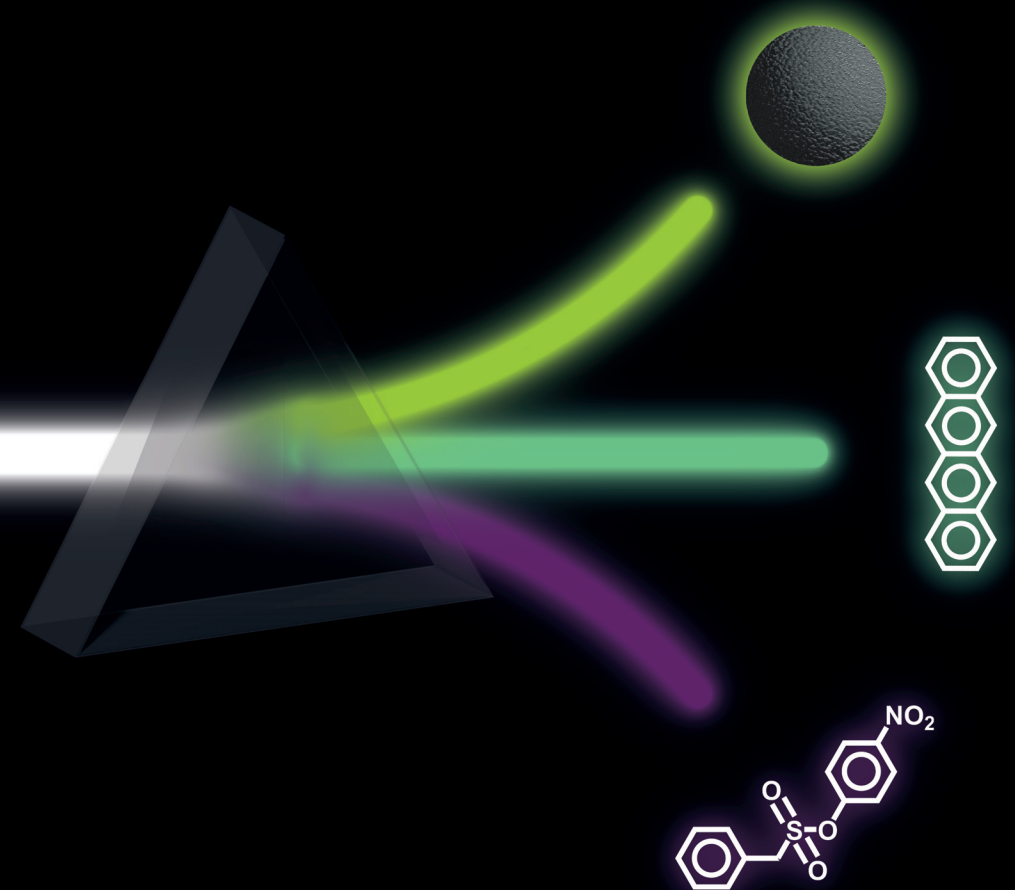


Nanoparticles, Surfaces, and Small Molecules:

Synthetic Methodology for Three Dimensions

Nanoparticles, Surfaces, and Small Molecules

Alyssa F.J. van den Boom



Alyssa F.J. van den Boom

Propositions

1. Not all Sulfur-Phenolate Exchange reactions are click reactions.
(this thesis)
2. Explicit introduction of oxygen prevents uncontrolled oxidation in silicon nanoparticles.
(this thesis)
3. Professors often have unrealistic expectations regarding the time required for experimental work.
4. Synthesis protocols resemble baking recipes in that not everyone will reach the same result after following the same steps.
5. The pampering of students at Dutch universities hampers them in their preparation for a working environment.
6. The rise in subscription-based services from manufacturers slows down innovation in those industries.
7. Gender quota reduce respect for female employees.

Propositions belonging to the thesis, entitled

Nanoparticles, Surfaces, and Small Molecules: Synthetic Methodology for Three Dimensions

Alyssa F.J. van den Boom

Wageningen, 20 June 2023

Nanoparticles, Surfaces, and Small Molecules:

Synthetic Methodology for Three Dimensions

Alyssa F. J. van den Boom

Thesis committee

Promotor

Prof. Dr H. Zuilhof
Professor of Organic Chemistry
Wageningen University & Research

Other members

Prof. Dr J.H.B. Sprakel, Wageningen University & Research
Prof. Dr L.D.A Siebbeles, Delft University of Technology
Dr J.C. Sootweg, University of Amsterdam
Dr M.M. Wienk, Eindhoven University of Technology

This research was conducted under the auspices of VLAG Graduate School (Biobased, Biomolecular, Chemical, Food and Nutrition Sciences).

Nanoparticles, Surfaces, and Small Molecules:

Synthetic Methodology for Three Dimensions

Alyssa F. J. van den Boom

Thesis

Submitted in fulfilment of the requirements for the degree of doctor
at Wageningen University

by the authority of the Rector Magnificus

Prof. Dr A.P.J. Mol,

in the presence of the

Thesis Committee appointed by the Academic Board

to be defended in public

on Tuesday 20 June 2023

at 11 a.m. in the Omnia Auditorium

Alyssa F. J. van den Boom

Nanoparticles, Surfaces, and Small Molecules: Synthetic Methodology for Three Dimensions,
198 pages.

PhD thesis, Wageningen University, Wageningen, The Netherlands (2023)
With references, with summary in English

ISBN 978-94-6447-579-1

DOI <https://doi.org/10.18174/586488>

Table of Contents

Chapter 1: General Introduction	7
Chapter 2: Fast room-temperature functionalization of silicon nanoparticles using alkyl silanols	31
Chapter 3: Improving triplet energy transfer from tetracene to silicon using a covalently-bound tetracene seed layer	59
Chapter 4: Sulfur-phenolate exchange as a fluorine-free approach to S(VI) exchange chemistry on sulfonyl moieties	93
Chapter 5: Sulphur-phenolate exchange as a mild, fast and high-yielding method towards the synthesis of sulfonamides	133
Chapter 6: General Discussion & Outlook	165
Summary	183
Acknowledgements	189
Curriculum Vitae	193
Overview of Completed Training Activities	195

Chapter 1

General Introduction

In response to global warming and the depletion of natural resources, humankind now needs to take steps to reduce its CO₂ footprint, minimize its energy consumption, and reduce the amount of harmful materials used and waste generated during production processes. These steps are necessary to preserve the earth for future generations: ice caps continue to melt, and an increase in extreme weather conditions is observed all over the world, with disastrous consequences for humans, animals, and plant life. To stop and maybe even reverse this process, a tremendous societal effort is needed; this requires close cooperation between governments, industry, consumers, and the scientific community. Chemistry is one field within the scientific community that can develop and contribute to solutions that address this global environmental crisis. In this thesis, we show our contribution to the end goal of zero emission and minimized waste through two major research lines: research into more efficient solar cells, and the development of novel click chemistry for the sustainable production of new materials and medicine. Both topics contribute to an improved, more environmentally friendly footprint, and will be further introduced and explained in this chapter.

Solar cells

Solar energy is one of the most important sources for the production of sustainable and renewable energy; converting solar energy into electricity does not produce CO₂, and – in contrast to fossil fuels such as oil and gas – solar energy is an (almost) infinite source of energy that will not be depleted over time. As a result, many countries invest heavily in solar energy as a sustainable energy source, with >9% of all electricity consumed in the Netherlands being produced from solar energy in 2021.¹ Nearly all of this energy was produced by photovoltaic cells, which convert solar energy into electricity via the photoelectric effect.² A schematic representation of the most common type of solar cell – using crystalline silicon – is shown in Figure 1. This design has many variations, all of which have been engineered to optimize energy conversion and minimize losses due to inefficient charge transfer and reflection. Two examples of these optimizations (also shown in

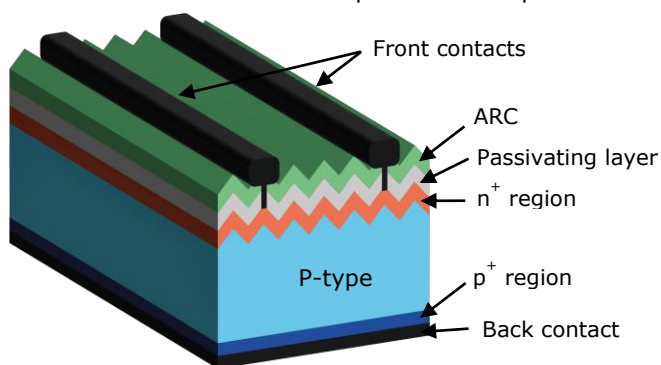


Figure 1: Schematic representation of a crystalline silicon solar cell.

Figure 1) are the addition of an anti-reflective coating (ARC) on top of the solar cell, and nanopatterning of the cell's surface, to minimize reflection and maximize absorption. With these and other optimizations in the design, silicon solar cells under controlled laboratory settings now operate at ~25% solar energy conversion efficiency, close to their theoretical limit of 29%.^{3,4} The reason for this – rather low – theoretical limit lies in the bandgap of the silicon material used to absorb the solar energy. When incoming photons have an energy lower than the bandgap of silicon, they will not cause excitation of electrons from the valence to the conduction band, and therefore do not produce a current in the solar cell. At the same time, when the photons have an energy higher than the bandgap, the excess energy is converted into heat, leading to further losses. For silicon, this leads to the data shown in Figure 2; other materials, *e.g.* germanium, show similar losses, with a minor shift due to the change in bandgap.^{3,4} As there is more energy to be gained from the high-energy photons than the low-energy photons,⁵ it is not surprising that there has been a lot of research on how to absorb these high-energy photons more efficiently. Here we will briefly discuss recent developments towards promising new materials and solar cell designs.

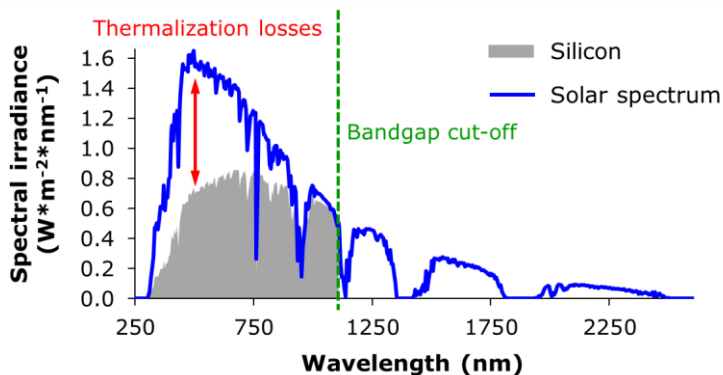


Figure 2: Energy mismatch between solar spectrum and silicon bandgap intrinsically limits solar energy conversion.

Perovskite solar cells

Perovskites are hybrid materials made from organic and inorganic building blocks, with the general formula ABX_3 , where A is an organic cation, B an inorganic cation, and X a halide (Figure 3).⁶ Perovskites provide a high degree of control over the bandgap, as all three components can be altered and tuned independently. In addition, perovskites can be made from low-cost materials, and are easy to process either as a solid or in solution, providing significant improvements over the production process for conventional

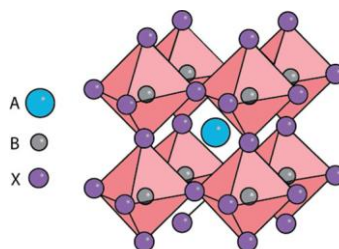


Figure 3: Crystal structure of a perovskite. Reprinted with permission from ⁹⁹. Copyright 2015 ACS.

(commercial) solar cells. Since their first introduction in 2009 (where an efficiency of 3.8% was reported),⁷ perovskites have developed rapidly, and lab-scale efficiencies of ~23% can now be reached.⁸ Unfortunately, the transfer to large-scale production and use has so far not been feasible for several reasons: the most efficient perovskite-based solar cells contain toxic lead cations that could leach into the environment during use,^{9,10} the long-term stability of perovskites is generally low, obligating users to replace the cells frequently to maintain solar cell performance,^{8,11–13} and the presence of surface defects that cause energy transfer barriers and defect trap states, leading to a reduced efficiency.^{14,15} Still, as new materials and techniques are developed to overcome these obstacles, the performance of perovskite solar cells is increasing steadily.^{9,10,14–16} Therefore, perovskites show promise to (at least partially) replace conventional solar cells in the coming years.

Tandem solar cells

One place where perovskites have already shown benefits is in the construction of tandem solar cells (TSCs).¹⁷ TSCs are solar cells in which the high-energy photons are absorbed in a different (part of the) solar cell than the low-energy photons (Figure 4). With this configuration, the well-established silicon- or germanium-based solar cell (low-energy photons) can be coupled to one or more novel solar cells based on *e.g.* perovskites (high-energy photons), to maximize the energy extracted from the solar spectrum.^{18–21} Alternatively, the whole TSC could be made from perovskites or polymers with systematically varied bandgaps.²² TSCs have shown great promise in breaking through the theoretical energy conversion limit, and certified efficiencies of ~30% have already been reported.^{18,23}

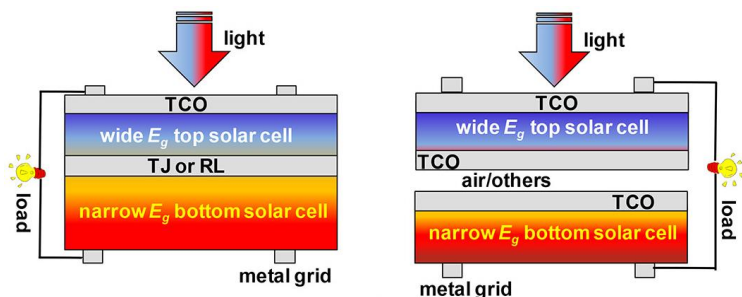


Figure 4: Schematic diagram of 2-terminal TSCs. TCO: transparent conductive oxide; TJ: tunnelling junction; RL: recombination layer. Reprinted with permission from ²⁴. Copyright 2020 ACS.

Despite these high efficiencies, the wide-spread use of TSCs is still limited. Ironically, the strength of a TSC – multiple (sub)cells working together – also causes issues in designing and creating a high-performance solar cell system,^{19,20,24} examples of which are: 1) the thickness of the top cell should be high enough to absorb as many high-energy photons as possible, yet low enough to allow the low-

energy photons to pass through; 2) both layers of the solar cell need to have an equal current at all times for the left design in Figure 4, as the whole system will always adapt to the lowest current, leading to a lower performance when there is a mis-match;²⁵ and 3) all electrodes and layers in between cells should be completely transparent to the solar spectrum, to maximize the energy available for absorption by the bottom layers.²⁶ As expected, these criteria require the use of special materials and specific production techniques for TSCs, leading to difficulties in scale-up and high manufacturing costs. In addition, the first two issues are partially dependent on the temperature, angle of incoming light, humidity, etc.,²⁵ further complicating the design and production of TSCs.¹⁸ As a result of all this, and the low life expectancy of the often-used perovskite solar (sub)cells, TSCs have so far not been able to replace commercial solar cells.

Sensitized solar cells

Another way to potentially lower production costs and push through the theoretical limit for solar cells is by sensitization. In this solar cell design, the absorption of light and charge carrier transport – processes that both occur within the bulk solar cell material in conventional solar cells – are divided over two separate materials:²⁷ light absorption occurs in the sensitizing layer, consisting of an organic dye (either as a liquid or solid) or quantum dots;^{27–32} meanwhile, charge separation occurs at the interface between the sensitizer and a semiconductor material, and charge transport occurs in the conduction band of the semiconductor, where the charges are transported to the charge collector. To prevent electron depletion of the sensitizing agent, an electrolyte is added to the cell, which is in turn regenerated by the counter electrode (Figure 5). This electrolyte can be present in liquid or solid form. Although liquid electrolytes generally show higher efficiencies, they (as well as liquid dyes) pose challenges due to the instability of the dye, corrosion of the cell by the electrolyte, and the need for proper encapsulation of the cell to prevent leaching of liquids into the environment. Therefore, this type of sensitized cell is not expected to be applicable on a large scale yet.

Another sensitization method has shown more promise: sensitization with up- or downconverting materials.³⁴ This method of sensitizing provides a similar effect as a tandem solar cell, yet here all light-absorbing materials are contained in the same (sub)cell.^{35,36} For upconverting materials, multiple low-energy photons produce one high-energy photon, which is absorbed by the semiconductor material in the cell. The opposite happens for downconverting materials: one high-energy photon is used to produce multiple low-energy photons, which are again absorbed by the semiconductor. In both cases, the semiconductor will also absorb photons directly from the sun, and produce a current in the usual way. Sensitization with up- or down-converters shows great promise to increase solar cell efficiencies to

beyond the Shockley–Queisser limit. This is especially the case for downconverters, which can, in principle, double the current generated by high-energy photons, while upconverters will halve the current generated by low-energy photons.³⁷

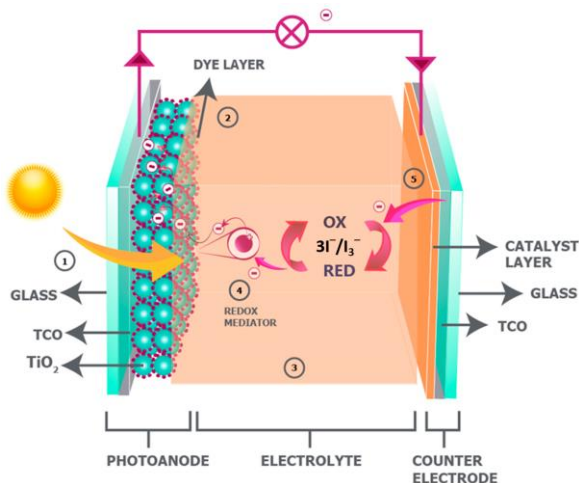


Figure 5: Schematic design of a dye-sensitized solar cell, using TiO_2 nanoparticles as the semiconductor, and the redox pair $3\text{I}^-/\text{I}_3^-$ as the electrolyte. The dye is represented as small purple dots on top of the semiconductor. Reprinted with permission from ³³.

There are several types of downconverters, like quantum dots and some organic dyes, but for the purposes of this introduction, we will focus on an especially promising class: organic molecules that cause downconversion through singlet fission (SF), a process schematically represented in Figure 6.

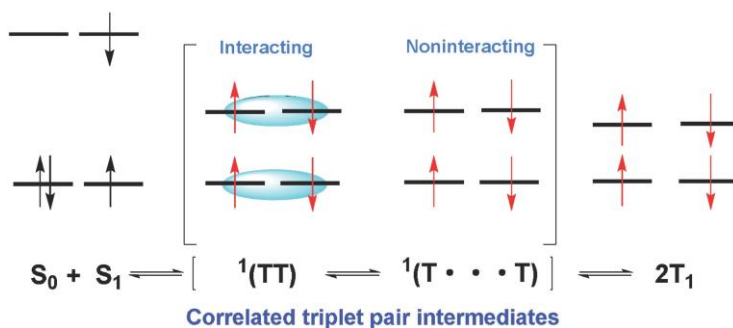


Figure 6: Overview of the SF process. A molecule is excited to the singlet state after absorption of a high-energy photon. This molecule falls back into a dark triplet state, simultaneously exciting another molecule into the triplet state. The triplet states are correlated, but slowly diffuse apart to generate two excited electrons. Reprinted with permission from ³⁸.

Though arguably no spectroscopic downconversion, as no low-energy photons are emitted, SF nevertheless produces two excited molecules (excitation energy divided over two molecules in a dark triplet state), each with an excited state energy

of about half the energy of the absorbed photon.³⁹ In fact, the lack of emission after SF is a benefit for optimizing the energy absorption within the solar cell. Instead of photons emitting in random directions, the excited electrons in the long-lived triplet state can be extracted in a unidirectional way towards the semiconductor material. However, the downside to this is the need for close contact between the sensitizing layer and the underlying semiconductor, as the energy from the electrons can only be transferred – *via* Dexter Energy Transfer (DET) – when there is a large overlap in the wavefunctions between the excited molecule and semiconductor (Figure 7).⁴⁰ Although challenging to achieve, some promising results have been reported for several SF molecule/semiconductor pairs, including: TIPS-tetracene and PbS quantum dots, tetracene and silicon (with a HfO_xN_y interlayer), pentacene and C_{60} , pentacene and PEDOT:PSS (with a P3HT interlayer), rubrene and C_{60} , pentacene and PbS/PbSe quantum dots,⁴¹ and tetracene and copper phthalocyanines.^{37,40,42–45}

From these previous studies, the results for sensitization of bulk crystalline silicon with SF materials are especially interesting. This method can potentially increase the efficiency of commercial silicon-based solar cells without compromising the robust and already optimized production process.⁴⁶ For these cases, the singlet fission material chosen is often tetracene. Tetracene has a triplet state with an energy slightly higher than the bandgap of silicon, making it an ideal partner for coupling to conventional solar cells. However, the current limitation of tetracene is that – when deposited as pure material – the orientation of tetracene is almost perpendicular to the silicon surface, leading to minimal triplet energy transfer to silicon.^{47,48} Many studies have tried to improve the efficiency of this energy transfer,⁴⁹ which was achieved to some extent with a very thin HfO_xN_y interlayer between the tetracene and silicon.⁴⁴ Triplet transfer was also observed for silicon surfaces without any passivation layer between the silicon and tetracene, after long-term exposure of the surfaces to air.⁴⁷ In this last case, the increase in triplet transfer was attributed to a change in the crystal structure of the tetracene, in which the molecules assumed a more parallel orientation with respect to the surface. This demonstrates the importance of tetracene's orientation on the silicon surface. If this orientation can be controlled during deposition, the triplet transfer can be optimized, to boost solar cell performance without completely redeveloping current commercial production processes. As a final interesting note, a recent study also showed that a sensitizing layer of tetracene increases the lifetime of the underlying silicon solar cell, as the absorption of high-energy photons by tetracene reduces the heat production in the silicon layer by thermalization processes.⁵⁰ As a longer lifetime reduces waste production, this provides an extra stimulus to develop tetracene-sensitized silicon solar cells.

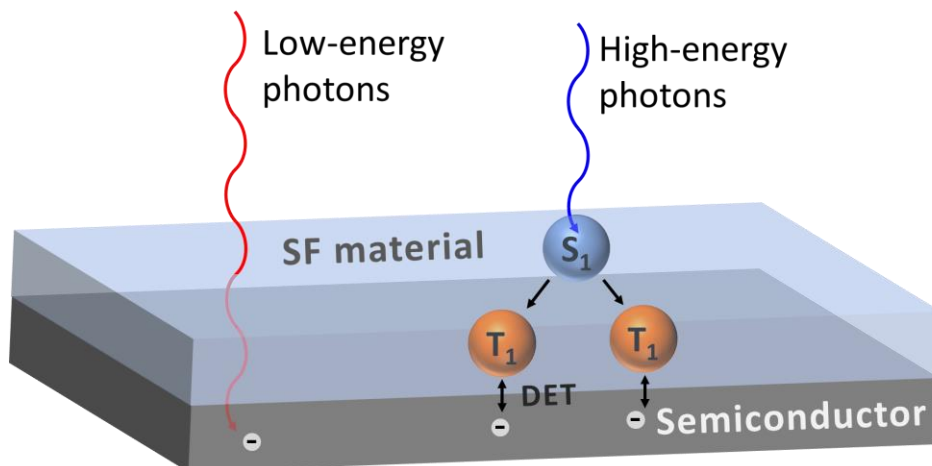


Figure 7: Schematic representation of a singlet-fission-sensitized solar cell, where high- and low-energy photons are absorbed in different layers within the cell, and two charges are generated from each high-energy photon.

Click Chemistry

The development of click chemistry is arguably one of the most important advances towards sustainable chemistry of the past 25 years. Using click chemistry, products that previously could only be obtained after many reaction steps and with low yields can now be produced with high yields in just a few reaction steps.^{51,52} The term “click” was coined in 2001 by Kolb, Finn, and Sharpless, where they also proposed several characteristics a reaction should have before it could be considered “click”:⁵³

“ The reaction must be *modular*, *wide in scope*, give *very high yields*, generate only *inoffensive byproducts* that can be removed by nonchromatographic methods, and be *stereospecific* (but not necessarily enantioselective). The required process characteristics include *simple reaction conditions* (ideally, the process should be insensitive to oxygen and water), *readily available starting materials and reagents*, the use of *no solvent or a solvent that is benign* (such as water) or *easily removed*, and *simple product isolation*. ”

As these characteristics are not quantified, there is some debate around which reactions can be considered click. Here, we will use the following criteria:

- the reaction should proceed with any molecule containing the reactive group, regardless of other functional groups present on the molecule
- the reaction conversion should be equal to the yield and near quantitative

- little to no heating is required, and the reaction can be performed under atmospheric conditions
- no toxic or corrosive solvents may be used, and the solvent should be easily removable
- products should be purified by recrystallization, extraction, precipitation, or a short isocratic column; this should not require the use of more than two techniques

These characteristics define an ecological funnel through which click chemistries appear more sustainable than other synthesis methods. Energy consumption is low, as heating is not required; minimal waste is produced due to the lack of byproducts and side reactions; and no extensive waste treatment is needed, as the solvents used are benign, and almost no purification is necessary. The above conditions also imply click reactions are suited for orthogonal synthesis, as reagents will only react to their specified targets. This means that multiple reaction steps can be performed in parallel or tandem within the same pot. As this removes the need for several cycles of isolation, deprotection, purification, drying, and redissolving of intermediates, this vastly reduces the energy requirements and waste production for reactions. Orthogonal synthesis has already been exploited in *e.g.* the synthesis of polymeric materials, where both polymer synthesis and functionalization could be performed without intermediate purification.^{54,55} In the following sections we will introduce three widely established click reactions, and elaborate on their applications. This list is by no means exhaustive, and only serves to provide a deeper understanding of the principles behind and the importance of click chemistry.

CuAAC reaction

The copper(I)-catalyzed azide-alkyne cycloaddition (CuAAC) reaction (Figure 8) was developed in 2002, and saw its first biological application in 2003, where the reaction was used to modify viral particles with fluorescent dyes.⁵⁶ At first, the use of toxic Cu(I) catalysts limited the use of CuAAC for biological applications;^{57,58} however, with the developments of biocompatible ligands, the amount of Cu(I) catalyst needed for the reaction was strongly reduced, thereby also reducing the toxic effects, and CuAAC became an invaluable tool in biological studies.⁵⁹ Since, CuAAC has been used to map the proteome, functionalize DNA,⁶⁰ study specific enzyme-substrate and protein-protein interactions, modify proteins,⁶¹ and to study post-translational modifications (PTMs).^{56,58,59} CuAAC has also found applications in polymer science,^{51,54,57} nanoparticle functionalization,⁶² target-guided synthesis,⁶³ and (solid-phase) synthesis for peptides, small molecules, drugs,⁶⁴ enzyme inhibitors, and polymers.^{59,63,65} Moreover, the product of the CuAAC reaction, a 1,2,3-triazole, can be used to create supramolecular complexes with other organic molecules or even (transition)metals.⁶⁶

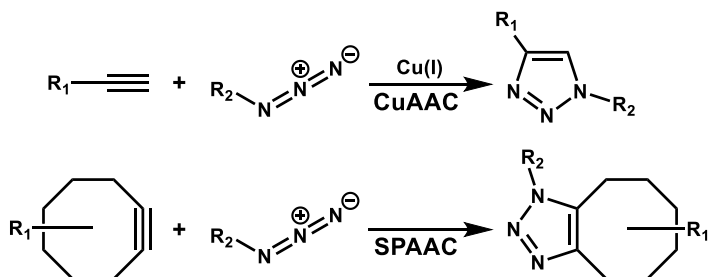


Figure 8: General reaction schemes for the CuAAC and SPAAC reactions.

In 2004, the need for a copper catalyst was eliminated with the introduction of SPAAC (strain-promoted alkyne-azide cycloaddition, Figure 8), where ring strain is employed to catalyze the reaction in the absence of copper.^{67,68} This has opened up the field of alkyne-azide cycloaddition reactions even more, and in 2022, Carolyn R. Bertozzi, Morten Meldal and K. Barry Sharpless were awarded the Nobel Prize in Chemistry for their work on CuAAC (Meldal & Sharpless), and the development and application of biorthogonal chemistry using – amongst others – SPAAC reactions (Bertozzi).⁶⁹

Thiol-ene

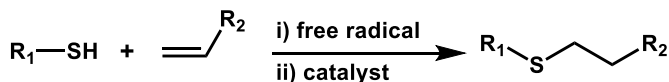


Figure 9: General reaction scheme for two thiol-ene reactions.

While CuAAC has become invaluable for biological studies, the thiol-ene click reaction has found its main application in material science. First noted in 1905,⁷⁰ the highly efficient reaction of thiols with C=C (-ene) bonds has grown into a widely applied tool in synthetic chemistry.^{71,72} Nowadays, two main thiol-ene reactions can be distinguished: free-radical addition of thiols to electron-rich / electron-poor C=C (or C≡C) bonds, and a catalyzed Michael addition of thiols to electron-deficient C=C bonds (Figure 9).⁷² Both reactions fulfill the requirements for a click reaction, and have found many uses, mainly in the production of polymers for high-end applications (microdevices, holographic diffractive materials, microfluidic devices, etc.).^{54,68,71} This is because cross-linked polymer networks made *via* radical thiol-ene click reactions have been reported as being the most homogeneous network structures ever made by free-radical polymerization, and generally display very narrow glass-transition regions.⁷² Other uses of the thiol-ene reaction in polymer science include the modification of existing polymers,^{54,55} and the synthesis of dendrimers and (nano)structures for drug delivery.^{57,68,71–74} In addition, due to their extremely high yields, thiol-ene click reactions were successfully applied for surface functionalization, where photolithography and nanopatterning – due to the possibility for light activation of the reagents – were possible with a high degree of

control;^{71,72} something that is not possible with CuAAC or SPAAC reactions. Apart from this, thiol-ene reactions are also excellent candidates for use in biological applications; as many proteins already contain native thiol groups, no prior modification of proteins is needed to create an active site. It is therefore not surprising that there are many examples of the use of thiol-ene reactions for binding of proteins to a surface, bioconjugation, (*e.g.* for use in vaccine development) or functionalization of amino-acid- or bio-based polymers.^{55,72,75,76}

Finally, one should note that thiols can also react to carbon-carbon triple bonds (-ynes) in the same way as for C=C bonds. In that case, the subsequent addition of two different thiols onto the same alkyne moiety allows the creation of a branched structure.⁵⁷

SuFEx

One of the latest additions to the list of click reactions is the Sulfur (VI) Fluoride Exchange (SuFEx) reaction:⁷⁷ a "SuFEx hub" containing a sulfonyl fluoride group is attacked by a nucleophile; the fluorine splits off as a leaving group, and the nucleophile is coupled to the SuFEx hub to afford a wide range of products (Figure 10). Discovered in 1927,⁷⁸ and re-introduced in 2014,⁷⁷ the strength of SuFEx reactions lies in the high stability of the starting S-F bond towards oxidation, reduction, and heat, as well as its poor reactivity before activation. This, combined with the wide availability and easy introduction of SuFEx hubs,⁷⁹⁻⁸² has led to a rapid increase in the use of SuFEx. Various examples of the use of SuFEx in polymers and biological applications are provided below. For a more detailed overview, and the use of SuFEx in other applications (*e.g.* surface modification), the reader is referred to some excellent recent reviews on the applications of SuFEx.^{80,83}

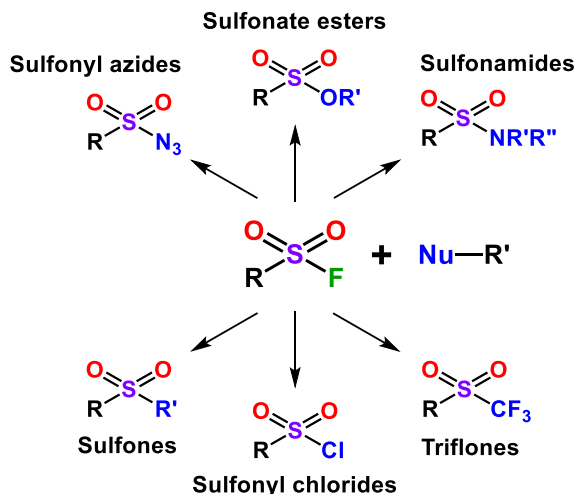


Figure 10: General reaction scheme for the SuFEx reaction, with an overview of product classes that can be obtained.

Polymers

The high reaction speed and yield of the (non-radical) SuFEx reaction make it ideal for the production of polymers. In 2014, the SuFEx reaction was used to create a sulfate analogue of poly(bisphenol A carbonate) in quantitative yield, that displayed superior resistance against chemical degradation.⁸⁴ In 2017, a wider selection of sulfonyl fluorides and silyl ethers were reacted to create a range of polymers in 10-60 min.⁸⁵ Additional functionalities on the monomers were not affected by the polymerization, and could be used for further functionalization of the polymer using orthogonal reactions such as CuAAC or thiol-ene. Later on, mono- and polydisperse sequence-controlled polymers were developed using a combination of SuFEx and CuAAC, thereby proving a demonstration how several click reactions can work together to create intricate materials.⁸⁰ More ambitious polymer designs were soon developed, such as chiral⁸⁶ or helical polymers,⁸⁷ and polymers with a pyrazoline-naphthylamide backbone for use in memory devices.⁸⁸ Besides for the construction of polymer backbones, SuFEx can also be used for post-polymerization modification; the small size and chemical robustness of the sulfonyl fluoride moiety provide a perfect active side that does not require protection during polymerization.^{80,89}

(Small molecules for) biological applications

The use of sulfonyl-fluoride-containing molecules as enzyme inhibitors has been well-established, and an extensive report on the biological activity of many sulfonyl-fluoride containing molecules was published as early as 1976, although the actual use of sulfonyl fluorides as enzyme inhibitors goes back decades.⁹⁰ Further reports followed in the '80s and '90s, where fluorosulfonyl-modified nucleotides were used as labeling and affinity probes for a range of proteins.⁷⁷ The success of the sulfonyl fluoride bond for these applications lies in its relatively slow reaction; when the -SO₂F compound is not complexed to the protein of interest, the residence time in the protein is too short to cause a reaction. However, in the case of complexation, reactions can occur, and the probe will form a covalent attachment to the protein. This proves a major advantage over the use of CuAAC and thiol-ene click reactions: no metal or radical catalyst is needed for the reaction, no prior modification of the proteins is needed, the SuFEx reaction is activated by water, and a reaction will only occur after a longer interaction time.^{77,91} It is therefore not surprising that with the development of SuFEx chemistry, many more examples of SO₂F-containing enzyme inhibitors and chemical probes can be found.^{77,79,80,92,93} Other uses of SuFEx chemistry are protein modification for the formation of biocompatible hydrogels,⁹¹ late-stage drug functionalization for screening purposes,^{81,92,94} and bioconjugation of alkyne-containing sulfonyl fluorides to proteins and DNA for further modification *via* CuAAC.^{80,95} As a final example of SuFEx in biological applications, the unnatural amino acid fluorosulfate-*L*-tyrosine was developed in 2018, which, after being incorporated into proteins, selectively reacted with lysine, histidine, and tyrosine

residues on nearby interacting proteins, generating covalent linkages between these proteins in living cells.⁹⁶

However, despite its many advantages, SuFEx still runs into limitation, one of which is the use of a fluorine leaving group. As fluorine-containing chemicals are investigated – and indeed banned – more and more for their toxicity to both humans and the environment, SuFEx is so far not a good candidate for ecologically friendly and sustainable click chemistry. To remedy this, alternatives to the fluorine leaving group in SuFEx have been developed. These are mainly based on the use of a sulfonyl chloride instead of the corresponding fluoride, the use of 1-sulfonimidoyl- or 1-sulfamimidoyl-3-methylimidazolium derivatives,⁹⁷ or the use of sulfonyl-triazoles.⁹⁸ For these last two, the starting material is difficult to prepare, while the use of sulfonyl chlorides – while popular before the introduction of SuFEx and widely available for a range of SuFEx hubs – suffers from poor hydrolytic stability. So, for SuFEx chemistry to grow further, it is important to address these issues, and find a stable starting material that does not yield fluorine-containing side products, yet provides the same benefits and high yields as “regular” SuFEx hubs.

Aim of this thesis

The aim of this thesis is to use new developments in several areas of research to aid in the transfer towards 100% sustainable energy production and low-energy costing, minimal-waste, non-toxic chemical synthesis. To this end, several projects were performed, the results of which can be found further on in this thesis.

First, we aimed to develop a room-temperature passivation method for hydrogen-terminated silicon nanoparticles. Nanoparticles in general have found many applications in bio-imaging, medicine, and solar cell applications, and hydrogen-terminated, crystalline silicon nanoparticles are of particular interest in this case. Not only due to the high natural abundance of silicon, but also due to their near-ideal electrical and electronic properties, and the lower toxicity compared to the often used cadmium- or lead-based nanoparticles. However, hydrogen-terminated silicon nanoparticles are highly susceptible to oxidation, and require passivation before use. Standard passivation methods often require high temperatures, long reaction times, or additional chemicals that end up as waste products after the passivation process. As this requires a lot of energy and waste treatment, we aimed to develop a room-temperature method, that required little to no solvent, and is faster and safer to use than conventional methods. This is described in **Chapter 2**.

Second, we aimed to improve the efficiency of silicon-based solar cells by sensitizing them with a covalent seed layer of tetracene derivatives. As explained, sensitization with tetracene provides one of the fastest ways to quickly boost solar cell efficiency without the need for drastic adjustments in existing solar cell production methods. Yet the almost parallel orientation of tetracene on the surface has so far limited the energy transfer. By attaching a covalent seed layer of tetracene derivatives with an improved orientation, we hoped to increase the energy transfer, thereby greatly increasing both the efficiency and lifetime of the solar cell. Efforts in this direction are outlined in **Chapter 3**.

Third and last, we aimed to both expand and improve upon the toolbox of click chemistry available to scientists. For this, we took the SuFEx reaction as a basis. Using a phenolate as the leaving group instead of fluorine, our goal was to reduce the production of toxic side products, decrease reaction times, and increase the scope of the reaction. With this, we aimed to increase the scope and sustainability of the SuFEx click reaction. The results of this research has been detailed in **Chapters 4 and 5**.

References

- (1) Rijksdienst voor Ondernemend Nederland. *Monitor Zon-PV 2022 in Nederland*; (2022).
- (2) Polman, A.; Knight, M.; Garnett, E. C.; Ehrler, B.; Sinke, W. C. Photovoltaic Materials: Present Efficiencies and Future Challenges. (2016), *Science* (1979), **352** (6283).
- (3) Rühle, S. Tabulated Values of the Shockley-Queisser Limit for Single Junction Solar Cells. (2016), *Solar Energy*, **130**, 139–147.
- (4) Alharbi, F. H.; Kais, S. Theoretical Limits of Photovoltaics Efficiency and Possible Improvements by Intuitive Approaches Learned from Photosynthesis and Quantum Coherence. (2015), *Renewable and Sustainable Energy Reviews*, **43**, 1073–1089.
- (5) American Society for Testing and Materials (ASTM), subcommittee G. 09. *Standard Tables for Reference Solar Spectral Irradiances: Direct Normal and Hemispherical on 37° Tilted Surface*; (2003).
- (6) Kim, J. Y.; Lee, J. W.; Jung, H. S.; Shin, H.; Park, N. G. High-Efficiency Perovskite Solar Cells. (2020), *Chem Rev*, **120** (15), 7867–7918.
- (7) Kojima, A.; Teshima, K.; Shirai, Y.; Miyasaka, T. Organometal Halide Perovskites as Visible-Light Sensitizers for Photovoltaic Cells. (2009), *J Am Chem Soc*, **131** (17), 6050–6051.
- (8) Rong, Y.; Hu, Y.; Mei, A.; Tan, H.; Saidaminov, M. I.; Seok, S. il; McGehee, M. D.; Sargent, E. H.; Han, H. Challenges for Commercializing Perovskite Solar Cells. (2018), *Science* (1979), **361** (6408).
- (9) Giustino, F.; Snaith, H. J. Toward Lead-Free Perovskite Solar Cells. (2016), *ACS Energy Lett*, **1** (6), 1233–1240.
- (10) Correa-Baena, J. P.; Abate, A.; Saliba, M.; Tress, W.; Jesper Jacobsson, T.; Grätzel, M.; Hagfeldt, A. The Rapid Evolution of Highly Efficient Perovskite Solar Cells. (2017), *Energy Environ Sci*, **10** (3), 710–727.
- (11) Green, M. A.; Ho-Baillie, A. Perovskite Solar Cells: The Birth of a New Era in Photovoltaics. (2017), *ACS Energy Lett*, **2** (4), 822–830.
- (12) Correa-Baena, J.-P.; Saliba, M.; Buonassisi, T.; Grätzel, M.; Abate, A.; Tress, W.; Hagfeldt, A. Promises and Challenges of Perovskite Solar Cells. (2017), *Science* (1979), **358**, 739–744.
- (13) Asghar, M. I.; Zhang, J.; Wang, H.; Lund, P. D. Device Stability of Perovskite Solar Cells – A Review. (2017), *Renewable and Sustainable Energy Reviews*, **77**, 131–146.
- (14) Mahapatra, A.; Prochowicz, D.; Tavakoli, M. M.; Trivedi, S.; Kumar, P.; Yadav, P. A Review of Aspects of Additive Engineering in Perovskite Solar Cells. (2020), *J Mater Chem A Mater*, **8** (1), 27–54.
- (15) Chen, J.; Park, N. G. Causes and Solutions of Recombination in Perovskite Solar Cells. (2019), *Advanced Materials*, **31** (47).
- (16) Wang, Z.; Shi, Z.; Li, T.; Chen, Y.; Huang, W. Stability of Perovskite Solar Cells: A Prospective on the Substitution of the A Cation and X Anion. (2017), *Angewandte Chemie International Edition*, **56**, 1190–1212.

- (17) Wali, Q.; Elumalai, N. K.; Iqbal, Y.; Uddin, A.; Jose, R. Tandem Perovskite Solar Cells. (2018), *Renewable and Sustainable Energy Reviews*, **84**, 89–110.
- (18) Todorov, T. K.; Bishop, D. M.; Lee, Y. S. Materials Perspectives for Next-Generation Low-Cost Tandem Solar Cells. (2018), *Solar Energy Materials and Solar Cells*, **180**, 350–357.
- (19) Anaya, M.; Lozano, G.; Calvo, M. E.; Míguez, H. ABX₃ Perovskites for Tandem Solar Cells. (2017), *Joule*, **1** (4), 769–793.
- (20) Lee, J. W.; Hsieh, Y. T.; de Marco, N.; Bae, S. H.; Han, Q.; Yang, Y. Halide Perovskites for Tandem Solar Cells. (2017), *Journal of Physical Chemistry Letters*, **8** (9), 1999–2011.
- (21) Tong, J.; Jiang, Q.; Zhang, F.; Kang, S. B.; Kim, D. H.; Zhu, K. Wide-Bandgap Metal Halide Perovskites for Tandem Solar Cells. (2021), *ACS Energy Lett*, **6** (1), 232–248.
- (22) You, J.; Dou, L.; Hong, Z.; Li, G.; Yang, Y. Recent Trends in Polymer Tandem Solar Cells Research. (2013), *Prog Polym Sci*, **38** (12), 1909–1928.
- (23) Tockhorn, P.; Sutter, J.; Cruz, A.; Wagner, P.; Jäger, K.; Yoo, D.; Lang, F.; Grischek, M.; Li, B.; Li, J.; Shargaieva, O.; Unger, E.; Al-Ashouri, A.; Köhnen, E.; Stolterfoht, M.; Neher, D.; Schlattmann, R.; Rech, B.; Stannowski, B.; Albrecht, S.; Becker, C. Nano-Optical Designs for High-Efficiency Monolithic Perovskite–Silicon Tandem Solar Cells. (2022), *Nat Nanotechnol*, **17** (11), 1214–1221.
- (24) Li, H.; Zhang, W. Perovskite Tandem Solar Cells: From Fundamentals to Commercial Deployment. (2020), *Chem Rev*, **120** (18), 9835–9950.
- (25) Dupré, O.; Niesen, B.; de Wolf, S.; Ballif, C. Field Performance versus Standard Test Condition Efficiency of Tandem Solar Cells and the Singular Case of Perovskites/Silicon Devices. (2018), *Journal of Physical Chemistry Letters*, **9** (2), 446–458.
- (26) Zhang, Z.; Li, Z.; Meng, L.; Lien, S. Y.; Gao, P. Perovskite-Based Tandem Solar Cells: Get the Most Out of the Sun. (2020), *Adv Funct Mater*, **30** (38).
- (27) Grätzel, M. Dye-Sensitized Solar Cells. (2003), *Journal of Photochemistry and Photobiology C: Photochemistry Reviews*, **4** (2), 145–153.
- (28) Nozik, A. J. Quantum Dot Solar Cells. (2002), *Physica E*, **14**, 115–120.
- (29) Giménez, S.; Mora-Seró, I.; MacOr, L.; Guijarro, N.; Lana-Villarreal, T.; Gómez, R.; Diguna, L. J.; Shen, Q.; Toyoda, T.; Bisquert, J. Improving the Performance of Colloidal Quantum-Dot-Sensitized Solar Cells. (2009), *Nanotechnology*, **20** (29).
- (30) O'Regan, B.; Grätzel, M. A Low-Cost, High-Efficiency Solar Cell Based on Dye-Sensitized Colloidal TiO₂ Films. (1991), *Nature*, **353**, 737–740.
- (31) Wang, H.; Zhang, X.; Gong, F.; Zhou, G.; Wang, Z. S. Novel Ester-Functionalized Solid-State Electrolyte for Highly Efficient All-Solid-State Dye-Sensitized Solar Cells. (2012), *Advanced Materials*, **24** (1), 121–124.
- (32) Kramer, I. J.; Sargent, E. H. The Architecture of Colloidal Quantum Dot Solar Cells: Materials to Devices. (2014), *Chem Rev*, **114** (1), 863–882.

- (33) Iftikhar, H.; Sonai, G. G.; Hashmi, S. G.; Nogueira, A. F.; Lund, P. D. Progress on Electrolytes Development in Dye-Sensitized Solar Cells. (2019), *Materials*, **12** (12), 1998.
- (34) Yu, D.; Yu, T.; Lin, H.; Zhuang, S.; Zhang, D. Recent Advances in Luminescent Downconversion: New Materials, Techniques, and Applications in Solar Cells. (2022), *Adv Opt Mater*, **10** (12), 2200014.
- (35) Macqueen, R. W.; Liebhaber, M.; Niederhausen, J.; Mews, M.; Gersmann, C.; Jäckle, S.; Jäger, K.; Tayebjee, M. J. Y.; Schmidt, T. W.; Rech, B.; Lips, K. Crystalline Silicon Solar Cells with Tetracene Interlayers: The Path to Silicon-Singlet Fission Heterojunction Devices. (2018), *Mater Horiz*, **5** (6), 1065–1075.
- (36) Futscher, M. H.; Rao, A.; Ehrler, B. The Potential of Singlet Fission Photon Multipliers as an Alternative to Silicon-Based Tandem Solar Cells. (2018), *ACS Energy Lett*, **3** (10), 2587–2592.
- (37) Xia, J.; Sanders, S. N.; Cheng, W.; Low, J. Z.; Liu, J.; Campos, L. M.; Sun, T. Singlet Fission: Progress and Prospects in Solar Cells. (2017), *Advanced Materials*, **29** (20), 1601652.
- (38) Xia, J.; Sanders, S. N.; Cheng, W.; Low, J. Z.; Liu, J.; Campos, L. M.; Sun, T. Singlet Fission: Progress and Prospects in Solar Cells. (2017), *Advanced Materials*, **29** (20), 1601652.
- (39) Ito, S.; Nagami, T.; Nakano, M. Molecular Design for Efficient Singlet Fission. (2018), *Journal of Photochemistry and Photobiology C: Photochemistry Reviews*, **34**, 85–120.
- (40) Rao, A.; Friend, R. H. Harnessing Singlet Exciton Fission to Break the Shockley-Queisser Limit. (2017), *Nat Rev Mater*, **2**, 17063.
- (41) Ehrler, B.; Wilson, M. W. B.; Rao, A.; Friend, R. H.; Greenham, N. C. Singlet Exciton Fission-Sensitized Infrared Quantum Dot Solar Cells. (2012), *Nano Lett*, **12** (2), 1053–1057.
- (42) Casillas, R.; Papadopoulos, I.; Ullrich, T.; Thiel, D.; Kunzmann, A.; Guldi, D. M. Molecular Insights and Concepts to Engineer Singlet Fission Energy Conversion Devices. (2020), *Energy Environ Sci*, **13** (9), 2741–2804.
- (43) Lee, J.; Jadhav, P.; Baldo, M. A. High Efficiency Organic Multilayer Photodetectors Based on Singlet Exciton Fission. (2009), *Appl Phys Lett*, **95** (3), 033301.
- (44) Einzinger, M.; Wu, T.; Kompalla, J. F.; Smith, H. L.; Perkinson, C. F.; Nienhaus, L.; Wieghold, S.; Congreve, D. N.; Kahn, A.; Bawendi, M. G.; Baldo, M. A. Sensitization of Silicon by Singlet Exciton Fission in Tetracene. (2019), *Nature*, **571** (7763), 90–94.
- (45) Lee, J.; Jadhav, P.; Reuswig, P. D.; Yost, S. R.; Thompson, N. J.; Congreve, D. N.; Hontz, E.; van Voorhis, T.; Baldo, M. A. Singlet Exciton Fission Photovoltaics. (2013), *Acc Chem Res*, **46** (6), 1300–1311.
- (46) Daiber, B.; Pujari, S. P.; Verboom, S.; Luxembourg, S. L.; Tabernig, S. W.; Futscher, M. H.; Lee, J.; Zuilhof, H.; Ehrler, B. A Method to Detect Triplet Exciton Transfer from Singlet Fission Materials into Silicon Solar Cells: Comparing Different Surface Treatments. (2020), *Journal of Chemical Physics*, **152** (11), 114201.

- (47) Daiber, B.; Maiti, S.; Ferro, S. M.; Bodin, J.; van den Boom, A. F. J.; Luxembourg, S. L.; Kinge, S.; Pujari, S. P.; Zuilhof, H.; Siebbeles, L. D. A.; Ehrler, B. Change in Tetracene Polymorphism Facilitates Triplet Transfer in Singlet Fission-Sensitized Silicon Solar Cells. (2020), *Journal of Physical Chemistry Letters*, **11** (20), 8703–8709.
- (48) Arias, D. H.; Ryerson, J. L.; Cook, J. D.; Damrauer, N. H.; Johnson, J. C. Polymorphism Influences Singlet Fission Rates in Tetracene Thin Films. (2016), *Chem Sci*, **7** (2), 1185–1191.
- (49) Niederhausen, J.; MacQueen, R. W.; Özkol, E.; Gersmann, C.; Futscher, M. H.; Liebhaber, M.; Friedrich, D.; Borgwardt, M.; Mazzio, K. A.; Amsalem, P.; Nguyen, M. H.; Daiber, B.; Mews, M.; Rappich, J.; Ruske, F.; Eichberger, R.; Lips, K. Energy-Level Alignment Tuning at Tetracene/c-Si Interfaces. (2020), *Journal of Physical Chemistry C*, **124** (51), 27867–27881.
- (50) Jiang, Y.; Nielsen, M. P.; Baldacchino, A. J.; Green, M. A.; McCamey, D. R.; Tayebjee, M. J. Y.; Schmidt, T. W.; Ekins-Daukes, N. J. Singlet Fission and Tandem Solar Cells Reduce Thermal Degradation and Enhance Lifespan. (2021), *Progress in Photovoltaics: Research and Applications*, **29** (8), 899–906.
- (51) Sumerlin, B. S.; Vogt, A. P. Macromolecular Engineering through Click Chemistry and Other Efficient Transformations. (2010), *Macromolecules*, **43** (1), 1–13.
- (52) Barner-Kowollik, C.; Inglis, A. J. Has Click Chemistry Lead to a Paradigm Shift in Polymer Material Design? (2009), *Macromol Chem Phys*, **210** (12), 987–992.
- (53) Kolb, H. C.; Finn, M. G.; Sharpless, K. B. Click Chemistry: Diverse Chemical Function from a Few Good Reactions. (2001), *Angewandte Chemie - International Edition*, **40** (11), 2004–2021.
- (54) Iha, R. K.; Wooley, K. L.; Nyström, A. M.; Burked, D. J.; Kade, M. J.; Hawker, C. J. Applications of Orthogonal “Click” Chemistries in the Synthesis of Functional Soft Materials. (2009), *Chem Rev*, **109** (11), 5620–5686.
- (55) Hvilsted, S. Facile Design of Biomaterials by “click” Chemistry. (2012), *Polym Int*, **61** (4), 485–494.
- (56) Parker, C. G.; Pratt, M. R. Click Chemistry in Proteomic Investigations. (2020), *Cell*, **180** (4), 605–632.
- (57) Xi, W.; Scott, T. F.; Kloxin, C. J.; Bowman, C. N. Click Chemistry in Materials Science. (2014), *Adv Funct Mater*, **24** (18), 2572–2590.
- (58) Best, M. D. Click Chemistry and Bioorthogonal Reactions: Unprecedented Selectivity in the Labeling of Biological Molecules. (2009), *Biochemistry*, **48** (28), 6571–6584.
- (59) Thirumurugan, P.; Matosiuk, D.; Jozwiak, K. Click Chemistry for Drug Development and Diverse Chemical-Biology Applications. (2013), *Chem Rev*, **113** (7), 4905–4979.
- (60) El-Sagheer, A. H.; Brown, T. Click Chemistry with DNA. (2010), *Chem Soc Rev*, **39** (4), 1388–1405.
- (61) Li, H.; Aneja, R.; Chaiken, I. Click Chemistry in Peptide-Based Drug Design. (2013), *Molecules*, **18** (8), 9797–9817.
- (62) Li, N.; Binder, W. H. Click-Chemistry for Nanoparticle-Modification. (2011), *J Mater Chem*, **21** (42), 16717–16734.

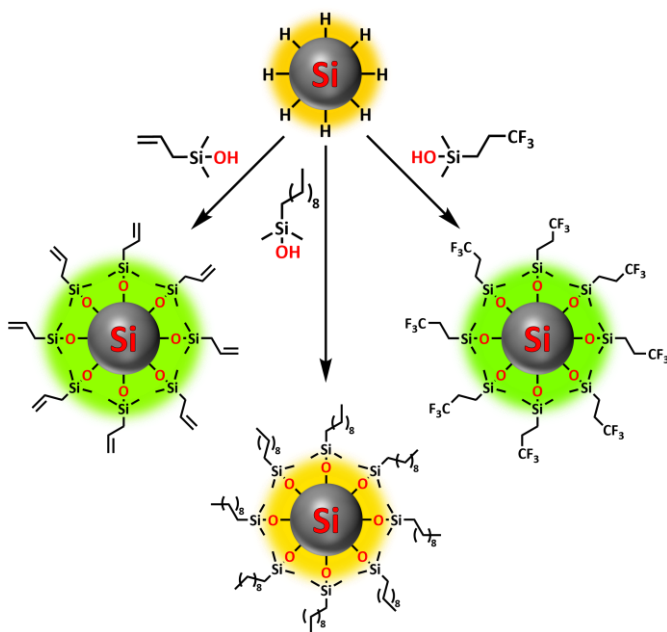
- (63) Mamidyala, S. K.; Finn, M. G. In Situ Click Chemistry: Probing the Binding Landscapes of Biological Molecules. (2010), *Chem Soc Rev*, **39** (4), 1252–1261.
- (64) Jiang, X.; Hao, X.; Jing, L.; Wu, G.; Kang, D.; Liu, X.; Zhan, P. Recent Applications of Click Chemistry in Drug Discovery. (2019), *Expert Opin Drug Discov*, **14** (8), 779–789.
- (65) Castro, V.; Rodríguez, H.; Albericio, F. CuAAC: An Efficient Click Chemistry Reaction on Solid Phase. (2016), *ACS Comb Sci*, **18** (1), 1–14.
- (66) Schulze, B.; Schubert, U. S. Beyond Click Chemistry-Supramolecular Interactions of 1,2,3-Triazoles. (2014), *Chem Soc Rev*, **43** (8), 2522–2571.
- (67) Agard, N. J.; Prescher, J. A.; Bertozzi, C. R. A Strain-Promoted [3 + 2] Azide–Alkyne Cycloaddition for Covalent Modification of Biomolecules in Living Systems. (2004), *J Am Chem Soc*, **126** (46), 15046–15047.
- (68) Remzi Becer, C.; Hoogenboom, R.; Schubert, U. S. Click Chemistry beyond Metal-Catalyzed Cycloaddition. (2009), *Angewandte Chemie - International Edition*, **48** (27), 4900–4908.
- (69) NobelPrize.org. *The Nobel Prize in Chemistry 2022*. Nobel Prize Outreach AB 2022. <https://www.nobelprize.org/prizes/chemistry/2022/press-release/> (accessed 2022-12-24).
- (70) Posner, T. Beiträge Zur Kenntniss Der Ungesättigten Verbindungen. II. Ueber Die Addition von Mercaptanen an Ungesättigte Kohlenwasserstoffe. (1905), *Berichte der deutschen chemischen Gesellschaft*, **38** (1), 646–657.
- (71) Hoyle, C. E.; Lowe, A. B.; Bowman, C. N. Thiol-Click Chemistry: A Multifaceted Toolbox for Small Molecule and Polymer Synthesis. (2010), *Chem Soc Rev*, **39** (4), 1355–1387.
- (72) Hoyle, C. E.; Bowman, C. N. Thiol-Ene Click Chemistry. (2010), *Angewandte Chemie - International Edition*, **49** (9), 1540–1573.
- (73) Lallana, E.; Sousa-Herves, A.; Fernandez-Trillo, F.; Riguera, R.; Fernandez-Megia, E. Click Chemistry for Drug Delivery Nanosystems. (2012), *Pharm Res*, **29** (1), 1–34.
- (74) Lallana, E.; Fernandez-Trillo, F.; Sousa-Herves, A.; Riguera, R.; Fernandez-Megia, E. Click Chemistry with Polymers, Dendrimers, and Hydrogels for Drug Delivery. (2012), *Pharm Res*, **29** (4), 1134–1142.
- (75) Habraken, G. J. M.; Koning, C. E.; Heuts, J. P. A.; Heise, A. Thiol Chemistry on Well-Defined Synthetic Polypeptides. (2009), *Chemical Communications*, No. 24, 3612–3614.
- (76) van Dijk, M.; Rijkers, D. T. S.; Liskamp, R. M. J.; van Nostrum, C. F.; Hennink, W. E. Synthesis and Applications of Biomedical and Pharmaceutical Polymers via Click Chemistry Methodologies. (2009), *Bioconj Chem*, **20** (11), 2001–2016.
- (77) Dong, J.; Krasnova, L.; Finn, M. G.; Barry Sharpless, K. Sulfur(VI) Fluoride Exchange (SuFEx): Another Good Reaction for Click Chemistry. (2014), *Angewandte Chemie - International Edition*, **53** (36), 9430–9448.
- (78) Steinkopf, W. Über Aromatische Sulfofluoride. (1927), *Journal für Praktische Chemie*, **117** (1), 1–82.

- (79) Meng, Y. P.; Wang, S. M.; Fang, W. Y.; Xie, Z. Z.; Leng, J.; Alsulami, H.; Qin, H. L. Ethenesulfonyl Fluoride (ESF) and Its Derivatives in SuFEx Click Chemistry and More. (2020), *Synthesis (Stuttg)*, **52** (5), 673–687.
- (80) Barrow, A. S.; Smedley, C. J.; Zheng, Q.; Li, S.; Dong, J.; Moses, J. E. The Growing Applications of SuFEx Click Chemistry. (2019), *Chem Soc Rev*, **48** (17), 4731–4758.
- (81) Abdul Fattah, T.; Saeed, A.; Albericio, F. Recent Advances towards Sulfur (VI) Fluoride Exchange (SuFEx) Click Chemistry. (2018), *J Fluor Chem*, **213**, 87–112.
- (82) Li, S.; Wu, P.; Moses, J. E.; Sharpless, K. B. Multidimensional SuFEx Click Chemistry: Sequential Sulfur(VI) Fluoride Exchange Connections of Diverse Modules Launched From An SOF 4 Hub . (2017), *Angewandte Chemie*, **129** (11), 2949–2954.
- (83) Yatvin, J.; Brooks, K.; Locklin, J. SuFEx on the Surface: A Flexible Platform for Postpolymerization Modification of Polymer Brushes. (2015), *Angewandte Chemie*, **127** (45), 13568–13571.
- (84) Dong, J.; Sharpless, K. B.; Kwisnek, L.; Oakdale, J. S.; Fokin, V. v. SuFEx-Based Synthesis of Polysulfates. (2014), *Angewandte Chemie International Edition*, **53** (36), 9466–9470.
- (85) Wang, H.; Zhou, F.; Ren, G.; Zheng, Q.; Chen, H.; Gao, B.; Klivansky, L.; Liu, Y.; Wu, B.; Xu, Q.; Lu, J.; Sharpless, K. B.; Wu, P. SuFEx-Based Polysulfonate Formation from Ethenesulfonyl Fluoride–Amine Adducts. (2017), *Angewandte Chemie International Edition*, **56** (37), 11203–11208.
- (86) Liang, D. D.; Pujari, S. P.; Subramaniam, M.; Besten, M.; Zuilhof, H. Configurationally Chiral SuFEx-Based Polymers. (2022), *Angew. Chem. Int. Ed.*, **61** (8), e202116158.
- (87) Li, S.; Li, G.; Gao, B.; Pujari, S. P.; Chen, X.; Kim, H.; Zhou, F.; Klivansky, L. M.; Liu, Y.; Driss, H.; Liang, D. D.; Lu, J.; Wu, P.; Zuilhof, H.; Moses, J.; Sharpless, K. B. SuFExable Polymers with Helical Structures Derived from Thionyl Tetrafluoride. (2021), *Nat Chem*, **13** (9), 858–867.
- (88) Xiao, X.; Zhou, F.; Jiang, J.; Chen, H.; Wang, L.; Chen, D.; Xu, Q.; Lu, J. Highly Efficient Polymerization via Sulfur(vi)-Fluoride Exchange (SuFEx): Novel Polysulfates Bearing a Pyrazoline–Naphthylamide Conjugated Moiety and Their Electrical Memory Performance. (2018), *Polym Chem*, **9** (8), 1040–1044.
- (89) Yatvin, J.; Brooks, K.; Locklin, J. SuFEx Click: New Materials from SOxF and Silyl Ethers. (2016), *Chemistry - A European Journal*, **22** (46), 16348–16354.
- (90) Silipo, C.; Hansch, C. Correlation Analysis of Baker's Studies on Enzyme Inhibition. 1. Guanine Deaminase, Xanthine Oxidase, Dihydrofolate Reductase, and Complement. (1976), *J Med Chem*, **19** (1), 62–71.
- (91) Dondoni, A.; Marra, A. SuFEx: A Metal-Free Click Ligation for Multivalent Biomolecules. (2017), *Org Biomol Chem*, **15** (7), 1549–1553.
- (92) Wilson Lucas, S.; Zijian Qin, R.; Rakesh, K. P.; Sharath Kumar, K. S.; Qin, H.-L. Chemical and Biology of Sulfur Fluoride Exchange (SuFEx) Click Chemistry for Drug Discovery. (2023), *Bioorg Chem*, **130**, 106227.
- (93) Jones, L. H.; Kelly, J. W. Structure-Based Design and Analysis of SuFEx Chemical Probes. (2020), *RSC Med Chem*, **11** (1), 10–17.

- (94) Liu, Z.; Li, J.; Li, S.; Li, G.; Sharpless, K. B.; Wu, P. SuFEx Click Chemistry Enabled Late-Stage Drug Functionalization. (2018), *J Am Chem Soc*, **140** (8), 2919–2925.
- (95) Liu, F.; Wang, H.; Li, S.; Bare, G. A. L.; Chen, X.; Wang, C.; Moses, J. E.; Wu, P.; Sharpless, K. B. Biocompatible SuFEx Click Chemistry: Thionyl Tetrafluoride (SO₂F₄)-Derived Connective Hubs for Bioconjugation to DNA and Proteins . (2019), *Angewandte Chemie*, **131** (24), 8113–8117.
- (96) Wang, N.; Yang, B.; Fu, C.; Zhu, H.; Zheng, F.; Kobayashi, T.; Liu, J.; Li, S.; Ma, C.; Wang, P. G.; Wang, Q.; Wang, L. Genetically Encoding Fluorosulfate- I - Tyrosine to React with Lysine, Histidine, and Tyrosine via SuFEx in Proteins in Vivo. (2018), *J Am Chem Soc*, **140** (15), 4995–4999.
- (97) Zasukha, S. v.; Timoshenko, V. M.; Tolmachev, A. A.; Pivnytska, V. O.; Gavrylenko, O.; Zherish, S.; Shermolovich, Y.; Grygorenko, O. O. Sulfonimidamides and Imidosulfuric Diamides: Compounds from an Underexplored Part of Biologically Relevant Chemical Space. (2019), *Chemistry - A European Journal*, **25** (28), 6928–6940.
- (98) Borne, A. L.; Brulet, J. W.; Yuan, K.; Hsu, K. L. Development and Biological Applications of Sulfur-Triazole Exchange (SuTEx) Chemistry. (2021), *RSC Chem Biol*, **2** (2), 322–337.
- (99) Green, M. A.; Jiang, Y.; Soufiani, A. M.; Ho-Baillie, A. Optical Properties of Photovoltaic Organic–Inorganic Lead Halide Perovskites. (2015), *J Phys Chem Lett*, **6** (23), 4774–4785.

Chapter 2

Fast room-temperature functionalization of silicon nanoparticles using alkyl silanols



This Chapter was published as:

Alyssa F.J. van den Boom, Sidharam P. Pujari, Fatma Bannani, Hafedh Driss, and Han Zuilhof (2020); Fast room-temperature functionalization of silicon nanoparticles using alkyl silanols; *Faraday Discussions*, **222**, 82-94.
<https://pubs.rsc.org/en/content/articlelanding/2020/FD/C9FD00102F>

Abstract: Silicon nanoparticles (Si NPs) are a good alternative to conventional heavy metal-containing quantum dots in many applications, due to their low toxicity, low cost, and the high natural abundance of the starting material. Recently, much synthetic progress has been made, and crystalline Si NPs can now be prepared in a matter of hours. However, the passivation of these particles is still a time-consuming and difficult process, usually requiring high temperatures and/or harsh reaction conditions. In this paper, we report an easy method for the room-temperature functionalization of hydrogen-terminated Si NPs. Using silanol compounds, a range of functionalized Si NPs could be produced in only 1 h reaction time at room temperature. The coated NPs were fully characterized to determine the efficiency of binding and the effects of coating on the optical properties of the NPs. It was found that Si NPs were effectively functionalized, and that coated NPs could be extracted from the reaction mixture in a straightforward manner. The silanol coating increases the quantum yield of fluorescence, decreases the spectral width, and causes a small (50 nm) blue-shift in both the excitation and emission spectra of the Si NPs, compared to unfunctionalized particles.

Introduction

Semiconductor nanoparticles have proven to be useful for many different applications, including bio-imaging,¹⁻³ LEDs,⁴⁻⁶ and solar cells.⁷⁻¹² Silicon nanoparticles (Si NPs) are, in this regard, particularly interesting, due to their low toxicity and the high natural abundance of the starting material.^{13,14} However, several issues have so far stood in the way of their widespread use. First, synthesis of the NPs is time-consuming and difficult, often requiring high temperatures or harsh chemicals.¹⁵⁻²⁵ Second, once the Si NPs are formed, they have to be rapidly passivated, to prevent loss of the original properties.²⁶ This is especially the case for hydrogen-terminated Si NPs (H-Si NPs). Such particles are of significant interest due to their near-ideal electronic and electrical properties, yet their susceptibility to oxidation requires extensive protection. In literature, passivation of H-Si NPs has been achieved by heating to 190 °C in the presence of a suitable ligand,²⁷ etching using phosphorous pentachloride followed by modification with an amine,^{20,28} thermally-promoted thiolation reactions,²⁹ reacting with bifunctional alkenes,²⁶ halogenation followed by a Grignard reaction,^{24,30} platinum-catalyzed reactions,^{23,25,31} or reactions in the presence of radical initiators.^{32,33} These procedures generally suffer from long reaction times and/or the use of harsh reaction conditions, making them less attractive for application on a larger scale. Furthermore, the type of ligand that can be attached in such procedures is usually limited by the reaction conditions used. In most cases, the ligand may also contain only one functional group, as having multiple functional groups interferes with the reaction. This limits the possibility for further functionalization. Clearly, an easy, fast, and versatile passivation method for H-Si NPs is still needed.

In this paper, we report the use of silanol compounds with a range of functional groups to passivate H-Si NPs (obtained *via* a microwave-based procedure developed in our group,³⁴ building upon earlier protocols from He's group for other types of Si NPs).^{35,36} This silanol reaction showed promise due to the discovery that flat Si surfaces could be readily functionalized in this manner,³⁷ yielding densely packed, hydrolytically stable monolayers in <1 h at room temperature. As this reaction proceeded without the need for additional solvents or catalysts, this constitutes a significant advantage over previously mentioned routes. Here, only mono-hydroxylated silanols were considered, as silanols with two or three hydroxyl groups might yield multilayers on the surface of the Si NPs, as reported for flat surfaces.³⁷ We show that passivation with silanols is an easy and fast method to obtain functionalized Si NPs. The silanol coating can easily be tuned by selecting silanols with different side groups, and due to the specificity of the reaction, even silanols with multiple functional groups can be used. Finally, we show it

is possible to obtain pure, passivated Si NPs with good optical properties in less than 4 h of combined reaction (1 h) and purification (3 h) time.

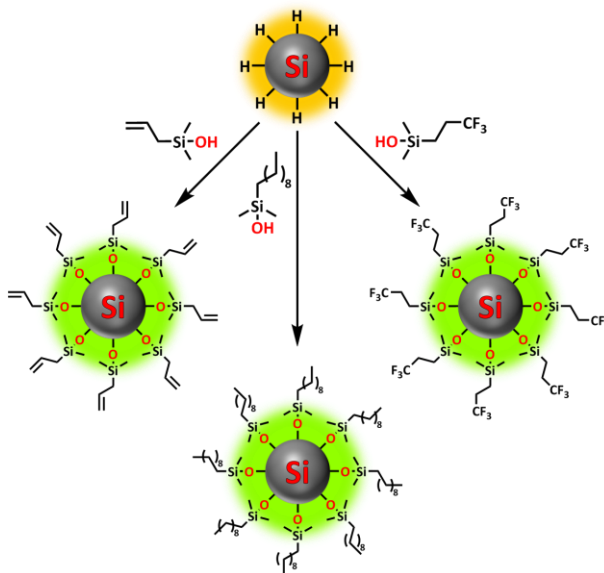


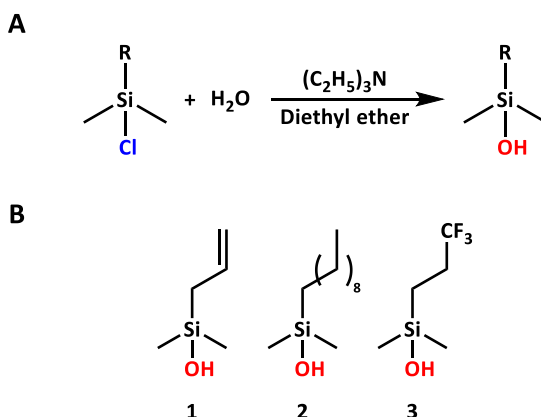
Figure 1: Overview image showing functionalization of silicon nanoparticles using various silanol compounds.

Experimental

Synthetic procedures

Synthesis of silanol compounds

Silanol compounds were synthesized from their corresponding chlorosilane using an adapted literature procedure (Scheme 1).³⁷ In brief, an alkyldimethylchlorosilane (1 equiv) was added to an ice-cold mixture of triethylamine (1.5 equiv), water (4 equiv), and diethyl ether. The mixture was stirred for 1 h at room temperature, after which the liquid phase was isolated. Hexane was added, and the diethyl ether was evaporated *in vacuo*. The reaction mixture was cooled on an ice bath, and washed with ice-cold 0.5 M aqueous HCl. The organic phase was dried using magnesium sulfate, and the solvent was evaporated *in vacuo* to obtain the silanol. Full characterization of the silanols used in this study can be found in the Supporting Information.



Scheme 1: A: Reaction scheme for silanol synthesis. **B:** Overview of silanols used in this study.

Synthesis of hydrogen-terminated silicon nanoparticles

H-Si NPs were prepared according to the protocol developed by Pujari *et al.*³⁴ In brief: inside a glovebox ($\text{O}_2 < 0.1$ ppm, $\text{H}_2\text{O} < 0.1$ ppm), 20 mg (0.10 mmol) of sodium ascorbate and 0.8 ml of DMSO were added to a microwave tube equipped with a stirrer bar. 0.2 mL (1.08 mmol) of triethoxysilane was added, after which the tube was quickly sealed and transported to the microwave. The mixture is allowed to react for 10 min at 170 °C while stirring at 600 rpm. After the reaction, the tube was allowed to cool down and transported back into the glovebox. There, it was opened, and the mixture was filtered with a 0.2 μm PTFE syringe filter. The filtered brown solution was directly used for passivation.

Functionalization of silicon nanoparticles

Inside a glovebox, 0.2 ml of the selected silanol is added to the filtered nanoparticle dispersion, and the resulting mixture is stirred for 1 h at room temperature. After this passivation step, the reaction mixture is taken out of the glovebox, and the DMSO is evaporated *in vacuo* (70 °C, 1 mbar); excess silanol is subsequently extracted using diethyl ether. After drying, the resulting dry brown flakes are finely ground with 15 ml of toluene, added in several small fractions, to extract the functionalized NPs; large particles are allowed to sediment after addition of each fraction, and the top layer of toluene is pipetted off. The combined toluene phases are dried prior to analysis. In a typical experiment, 20-35 mg of functionalized Si NPs were obtained in this way, depending on the ligand and the number of toluene fractions used.

Preparation of water-soluble particles

To prepare water-soluble Si NPs, a thiol sugar was attached to the allyldimethylsilanol-functionalized Si NPs *via* a thiol-ene click reaction. To a purified sample of 30 mg of the functionalized Si NPs, a solution of 0.36 g (1.0 mmol) 1-thio- β -D-glucose tetraacetate and 0.05 g (0.2 mmol) 2,2-dimethoxy-2-phenylacetophenone (DMPA) in 1:1 chlorobenzene and DMF was added inside a glovebox.^{38,39} The reaction mixture was stirred at room temperature for 3.5 h with 365 nm light irradiation. The distance between the lamp and the solution was ~ 4 cm, so as not to heat the sample. The lamp was removed, and the solvents were evaporated *in vacuo*. A light brown gel formed, from which Si NPs and DMPA were extracted using chlorobenzene. The solvent was again removed *in vacuo*, and the functionalized Si NPs were extracted using diethyl ether.

To de-protect the acetate-capped sugar, the Si NPs were dispersed in a 0.015 M solution of sodium methoxide in methanol.⁴⁰ The reaction mixture was stirred for 45 min, and the sodium methoxide was precipitated out of solution by the addition of anhydrous pentane. The solvents of the clear dispersion were removed *in vacuo* to obtain 27 mg of dry thioglucose-coated Si NPs for analysis.

Materials and methods

NMR measurements were conducted on a 400 MHz Bruker Avance III, and resulting data were analyzed using MestReNova software, version 10.0.2-15465.

IR measurements were performed on a Bruker Tensor 27 spectrometer equipped with a diamond ATR accessory (32 scans; 4 cm^{-1} resolution). For the Si NP samples, the dried Si NP powder was firmly pressed onto the ATR crystal; for the pure silanols, a drop was placed on the crystal.

XPS measurements were performed on a Jeol JPS-9200 photoelectron spectrometer, using a 12 kV and 20 mA monochromatic Al K α source. The analyzer pass energy was 10 eV, and the take-off angle between sample and detector was set at 80°. Data was analyzed using the program CasaXPS, version 2.3.18PR1.0. Samples were prepared by drop coating a Si NP solution onto a cleaned gold surface.

TEM measurements were performed on a Jeol JEM-1400 plus (WEMC - TEM 120KV). Samples were prepared by evaporating a drop of dilute Si NP solution in chloroform onto an ultrathin Carbon Type-A support film with a 400 mesh on top of a copper grid with an approximate hole size of 42 μm (TED PELLA, Inc.). Samples were allowed to dry for 30 min prior to imaging.

High-resolution TEM measurements were performed on a Tecnai G2 F20 Super Twin TEM microscope at 200 kV with a LaB6 emitter. The microscope was equipped with a high-angle annular dark-field (HAADF) detector for scanning transmission electron microscopy (STEM) imaging. STEM imaging and all analytical work was performed with a probe size of 1 nm, resulting in a beam current of about 0.5 nA. TEM images were collected using a GATAN US1000 2K HR 200 kV CCD camera. The CCD line traces were collected fully automatically using the Tecnai G2 user interface and processed with both Digital Micrograph software Version 2.3 and the Tecnai Imaging and Analysis (TIA) software Version 1.9.162.

Optical properties (in DMSO, unless noted otherwise) were studied using an Edinburgh Instruments FLS900 fluorescence spectrometer (continuous: 450 W xenon lamp as the excitation source; for lifetime: 444 nm LED laser) for the fluorescent properties, and a Varian Cary 50 UV-Vis spectrophotometer for the absorption measurements (scan rate 600 nm/min; spectra corrected for solvent absorption). Results were fitted with a 3-exponential decay. For the quantum yield, fluorescein in 0.1 M aqueous NaOH was used as a reference, with an absolute quantum yield of 0.88 ± 0.03 .⁴¹

Results and discussion

Silanol-based functionalization of silicon nanoparticles

The passivation of H-Si NPs with silanol compounds (Figure 1) proceeded readily at room temperature with a straightforward procedure: the silanol was simply added to a H-Si NP suspension in DMSO (as obtained without further purification after Si NP synthesis), and the mixture was stirred for 1 h at room temperature. The ease of this reaction is in line with the calculated exothermicity, namely $\Delta H = -16.9$ kcal/mol in DMSO, as obtained from quantum-chemical wB97XD/6-311+G(d,p) calculations using a dielectric SMD model mimicking DMSO. The reason for the extra 30 min of stirring time, compared to the analogous reaction on flat surfaces,³⁷ was to ensure a high packing density on the Si NP surface, as this would minimize future oxidation. Escorihuela *et al.* further reported that for flat surfaces, the reaction speed could be increased by irradiation with UV light. However, this was not tested here, as the subsequent (relatively slow) evaporation of DMSO *in vacuo* meant the Si NPs would be exposed to silanol for at least 2 h anyway.

For both silanols **1** and **3**, excess silanol was removed simultaneously with DMSO, simplifying the purification procedure; only one extraction step with diethyl ether was necessary to remove remaining traces of unbound silanol and obtain a dry powder. Meanwhile, **2** could not be removed by vacuum at

the current temperature. Therefore, for this silanol, three extractions with diethyl ether were performed to obtain a dry powder. In all cases, an estimated yield of $\sim 45\%$ was obtained, assuming all Si NP surface atoms had reacted with the silanol, and no Si-H bonds remained. To confirm the passivation process did not affect the size of the Si NPs, TEM imaging was performed. For both passivated and non-passivated Si NPs, the average size of the particles was around 6 ± 1 nm (Figure S13), slightly (~ 1.5 nm) smaller than previously reported by Pujari *et al.* for H-Si NPs synthesized under similar conditions.³⁴ High-resolution TEM of single Si NPs confirmed the crystallinity of the functionalized NP, in line with data shown by Pujari *et al.*³⁴ Additionally, the interplanar spacing of the crystalline particles was measured to be 0.31 nm in the (111) direction, and 0.19 nm in the (110) direction (**Error! Reference source not found.**D and E). This corresponds to literature values found for crystalline silicon wafers (1.92 and 3.13 Å,

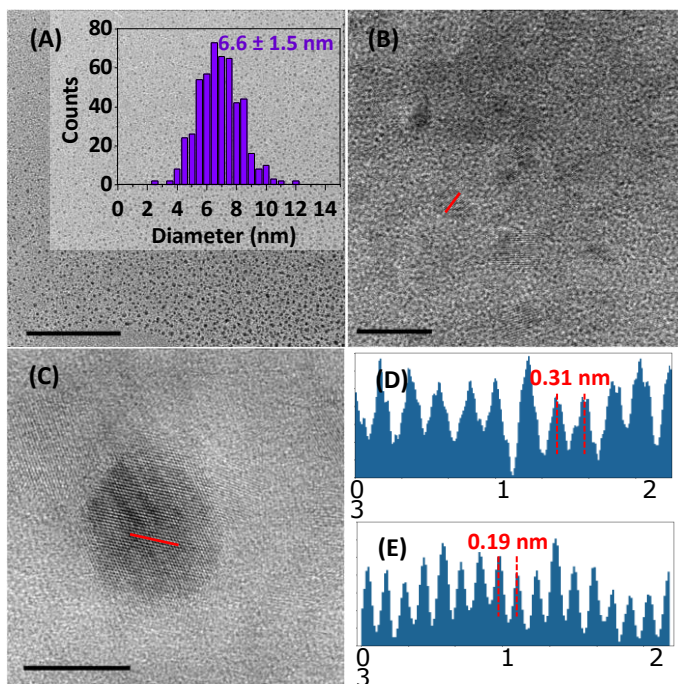


Figure 2: High-resolution TEM images of **3**-Si NPs. Scale bars are 200 nm (**A**) and 10 nm (**B** & **C**). The insert in **A** shows the size distribution. **D** shows the interplanar spacing of a Si(111) NP measured along the red line in **C**, and **E** the spacing of a Si(110) NP measured in **B**. respectively).⁴²

Recently, a paper by Oliynyk *et al.* raised the question whether Si NPs could really be formed in a microwave reaction.⁴³ Even though they

specifically doubted the formation in an aqueous solution, and suggested the formation of fluorescent NPs of a carbon or hybrid composition, their investigation is also relevant here. Based on the interplanar crystal spacing found, and the silicon signal observed using XPS (*vide infra*), we would argue that crystalline Si NPs were indeed formed in this reaction, rather than hybrid organo-silicon or carbon NPs. Furthermore, Oliinyk *et al.* contributed the source of fluorescence in the paper by Zhong *et al.*³⁶ to the formation of carbon nanoparticles and/or organic fluorophores. If this had been the case here, the organic fluorophores should have been visible in the NMR and IR spectra discussed below. However, in these spectra, only signals from the silanol coating could be seen, indicating no other functional groups were present in the sample. Combined, these data imply the formation of well-defined, fluorescent, crystalline Si NPs, rather than non-crystalline and hybrid carbon nanodots, in the microwave reaction described above.

Characterization of silanol-functionalized particles

NMR spectroscopy

The passivated particles were first characterized using NMR, to determine the purity and success of passivation. A representative spectrum of Si NPs passivated with compound **1** (**1**-Si NPs) is shown in Figure 3 (for remaining spectra, see Supporting Information S2). For clarity, the spectrum of the pure silanol is shown underneath in light grey. All signals belonging to the alkyl groups of the silanol can clearly be seen in the spectrum of the functionalized Si NPs, while the signal from the -OH group has disappeared (5.55 ppm in DMSO- d_6 , Figure S1). This indicates that the silanol has successfully reacted *via* the -OH group. In addition, the integration ratio of the peaks closely matches the ratio found for the unbound silanol, although some deviation is sometimes found due to the low signal of the functionalized NPs.

Binding is further confirmed by the broadening of the silanol peaks, caused by attachment of the organic compound to a slowly-rotating NP.^{19,25} Since rotation speed is related to size, more severe peak broadening is observed for larger particles. This is why the peak broadening here is more severe compared to the spectra of the 1-4 nm NPs reported in literature.^{19,25} Meanwhile, ^1H NMR on TiO_2 NPs of $\sim 10.4 \times 7.4$ nm showed spectra with nearly unresolvable peaks.^{44,45}

Final proof of successful binding is given by the slight change in chemical shift for hydrogen atoms belonging to the methyl groups of the silanol (Figure 3, ~ 0.2 ppm). This shift is upfield when measured in CDCl_3 , and downfield when measured in DMSO- d_6 . Hydrogen atoms further up the alkyl chain of the silanol seem unaffected by the Si NP surface. In addition to this, only small contaminant peaks can be found in the spectrum, indicating the purification was successful. Since NPs, due to their slow-tumbling nature,

only give very small signals compared to organic compounds, any contaminants are clearly visible in the spectrum.

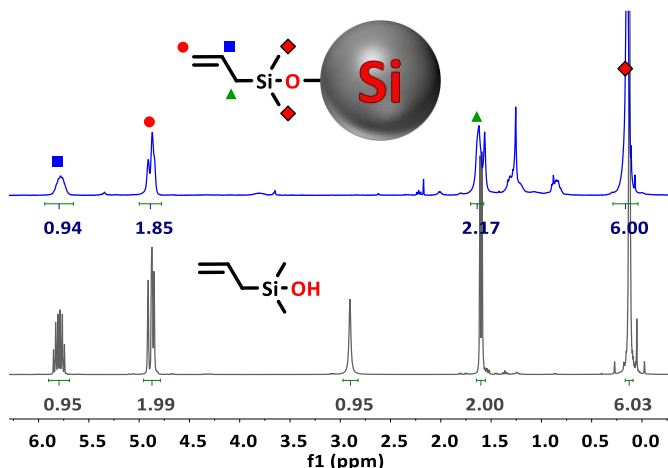


Figure 2: ^1H NMR spectrum of **1-Si NPs** (top) and pure unbound **1** (bottom) in CDCl_3 .

IR spectroscopy

Since NMR analysis only yielded low signals and broad peaks, ATR-IR was used as extra confirmation of successful silanol attachment. Figure 4 presents the ATR-IR spectrum of **1**-functionalized Si NPs (**1-Si NPs**), compared to that of the dimerized form of **1** (**1₂**). Both spectra contain a narrow band at 1257 cm^{-1} , indicative of the presence of Si-CH₃ groups.^{24,31,46} Other characteristic peaks of the silanol can also be seen in the **1-Si NP** spectrum, such as the C=C bond vibrations at 1632 , 990 , 932 , and 893 cm^{-1} , and the =C-H vibration at 3080 cm^{-1} . Additionally, the strong band at 1059 cm^{-1} indicates the presence of a Si-O-Si bond, as expected after passivation, while the absence of a broad peak at $\sim 3270\text{ cm}^{-1}$ reflects the disappearance of the -OH group.

For this sample in particular, the IR spectrum is interesting, as it provides further evidence that the silanol has indeed reacted *via* the -OH group, rather than the vinyl group. Not only would binding via the vinyl group lead to the disappearance of the C=C signals at 1632 , 990 , 932 and 893 cm^{-1} , it would also lead to the formation of a new signal at around 1210 cm^{-1} .⁴⁶

The absence of this latter peak is not directly clear from the spectrum in Figure 4. However, when the difference spectrum between passivated and non-passivated Si NPs is plotted, the lack of signal in this region becomes clear (Figure S5). In addition, further signals characteristic to **1** also show up in the difference spectrum, including several peaks in the fingerprint region. This is also observed for the other passivations: the difference spectrum shows characteristic peaks belonging to the silanol used during the reaction

(Supporting Information, Figures S6, S7). Only for **2**-Si NPs the comparison is less clear, due to the small number of characteristic peaks that can be uniquely attributed to **2**.

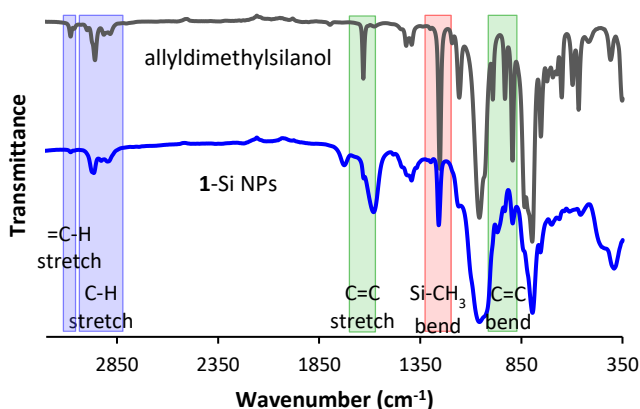


Figure 3: ATR-IR spectra of **1**₂ and **1**-Si NPs. Several notable peaks have been highlighted.

XPS analysis

To confirm that the IR signal around 1060 cm^{-1} is indeed due to the binding of the silanol, and not primarily a result of oxidation, XPS analysis was performed. For a well-passivated, non-oxidized sample, a peak $<101\text{ eV}$ is expected in the silicon 2p narrow scan. Meanwhile, for a completely oxidized sample, the peak should be found at $>103\text{ eV}$.³⁴ For the silanol-coated particles, a clear peak was found at 101.8 eV , indicating the Si NPs are partially oxidized (Figure 5, wide scan in Figure S8). This is in line with the nature of the silanol functionalization, in which for every silanol ligand attached to the Si NPs, two silicon atoms will be directly bound to an oxygen atom. These silicon atoms need not always be located at the surface of the Si NP, as the oxygen atom can “bury” itself inside the Si NP. As a result, the binding energy of >2 silicon atoms can be affected, resulting in an average Si 2p binding energy of 102 eV . In addition, a small fraction of oxidation of the initial Si NP core is typically observed under these conditions, which can – in principle – be removed by HF etching.³⁴ Since the silanol functionalization itself adds oxygen to the NP, such etching was not performed in this case. This Si 2p binding energy of 101.8 eV was found for all functionalized Si NPs, with minor (0.3 eV) differences likely due to charging effects in the XPS.⁴⁷ As no peak at $>103\text{ eV}$ is present in Figure 5, we tentatively attribute the peak at 1060 cm^{-1} , as observed in the IR spectrum,

to the Si-O-Si bonds from the silanol functionalization, rather than oxidation by atmospheric oxygen.

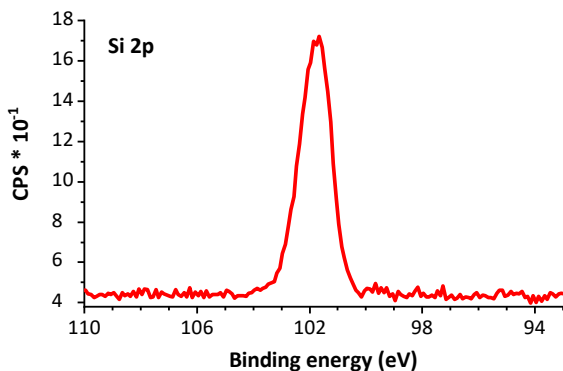


Figure 4: XPS silicon 2p narrow scan of **2**-Si NPs. The peak is centered around 101.8 eV.

Optical properties

Next, the effect of the silanol coating on the optical properties of the Si NPs was determined. To this end, the properties were compared to those of H-Si NPs. It was shown that passivation with silanols leads to a ~ 50 nm blue-shift in both the excitation and emission spectrum (Figure 6). This is likely due to the introduction of oxygen atoms into the Si NPs during the silanol coating, which has already been shown to lead to a blue-shift in the spectra.²⁹ Interestingly, no shift was observed for **2**-Si NPs (Table 1). It is likely that some minor oxidation of **1**- and **3**-Si NPs occurred during processing, as the smaller dimethylsilanol ligands, due to their bulkiness, cannot reach 100% passivation. Meanwhile, the large, hydrophobic alkyl chain of **2** is more effective in blocking incoming oxidants, and will therefore offer better protection against oxidation. Indeed, XPS on **3**-Si NPs after measurement of the optical properties shows the presence of a small amount of silicon oxide (Figure S9). Besides shifting the positions of the excitation and emission maxima, the silanol coating seems to reduce the spectral width of the Si NPs. For non-passivated Si NPs, the spectral widths of the excitation and emission spectra were 0.68 and 0.53 eV, respectively. For **1**-passivated Si NPs the excitation width decreased to 0.57 eV, and for **3**-Si NPs the excitation and emission width decreased to 0.43 and 0.41 eV, respectively. Meanwhile, no change in spectral width was observed for **2**-Si NPs; the excitation spectrum had a spectral width of 0.69 eV, and the emission spectrum a width of 0.50 eV.

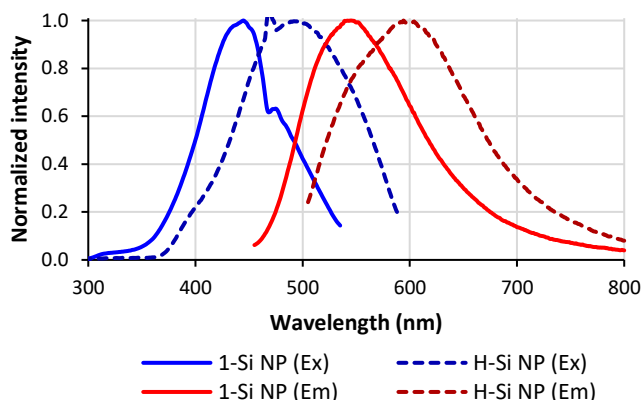


Figure 6: Optical properties of Si NPs. Full lines: Si NPs passivated with **1**; dashed lines: non-passivated Si NPs. Excitation spectra are shown in blue, emission spectra in red.

Finally, also the fluorescence lifetime and quantum yield were affected by the passivation process. The average fluorescence lifetime of **3**-Si NPs increased from 4.1 to 6.9 ns after passivation, while for **2**-Si NPs the lifetime decreased to 3.3 ns. These short ns lifetimes are typical for Si NPs with an alkyl-termination, prepared using wet-chemical methods, as shown in previous studies on free-standing Si NPs.^{31,48–52} In addition, it has been shown that an electronegative capping (such as a silanol) or an electronegative environment (such as DMSO) can also cause short ns lifetimes for Si NPs.⁵³

The quantum yield of the Si NPs increased for all silanols, though the increase for **2**-Si NPs was not as large as for the other silanols. This increase could be partially due to the purification procedure for the passivated Si NPs: as the H-Si NP sample was not purified before quantum yield determination (to minimize oxidation), this sample contains traces of non-fluorescent impurities that increase the optical absorption of the sample, and thereby slightly decrease the apparent quantum yield for the H-Si NPs compared to the purified samples. The quantum yield for these silanol-functionalized Si NPs compares favorably compared to other modes of functionalization.³⁴

Table 1: Optical properties of silanol-coated Si NPs.

Sample	$\lambda_{\text{ex max}}$ (nm)	$\lambda_{\text{em max}}$ (nm)	Average lifetime (ns)	Quantum yield
H-Si NP	496	594	4.1	16% ^a
1 -Si NP	445	545	4.2	30% ^a
2 -Si NP	495	589	3.3	20% ^a
3 -Si NP	443	539	6.9	27% ^a
ThioglucoSe Si NPs	370	460	-	35% ^b

^a QY w.r.t. fluorescein in 0.1 M NaOH. ^b QY w.r.t. quinine sulfate.

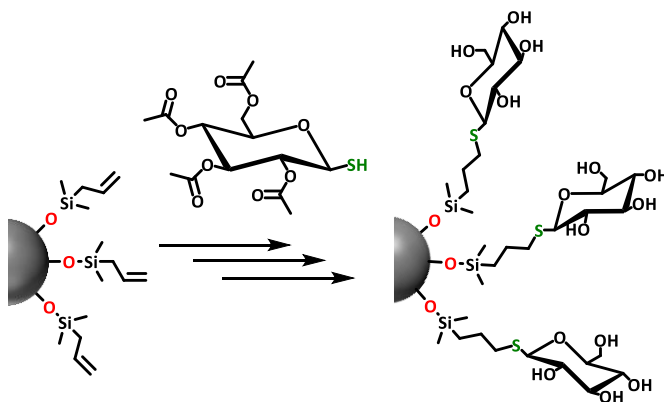
Reactivity of silanol-based Si NPs: Water-soluble, glucose-coated Si NPs

Figure 7: Schematic overview of the synthesis of water-soluble, glucose-coated Si NPs.

As a proof of concept, to show that water-soluble, bio-functional Si NPs could be prepared in this manner, 1-thio- β -D-glucose tetraacetate was reacted to **1**-Si NPs *via* a thiol-ene click reaction (Figure 7 & 8). Previous research on thiol-ene click reactions used a reaction time of 1 h.⁴⁷ Here, due to the size and bulkiness of the sugar ligand, a longer reaction time of 3.5 h was used, to ensure a higher packing density. Due to the extensive purification needed during synthesis of these NPs, and the small scale of the experiment (30 mg of H-Si NPs), this reaction yielded only 27 mg. Successful binding of the protected thiol-sugar was confirmed by IR, with the disappearance of the S-H stretch vibration after the click reaction (Figure S15). After deprotection, the thioglucose-coated Si NPs were dispersed in water for fluorescence measurements. An excitation maximum of 370 nm and an emission maximum of 460 nm were found, with a quantum yield of 35% compared to quinine sulfate (Figure S12). This is a significant blue-shift compared to the Si NPs coated only with silanol, likely due to UV-induced oxidation.

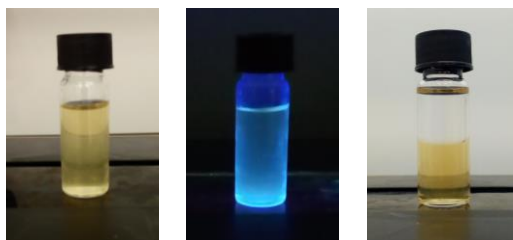


Figure 8: glucose-coated Si NPs in water under normal light (left) and 365 nm irradiation (middle). The right picture shows the solubility of glucose-coated Si NPs in hexane (top layer) and water (bottom layer).

Conclusions

We have demonstrated a fast, easy, and efficient way to passivate hydrogen-terminated Si nanoparticles (H-Si NPs) using silanol compounds at room temperature. The reaction was specific enough to allow the presence of other functional groups in the silanol ligand, and both the passivation and purification of the Si NPs were simple procedures with opportunities for scale-up. The silanol-coated Si NPs produced here showed little oxidation and improved quantum yields. Finally, purified silanol-coated Si NPs could be produced and purified from hydrogen-terminated Si NPs in under 4 h, showing a significant improvement over previous methods for H-Si NP functionalization.

Acknowledgements

The authors acknowledge funding from the Netherlands Organization for Scientific Research (NWO) in the framework of the Materials for Sustainability program. Low-resolution electron microscopy work was performed at the Wageningen Electron Microscopy Center (WEMC) of Wageningen University. Barend van Lagen is acknowledged for helpful instrumental assistance.

References

- 1 X. Cheng, S. B. Lowe, P. J. Reece and J. J. Gooding, *Chem. Soc. Rev.*, 2014 **43**, 2680.
- 2 Y. Su, X. Ji and Y. He, *Adv. Mater.*, 2016 **28**, 10567.
- 3 S. Wu, Y. Zhong, Y. Zhou, B. Song, B. Chu, X. Ji, Y. Wu, Y. Su and Y. He, *J. Am. Chem. Soc.*, 2015 **137**, 14726.
- 4 B. Ghosh, Y. Masuda, Y. Wakayama, Y. Imanaka, J. Inoue, K. Hashi, K. Deguchi, H. Yamada, Y. Sakka, S. Ohki et al., *Adv. Funct. Mater.*, 2014 **24**, 7151.
- 5 S. Coe, W.-K. Woo, M. Bawendi and V. Bulovic, *Nature*, 2002 **420**, 800.
- 6 L. Yang, Y. Liu, Y.-L. Zhong, X.-X. Jiang, B. Song, X.-Y. Ji, Y.-Y. Su, L.-S. Liao and Y. He, *Appl. Phys. Lett.*, 2015 **106**, 173109.
- 7 I. Robel, V. Subramanian, M. Kuno and P. V Kamat, *J. Am. Chem. Soc.*, 2006 **128**, 2385.
- 8 G. Y. Kwak, T. G. Kim, S. Hong, A. Kim, M. H. Ha and K. J. Kim, *Sol. Energy*, 2018 **164**, 89.
- 9 B. Liu, J. Hu, L. Jia, J. Liu, X. Ren, X. Zhang, X. Guo and S. (Frank) Liu, *Sol. Energy*, 2018 **167**, 102.
- 10 T. Subramani, J. Chen, Y. L. Sun, W. Jevasuwan and N. Fukata, *Nano Energy*, 2017 **35**, 154.
- 11 J. Duan, H. Zhang, Q. Tang, B. He and L. Yu, *J. Mater. Chem. A*, 2015 **3**, 17497.
- 12 B. Song and Y. He, *Nano Today*, 2019 **26**, 149.
- 13 S. Bhattacharjee, I. M. C. M. Rietjens, M. P. Singh, T. M. Atkins, T. K. Purkait, Z. Xu, S. Regli, A. Shukaliak, R. J. Clark, B. S. Mitchell et al., *Nanoscale*, 2013 **5**, 4870.
- 14 L. Ruizendaal, S. Bhattacharjee, K. Pournazari, M. Rosso-Vasic, L. H. J. De Haan, G. M. Alink, A. T. M. Marcelis and H. Zuilhof, *Nanotoxicology*, 2009 **3**, 339.
- 15 X. Li, Y. He, S. S. Talukdar and M. T. Swihart, *Langmuir*, 2003 **19**, 8490.
- 16 F. Erogbogbo, K. T. Yong, R. Hu, W. C. Law, H. Ding, C. W. Chang, P. N. Prasad and M. T. Swihart, *ACS Nano*, 2010 **4**, 5131.
- 17 W. Ren, Y. Wang, Q. Tan, J. Yu, U. J. Etim, Z. Zhong and F. Su, *Electrochim. Acta*, 2019 **320**, 134625.
- 18 F. Erogbogbo, C. A. Tien, C. W. Chang, K. T. Yong, W. C. Law, H. Ding, I. Roy, M. T. Swihart and P. N. Prasad, *Bioconjug. Chem.*, 2011 **22**, 1081.
- 19 A. Shiohara, S. Hanada, S. Prabakar, K. Fujioka, T. H. Lim, K. Yamamoto, P. T. Northcote and R. D. Tilley, *J. Am. Chem. Soc.*, 2010 **132**, 248.
- 20 M. Dasog, G. B. De los Reyes, L. V Titova, F. A. Hegmann and J. G. C. Veinot, *ACS Nano*, 2014 **8**, 9636.
- 21 C. M. Hessel, E. J. Henderson and J. G. C. Veinot, *Chem. Mater.*, 2006 **18**, 6139.
- 22 Z. Kang, Y. Liu, C. H. A. Tsang, D. D. D. Ma, X. Fan, N.-B. Wong and S.-T. Lee, *Adv. Mater.*, 2009 **21**, 661.
- 23 M. Rosso-vasic, E. Spruijt, Z. Popović, K. Overgaag, B. van Lagen, B. Grandidier, D. Vanmaekelbergh, D. Domínguez-Gutiérrez, L. De Cola and H. Zuilhof, *J. Mater. Chem.*, 2009 **19**, 5926.
- 24 C.-S. Yang, R. A. Bley, S. M. Kauzlarich, H. W. H. Lee and G. R. Delgado, *J. Am.*

- Chem. Soc.*, 1999 **121**, 5191.
- 25 W. Biesta, B. van Lagen, V. S. Gevaert, A. T. M. Marcelis, J. M. J. Paulusse, M. W. F. Nielen and H. Zuilhof, *Chem. Mater.*, 2012 **24**, 4311.
 - 26 Y. Yu, C. M. Hessel, T. D. Bogart, M. G. Panthani, M. R. Rasch and B. A. Korgel, *Langmuir*, 2013 **29**, 1533.
 - 27 J. A. Kelly, A. M. Shukaliak, M. D. Fleischauer and J. G. C. Veinot, *J. Am. Chem. Soc.*, 2011 **133**, 9564.
 - 28 M. Dasog and J. G. C. Veinot, *Phys. Status Solidi A*, 2012 **209**, 1844.
 - 29 Y. Yu, C. E. Rowland, R. D. Schaller and B. A. Korgel, *Langmuir*, 2015 **31**, 6886.
 - 30 M. Dasog, K. Bader and J. G. C. Veinot, *Chem. Mater.*, 2015 **27**, 1153.
 - 31 M. Rosso-vasic, E. Spruijt, B. Van Lagen, L. De Cola and H. Zuilhof, *Small*, 2008 **4**, 1835.
 - 32 I. M. D. Höhlein, J. Kehrle, T. K. Purkait, J. G. C. Veinot and B. Rieger, *Nanoscale*, 2015 **7**, 914.
 - 33 J. M. Buriak, *Chem. Mater.*, 2014 **26**, 763.
 - 34 S. P. Pujari, H. Driss, F. Bannani, B. van Lagen and H. Zuilhof, *Chem. Mater.*, 2018 **30**, 6503.
 - 35 Y. Zhong, X. Sun, S. Wang, F. Peng, F. Bao, Y. Su, Y. Li, S.-T. Lee and Y. He, *ACS Nano*, 2015 **9**, 5958.
 - 36 Y. Zhong, F. Peng, F. Bao, S. Wang, X. Ji, L. Yang, Y. Su, S.-T. Lee and Y. He, *J. Am. Chem. Soc.*, 2013 **135**, 8350.
 - 37 J. Escorihuela and H. Zuilhof, *J. Am. Chem. Soc.*, 2017 **139**, 5870.
 - 38 N. S. Bhairamadgi, S. Gangarapu, M. A. Caipa Campos, J. M. J. Paulusse, C. J. M. Van Rijn and H. Zuilhof, *Langmuir*, 2013 **29**, 4535.
 - 39 M. A. C. Campos, J. M. J. Paulusse and H. Zuilhof, *Chem. Commun.*, 2010 **46**, 5512.
 - 40 K. Ágoston, A. Dobó, J. Rákó, J. Kerékgyártó and Z. Szirmai, *Carbohydr. Res.*, 2001 **330**, 183.
 - 41 K. Suzuki, A. Kobayashi, S. Kaneko, K. Takehira, T. Yoshihara, H. Ishida, Y. Shiina, S. Oishi and S. Tobita, *Phys. Chem. Chem. Phys.*, 2009 **11**, 9850.
 - 42 C. Xiao, J. Guo, P. Zhang, C. Chen, L. Chen and L. Qian, *Sci. Rep.*, 2017 **7**, 40750.
 - 43 B. V. Oliinyk, D. Korytko, V. Lysenko and S. Alekseev, *Chem. Mater.*, 2019 DOI: 10.1021/acs.chemmater.9b01067.
 - 44 E. Schechtel, R. Dören, H. Frerichs, M. Panthöfer, M. Mondeshki and W. Tremel, *Langmuir*, 2019 DOI: 10.1021/acs.langmuir.9b02496.
 - 45 Z. Hens and J. C. Martins, *Chem. Mater.*, 2013 **25**, 1211.
 - 46 P. J. Launer and B. Arkles, *Silicon Compd. Silanes Silicones*, 2013 175.
 - 47 L. Ruizendaal, S. P. Pujari, V. Gevaerts, J. M. J. Paulusse and H. Zuilhof, *Chem. Asian J.*, 2011 **6**, 2776.
 - 48 K. Dohnalová, A. N. Poddubny, A. A. Prokofiev, W. D. De Boer, C. P. Umesh, J. M. Paulusse, H. Zuilhof and T. Gregorkiewicz, *Light Sci. Appl.*, 2013 **2**, e47.
 - 49 K. Dohnalová, A. Fučíková, C. P. Umesh, J. Humpolíčková, J. M. J. Paulusse, J. Valenta, H. Zuilhof, M. Hof and T. Gregorkiewicz, *Small*, 2012 **8**, 3185.
 - 50 D. S. English, L. E. Pell, Z. Yu, P. F. Barbara and B. A. Korgel, *Nano Lett.*, 2002 **2**, 681.

Chapter 2

- 51 K. Kůsova, O. Cibulka, K. Dohnalová, I. Pelant, J. Valenta, A. Fučíková, K. Žídek, J. Lang, J. Englich, P. Matějka et al., *ACS Nano*, 2010 **4**, 4495.
- 52 J. H. Warner, A. Hoshino, K. Yamamoto and R. D. Tilley, *Angew. Chemie - Int. Ed.*, 2005 **44**, 4550.
- 53 A. N. Poddubny and K. Dohnalová, *Phys. Rev. B*, 2014 **90**, 245439.

Supporting Information

S1. Experimental details

DMSO (anhydrous, $\geq 99.9\%$), pentane (anhydrous, $\geq 99\%$), triethoxysilane (95%), sodium L-ascorbate ($\geq 99.0\%$), diethyl ether, allyl(chloro)dimethylsilane (97%), 1-thio- β -D-glucose tetraacetate (97%), hydrochloric acid (37% in water), sodium methoxide (0.5 M solution in methanol), chlorobenzene ($\geq 99.5\%$), 2,2-dimethoxy-2-phenylacetophenone (99%), quinine for fluorescence (anhydrous, $\geq 98\%$), magnesium sulfate (anhydrous, 98%), and triethylamine ($\geq 99\%$) were purchased from Sigma Aldrich. Toluene ($\geq 99.5\%$) was purchased from Merck. 30 vol% sulfuric acid was purchased from Chem-Lab NV. n-Hexane ($\geq 95\%$) and methanol ($\geq 99.8\%$) were purchased from Biosolve. N-Decyldimethylchlorosilane (97%) and (3,3,3-trifluoropropyl)dimethylchlorosilane (97%) were purchased from abcr. Wherever water is mentioned, milli-Q water should be read, produced using a Milli-Q Integral 3 system (Millipore). DMSO was immediately placed in a glovebox upon arrival, and both DMSO and methanol were (further) dried with activated molecular sieves before use. All other chemicals were used as received.

Silanols were prepared on a 5 ml scale in 100 mL round-bottom flasks. The volume of diethyl ether was 10x the volume of chlorosilane (50 mL), and the volume of hexane was equal to the volume of diethyl ether. Washing was done with 2 x 25 mL of ice-cold 0.5M HCl in water. Due to its susceptibility to dimerization, allyldimethylsilanol was prepared fresh for each experiment. For IR results, only notable peaks are mentioned.

Allyldimethylsilanol (1): Yield: 80%. ^1H NMR (400 MHz, DMSO- d_6): δ = 0.00 (s, 6H), 1.50 (d, J = 8.2 Hz, 2H), 4.81 (m, 2H), 5.46 (s, 1H), 5.77 (tdd, J = 17.0, 10.1, 8.1 Hz, 1H). IR (ATR): ν = 3289, 3079, 1631, 1254, 990, 932, 893 cm^{-1} . MS ($\text{C}_5\text{H}_{11}\text{SiO}$): calculated m/z = 115.0579 [$\text{M} - \text{H}$] $^-$, found 175.0246 [$\text{M} + \text{OAc}$] $^-$

n-Decyldimethylsilanol (2): Yield: 90%. ^1H NMR (400 MHz, DMSO- d_6): δ = -0.03 (s, 6H), 0.45 (t, J = 7.5 Hz, 2H), 0.85 (t, J = 7.5 Hz, 3H), 1.24 (m, 16H), 5.22 (s, 1H). IR (ATR): ν = 3271, 2921, 1250 cm^{-1} . MS ($\text{C}_{12}\text{H}_{28}\text{SiO}$): calculated m/z = 215.1831 [$\text{M} - \text{H}$] $^-$, found 215.1836.

(3,3,3-Trifluoropropyl)dimethylsilanol (3): Yield: 83%. (400 MHz, DMSO- d_6): δ = 0.04 (s, 6H), 0.64 (m, 2H), 2.16 (m, 2H), 5.55 (s, 1H). IR (ATR): ν = 3277, 2962, 1259, 1203 cm^{-1} . MS ($\text{C}_5\text{H}_{11}\text{F}_3\text{SiO}$): calculated m/z = 171.0453 [$\text{M} - \text{H}$] $^-$, found 171.0457.

S2. NMR Spectra

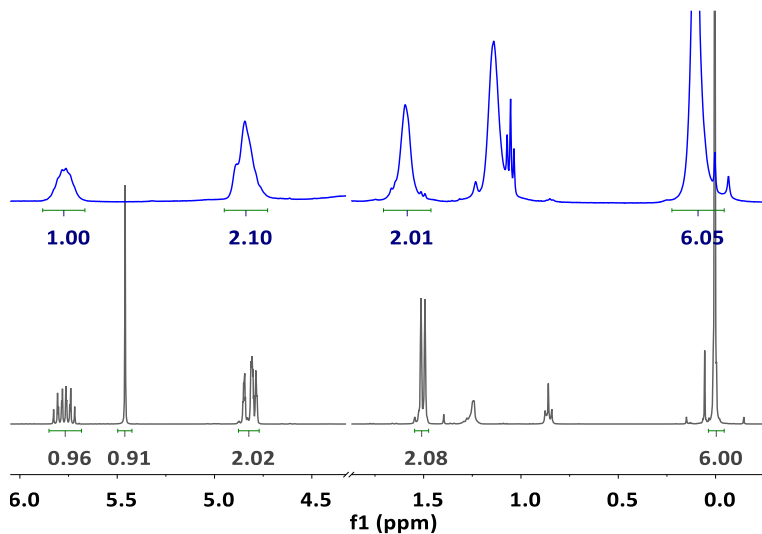


Figure S1: ^1H NMR spectrum of **1-Si NPs** (top) and unbound **1** (bottom) in DMSO-d_6 .

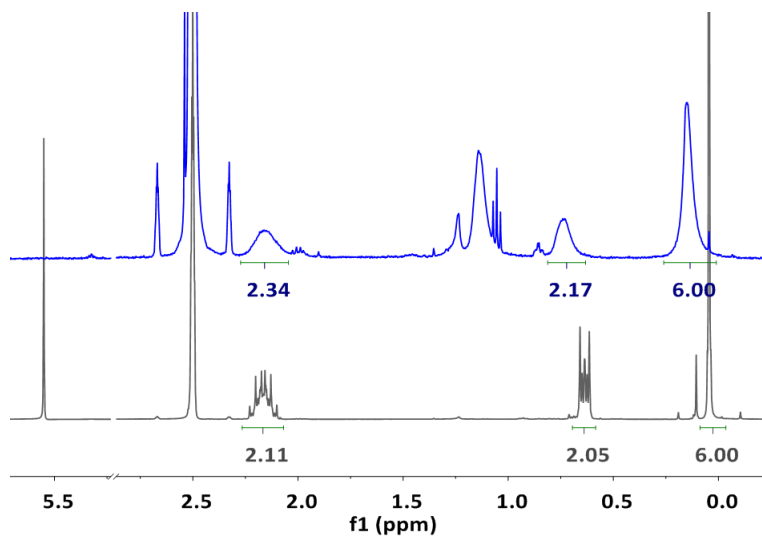


Figure S2: ^1H NMR spectrum of **3-Si NPs** (top) and unbound **3** (bottom) in DMSO-d_6 .

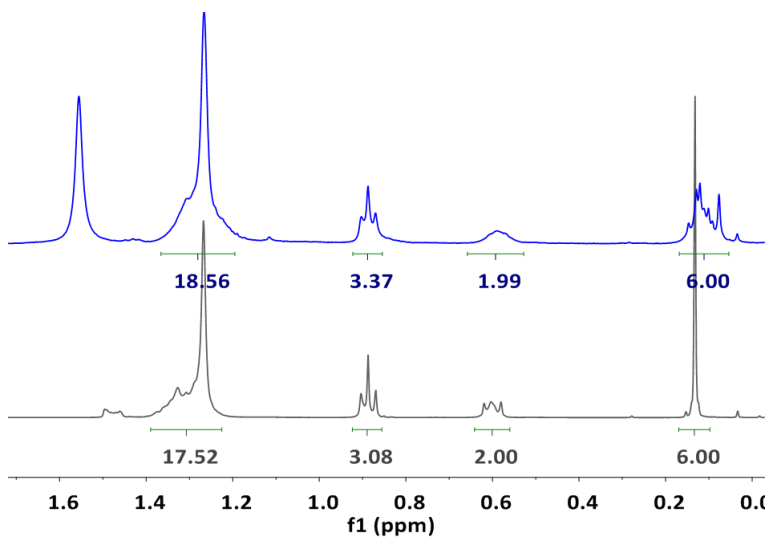


Figure S3: ^1H NMR spectrum of **2-Si NPs** (top) and unbound **2** (bottom) in CDCl_3 .

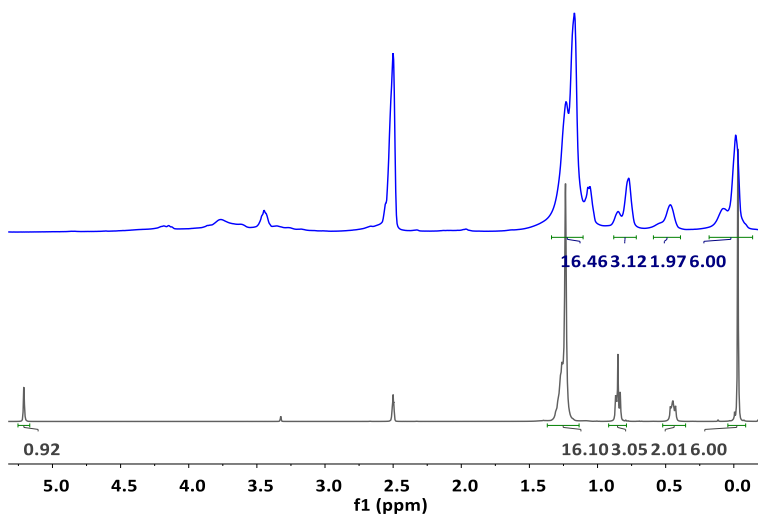


Figure S4: ^1H NMR spectrum of **2-Si NPs** (top) and unbound **2** (bottom) in DMSO-d_6 .

S3. IR Spectra

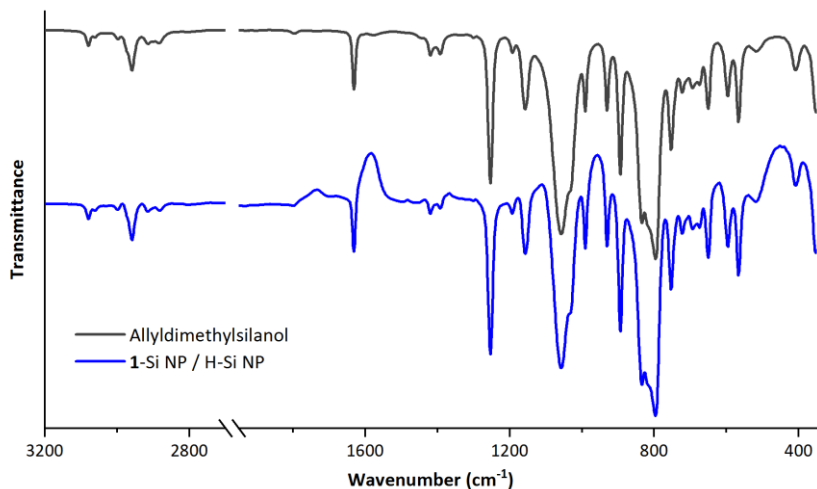


Figure S5: Top: ATR-IR spectrum of **1**. Bottom: ATR-IR difference spectrum between **1**-Si NPs and H-Si NPs. As a background, (partially) oxidized H-Si NPs were used.

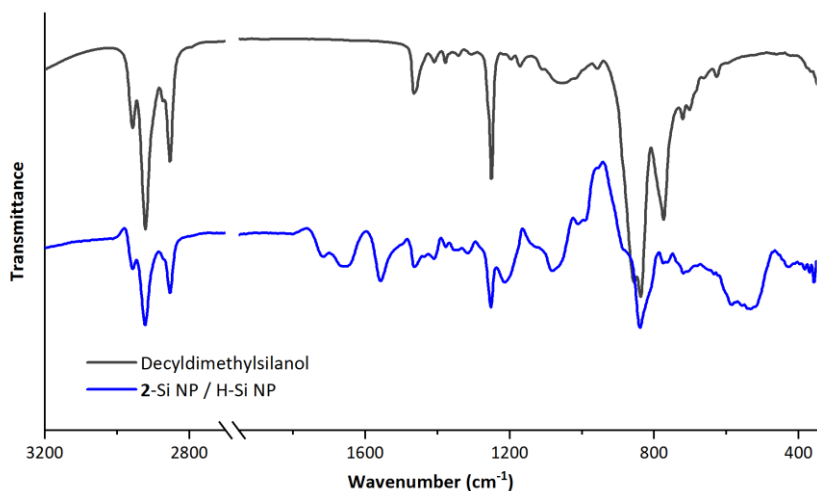


Figure S6: Top: ATR-IR spectrum of **2**. Bottom: ATR-IR difference spectrum between **2**-Si NPs and H-Si NPs. As a background, (partially) oxidized H-Si NPs were used.

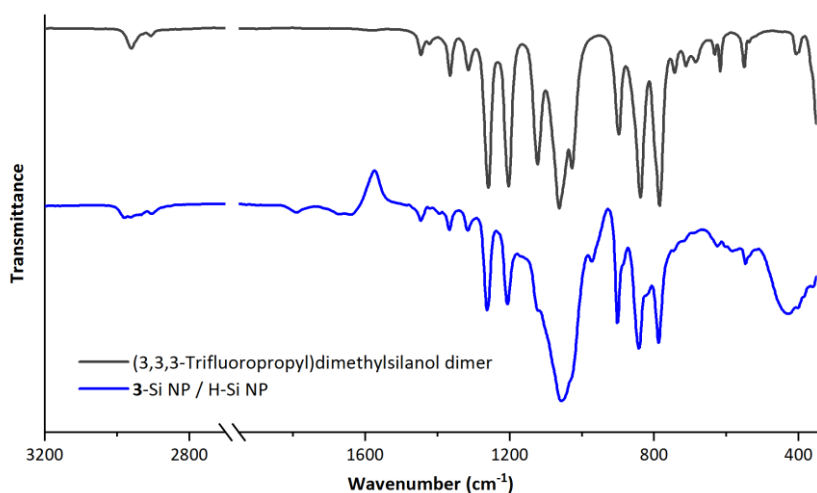


Figure S7: Top: ATR-IR spectrum of **3**₂. Bottom: ATR-IR difference spectrum between **3**-Si NPs and H-Si NPs. As a background, (partially) oxidized H-Si NPs were used.

S4. XPS Spectra

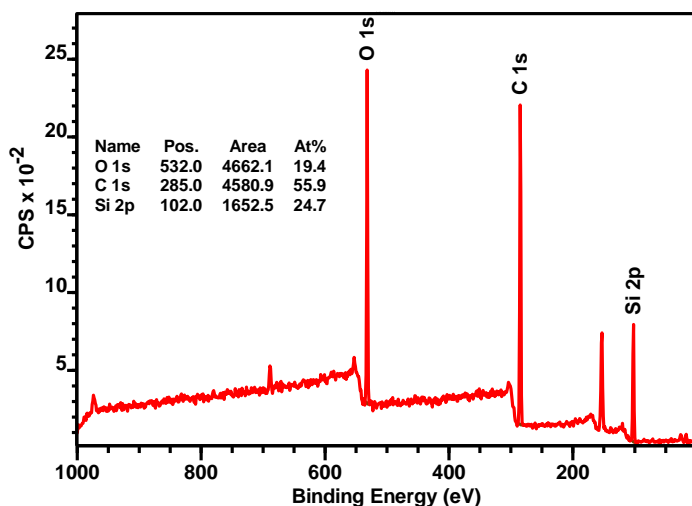


Figure S8: XPS wide scan of **2**-Si NPs drop-coated onto a cleaned gold surface. Spectrum is calibrated on the C 1s peak, which is set to 285 eV.

As can be seen in Figure S8, the ratio of carbon to oxygen to silicon does not match with the predicted values. The silicon peak should be higher, and the C:O ratio should be 12:1. The increased oxygen ratio could indicate oxidation, yet the silicon narrow scan suggests this is not dominant. Therefore, the increased oxygen and carbon likely arise from environmental contaminants, as the XPS samples were prepared in a regular fume hood, instead of the glovebox. This is further confirmed

by the presence of a small fluorine peak, likely derived from the Teflon tweezers used to handle the surfaces. Environmental contaminants can also be seen in the wide and carbon narrow scan of **3**-Si NPs (Figure S9 top row). The ratio in the carbon peaks belonging to CF_3 , $\text{CH}_2\text{-CF}_3$, and $\text{Si-C} / \text{C-C}$ should be 1:1:3, respectively. Instead, the last peak is much higher due to the presence of atmospheric contaminants.

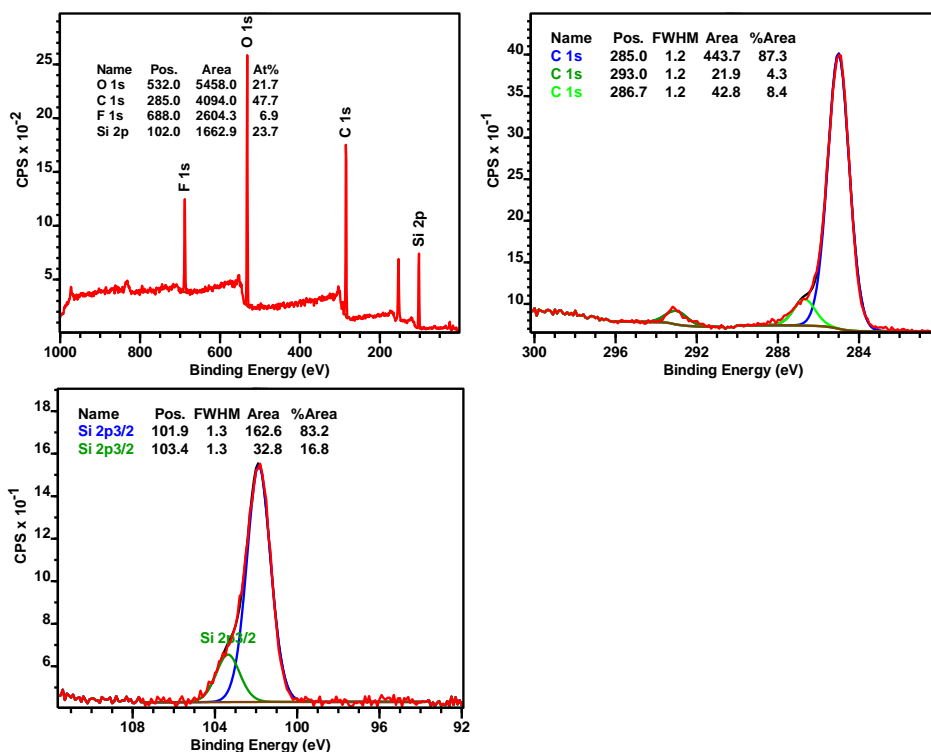


Figure S9: XPS wide (top left), carbon 1s narrow (top right), and silicon 2p narrow (bottom) spectra of **3**-Si NPs.

S5. Optical properties

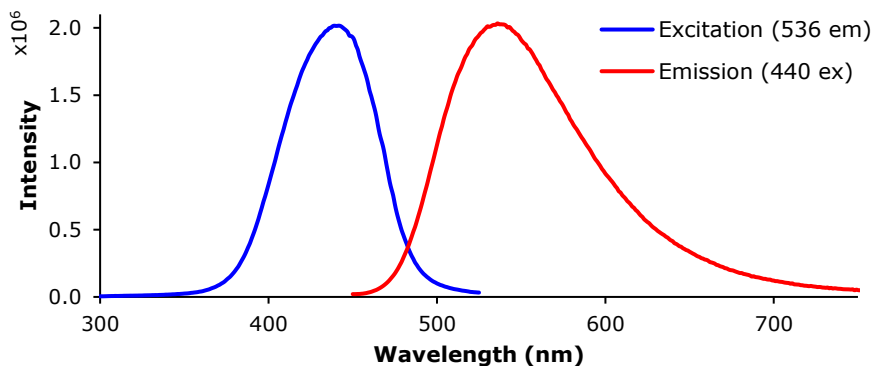


Figure S10: Excitation and emission spectrum of **3**-Si NPs.

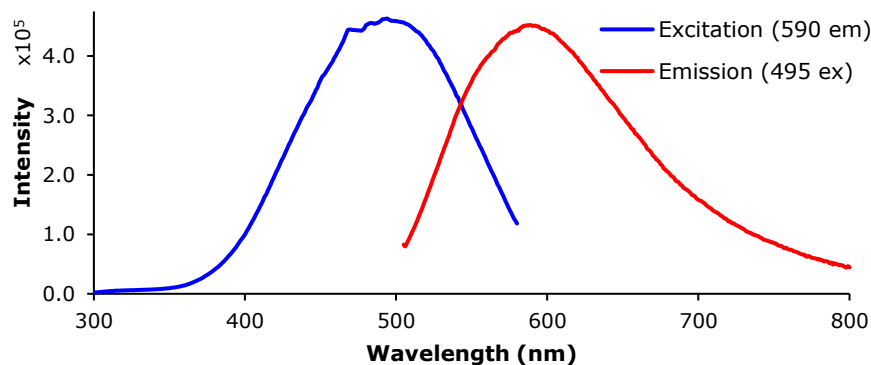


Figure S11: Excitation and emission spectrum of **2**-Si NPs.

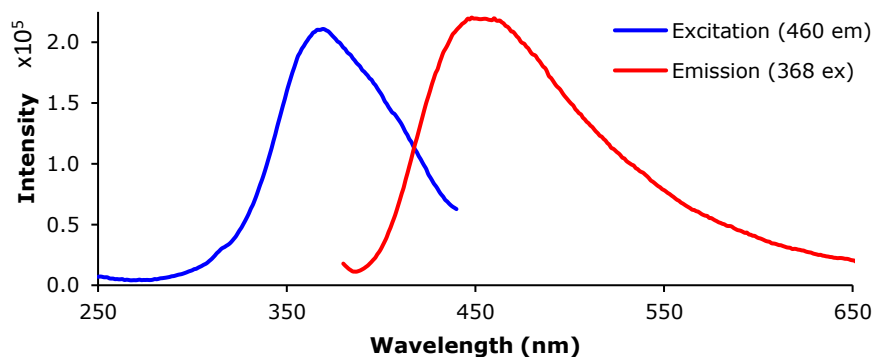


Figure S12: Excitation and emission spectrum of water-soluble, 1-thio-glucose-coated Si NPs.

S6. TEM results

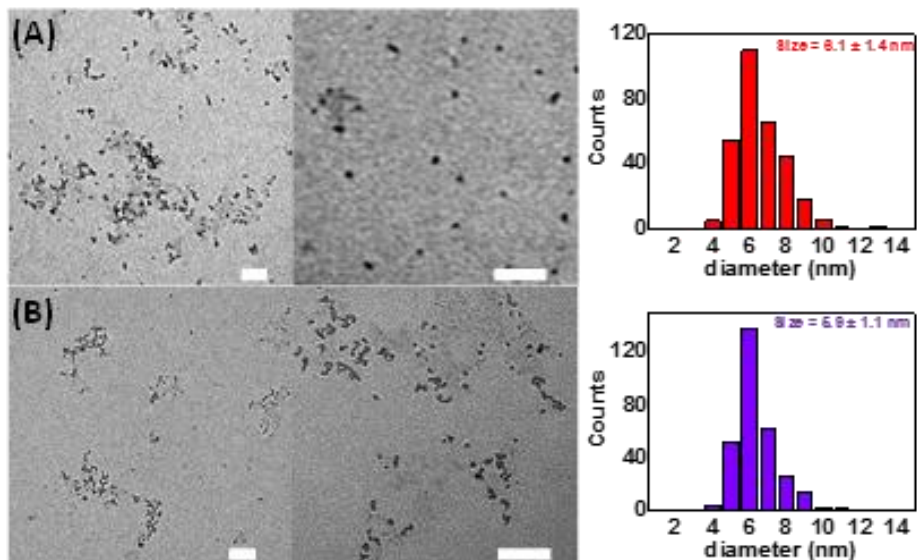


Figure S13: TEM images and size distributions of H-Si NPs (A) and 3-Si NPs (B). The scale bar represents 50 nm, and the size distribution was determined from 300 particles.

S7. Sugar-coated Si NPs characterization

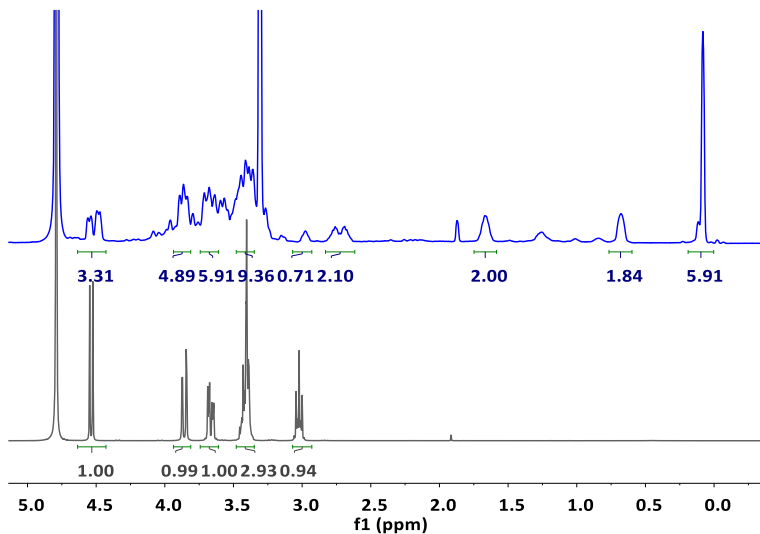


Figure S14: ^1H NMR spectrum of 1-thio-glucose-coated Si NPs in D_2O .

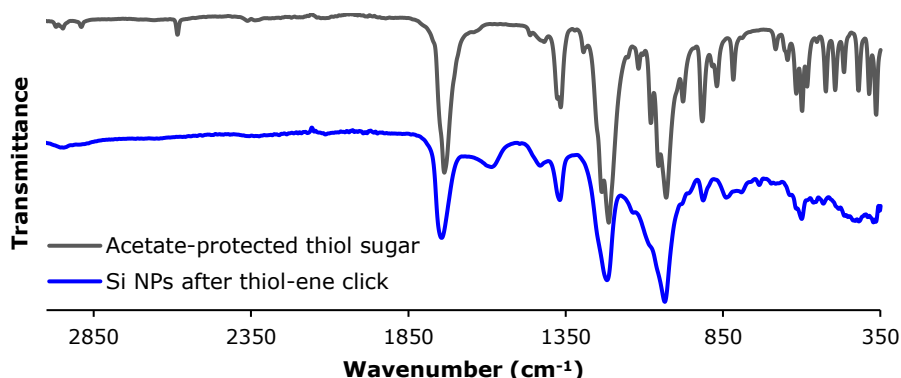


Figure S15: IR spectrum of **1**-Si NPs after a thiol-ene click reaction with 1-thio- β -D-glucose tetraacetate.

S8. Reaction enthalpy calculation

To calculate the reaction enthalpy for the functionalization of the Si NPs via wB97XD/6-311+G(d,p) calculations, the following structures were used (Figure S16): a model Si_8 compound was used to represent the hydrogen-terminated Si NP. It is assumed the use of this model compound has little effect on the enthalpy calculation. The energies of all structures were calculated under both vacuum and solvent conditions, where the dielectric SMD model was used to mimic DMSO as the solvent. The results can be found in Table S1.

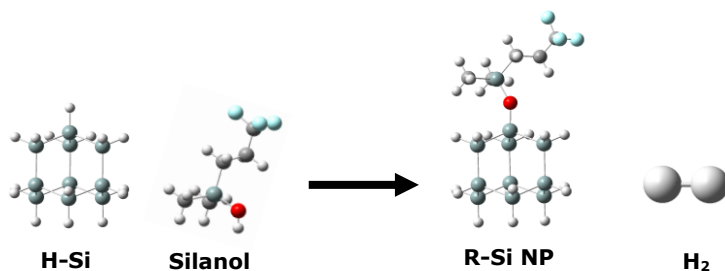


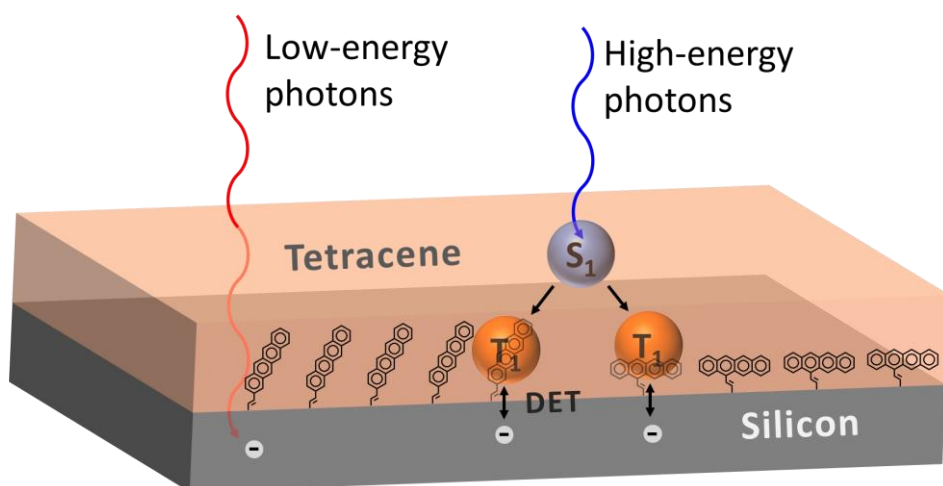
Figure S16: Chemical structures used for the calculation of the reaction enthalpy.

Table S1: Energy calculations for the structures shown in Figure S16.

	H-Si NP	Silanol	R-Si NP	H ₂	ΔH
E_{vacuum} (Hartree)	-2904.507	-861.356	-3764.722	-1.163	-0.02
E_{vacuum} (kcal/mol)	-1822604.1	-540508.8	-2362396.8	-729.6	-13.5
E_{DMSO} (Hartree)	-2904.510	-861.347	-3764.720	-1.164	-0.03
E_{DMSO} (kcal/mol)	-1822606.2	-540502.8	-2362395.7	-730.2	-16.9

Chapter 3

Improving triplet energy transfer from tetracene to silicon using a covalently-bound tetracene seed layer



An adapted version of this Chapter was submitted as:

Alyssa F. J. van den Boom, Silvia Ferro, María Gelvez Rueda, Han Zuilhof, and Bruno Ehrler; Towards improving triplet energy transfer from tetracene to silicon using a covalently-bound tetracene seed layer.

Abstract: Due to many technological advancements over the past years, silicon solar cells are, under controlled lab conditions, now operating close to the Shockley & Queisser limit, their theoretical maximum efficiency. To increase their efficiency beyond this theoretical limit, it is necessary to decrease energy losses occurring for high-energy photons. One of the more promising ways to do this is to add a sensitizing layer of singlet-fission material, which can in principle double the current generated by high-energy photons, and significantly reduce energy losses within the solar cell. Here, we construct a model of such a solar cell, using Si(111) surfaces and tetracene. To increase the energy transfer between the two layers, a series of tetracene derivatives was synthesized, which were covalently attached onto the silicon surface as a seed layer. Using XRD, a shift in crystal structure and ordering of the tetracene close to the seed layer can be observed. Unfortunately, the effect on the energy transfer was limited, showing a need for further investigations into the effect of the seed layer.

Solar energy conversion plays an important role in the development towards 100% sustainable energy production. Up to now, the main way of converting solar energy into electricity is by using photovoltaic solar panels. These panels are generally made of silicon, due to its wide availability, its established place in the semiconductor industry, the resulting relatively low cost of highly pure material, and because – theoretically speaking – silicon has one of the most optimal bandgaps for solar energy conversion, as calculated by Shockley & Queisser in 1961.^{1–3} Yet even with an almost ideal bandgap, the maximum conversion for silicon is still limited to 29% of all available solar energy.⁴ This is mostly a result of the fixed and relatively low-energy bandgap of silicon: photons with an energy higher than the bandgap – meaning all photons with a wavelength shorter than ~ 1100 nm – lose all of their energy in excess to the bandgap of silicon to thermal losses after absorption, resulting in highly inefficient use of a large part of the solar spectrum. It is therefore not surprising that much research has been performed on improving the efficiency with which these high-energy photons are absorbed and converted into electricity, as a means of boosting photovoltaic solar cell performance. This has *e.g.* been done by the development of tandem solar cells (TSCs), in which the high-energy photons are absorbed by a different material within the solar cell from the material that absorbs the low-energy photons.⁵ The best-performing of such cells are generally made – in part – of perovskites, as these materials have easily tunable bandgaps, and are easy to process. However, perovskites often suffer from low stability, decreasing the lifetime of the TSC.⁶ Moreover, when the two sub-cells are connected in series, a tandem cell requires current-matching between them, which is technically challenging, and to some extent dependent on the incident lighting conditions.^{7,8}

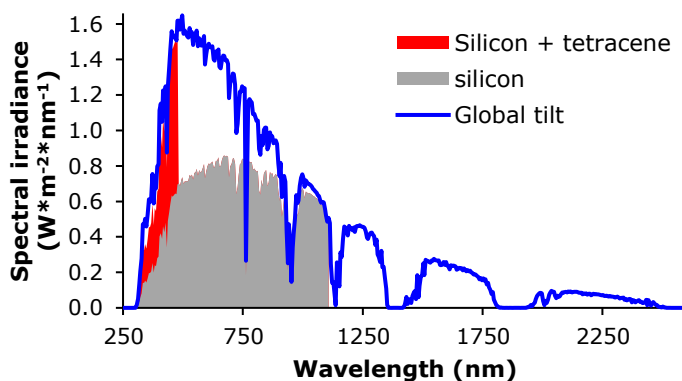


Figure 1: Theoretical maximum energy extracted from the solar spectrum by a silicon solar cell with and without a tetracene sensitizing layer, based solely on the bandgaps involved. Loss mechanisms besides thermalization losses are disregarded.⁹

Another promising approach to better utilize the high-energy light is to use sensitizing layers on top of conventional solar cells. These sensitizing layers are

ideally made from materials that can undergo a process called singlet fission, which can, in principle, double the current coming from high-energy photons.^{10,11} The singlet fission process itself can be roughly described by two steps:^{12,13} first, a high-energy photon is absorbed by one molecule to create an excited singlet exciton state; then, the excited singlet state falls back to a lower-energy triplet state, while the excess energy is simultaneously transferred to an adjacent molecule and used to excite this second molecule into the triplet state as well. After this last step, the two molecules are both trapped in the excited triplet states. Due to the nature of the triplet state, recombining to the ground state is formally spin-forbidden, which in practice means these excited states decay relatively slowly, yet the energy of these excited systems can be extracted using a suitable (semi-) conductor, to yield two electrons with about half the energy of the original photon. Using this solar cell design, an increase in maximum solar cell efficiency from 29 to 35% can be achieved, depending on the materials used (Figure 1).¹⁴

In this work, we prepared a model system for such a singlet-fission sensitized solar cell, using tetracene as the singlet fission material, and silicon as the underlying solar cell material. Tetracene has a triplet energy that is almost perfectly matched to the bandgap of silicon,¹⁵ and furthermore has the benefit that – when applied on top of a silicon solar cell – lowers the temperature in and extends the lifetime of the underlying silicon solar cell by reducing heat production due to thermalization losses.¹⁶ Moreover, tetracene has already been used previously for the sensitization of other materials, such as buckyballs^{17,18} (with an interfacial layer of copper phthalocyanine),^{19,20} or PbS nanoparticles,^{21,22} and in all cases showed energy transfer to the underlying substrate. There have even been previous examples of silicon solar cells with a tetracene sensitizing layer, yet the efficiency of these cells was either not increased, or only very little, and interfacial layers or modification of the silicon surface were needed to facilitate the increase in efficiency.^{14,15,23} Here, our approach is to covalently attach a seed layer of tetracene derivatives to the silicon surface, and subsequently deposit further layers of tetracene on top of this seed layer. The seed layer serves to orient the deposited tetracene layers for optimal energy transfer, as previous studies have shown that tetracene tends to orient itself almost perpendicular to the silicon surface when deposited.²⁴ Such an orientation leads to a low overlap in wavefunctions between the tetracene and silicon – and therefore a low energy transfer efficiency. However, when the orientation of the tetracene on the silicon surface is changed to a more parallel orientation, energy transfer to silicon is increased significantly.²⁵

Two tetracene derivatives were designed for this study: one with a linker on the 5-position (**1**), and one with a linker on the 2-position (**2**, Figure 2). Derivative **1** is expected to have a more favorable orientation when attached to silicon, but the presence of the linker on the 5-position – where the electron density is highest in the LUMO and during excitation to the S_1 state^{26,27} – implies that the physical

and optical properties of this derivative will show a significant shift compared to those of unmodified tetracene. This shift would certainly be larger than the shift expected for **2**,²⁸ where the linker is at a position of relatively low electron density, meaning its properties will be largely similar to those of tetracene. However, the orientation on the surface will be more perpendicular compared to derivative **1**, causing the wavefunction overlap with the silicon surface to be lower.

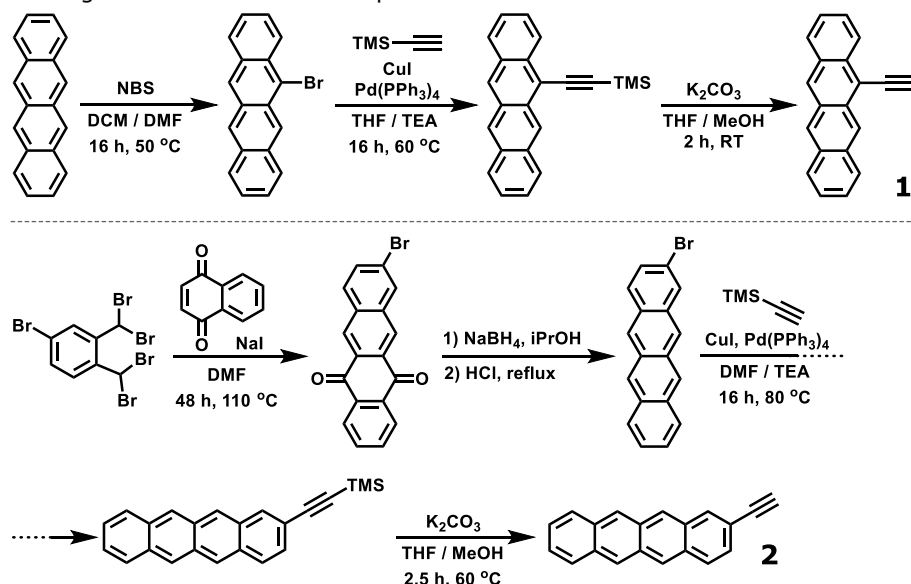


Figure 2: Synthesis schemes for tetracene derivatives **1** and **2**.

The effects of the linker position could already clearly be seen during synthesis: while derivative **1** displayed good solubility, derivative **2** showed an extremely poor solubility in most common organic solvents, in line with the behavior of unfunctionalized tetracene. Still, both derivatives could be obtained on a multiple-gram scale, thereby showing promise for further scale-up. When recording the optical properties, using a trimethylsilyl group to protect the highly reactive ethynyl moiety, the differences between **1** and **2** were further highlighted (Figure 3). Here, again, the spectra for derivative **2** more closely resemble the properties of tetracene itself, with three clear vibronic peaks in both the excitation, emission, and absorption spectra, and only a ~10 nm red-shift for all peaks with respect to tetracene (Table 1). In terms of energy, this shift in wavelengths corresponds to a 0.05 eV difference for the excitation energies, and a 0.06 eV difference for the emission energies. For **1**, the shift in excitation and emission energies is larger (0.16 eV for the excitation, and 0.20 eV for the emission), and the peaks themselves are broader compared to both tetracene and **2**. These results for **1** are in line with previous studies on tetracene dimers, where a similar linker structure was used.^{29,30} Those studies also confirmed that the singlet fission capabilities of the dimers were intact, both in solution and in thin films. Therefore, the observed

shifts in optical properties are not expected to negatively impact the energy transfer in our model system. In fact, the small red-shift observed for especially **2** may even be beneficial, by funneling the triplet energy from the deposited unfunctionalized tetracene layer to the functionalized seed layer in the final solar cell. Indeed, such “cascade” systems using tetracene derivatives have already been proven to increase the efficiency of tetracene-sensitized solar cells.¹⁸

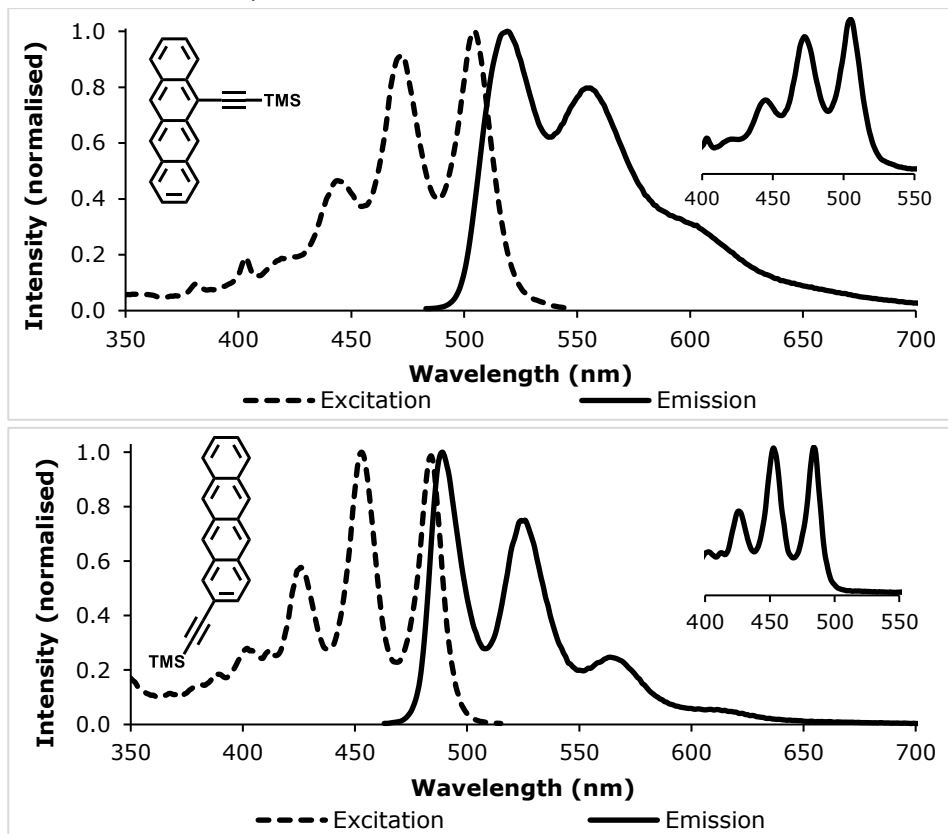


Figure 3: Excitation and emission spectra of trimethylsilyl-protected **1** (top) and **2** (bottom) in DCM. The inserts in the top right corners show the absorption spectra.

Table 1: Excitation and emission maxima for tetracene, 5-((trimethylsilyl)-ethynyl)tetracene (**1-TMS**), and 2-((trimethylsilyl)ethynyl)tetracene (**2-TMS**).

	Excitation maxima (nm)			Emission maxima (nm)		
	419	445	475	478	512	550
Tetracene						
1-TMS	444	472	504	519	556	605
2-TMS	426	453	484	489	526	564

After measuring the properties of both derivatives in solution, solar cell model devices were created by functionalizing hydrogen-terminated silicon (111) surfaces (H-Si(111)) with **1** and **2** (Figure 4). It is for this purpose that an ethynyl linker

was used, as this linker has several advantages over other functional groups when it comes to functionalizing H-Si(111):³¹ 1) the ethynyl linker is the smallest linker containing a terminal alkyne, ensuring the distance of the seed layer to the silicon surface is as small as possible; 2) alkynes react faster and under milder conditions to H-Si(111) than other carbon-based linkers;³² 3) alkynes provide good packing densities and even monolayers;^{33,34} and 4) after modification, alkenyl-linked monolayers show better stability than alkyl-linked monolayers, probably due to their higher density on the surface.^{35,36} Since the tetracene monolayer we attach to Si(111) has some distinct aromatic signals, it should be possible to confirm successful modification using IR. However, the IR spectrum that was recorded showed almost no signal (Supporting Information, Figure S3), and could not be used to confidently state successful modification had taken place. Therefore, two fluorinated derivatives of **1** and **2** were prepared, according to the synthesis outlined in Figure 5. After functionalization of fresh surfaces with these fluorinated derivatives, attachment could easily be confirmed using XPS, by looking for the presence of a fluorine peak in the wide scan. Since the surfaces were sonicated in DCM after functionalization, any physisorbed tetracene is removed prior to the XPS measurements, ensuring that the fluorine signal observed comes from covalently bound tetracene moieties. To confirm covalent attachment even further, several surfaces were rubbed over fiber-free paper before XPS measurements, and no difference in the fluorine signal was observed between these and only sonicated samples. Due to the similarity between the fluorinated and non-fluorinated tetracene derivatives, we assume successful attachment of the non-fluorinated **1** and **2** occurred to a similar degree as found for **1F** and **2F**.

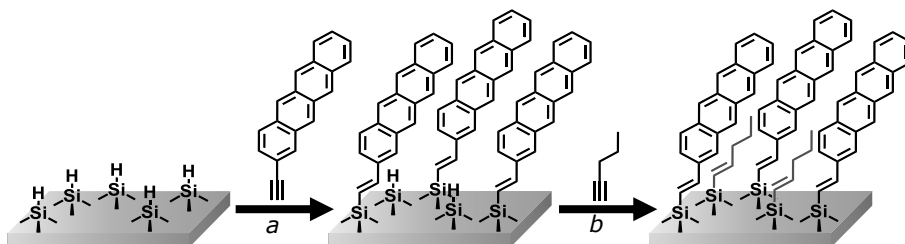


Figure 4: Schematic representation of the surface functionalization reactions. a) functionalization with 2-ethynyltetracene; b) backfilling with 1-pentyne.

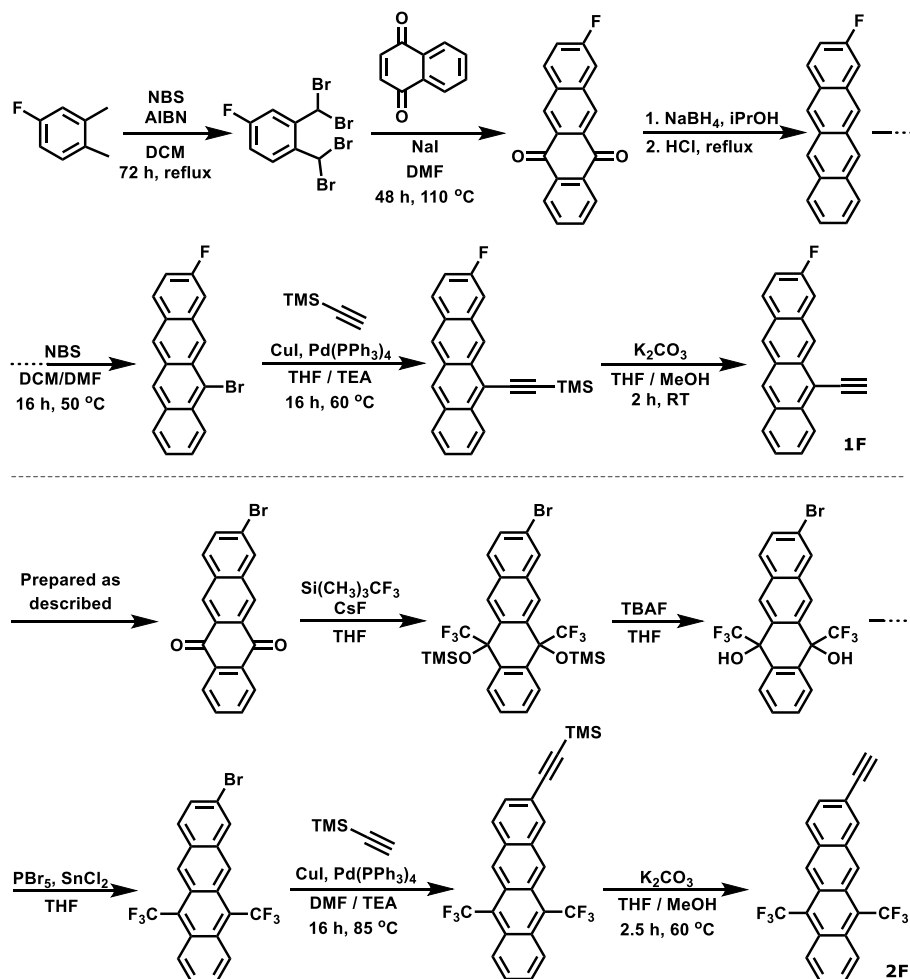


Figure 5: Synthesis schemes for **1F** and **2F**, the fluorinated versions of tetracene derivatives **1** and **2** for XPS analysis.

For surfaces functionalized with **1F**, a ratio of C/F of 21.4:1 is found in the XPS wide scan, close to the expected ratio of 20:1 (Figure 6). The amount of carbon is slightly higher due to a backfilling reaction with 1-pentyne, performed after functionalization with **1F**. This backfilling is done to prevent the oxidation of unfunctionalized Si-H sites, which would lead to the formation of an insulating layer of SiO_x on the silicon surface, that in turn would reduce the energy transfer efficiency in the final solar cell.^{37,38} Based on the C/F ratio, the final surface is functionalized with a ratio of 4:1 **1F**/1-pentyne. And indeed, after several weeks exposure to ambient atmosphere, the amount of surface oxidation for a backfilled surface is only 3.8% (Figure 6 right), instead of the 4.9% observed for non-backfilled surfaces (Supporting Information, Figure S4), demonstrating a reduction

in oxidation. As expected, full passivation was not achieved – even with backfilling – due to the molecular footprint of **1F**, which apparently limits access to the surface for the 1-pentyne, thus hampering full backfilling. Future work into the use of smaller, gaseous alkynes as backfilling materials would be highly useful to further decrease oxidation.

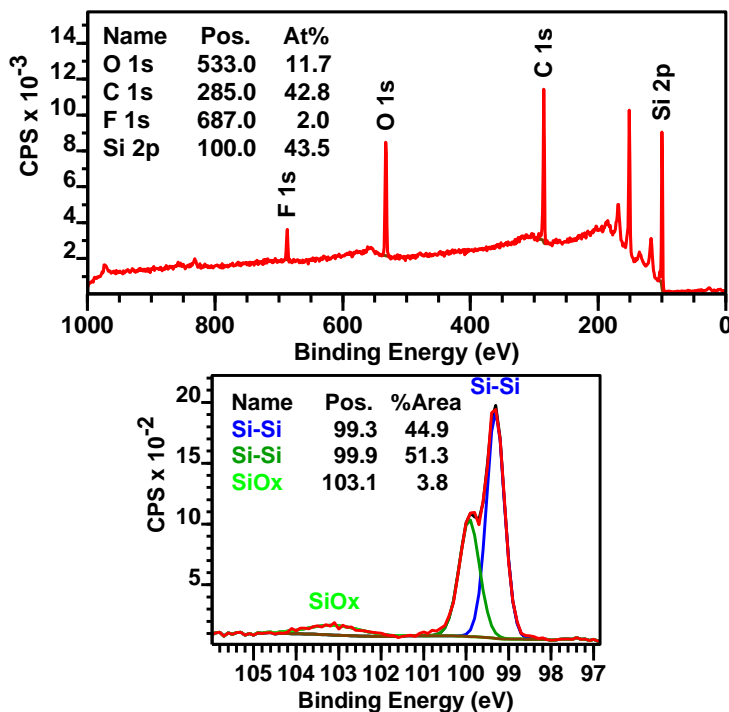


Figure 6: XPS wide (top) and Si 2p narrow (bottom) scans of a representative surface functionalized with **1F** after backfilling with 1-pentyne.

For surfaces functionalized with **2F**, the ratio of C/F is a lot higher than the theoretical ratio of 22:6 ratio (Figure 7). This is not unexpected, as the two bulky -CF₃ groups on **2F** likely lead to a low packing density of this derivative on the surface. Still, the more perpendicular orientation leaves more openings for backfilling, resulting in a surface with a ratio of ~1:8 for **2F**/1-pentyne. The increased amount of backfilling can also be seen in the lower amount of surface oxidation: with backfilling, 2.7% of Si-O_x is observed after several weeks in ambient atmosphere, while this increases to 7.5% without backfilling. This demonstrates the importance of the backfilling procedure for **2F**-functionalized surfaces, which decreases oxidation by roughly two-thirds.

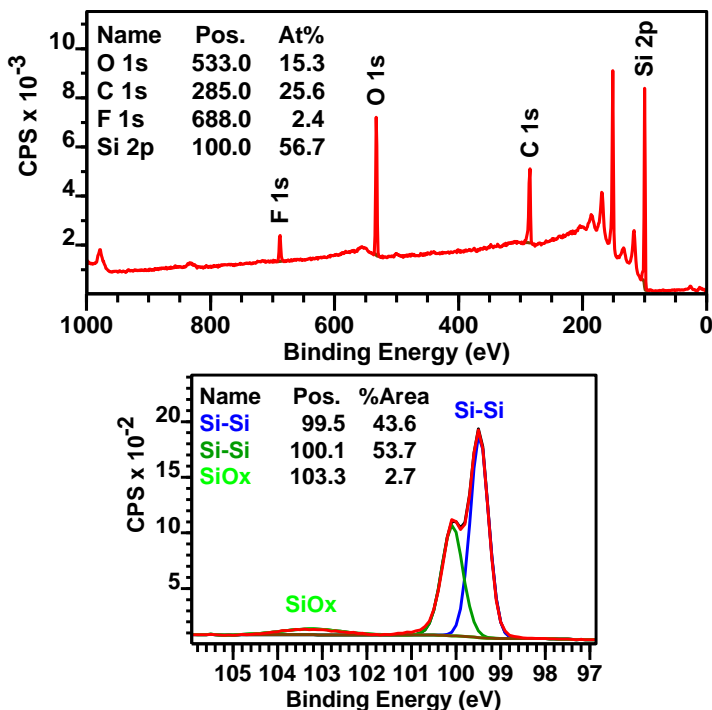


Figure 7: XPS wide (top) and Si 2p narrow (bottom) scans of a representative surface functionalized with **2F** after backfilling with 1-pentyne.

After confirming the presence of a covalent seed layer, a 100 nm layer of underivatized tetracene was deposited on silicon surfaces functionalized with **1** and **2**, as well as on a surface functionalized with only 1-pentyne, used as a control sample. The crystallinity of the deposited layers was checked with XRD, and an interesting result was found: where surfaces functionalized with 2-ethynyltetracene showed good crystallinity of the tetracene layer, surfaces functionalized with 5-ethynyltetracene showed little to no crystallinity (Figure 8). In fact, the crystallinity of these last surfaces was even lower than that of the reference sample functionalized with only 1-pentyne. Perhaps the tetracene deposited on the surface functionalized with **1** cannot interact properly with the covalently-bound tetracene derivatives due to unfavorable interactions with the tips of the 1-pentyne molecules in between the molecules of **1**, as both these molecules have a similar “height” on the surface (Figure 9). In that case, backfilling with a shorter alkyne might improve the interaction between **1** and tetracene. This was not attempted here due to a lack of suitable equipment to work with these shorter alkynes, which are present as gases at room temperature.

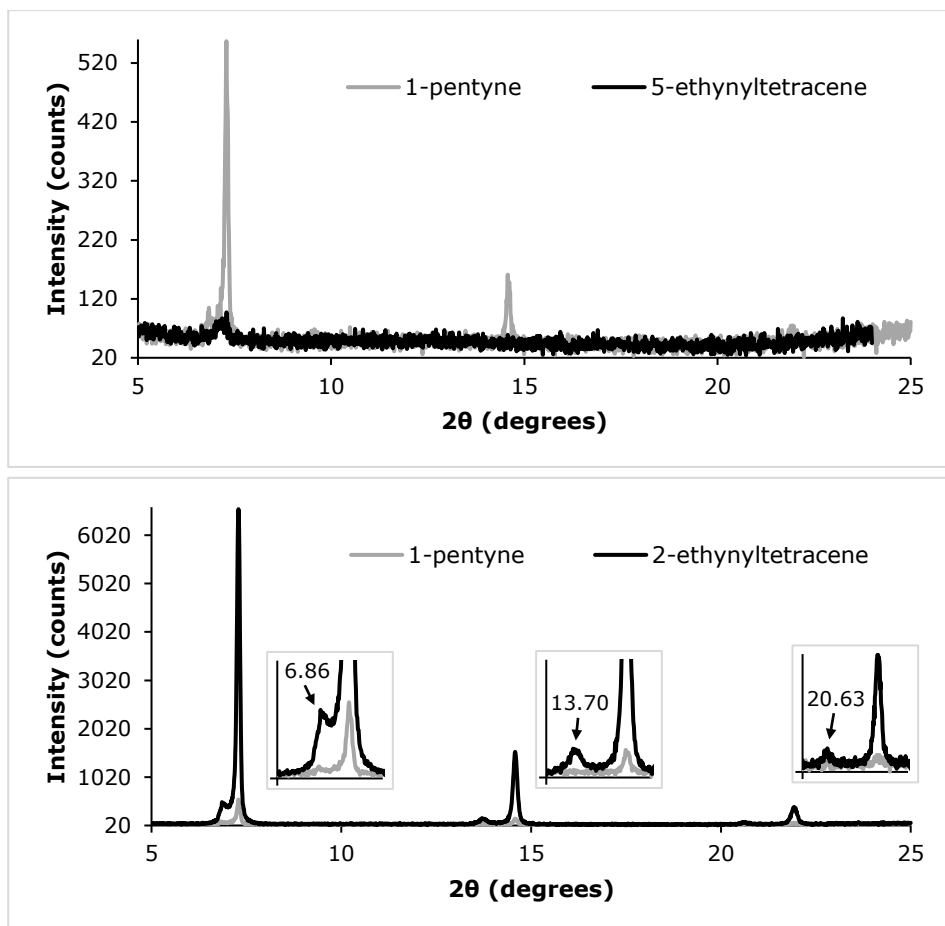


Figure 8: XRD spectra of Si (111) surfaces functionalized with **1** (top) and **2** (bottom), and covered with a 100 nm layer of tetracene. The spectrum of a surface functionalized with 1-pentyne and covered with 100 nm of tetracene is shown in gray as a reference. The spectrum for **2** also contains zoomed-in sections as inserts, to show the smaller peaks belonging to another tetracene polymorph.

For surfaces functionalized with 2-ethynyltetracene, a small orienting effect of the seed layer can be observed in the XRD spectrum (Figure 8, bottom); next to each of the larger peaks also found in the control sample, smaller peaks are found at slightly lower 2θ values, indicating the presence of a different tetracene polymorph in these samples. The 2θ values of these smaller peaks match those of the tetracene polymorph (Tc II) for which faster singlet fission and successful energy transfer to silicon were previously observed.^{25,39} Since neither surfaces functionalized with **1** or 1-pentyne show peaks at these lower 2θ values, this second tetracene polymorph is presumed to be present in the tetracene layers close to the 2-ethynyltetracene seed layer. Similar results were also found using 2D XRD

measurements (see Supporting Information). This is interesting, as this would imply there is a change of crystal structure partway through the tetracene layer. As it has previously been demonstrated that the orientation of tetracene molecules with respect to each other affects the diffusion of the correlated triplet-triplet state,⁴⁰ it would be interesting to further study the singlet fission behavior at the interface between these two crystal structures. Unfortunately, it lies outside the capabilities of the current work to perform such detailed studies.

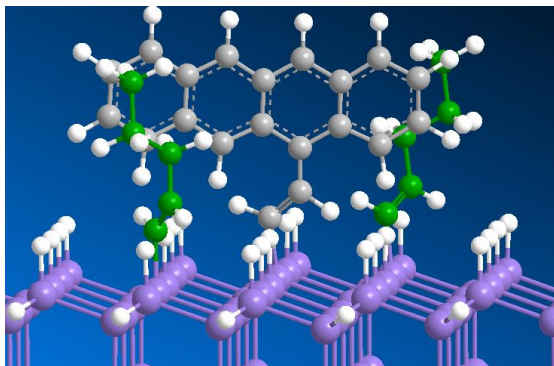


Figure 9: Chemical model for a surface functionalized with **1** and 1-pentyne. For clarity, the 1-pentyne molecules are shown in green.

However, to further study the orientating effect of **2**, GIWAX measurements were performed to investigate the degree of order in the tetracene layers on top of the seed layers. Again, surfaces functionalized with **1**, due to their lack of crystallinity in the tetracene layer, showed no signs of ordering in the tetracene layer (see Supporting Information), while surfaces with only 1-pentyne showed a slightly larger peak, indicating a small increase in ordering of the tetracene. However, the sample functionalized with **2** showed excellent ordering, with a large peak at 270° , and two smaller side peaks at a 15° distance (255° and 285° , Figure 10). These results further indicate that **2**, when applied as a covalently bound seed layer, can help orient subsequently deposited tetracene layers into a well-ordered crystal structure.

We next studied the effect of the covalent layer on the energy transfer efficiency. As previous studies indicated that the diffusion distance of excitons is greater in a well-ordered, crystalline sample,⁴¹ we expected a similar superior performance of samples functionalized with **2** in these final measurements, especially when also considering the presence of the tetracene polymorph Tc II near the seed layer – which, as mentioned, has already been shown to transfer more energy to silicon.²⁵ However, and to our dismay, no such performance was found. All three surfaces showed poor energy transfer, with no signs of triplet energy transfer to the silicon surface (Figure 11). The magnetic-field-dependent photocurrent that is observed instead seems to point to either direct singlet energy

transfer from the tetracene to the silicon, or towards indirect transfer after radiative decay of the singlet excitons of the tetracene into photons that are then absorbed by the silicon. Perhaps, as the orientation of the majority of the tetracene layer on the **2**-functionalized surface is still mainly in the less transfer-efficient polymorph Tc I, the small layer of tetracene in the TC II polymorph orientation close to the silicon surface – as observed in the XRD spectra – is not enough to increase the overall energy transfer efficiency.

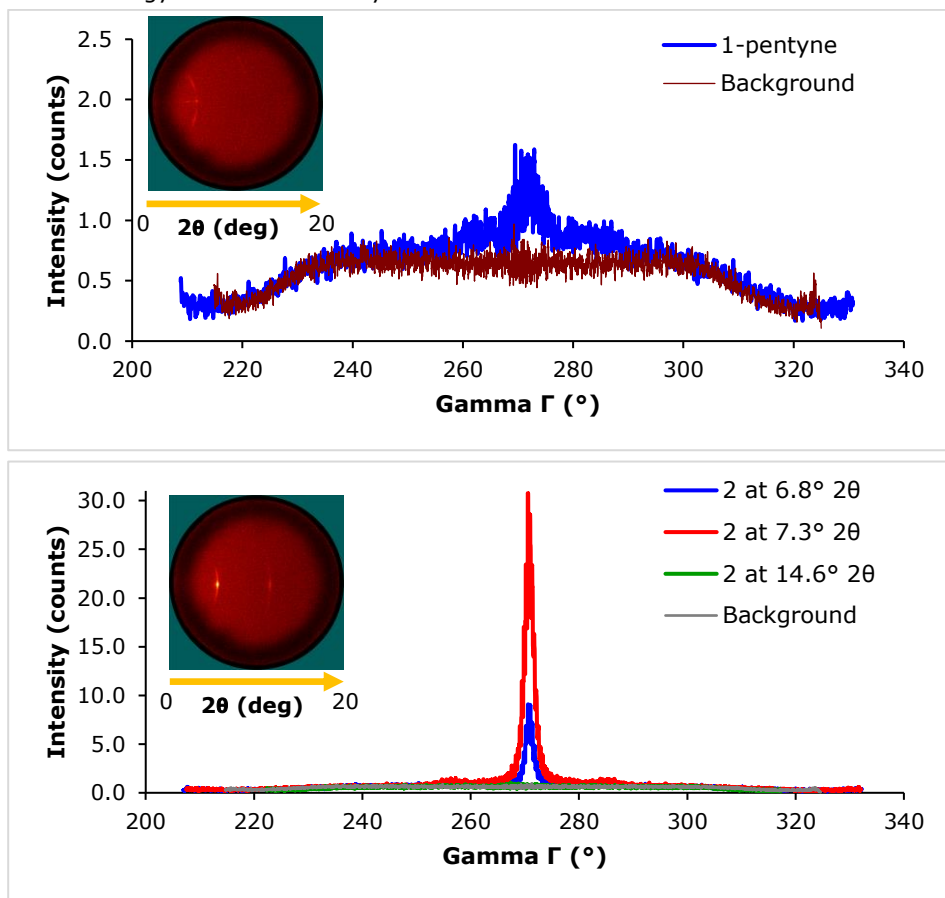


Figure 10: GIWAX spectrum of surfaces functionalized with 1-pentynyl (top) and **2** + 1-pentynyl (bottom). The spectrum of 1-pentynyl was recorded at 7.3°. Background spectra were recorded at 2θ angles where no signal was visible. The inserts show pictures of the surfaces during the GIWAX measurements, where a lighter color indicates a higher intensity signal.

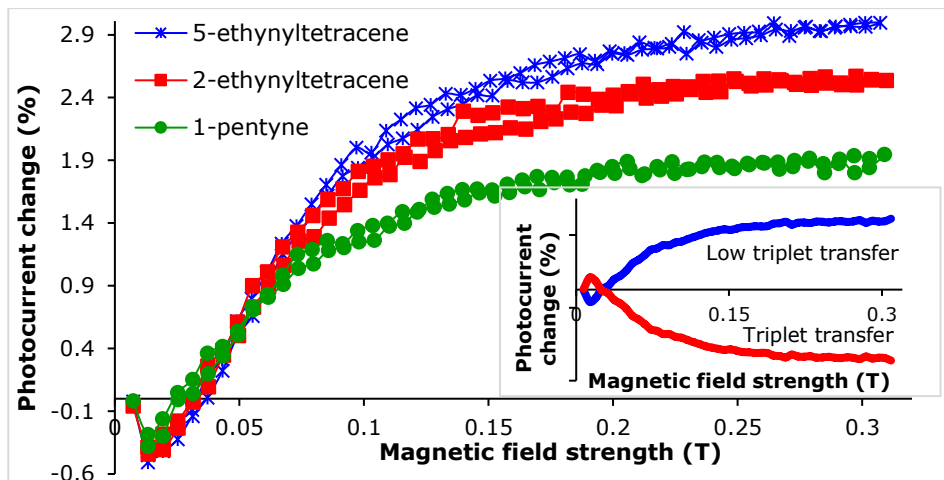


Figure 11: Magnetic-field-dependent photocurrent measurements of surfaces functionalized with 5-ethynyltetracene (**1**), 2-ethynyltetracene (**2**), and 1-pentyne. The insert in the bottom right corner shows a schematic representation of the expected result in the case of low and high triplet energy transfer to silicon.

In conclusion, we have shown that it is possible to attach a covalent seed layer of novel tetracene derivatives onto a hydrogen-terminated silicon surface. Modifying the tetracene on the 2- position is in this respect preferred, as this leads to a better preservation of the optical properties compared to the unmodified tetracene. Apart from this, surfaces functionalized with a tetracene moiety bound *via* the 2- position show a greater ability to orient subsequently deposited tetracene layers into the more favorable tetracene polymorph Tc II, and are slightly more resistant against oxidation after backfilling. Unfortunately, there is no (clear) increase in the triplet energy transfer efficiency from tetracene to silicon with any of the functionalized surfaces tested here. In addition, even when a seed layer seems capable of orienting subsequent tetracene layers into a more favorable orientation for energy transfer, this effect seems to be limited to the tetracene layers closest to the surface, with layers further away assuming the preferred – more parallel – orientation of tetracene. This was demonstrated using XRD, where peaks at the 2θ values belonging to the TC II polymorph were observed only after functionalization of the surface with **2**, and only as small peaks next to larger peaks belonging to the Tc I polymorph, indicating the majority of the deposited tetracene layer is still present as the Tc I polymorph. Further research into this phenomenon, as well as longer linker groups and alternative linker positions, together with the aforementioned need to optimize the backfilling process, is therefore needed to make singlet fission-sensitized silicon solar cells a viable alternative to conventional solar cells.

References

- (1) Polman, A.; Knight, M.; Garnett, E. C.; Ehrler, B.; Sinke, W. C. Photovoltaic Materials: Present Efficiencies and Future Challenges. (2016), *Science* (1979), **352** (6283).
- (2) Rühle, S. Tabulated Values of the Shockley-Queisser Limit for Single Junction Solar Cells. (2016), *Solar Energy*, **130**, 139–147.
- (3) Shockley, W.; Queisser, H. J. Detailed Balance Limit of Efficiency of P-n Junction Solar Cells. (1961), *J Appl Phys*, **32** (3), 510–519.
- (4) Tiedje, T.; Yablonovitch, E.; Cody, G. D.; Brooks, B. G. Limiting Efficiency of Silicon Solar Cells. (1984), *IEEE Trans Electron Devices*, **31** (5), 711–716.
- (5) Li, H.; Zhang, W. Perovskite Tandem Solar Cells: From Fundamentals to Commercial Deployment. *Chemical Reviews*. American Chemical Society September 23, 2020, pp 9835–9950.
- (6) Asghar, M. I.; Zhang, J.; Wang, H.; Lund, P. D. Device Stability of Perovskite Solar Cells – A Review. (2017), *Renew. and Sustain. Energy Rev*, **77**, 131–146.
- (7) Li, H.; Zhang, W. Perovskite Tandem Solar Cells: From Fundamentals to Commercial Deployment. (2020), *Chem Rev*, **120** (18), 9835–9950.
- (8) Dupré, O.; Niesen, B.; de Wolf, S.; Ballif, C. Field Performance versus Standard Test Condition Efficiency of Tandem Solar Cells and the Singular Case of Perovskites/Silicon Devices. (2018), *J. Phys. Chem. Lett.*, **9** (2), 446–458.
- (9) American Society for Testing and Materials (ASTM), subcommittee G. 09. *Standard Tables for Reference Solar Spectral Irradiances: Direct Normal and Hemispherical on 37° Tilted Surface*; (2003).
- (10) Dexter, D. L. Two Ideas on Energy Transfer Phenomena: Ion-Pair Effects Involving the OH Stretching Mode, and Sensitization of Photovoltaic Cells. (1979), *J Lumin*, **18**, 779–784.
- (11) Rao, A.; Friend, R. H. Harnessing Singlet Exciton Fission to Break the Shockley–Queisser Limit. (2017), *Nat Rev Mater*, **2** (11), 17063.
- (12) Burdett, J. J.; Bardeen, C. J. The Dynamics of Singlet Fission in Crystalline Tetracene and Covalent Analogs. (2013), *Acc. Chem. Res.*, **46** (6), 1312–1320.
- (13) Zimmerman, P. M.; Bell, F.; Casanova, D.; Head-Gordon, M. Mechanism for Singlet Fission in Pentacene and Tetracene: From Single Exciton to Two Triplets. (2011), *J Am Chem Soc*, **133** (49), 19944–19952.
- (14) Einzinger, M.; Wu, T.; Kompalla, J. F.; Smith, H. L.; Perkinson, C. F.; Nienhaus, L.; Wieghold, S.; Congreve, D. N.; Kahn, A.; Bawendi, M. G.; Baldo, M. A. Sensitization of Silicon by Singlet Exciton Fission in Tetracene. (2019), *Nature*, **571** (7763), 90–94.
- (15) Niederhausen, J.; MacQueen, R. W.; Özkol, E.; Gersmann, C.; Futscher, M. H.; Liebhaber, M.; Friedrich, D.; Borgwardt, M.; Mazzio, K. A.; Amsalem, P.; Nguyen, M. H.; Daiber, B.; Mews, M.; Rappich, J.; Ruske, F.; Eichberger, R.; Lips, K. Energy-Level Alignment Tuning at Tetracene/c-Si Interfaces. (2020), *Journal of Physical Chemistry C*, **124** (51), 27867–27881.
- (16) Jiang, Y.; Nielsen, M. P.; Baldacchino, A. J.; Green, M. A.; McCamey, D. R.; Tayebjee, M. J. Y.; Schmidt, T. W.; Ekins-Daukes, N. J. Singlet Fission and

- Tandem Solar Cells Reduce Thermal Degradation and Enhance Lifespan. (2021), *Progress in Photovoltaics: Research and Applications*, **29** (8), 899–906.
- (17) Chan, W. L.; Tritsch, J. R.; Zhu, X. Y. Harvesting Singlet Fission for Solar Energy Conversion: One- Versus Two-Electron Transfer from the Quantum Mechanical Superposition. (2012), *J Am Chem Soc*, **134** (44), 18295–18302.
 - (18) Schlenker, C. W.; Barlier, V. S.; Chin, S. W.; Whited, M. T.; McAnally, R. E.; Forrest, S. R.; Thompson, M. E. Cascade Organic Solar Cells. (2011), *Chemistry of Materials*, **23** (18), 4132–4140.
 - (19) Jadhav, P. J.; Mohanty, A.; Sussman, J.; Lee, J.; Baldo, M. A. Singlet Exciton Fission in Nanostructured Organic Solar Cells. (2011), *Nano Lett*, **11** (4), 1495–1498.
 - (20) Tritsch, J. R.; Chan, W. L.; Wu, X.; Monahan, N. R.; Zhu, X. Y. Harvesting Singlet Fission for Solar Energy Conversion via Triplet Energy Transfer. (2013), *Nat Commun*, **4**, 2679.
 - (21) Thompson, N. J.; Wilson, M. W. B.; Congreve, D. N.; Brown, P. R.; Scherer, J. M.; Bischof, T. S.; Wu, M.; Geva, N.; Welborn, M.; van Voorhis, T.; Bulovi, V.; Bawendi, M. G.; Baldo, M. A. Energy Harvesting of Non-Emissive Triplet Excitons in Tetracene by Emissive PbS Nanocrystals. (2014), *Nat Mater*, **13** (1), 1039–1043.
 - (22) Gish, M. K.; Pace, N. A.; Rumbles, G.; Johnson, J. C. Emerging Design Principles for Enhanced Solar Energy Utilization with Singlet Fission. (2019), *Journal of Physical Chemistry C*, **123** (7), 3923–3934.
 - (23) Macqueen, R. W.; Liebhaber, M.; Niederhausen, J.; Mews, M.; Gersmann, C.; Jäckle, S.; Jäger, K.; Tayebjee, M. J. Y.; Schmidt, T. W.; Rech, B.; Lips, K. Crystalline Silicon Solar Cells with Tetracene Interlayers: The Path to Silicon-Singlet Fission Heterojunction Devices. (2018), *Mater Horiz*, **5** (6), 1065–1075.
 - (24) Niederhausen, J.; Macqueen, R. W.; Lips, K.; Aldahhak, H.; Schmidt, W. G.; Gerstmann, U. Tetracene Ultrathin Film Growth on Hydrogen-Passivated Silicon. (2020), *Langmuir*, **36** (31), 9099–9113.
 - (25) Daiber, B.; Maiti, S.; Ferro, S. M.; Bodin, J.; van den Boom, A. F. J.; Luxembourg, S. L.; Kinge, S.; Pujari, S. P.; Zuilhof, H.; Siebbeles, L. D. A.; Ehrler, B. Change in Tetracene Polymorphism Facilitates Triplet Transfer in Singlet Fission-Sensitized Silicon Solar Cells. (2020), *Journal of Physical Chemistry Letters*, **11** (20), 8703–8709.
 - (26) Estévez-Fregoso, M.; Hernández-Trujillo, J. Electron Delocalization and Electron Density of Small Polycyclic Aromatic Hydrocarbons in Singlet Excited States. (2016), *Physical Chemistry Chemical Physics*, **18** (17), 11792–11799.
 - (27) Plasser, F.; Mewes, S. A.; Dreuw, A.; González, L. Detailed Wave Function Analysis for Multireference Methods: Implementation in the Molcas Program Package and Applications to Tetracene. (2017), *J Chem Theory Comput*, **13** (11), 5343–5353.
 - (28) Pati, Y. A.; Ramasesha, S. Exact Solution of the PPP Model for Correlated Electronic States of Tetracene and Substituted Tetracene. (2014), *Journal of Physical Chemistry A*, **118** (23), 4048–4055.

- (29) Korovina, N. V.; Joy, J.; Feng, X.; Feltenberger, C.; Krylov, A. I.; Bradforth, S. E.; Thompson, M. E. Linker-Dependent Singlet Fission in Tetracene Dimers. (2018), *J Am Chem Soc*, **140** (32), 10179–10190.
- (30) Korovina, N. V.; Das, S.; Nett, Z.; Feng, X.; Joy, J.; Haiges, R.; Krylov, A. I.; Bradforth, S. E.; Thompson, M. E. Singlet Fission in a Covalently Linked Cofacial Alkynyltetracene Dimer - Supporting Information. (2016), *J Am Chem Soc*, **138** (2), 617–627.
- (31) Li, Y.; Calder, S.; Yaffe, O.; Cahen, D.; Haick, H.; Kronik, L.; Zuilhof, H. Hybrids of Organic Molecules and Flat, Oxide-Free Silicon: High-Density Monolayers, Electronic Properties, and Functionalization. (2012), *Langmuir*, **28** (26), 9920–9929.
- (32) Coletti, C.; Marrone, A.; Giorgi, G.; Sgamellotti, A.; Cerofolini, G.; Re, N. Nonradical Mechanisms for the Uncatalyzed Thermal Functionalization of Silicon Surfaces by Alkenes and Alkynes: A Density Functional Study. (2006), *Langmuir*, **22** (24), 9949–9956.
- (33) Scheres, L.; Giesbers, M.; Zuilhof, H. Organic Monolayers onto Oxide-Free Silicon with Improved Surface Coverage: Alkynes versus Alkenes. (2010), *Langmuir*, **26** (7), 4790–4795.
- (34) Ciampi, S.; Harper, J. B.; Gooding, J. J. Wet Chemical Routes to the Assembly of Organic Monolayers on Silicon Surfaces via the Formation of Si-C Bonds: Surface Preparation, Passivation and Functionalization. (2010), *Chem Soc Rev*, **39** (6), 2158–2183.
- (35) Puniredd, S. R.; Assad, O.; Haick, H. Highly Stable Organic Monolayers for Reacting Silicon with Further Functionalities: The Effect of the C-C Bond Nearest the Silicon Surface. (2008), *J Am Chem Soc*, **130** (41), 13727–13734.
- (36) Puniredd, S. R.; Assad, O.; Haick, H. Highly Stable Organic Modification of Si(111) Surfaces: Towards Reacting Si with Further Functionalities While Preserving the Desirable Chemical Properties of Full Si-C atop Site Terminations. (2008), *J Am Chem Soc*, **130** (29), 9184–9185.
- (37) Haick, H.; Hurley, P. T.; Hochbaum, A. I.; Yang, P.; Lewis, N. S. Electrical Characteristics and Chemical Stability of Non-Oxidized, Methyl-Terminated Silicon Nanowires. (2006), *J Am Chem Soc*, **128** (28), 8990–8991.
- (38) Fonash, S. J. Chapter Five - Semiconductor–Semiconductor Heterojunction Cells. In *Solar Cell Device Physics (Second Edition)*; Fonash, S. J., Ed.; Academic Press: Boston, (2010); pp 183–262.
- (39) Arias, D. H.; Ryerson, J. L.; Cook, J. D.; Damrauer, N. H.; Johnson, J. C. Polymorphism Influences Singlet Fission Rates in Tetracene Thin Films. (2016), *Chem Sci*, **7** (2), 1185–1191.
- (40) Abraham, V.; Mayhall, N. J. Revealing the Contest between Triplet-Triplet Exchange and Triplet-Triplet Energy Transfer Coupling in Correlated Triplet Pair States in Singlet Fission. (2021), *J. Phys. Chem. Lett.*, **12** (43), 10505–10514.
- (41) Akselrod, G. M.; Deotare, P. B.; Thompson, N. J.; Lee, J.; Tisdale, W. A.; Baldo, M. A.; Menon, V. M.; Bulovic, V. Visualization of Exciton Transport in Ordered and Disordered Molecular Solids. (2014), *Nat Commun*, **5**, 3646.

Supporting Information

General information

All chemicals were purchased from either Merck Life Science N.V. or abcr, and used as received. Double side polished silicon(111) wafers with a diameter of 76.2 ± 0.3 mm were purchased from SIEGERT WAFER GmbH (FZ growth, prime grade, N type, Ph-doped, 381 ± 25 μm thickness), and cut into 1x1 cm squares using a laser cutter.

NMR measurements were conducted on a 400 MHz Bruker Avance III at 298K, and the resulting data were analyzed using MestReNova software, version 14.1.0-24037. Spectra were calibrated relative to signals corresponding to the non-deuterated solvents (CDCl_3 solvent peak) – at 7.26 ppm for ^1H spectra, and 77.16 ppm for ^{13}C spectra. For spectra recorded in DMSO-d_6 , ^1H spectra were calibrated to the non-deuterated solvent peak at 2.50 ppm. Abbreviations used in the description of NMR data are as follows: chemical shift (δ = ppm), multiplicity (s = singlet, d = doublet, t = triplet, q = quartet, p = pentet, sextet = sext, h = heptet, dd = doublet of doublets, dt = doublet of triplets, m = multiplet), coupling constant (J , Hz).

High-resolution mass spectra (HRMS) were recorded on a Thermo Scientific Exactive 1.1 with an orbitrap mass analyzer, using a DART gun from Ion Sense. The temperature of the DART gun was set to 450-550 $^\circ\text{C}$, with a helium gas flow. Data were analyzed using Thermo Xcalibur software, version 2.2 SP1.48.

IR spectra were recorded on a Bruker Tensor 27 spectrometer equipped with a diamond ATR accessory (64 scans; 4 cm^{-1} resolution; range 4000-350 cm^{-1}). Strong or indicative peaks in the region 4000-1000 cm^{-1} are mentioned for each novel compound.

IR-RAS spectra were recorded on a Bruker Tensor 27 with MCT detector equipped with a Seagull™ Variable Angle Reflection Accessory. A germanium crystal was used to perform Ge-ATR measurements using P polarization and a mirror angle of 68°. A total of 2048 scans were performed per sample, with a resolution of 4 cm^{-1} .

XPS measurements were performed on a Jeol JPS-9200 photoelectron spectrometer, using a 12 kV and 20 mA monochromatic Al K α source. The analyzer pass energy was 10 eV, and the take-off angle between sample and detector was set at 80°. Data was analyzed using the program CasaXPS, version 2.3.18PR1.0.

Optical properties (in DCM) were studied using an Edinburgh Instruments FLS900 fluorescence spectrometer, using a 450 W xenon lamp as the excitation source. For

the UV-Vis absorption spectra, a Varian Cary 50 UV-Vis spectrophotometer was used, with a scan rate of 600 nm/min. Absorption spectra were corrected for solvent absorption.

Tetracene deposition 30 nm or 100 nm tetracene layers were deposited on silicon surfaces using an evaporation chamber by Angstrom Engineering Inc, at a base pressure below 7×10^{-7} mbar. Tetracene was purchased from Sigma-aldrich (99.99% purity) and used as is. The deposition was 1 \AA/s in all cases.

Magnetic-field-dependent photocurrent measurements were performed using a home-built setup. The magnetic field is applied by an electromagnet, made up by two Helmholtz coils and calibrated using a Hall effect sensor. The magnetic field is applied by sending a current of up to 5 Amperes through the magnet, resulting in a magnetic field of up to 0.35 T. The field is oriented parallel to the sample surface. The excitation source is a 520 nm diode laser, installed in a Thorlabs temperature controlled laser housing. The cw laser power is around 10 mW with a laser spot size of approx. 1 mm. The photocurrent is measured with a Keithly 2636A Source measure unit.

1D XRD measurements were conducted using a Bruker D8 Advance diffractometer (Bragg-Brentano) with a Co-K α source ($\lambda = 1.7889 \text{ \AA}$, 35 kV, 40 mA) and a Lynxeye position sensitive detector

2D GIWAX XRD measurements were conducted using a Bruker D8 Discover with a Co-K α GIWAX source (1mS microfocus tube, 50 kV, 1000 mA) and a VANTEC500 2D-detector. Samples were measured under the following conditions: 2.0 mm collimator, 600 s/step, and a 4° X-ray incidence angle.

Experimental details

Synthesis of tetracene

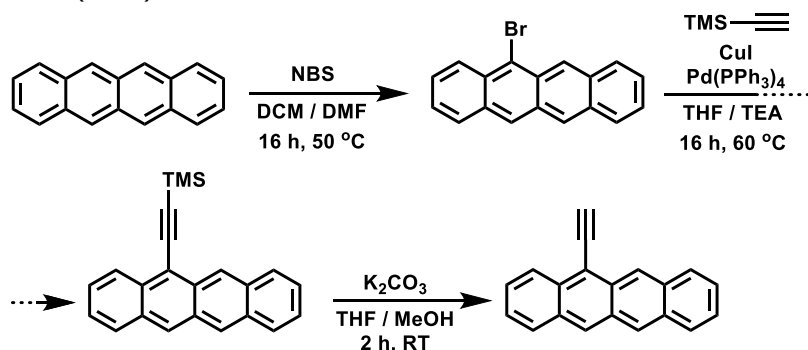
Tetracene was prepared according to the procedure described in Kulkarni *et al.* (2018).¹ In short, 2.50 g (9.68 mmol, 1 equiv) of 5,12-naphthacenequinone was dissolved in 220 ml each of methanol and THF. While stirring, 1.65 g (43.62 mmol, 4.5 equiv) of NaBH $_4$ was slowly added, and the reaction mixture was allowed to stir for another hour at room temperature. Then, the mixture was neutralized with (glacial) acetic acid, and transferred to an extraction funnel. Here, 150 ml of both brine and DCM are added, and the organic layer is separated. The organic layer is washed with 2x 150 ml of brine, and the combined water layers are back-extracted with 150 ml of DCM. The organic layers are combined, dried over magnesium sulfate, and concentrated on a rotavapor to yield 2.34 g (8.93 mmol) of 5,12-dihydrotetracene-5,12-diol as a yellow solid.

Improving triplet energy transfer from tetracene to silicon using a covalently-bound tetracene seed layer

This solid was dissolved in 270 ml of THF, and a mixture of 3.41 g (18.00 mmol, 2 equiv) of SnCl_2 in 4.3 ml of 37% HCl was added dropwise under vigorous stirring. After addition was complete, the reaction was allowed to stir for 1 hour at room temperature. Then, the mixture was filtered, and the solid washed with 1M HCl, water, and methanol, to give 1.32 g (5.78 mmol) of tetracene as orange needles. **^1H NMR (400 MHz, CDCl_3):** δ 8.67 (s, 4H), 8.00 (dd, J = 6.2, 3.3 Hz, 4H), 7.40 (dd, J = 6.8, 3.2 Hz, 4H). These values match those reported by Kulkarni *et al.* (2018).

Synthesis of 5-ethynyltetracene (1)

5-ethynyltetracene was prepared according to the procedure described by Korovina *et al.* (2016).²



5-bromotetracene

In a three-necked flask equipped with a stir bar, 1.00 g (4.38 mmol, 1 equiv) of tetracene was suspended in 250 ml of dry DCM, and the suspension was sonicated for 30 minutes. Meanwhile, an addition funnel was charged with 0.86 g (4.83 mmol, 1.1 equiv) of n-bromosuccinimide (NBS), 70 ml of dry DCM, and 15 ml of dry DMF. This solution was flushed with argon for 10 minutes, after which the addition funnel was installed onto the three-necked flask under argon flow. A condenser was added, and the tetracene suspension was heated to 50 °C under argon. Then, the NBS solution was added dropwise, over a period of 2h. Next, the reaction mixture was allowed to stir overnight at 50 °C, in the dark, under argon. The mixture was cooled down to room temperature, and the DCM was removed on a rotavapor. 30 ml of methanol was added to the resulting slurry, and the mixture was cooled down to 0 °C. 5 ml of water was added dropwise, and the red solids were collected by vacuum filtration. The solids were washed with cold water and methanol to yield 1.25 g (4.08 mmol, 93%) of 5-bromotetracene as a red solid.

^1H NMR (400 MHz, CDCl_3): δ 9.14 (s, 1H), 8.64 (d, J = 3.8 Hz, 2H), 8.48 (d, J = 8.9 Hz, 1H), 8.08 (d, J = 7.4 Hz, 1H), 8.02 – 7.94 (m, 2H), 7.56 – 7.50 (m, 1H), 7.48 – 7.38 (m, 3H).

5-((trimethylsilyl)ethynyl)tetracene:

The 5-bromotetracene was transferred into a three-necked flask, together with 34 mg (0.18 mmol) of CuI, 162 mg (0.14 mmol) of Pd(PPh₃)₄, and 30 ml of dry THF. The resulting solution was flushed with argon for 15 min. Meanwhile, an addition funnel was filled with a solution of 0.90 ml (6.37 mmol, 1.6 equiv) of (trimethylsilyl)acetylene in 25 ml of triethylamine, and this solution was also flushed with argon for 15 min, before the addition funnel was installed onto the three-necked flask. A condenser was added, and the 5-bromotetracene solution was heated to 60 °C. The (trimethylsilyl)acetylene solution was added dropwise, and the reaction mixture was allowed to stir overnight at 60 °C, in the dark, under argon atmosphere.

After cooling down, the reaction mixture was added to a separation funnel containing 50 ml of DCM. The organic layer was washed with 3x 20 ml of a saturated ammonium chloride solution, and the combined water layers were back-extracted with 20 ml of DCM. The organic layers were combined, dried over MgSO₄, and concentrated on a rotavapor. The crude product was then further purified using flash chromatography (silica gel, mobile phase: hexane) to yield 1.01 g (3.10 mmol, 76%) of 5-((trimethylsilyl)ethynyl)tetracene as a red solid.

¹H NMR (400 MHz, CDCl₃): δ 9.18 (s, 1H), 8.66 (s, 2H), 8.55 (dd, *J* = 8.8, 1.0 Hz, 1H), 8.10 – 8.07 (m, 1H), 8.03 – 7.97 (m, 2H), 7.55 – 7.50 (m, 1H), 7.46 – 7.41 (m, 3H), 0.48 (s, 9H). These values match those reported in ².

5-ethynyltetracene:

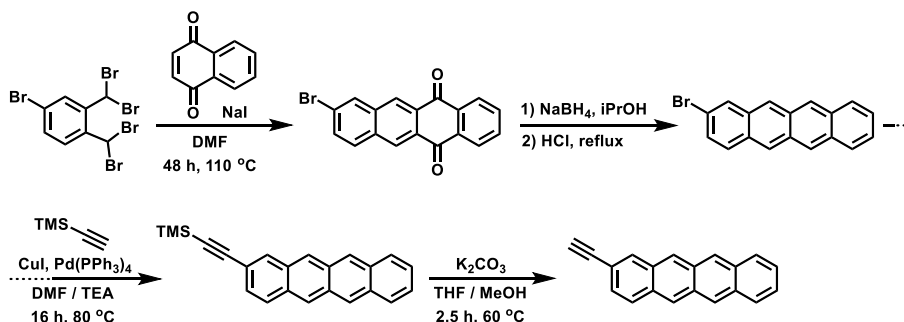
0.15 g (0.46 mmol, 1 equiv) of 5-((trimethylsilyl)ethynyl)tetracene was added to a round bottom flask under argon, along with 0.23 g (1.66 mmol, 3.6 equiv) of potassium carbonate. Next, still under argon, 4.5 ml of dry THF, and 2.8 ml of dry methanol were added. The resulting suspension was allowed to stir for 2h, in the dark, under argon. Afterwards, the solvent was removed on a rotavapor, and the product was passed through a silica plug using dry DCM. The solvent was again evaporated, and the product was transported into a glovebox, where it was immediately used for surface functionalisation.

¹H NMR (400 MHz, CDCl₃): δ 9.26 (s, 1H), 8.71 (d, *J* = 6.2 Hz, 2H), 8.63 (d, *J* = 7.8 Hz, 1H), 8.16 – 8.10 (m, 1H), 8.08 – 8.01 (m, 2H), 7.61 – 7.54 (m, 1H), 7.53 – 7.45 (m, 3H), 4.18 (s, 1H). These values match those reported in ².

Synthesis of 2-ethynyltetracene (2)

For the synthesis of 2-ethynyltetracene, 2-bromotetracene was first prepared according to a procedure from Zhao *et al.* (2020).³ Then, an adapted procedure from the one described above for 5-ethynyltetracene was followed.

Improving triplet energy transfer from tetracene to silicon using a covalently-bound tetracene seed layer



8-bromotetracene-5,12-dione

A round bottom flask under argon was charged with 3.94 g (26.28 mmol, 4.2 equiv) of NaI, and 1.00 g (6.31 mmol, 1 equiv) of 1,4-naphthoquinone. 30 ml of DMF was added, followed by 3.29 g (6.57 mmol, 1.04 equiv) of $\alpha,\alpha,\alpha,\alpha$ -tetrabromo-4-bromo-o-xylene. The resulting mixture was stirred at 110 °C for 48h. After cooling down, the precipitated solid was collected using vacuum filtration, washed with water, methanol, and acetone, and dried under vacuum to yield 1.41 g (4.17 mmol, 66%) of 8-bromotetracene-5,12-dione as a golden-yellow, shiny solid.

¹H NMR (400 MHz, CDCl₃): δ 8.84 (s, 1H), 8.78 (s, 1H), 8.41 (dd, J = 5.8, 3.4 Hz, 2H), 8.28 (s, 1H), 7.99 (d, J = 8.8 Hz, 1H), 7.85 (dd, J = 6.0, 3.3 Hz, 2H), 7.78 (d, J = 8.7 Hz, 1H). These values match data from ³.

2-bromotetracene

The fresh 8-bromotetracene-5,12-dione was dissolved in 140 ml of isopropanol, and 2.18 g (57.63 mmol, 14 equiv) of NaBH₄ was added. A condenser was installed onto the flask, and the reaction mixture was allowed to reflux at 95 °C for 24h in the dark. After cooling down, the mixture was placed on an ice bath, and 140 ml of a 2M aqueous HCl solution was added dropwise. The mixture was heated to 105 °C, and allowed to reflux for 3h. After cooling, the solids were collected using vacuum filtration, and washed with water, methanol, acetone, and hexane, to yield 0.97 g (3.14 mmol, 75%) of 2-bromotetracene as an orange solid.

Note: the solubility of 2-bromotetracene is exceptionally low in common organic solvents.

¹H NMR (400 MHz, CDCl₃): δ 8.71 – 8.61 (m, 3H), 8.57 (s, 1H), 8.18 (s, 1H), 8.03 – 7.97 (m, 2H), 7.88 (d, J = 9.1 Hz, 1H), 7.46 – 7.37 (m, 3H). These values match data from ³.

2-((trimethylsilyl)ethynyl)tetracene

The thus prepared 2-bromotetracene was dissolved in 28 ml of dry DMF in a three-necked flask under argon, and 32 mg (0.17 mmol) CuI and 152 mg (0.13 mmol) Pd(PPh₃)₄ were added. The resulting suspension was flushed with argon for 15 minutes. Meanwhile, 0.7 ml (5.16 mmol, 1.6 equiv) of (trimethylsilyl)acetylene was

dissolved in 24 ml of triethylamine in an addition funnel under argon. The addition funnel was installed onto the three-necked flask, along with a condenser, and the flask was heated to 85 °C. The (trimethylsilyl)acetylene solution was added dropwise, and the reaction was allowed to stir overnight at 85 °C, in the dark, under argon.

The mixture was cooled down, diluted with hexane, and cooled down further on an ice bath. The solids were collected using vacuum filtration, and washed with water, methanol, acetone, and hexane, to yield 0.67 g (2.06 mmol, 66%) of 2-((trimethylsilyl)ethynyl)tetracene as a red solid.

Note: the solubility of 2-((trimethylsilyl)ethynyl)tetracene is exceptionally low in common organic solvents.

¹H NMR (400 MHz, CDCl₃): δ 8.65 (d, *J* = 6.7 Hz, 2H), 8.60 (s, 2H), 8.17 (s, 1H), 8.00 (dd, *J* = 6.6, 3.2 Hz, 2H), 7.91 (d, *J* = 8.9 Hz, 1H), 7.41 (dd, *J* = 6.6, 3.2 Hz, 2H), 7.36 (dd, *J* = 8.8, 1.5 Hz, 1H), 0.31 (s, 9H). **¹³C NMR (101 MHz, CDCl₃):** δ 132.9, 128.4, 127.4, 126.8, 126.5, 125.6, 0.2. **IR:** $\tilde{\nu}_{\text{max}}$ = 2955, 2899, 2146, 1462, 1294, 1248, 1169, 955, 904, 868, 837, 802, 758, 733, 642, 467 cm⁻¹ **HRMS:** *m/z* C₂₃H₂₁Si⁺ ([M+H]⁺): calculated 325.1407, found 325.1406.

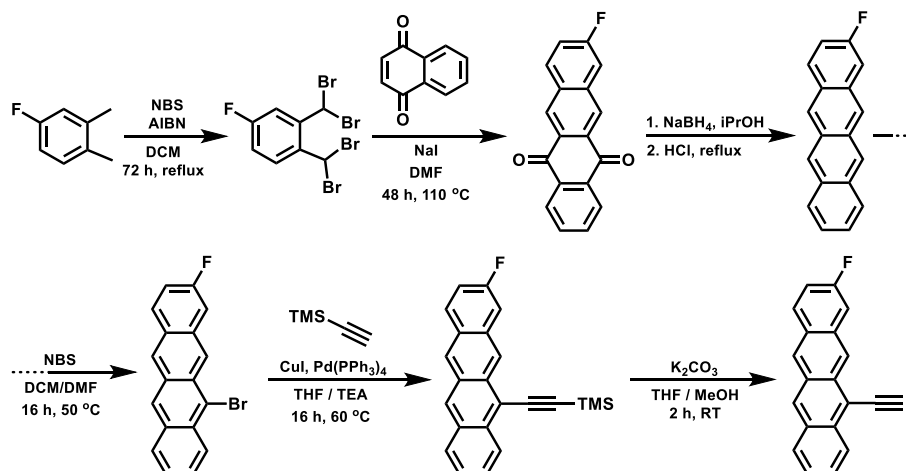
2-ethynyltetracene

To deprotect the 2-((trimethylsilyl)ethynyl)tetracene for use in surface functionalisation, 25 mg (0.077 mmol) of the compound was added to a Schlenk flask equipped with a stir bar, along with 38 mg (0.275 mmol, 3.6 equiv) of K₂CO₃. The flask was flushed with argon, after which 4.0 ml of THF and 2.7 ml of methanol were added under argon flow. The flask was sealed, heated to 60 °C under argon, and stirred in the dark for 2.5 h. Afterwards, the mixture was cooled down to room temperature, and the solvents were evaporated. The crude product was passed through a silica plug with ~500 ml of hot, dry DCM, and the solvents were again evaporated. The thus purified product was transferred into a glovebox, where it was immediately used for surface functionalisation.

Note: the solubility of 2-ethynyltetracene is exceptionally low in common organic solvents.

¹H NMR (400 MHz, CDCl₃): δ 8.66 (d, *J* = 5.4 Hz, 2H), 8.63 (s, 2H), 8.21 (s, 1H), 8.00 (dd, *J* = 6.5, 3.3 Hz, 2H), 7.94 (d, *J* = 8.9 Hz, 1H), 7.42 (dd, *J* = 6.7, 3.2 Hz, 2H), 7.38 (dd, *J* = 8.8, 1.6 Hz, 1H), 3.22 (s, 1H). This compound is unstable, and could therefore not be further characterized. Full characterization was therefore performed on 2-((trimethylsilyl)ethynyl)tetracene.

Synthesis of 2-fluoro-6-((trimethylsilyl)ethynyl)tetracene (1F)



4-fluoro- $\alpha,\alpha,\alpha,\alpha$ -tetrabromoxylene was prepared according to the procedure described by Zhao *et al.* (2020).³ 7.10 g (40.21 mmol) of *n*-bromosuccinimide (NBS) was suspended in 38 ml of DCM, and to this were added 2.5 g (20.14 mmol) of 4-fluoro-*o*-xylol and 0.11 g (0.65 mmol) of azobis(isobutyronitrile) (AIBN). This mixture was then refluxed for 72 h, adding another 7.10 g of NBS and 0.11 g of AIBN after 24 h and 48 h. After cooling down, the mixture was filtered, and the solids washed with DCM. The combined filtrate and washing solution were then washed 3x with water, aqueous $\text{Na}_2\text{S}_2\text{O}_3$, and brine. The organic layer was isolated, dried over MgSO_4 , and concentrated on a rotavap. The crude product was further purified using column chromatography (silica gel, eluent: hexane) to yield 3.91 g (8.88 mmol, 44%) of off-white solids.

8-fluoro-5,12-naphthacenequinone was prepared in the same way as 8-bromotetracene-5,12-dione – starting with 3.69 g (8.39 mmol) of 4-fluoro- $\alpha,\alpha,\alpha,\alpha$ -tetrabromoxylene – to yield 0.68 g (2.46 mmol, 29%) of gold-yellow solids.

^1H NMR (400 MHz, CDCl_3): δ 8.87 (s, 1H), 8.80 (s, 1H), 8.41 (dd, J = 6.1, 3.1 Hz, 2H), 8.13 (dd, J = 9.0, 5.5 Hz, 1H), 7.84 (dd, J = 5.8, 3.3 Hz, 2H), 7.73 (dd, J = 9.2, 2.5 Hz, 1H), 7.49 (td, J = 8.7, 2.5 Hz, 1H). **^{13}C NMR (101 MHz, CDCl_3):** δ 183.07, 182.85, 164.04, 161.51, 134.50, 134.43, 133.03, 132.94, 129.70, 128.84, 128.78, 127.73, 127.71, 120.41, 120.15, 113.55, 113.35.

2-fluototetracene was prepared from 8-fluoro-5,12-naphthacenequinone according to the procedure described for 2-bromotetracene, to yield 0.52 g (2.11 mmol, 86%) of orange solids.

Note: the solubility of 2-fluorotetracene is exceptionally low in common organic solvents.

¹H NMR (400 MHz, CDCl₃): δ 8.67 (d, *J* = 6.9 Hz, 2H), 8.61 (d, *J* = 17.0 Hz, 2H), 8.05 – 7.95 (m, 3H), 7.56 (d, *J* = 10.2 Hz, 1H), 7.44 – 7.38 (m, 2H), 7.22 (d, *J* = 9.5 Hz, 1H).

These values match previously reported data for this compound.⁴

11-bromo-2-fluorotetracene was prepared from 0.43 g (1.75 mmol) of 2-fluorotetracene according to the procedure described for 5-bromotetracene, to yield 0.52 g (1.61 mmol, 92%) of orange solids.

¹H NMR (400 MHz, CDCl₃): δ 9.08 (d, *J* = 8.5 Hz, 1H), 8.67 (s, 2H), 8.49 (d, *J* = 9.0 Hz, 1H), 8.09 (d, *J* = 10.5 Hz, 1H), 8.04 – 7.96 (m, 2H), 7.61 – 7.39 (m, 3H).

5-((trimethylsilyl)ethynyl)-8-fluorotetracene was prepared from 0.52 g of 11-bromo-2-fluorotetracene according to the procedure described for 5-((trimethylsilyl)ethynyl)tetracene, to yield 0.55 g (1.61 mmol, 100%) of red solids.

¹H NMR (400 MHz, CDCl₃): δ 9.09 (d, *J* = 13.4 Hz, 1H), 8.65 – 8.60 (m, 2H), 8.12 – 8.05 (m, 1H), 8.01 – 7.96 (m, 2H), 7.57 – 7.50 (m, 1H), 7.50 – 7.40 (m, 2H), 7.23 (ddd, *J* = 7.8, 2.5, 1.5 Hz, 1H), 0.49 (d, *J* = 1.2 Hz, 9H). **¹³C NMR (101 MHz, CDCl₃):** δ 131.6, 131.5, 128.5, 128.4, 128.3 (d, *J* = 2.9 Hz), 128.1, 127.8, 127.4, 127.1, 126.7, 125.7, 125.3, 125.1, 124.7, 124.2 (d, *J* = 8.5 Hz), 117.6, 109.5 (d, *J* = 20.7 Hz), 108.5 (d, *J* = 22.6 Hz), 101.5 (d, *J* = 23.1 Hz). **¹⁹F NMR (376 MHz, CDCl₃):** δ -111.13 (m). **IR:** $\tilde{\nu}_{\text{max}}$ = 3051, 2958, 2139, 1637, 1468, 1248, 1174, 1157, 891, 839, 733, 644, 463, 436. **HRMS:** *m/z* C₂₃H₂₀FSi⁺ ([M+H]⁺): calculated 343.1313, found 343.1311.

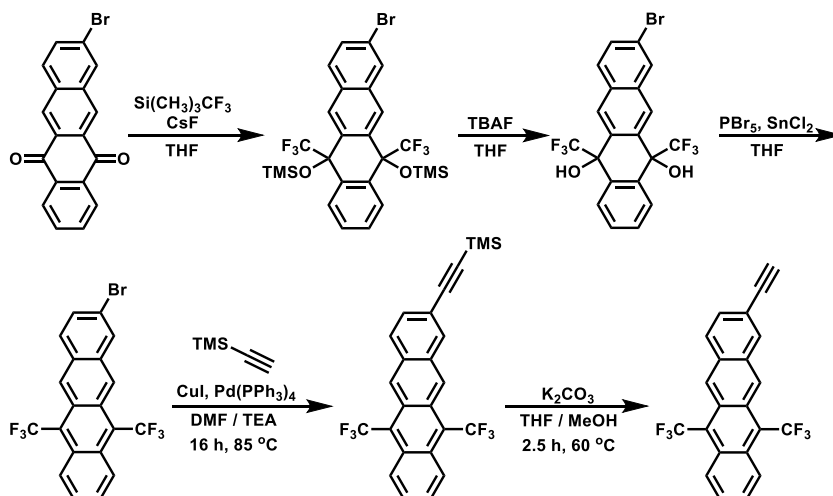
11-ethynyl-2-fluorotetracene was prepared from 0.2 g (0.58 mmol) of 5-((trimethylsilyl)ethynyl)-8-fluorotetracene according to the procedure for 5-ethynyltetracene. Quantitative yield.

¹H NMR (400 MHz, CDCl₃): δ 9.14 (d, *J* = 12.8 Hz, 1H), 8.68 (t, *J* = 4.7 Hz, 2H), 8.57 (d, *J* = 9.4 Hz, 1H), 8.08 (d, *J* = 7.1 Hz, 1H), 8.04 – 7.99 (m, 2H), 7.60 – 7.50 (m, 1H), 7.50 – 7.41 (m, 2H), 7.24 (s, 1H), 4.15 (s, 1H). This compound is unstable, and could therefore not be characterized further. Full characterization was therefore performed on 5-((trimethylsilyl)ethynyl)-8-fluorotetracene.

Synthesis of 2-ethynyl-6,11-bis(trifluoromethyl)tetracene (2F)

For the synthesis up to 2-bromo-6,11-bis(trifluoromethyl)tetracene, an adapted procedure from Schwaben *et al.* (2015) was used.⁵ All following products were prepared using protocols already described above.

Improving triplet energy transfer from tetracene to silicon using a covalently-bound tetracene seed layer



2-bromo-6,11-bis(trifluoromethyl)tetracene

A round bottom flask under argon was charged with 1.32 g of 8-bromotetracene-5,12-dione (3.91 mmol, 1 equiv) and 26 ml of dry THF. To this, 1.28 ml (8.60 mmol, 2.2 equiv) of trimethyl(trifluoromethyl)silane was added, and the suspension was cooled to 0 °C. 5.9 mg (0.04 mmol, 1 mol%) of CsF was added, and the reaction was stirred for 10 minutes. Then, the mixture was allowed to warm to room temperature, and stirred for another 1.5 h. The solvent was evaporated, and the crude product was purified using column chromatography (silica gel, 15:2 hexane/MTBE) to yield the intermediate ((8-bromo-5,12-bis(trifluoromethyl)-5,12-dihydrotetracene-5,12-diyl)bis(oxy))bis(trimethylsilane). **¹H NMR (400 MHz, CDCl₃):** δ 8.44 (d, *J* = 2.4 Hz, 1H), 8.39 (d, *J* = 2.5 Hz, 1H), 8.16 (s, 1H), 8.01 (dt, *J* = 5.9, 2.9 Hz, 2H), 7.85 (d, *J* = 8.7 Hz, 1H), 7.67 (dd, *J* = 8.8, 2.0 Hz, 1H), 7.55 (dd, *J* = 6.1, 3.4 Hz, 2H), -0.05 (d, *J* = 4.4 Hz, 18H).

This intermediate was dissolved in 27 ml of dry THF, and the solution was cooled down to 0 °C. Then, 8.6 ml of a 1M solution of TBAF in dry THF (8.60 mmol, 2.2 equiv) was added dropwise, after which the reaction mixture was allowed to warm to room temperature. The reaction was stirred for 30 minutes, and transferred to an extraction funnel. DCM and brine (27 ml each) were added, and the layers were separated. The water phase was extracted with 3x 27 ml of DCM. The organic layers were combined, dried, and concentrated under vacuum. The crude product was purified using column chromatography (silica gel, 5:1 to 1:1 hexane/MTBE) to yield the intermediate 8-bromo-5,12-bis(trifluoromethyl)-5,12-dihydrotetracene-5,12-diol. **¹H NMR (400 MHz, DMSO-*d*₆):** δ 8.57 (d, *J* = 5.0 Hz, 2H), 8.46 (d, *J* = 2.0 Hz, 1H), 8.11 (d, *J* = 8.8 Hz, 1H), 8.02 (dd, *J* = 5.8, 3.3 Hz, 2H), 7.81 (d, *J* = 7.5 Hz, 2H), 7.74 (dd, *J* = 8.8, 2.0 Hz, 1H), 7.61 (dt, *J* = 7.2, 3.6 Hz, 2H).

This intermediate was again dissolved in 22 ml of dry THF at room temperature, and 6.7 g (14.82 mmol, 4 equiv) of phosphorus pentabromide was added in portions. The reaction mixture was heated to 50 °C, and stirred for 18 h. After this

time, 7.01 g (37 mmol, 10 equiv) of SnCl_2 was added, and the reaction was stirred for another 10 minutes at 50 °C. Next, the mixture was cooled to room temperature, and diluted with 215 ml of diethyl ether in an extraction funnel. 110 ml of a saturated solution of NaHCO_3 was added slowly, and the organic phase was isolated, washed with 45 ml of brine, dried, and concentrated under vacuum. The resulting solids were washed with hexane, and dried to yield 0.94 g (2.11 mmol, 54%) of 2-bromo-6,11-bis(trifluoromethyl)tetracene. **^1H NMR (400 MHz, CDCl_3):** δ 8.52 (d, J = 2.2 Hz, 1H), 8.46 (d, J = 2.2 Hz, 1H), 8.13 (d, J = 1.9 Hz, 1H), 8.09 (dt, J = 5.8, 2.8 Hz, 2H), 7.83 (d, J = 8.8 Hz, 1H), 7.65 (dd, J = 8.7, 1.9 Hz, 1H), 7.59 (dd, J = 6.0, 3.4 Hz, 2H).

((6,11-bis(trifluoromethyl)tetracene-2-yl)ethynyl)trimethylsilane

((6,11-bis(trifluoromethyl)tetracene-2-yl)ethynyl)trimethylsilane was prepared in the same way as 2-((trimethylsilyl)ethynyl)tetracene, but using column chromatography (silica gel, 30% diethyl ether in hexane) to purify the final product as beige solids. **^1H NMR (400 MHz, CDCl_3):** δ 8.49 (dd, J = 7.7, 2.2 Hz, 2H), 8.14 – 8.05 (m, 3H), 7.89 (d, J = 8.5 Hz, 1H), 7.65 – 7.57 (m, 3H), 0.30 (s, 9H). **^{13}C NMR (101 MHz, CDCl_3):** δ 133.23, 132.76, 132.58, 132.34, 130.84, 130.79, 130.57, 130.07, 128.82 (q, J = 2.7 Hz), 128.64 (q, J = 3.0 Hz), 128.41, 125.64, 122.72, 104.81, 96.41, 73.63 (q, J = 28.0 Hz), 73.61 (q, J = 28.0 Hz), 0.08. **^{19}F NMR (376 MHz, CDCl_3):** δ -78.28 (s), -78.39 (s). **IR:** $\tilde{\nu}_{\text{max}}$ = 3078, 2958, 2152, 1331, 1252, 1205, 1159, 1034, 976, 912, 847, 760, 737, 688, 640. **HRMS:** m/z $\text{C}_{25}\text{H}_{19}\text{F}_6\text{Si}^+$ ($[\text{M}+\text{H}]^+$): calculated 461.1155, found 461.1192.

After deprotection using the same protocol as for 2-ethynyltetracene, the title compound 2-ethynyl-6,11-bis(trifluoromethyl)tetracene was obtained as an off-white solid in quantitative yield. This compound is unstable, and could therefore not be characterized. Full characterization was therefore performed on ((6,11-bis(trifluoromethyl)tetracene-2-yl)ethynyl)trimethylsilane.

Surface functionalization and backfilling

Double side polished silicon (111) surfaces of 1x1 cm were cleaned before etching and functionalisation by sonicating them for 10 minutes each in isopropanol, hexane, acetone, and DCM. After the final sonication step, the surfaces were blown dry with a stream of nitrogen, and submitted to a 10-minute plasma treatment in a plasma oven, using oxygen gas to generate the plasma. Then, the surfaces were transported into an oxygen-free glovebox (O_2 = 0%). Here, they were etched with a solution of 40% NH_4F in water for 15 minutes, under constant bubbling with nitrogen gas to remove bubbles formed during etching. After etching, the surfaces were washed extensively with deoxygenated water, and blown dry with a stream of nitrogen. The thus prepared surfaces were immediately used for functionalisation by fully immersing them in either an argon-purged solution of tetracene derivative

in dry toluene, or neat 1-pentyne for the reference surface. The immersed surfaces were heated to 90 °C, and allowed to react overnight. The next day, the surfaces were removed from the solution, and sonicated for 10 minutes in dry DCM to remove any physisorbed 1-pentyne or tetracene derivative. The surfaces functionalised with tetracene derivative were then submerged in neat 1-pentyne for backfilling. Again, the surfaces were allowed to react at 90 °C overnight, and cleaned by sonicating in dry DCM.

Supplementary figures

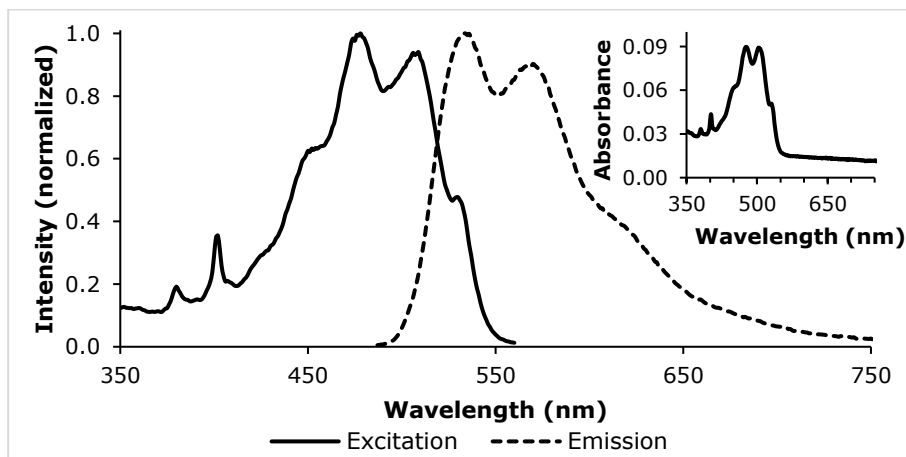


Figure S1: Excitation and emission scan for trimethylsilyl-protected **1F** in DCM. The insert shows the absorption spectrum in the same region.

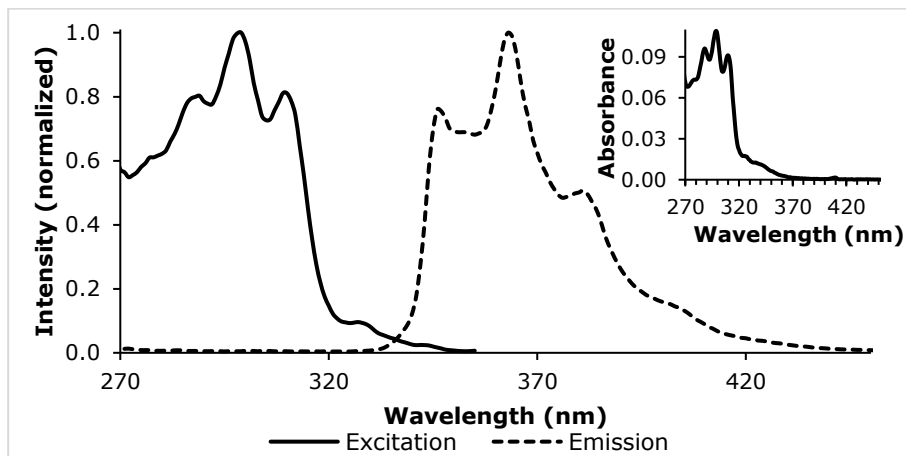


Figure S2: Excitation and emission scan for trimethylsilyl-protected **2F** in DCM. The insert shows the absorption spectrum in the same region.

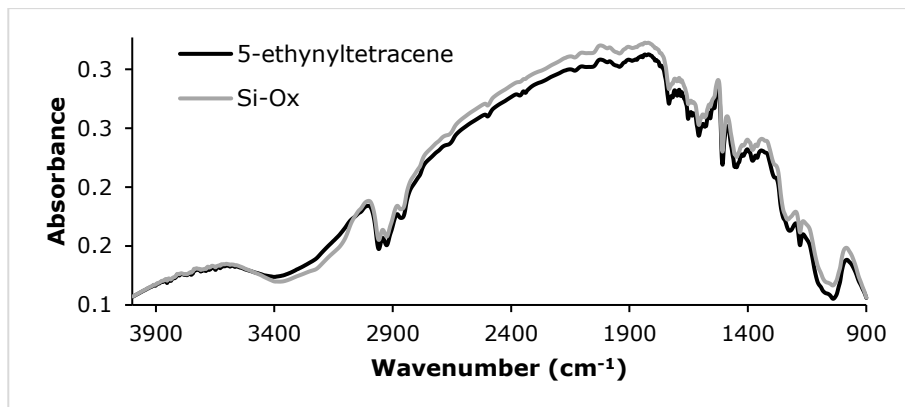


Figure S3: IR-RAS spectrum of a Si(111) surface functionalized with **1**. The spectrum of a cleaned, non-etched Si(111) is shown as a background.

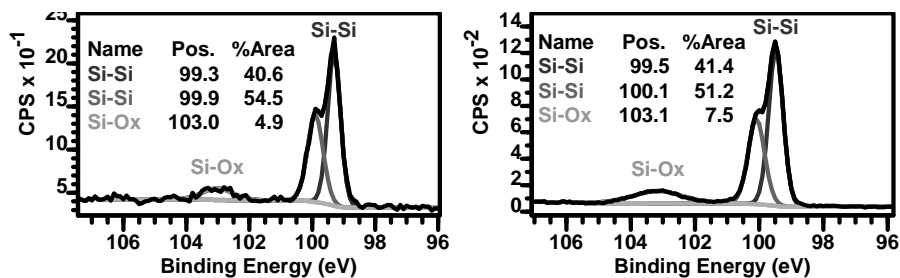


Figure S4: Si 2p narrow scans of non-backfilled surfaces functionalized with **1F** (left) and **2F** (right) after several weeks exposure to ambient atmosphere.

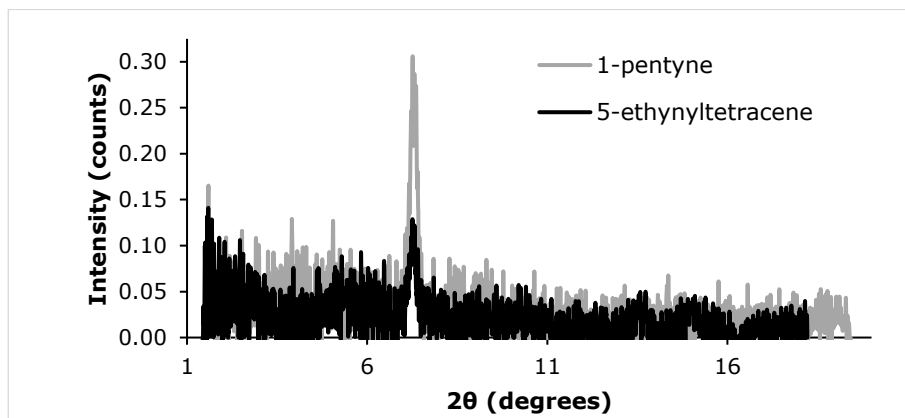


Figure S5: 2D XRD measurement on a surface functionalized with **1**. A spectrum of a surface functionalized with 1-pentyne is shown as a background spectrum.

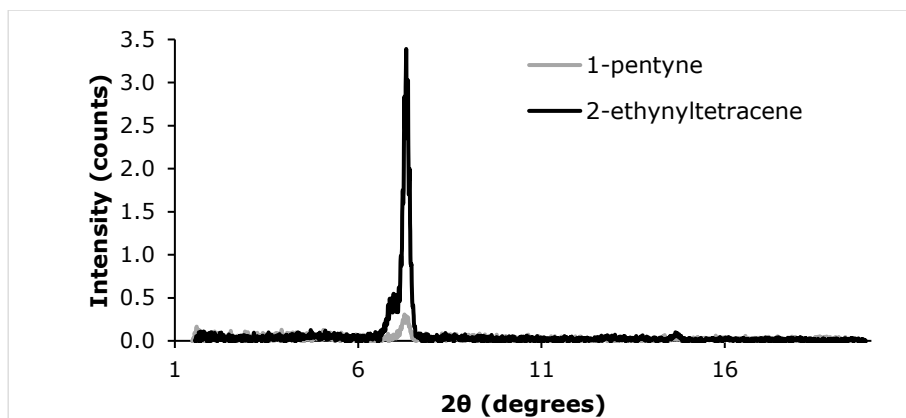


Figure S6: 2D XRD measurement on a surface functionalized with **2**. A spectrum of a surface functionalized with 1-pentyne is shown as a background spectrum.

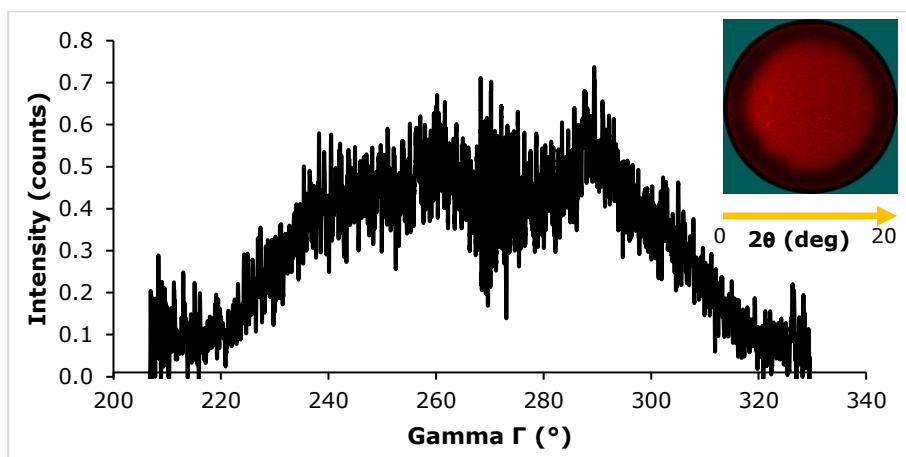


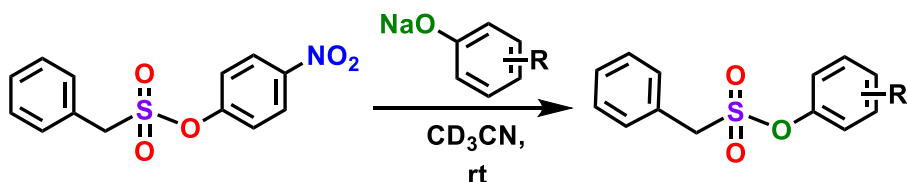
Figure S7: GIWAX spectrum of a surface functionalized with **1**, recorded at 7.3° 2θ. Data has been corrected for background signals by recording a background spectrum at a 2θ angle where no signal was present. The insert shows a picture of the surface during the GIWAX measurement, where a lighter colour indicates a higher intensity signal.

References

- (1) Kulkarni, G. C.; Morales-Cruz, J. L.; Hussain, W. A.; Garvey, I. J.; Plunkett, K. N. Electron Acceptors Based on Cyclopentannulated Tetracenes. (2018), *Synlett*, **29** (19), 2572–2576.
- (2) Korovina, N. V.; Das, S.; Nett, Z.; Feng, X.; Joy, J.; Haiges, R.; Krylov, A. I.; Bradforth, S. E.; Thompson, M. E. Singlet Fission in a Covalently Linked Cofacial Alkynyltetracene Dimer. (2016), *Journal of the American Chemical Society*, **138** (2), 617–627.
- (3) Zhao, L.; Kaiser, R. I.; Lu, W.; Ahmed, M.; Evseev, M. M.; Bashkirov, E. K.; Azyazov, V. N.; Tönshoff, C.; Reicherter, F.; Bettinger, H. F.; Mebel, A. M. A Free-Radical Prompted Barrierless Gas-Phase Synthesis of Pentacene. (2020), *Angewandte Chemie International Edition*, **59** (28), 11334–11338.
- (4) Woodward, S.; Ackermann, M.; Ahirwar, S. K.; Burroughs, L.; Garrett, M. R.; Ritchie, J.; Shine, J.; Tyril, B.; Simpson, K.; Woodward, P. Straightforward Synthesis of 2- and 2,8-Substituted Tetracenes. (2017), *Chemistry – A European Journal*, **23** (32), 7819–7824.
- (5) Schwaben, J.; Münster, N.; Klues, M.; Breuer, T.; Hofmann, P.; Harms, K.; Witte, G.; Koert, U. Efficient Syntheses of Novel Fluoro-Substituted Pentacenes and Azapentacenes: Molecular and Solid-State Properties. (2015), *Chemistry – A European Journal*, **21** (39), 13758–13771.

Chapter 4

Sulfur-Phenolate Exchange as a fluorine-free approach to S(VI) exchange chemistry on sulfonyl moieties



This Chapter was published as:

Alyssa F.J. van den Boom, Muthusamy Subramaniam and Han Zuilhof (2022); Sulfur-Phenolate Exchange as a fluorine-free approach to S(VI) exchange chemistry on sulfonyl moieties; *Organic Letters*, **24**, 8621-8626.
<https://pubs.acs.org/doi/10.1021/acs.orglett.2c03421>

Abstract: SuFEx chemistry has recently evolved as a next-generation click chemistry. However, in most SuFEx syntheses additional reagents/catalysts and carefully controlled conditions are still needed. Here, we aim to further generalize S(VI) exchange chemistry, using 4-nitrophenyl phenylmethanesulfonate as example, in which the nitrophenolate group is exchanged for a wide range of (substituted) phenols and alkyl alcohols. Quantitative yields were reached within 10 min under ambient conditions, and required only filtering through silica as work-up.

Over the past few decades, an ever-growing toolbox of click reactions has been developed, which has revolutionized the molecular sciences. Well-known examples are e.g. the copper(I)-catalyzed alkyne-azide cycloaddition, strain-promoted variants thereof, or thiol-ene radical additions.^{1,2} One of the most recent additions is the sulfur fluoride exchange (SuFEx) reaction, in which an S-F bond is replaced by an S-O or S-N bond.³ This reaction is both facile and high yielding, and has been shown to be highly useful for fields from medicinal chemistry to polymer chemistry.⁴⁻⁸ The original scope of the reaction was focused on silyl-protected phenols⁹⁻¹³ and (unprotected) amines.^{14,15} More recent extensions opened this up, and allowed for the first intrinsically enantiospecific click reaction, namely the catalyst-free reaction of (sodium) phenolates to chiral sulfonimidoyl fluorides.^{16,17} Furthermore, addition of hexamethyl disilazane and base as catalysts recently extended the scope to saturated alcohols,¹⁸ BF₃ catalysis allowed coupling of terminal alkynes,¹⁹ and the use of 1-hydroxybenzotriazole (HOBt) together with TMDS and DIPEA allowed the formation of sulfonamides.²⁰

While SuFEx chemistry is generally considered as fast and easy, the addition of extra reagents, catalysts, or use of inert atmosphere is typically needed to reach high yields [Examples of additional reagents or catalysts used in literature: BTMG (yield without 77%, yield with >99%);¹⁸ [Ph₃P=N-PPh₃]⁺[HF₂]⁻ (yield 99%);⁹ tris(dimethylamino)sulfonium bifluoride¹¹]. Finally, the involvement of fluorine does provide the S-F reagents with a remarkable combination of stability and specific reactivity, but makes the SuFEx chemistry less attractive from both an environmental and industrial point of view, due to the temporary formation of surface-etching fluoride anions, the toxicity of fluoride anions, and government regulations that increasingly restrict the use of fluorine-containing chemicals. Evidently, there is need for a catalyst-free, rapid, high-yielding and easy-to-handle S(VI) exchange chemistry that does not involve fluorine. Some important steps have already been taken in this direction, by the synthesis of 1-sulfonimidoyl- and 1-sulfamidoyl-3-methylimidazolium derivatives that can be used to produce sulfonimidamides and imidosulfuric diamides,²¹ and the use of sulfonyl-triazoles for the synthesis of sulfonyl esters.²²

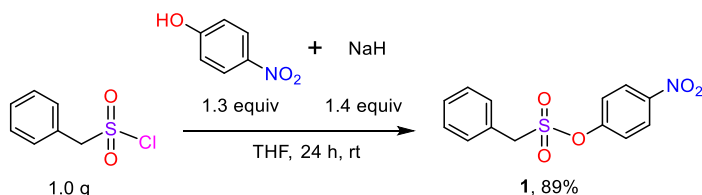


Figure 1. Synthesis of the starting compound 4-nitrophenyl phenylmethanesulfonate (**1**).

In this work, we hope to expand upon these first steps, by presenting a generalized, fluorine-free version of S(VI) exchange chemistry – a Sulfur Phenolate Exchange reaction (SuPhenEx) – for SO₂X moieties in which nitrophenolate is the leaving group instead of fluoride. This approach is similar to previous studies on sulfonimidoyl moieties.¹⁷ Using 4-nitrophenyl phenylmethanesulfonate (**1**) as starting material, we produce a wide range of products *via* a simple, uncatalyzed exchange reaction with a large selection of (natural) phenols and alkyl alcohols. The starting material for all reactions described hereafter, *i.e.*, 4-nitrophenyl phenylmethanesulfonate (**1**), was prepared on a multi-gram scale from phenylmethanesulfonyl chloride and 4-nitrophenol (Figure 1). The crystalline material showed good stability for multiple weeks under ambient conditions, while a solution of **1** in 20% DMSO in water was stable for at least 9 days without signs of degradation, clearly demonstrating the high stability and easy-to-handle nature of the starting material **1**, which allows bulk production and long-term storage. Compound **1** was then used to generate a large range of S(VI) exchange products via a phenolate exchange reaction (Table 1). This reaction hinges on the strong electron-withdrawing nature of the *p*-NO₂ group on the nitrophenolate, which makes it an excellent leaving group in the exchange reaction. As a small added benefit, the strong orange color of the displaced nitrophenolate allows rough tracking of the reaction progress by eye. The exchange reaction does also work starting from less electron-withdrawing groups, like 4-CN or 4-Cl, yet the use of these starting materials drastically increases the reaction time; the conversion to product **3a**, which takes <5 min using **1**, takes 20 min using **3k-p**, or 40 min using **3f** as a starting material. Still, the conversions remained clean, with typically 85-95% isolated yield and no by-products.

As can be seen in Table 1, most products were formed with excellent yields (100%, as determined by NMR) after just 5 min of reaction time. Previous procedures to produce already-described products from Table 1 involved stirring for 1-24 h, in dry solvents, on an ice bath, under inert atmosphere, using phenylmethanesulfonyl chloride as the starting material.²³ Here, we simply stir at room temperature under ambient atmosphere, using non-dried deuterated acetonitrile. Yet, for most known products from Table 1, the yield obtained using our simple and robust method is at least as high as yields obtained previously.^{18,24,25} Additionally, the reaction time is significantly shorter, and the work-up typically consisted only of a simple filtering step through a short silica plug. To confirm the accuracy of the NMR yield, we repeated several reactions on a 0.51 mmol **1** scale, and isolated the products. The thus obtained isolated yields – given in brackets in Table 1 – were all within 5% of the NMR yields reported above.

Sulfur-Phenolate Exchange as a fluorine-free approach to S(VI) exchange chemistry on sulfonyl moieties

Table 1. Reaction times and yields for the exchange reaction of **1** with a range of substrates.

1, 0.1 mmol	2, 1.1 equiv	3		
3a , < 5 min, 100% (95%)		3b-o , < 5 min, 100% 3b-m , < 5 min, 100% 3b-p , < 5 min, 100%	3c , 3 h, 75% ^[a] (75%)	3d , < 5 min, 100% (96%)
3e , < 5 min, 100% (100%)		3f , 75 min, 100% (99%)	3g-o , 10 min, 100% (95%) 3g-m , 7 min, 100% 3g-p , < 5 min, 100%	3h-o , 1 h, 100% 3h-m , < 5 min, 100% 3h-p , < 5 min, 100%
3i , < 5 min, 100%		3j , 30 min, 100% (100%)	3k-o , no reaction 3k-p , 24 h, 100%	3l , < 5 min, 100%
3m , 30 min, 100%		3n-o , partial degradation of 1 3n-p , degradation of 1	3o-o , < 5 min, 100% 3o-p , < 5 min, 100%	
3p , 1 h, 100%		3q , 10 min, 100% (96%)	3r , < 5 min, 100%	3s , 1 h, 100%
3t , degradation of 1		3u , 3 h, 90% (85%)	3v , < 5 min, 100%	3w , 3 h, 100%
3x , no reaction		3y , degradation of 1	3z , degradation of 1	3aa , 10 min, 100%
3ab , 1 h, 100% ^[b]		3ac , 1 h, 100% ^[b]	3ad , no reaction	3ae , 1 h, 100%
3af , 24 h, 100%				

Yield was determined by NMR measurements, after filtering through a short silica plug. For several compounds, an isolated yield was also determined (yield in brackets). ^[a] 75% yield for addition via the hydroxyl moiety, 25% yield for addition via the amine moiety. ^[b] 2.1 equiv of NaH, 2.1 equiv **1**, 2 equiv phenol.

The base used in this reaction to generate the reactive phenolate is somewhat dependent on the substrate. Often NaH is favored for two reasons: 1) the base is removed as hydrogen gas during the deprotonation step; 2) the sodium cation precipitates with the nitrophenolate, allowing this side product of the reaction to be filtered off. However, for some phenols containing additional base-sensitive groups (e.g. **2n**, **2y**, **2z**), treatment with NaH caused degradation. For phenols **2y** and **2z**,

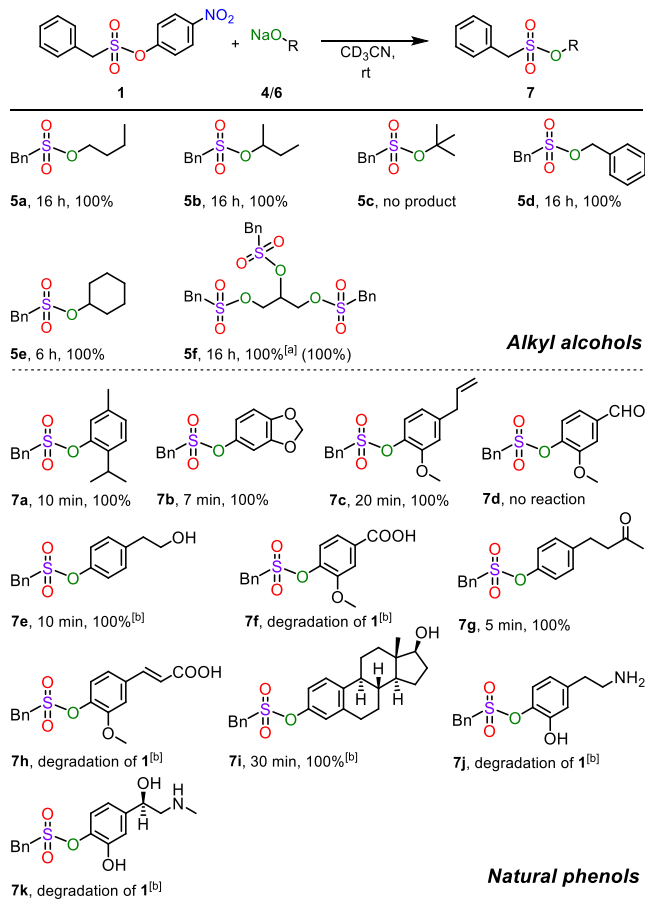
the milder organic bases BTMG or DBU were shown to be a better choice to provide the desired product, though for compound **3z**, purification to a pure product was not possible without causing (partial) degradation. Phenol **2n** still only showed degradation products regardless of base, but product **3y** could be isolated and purified following a reaction of **1** and **2y** with either BTMG or DBU. However, with these bases, a column or extraction was needed to purify the final product, instead of the simple filtering through silica required for NaH reactions. Several other common bases were also tested for their ability to perform the exchange reaction, but these typically yielded lower yields (Supporting Info, Table S1). Apart from this, there were also some phenols – those containing electron-withdrawing groups on the *ortho* position (**2k-o**, **2x**, **2ad**) – that did not react at all under the conditions specified above. This is attributed to the combination of reaction-diminishing steric and electronic effects, as phenols containing other bulky, but electron-donating, groups at the *ortho* position (**2o-o**, **2ae**) did give 100% yield, albeit at a reduced reaction rate. Here especially **2ae** is remarkable, as the corresponding reaction product on sulfonimidoyl fluorides did not give significant amounts of substitution products.¹⁶

After these first results, the scope of the exchange reaction was investigated, by testing the ability of the nitrophenolate on **1** to exchange with a range of alkyl alcohols **4a-f** and naturally occurring phenols **6a-k** (Table 2). Similar to the phenols in Table 1, a quantitative yield was obtained for most of the alkyl alcohols; only for the sterically hindered *tert*-butyl alcohol **4c**, no product was formed. The efficacy is perhaps most clearly shown for the reaction with glycerol (**4f**): even with only a minor excess of **1** (3.1 equiv), only one product, displaying triple addition of **1** to glycerol, is observed upon work-up. This marks a significant step forward, as under classical SuFEx conditions saturated alcohols are typically under-reactive, and can only be induced to react upon addition of both HMDS and BTMG, as shown by Moses' group.¹⁸ Here, no additional agents are needed to obtain quantitative sulfonate product formation with saturated alcohols.

While the yields for saturated alcohols are as high as observed for phenols, there is a significant increase in reaction time needed to reach full conversion: 6 – 16 h compared to the typically < 5 min for the phenols. This clearly shows the difference in reactivity between phenols and alkyl alcohols under these conditions. However, when 1 equiv of 15-crown-5 was added to capture the Na⁺ ion, the reaction time for alkyl alcohols (tested for **4a** and **4e**) is decreased to less than 15 min, close to the reaction times observed for most phenols. Such addition also helped to speed up the reaction for some of the slower-reacting phenols, such as **2w** or **2af**. As the addition of 15-crown-5 ether prevents the formation – and therefore precipitation – of the sodium 4-nitrophenolate salt, we conclude that, while advantageous from the point of easy purification, precipitation of the sodium nitrophenolate – as a means of removing one of the products of the reaction – is not an essential component of the driving force of the reaction.

Sulfur-Phenolate Exchange as a fluorine-free approach to S(VI) exchange chemistry on sulfonyl moieties

Table 2. Extension of scope of the S(VI) exchange reaction from **1**: saturated alcohols and natural phenols.



Yields were determined by ¹H NMR measurements. Reaction conditions: 0.10 mmol **1** and 1.1 equiv **4/6** in 0.6 ml CD₃CN. ^[a] 3 equiv NaH & 3.1 eq **1** used. ^[b] 2 equiv NaH used

When looking at the results for the naturally occurring phenols, a similar trend is observed as for phenols **2a-2af**. Again, phenols containing an additional base-sensitive acid group (**6f**, **6h**) show degradation upon interaction with NaH, while most other phenols again give quantitative yields. Also phenols with two hydroxyl groups (**6j** and **6k**) situated *ortho* to each other show degradation, though in this case this is likely due to a strong electronic repulsion between the additional (deprotonated) hydroxyl group on the attacking phenolate and the oxygen atoms on the sulfonyl group during the nucleophilic attack of the phenolate, as these atoms will be in close proximity to each other in the transition state. As a result of this strong electronic repulsion, the attacking phenolate cannot approach close enough to form the desired product, and degradation of **1** occurs instead. Finally, the phenol containing an aldehyde group (**6d**) gave no reaction, while this

functionality led to degradation before (**2n-p**). Apparently, the additional methoxy group on the *ortho*-position prevents degradation, yet the presence of the aldehyde moiety still prevents exchange with the nitrophenolate on **1**.

To investigate whether not just benzylic sulfonates, but also aryl sulfonates would undergo this transformation, we repeated the exchange reaction for phenols **2a**, **2e**, **2k-p**, and alcohol **4b** using 4-nitrophenyl 4-methylbenzene sulfonate. The selected phenols and alcohol represent the full range of electron-donating to electron-withdrawing aryl substituents, as well as an aliphatic alcohol. All reactions gave good yields, though the reaction times were increased compared to the reaction with **1**: 40 min for **2a** (100% yield), 10 min for **2e** (100% yield), 85% conversion after 5 days for **2k-p**, and 95% conversion after 5 days for **4b**. This indicates that, while aryl sulfonates can be used, the reactivity is greatly decreased compared to benzylic sulfonates.

To further explore the relevance of this reaction, we investigated its potential for dynamic covalent chemistry, as such a feature would significantly widen the applicability of this exchange chemistry in the field of materials and polymer science. In principle, a leaving group phenolate can – if it is sufficiently nucleophilic – re-attach to the sulfonate to regain the starting material. This was not observed for any of the phenols or alcohols tested here, as the nitro group on the nitrophenol has a much stronger electron-withdrawing effect than any other substituent or alcohol tested. However, for more nucleophilic phenolates such exchange might be feasible. So, to test this, product **3f** (1 equiv) was exposed to 1 equiv of NaH and 1 equiv of 4-bromophenol (**2h-p**). At the same time, product **3h-p** (1 equiv) was exposed to 1 equiv of NaH and 1 equiv of 4-chlorophenol (**2f**). As 4-bromophenol and 4-chlorophenol have a similar electron-withdrawing effect (Hammett parameter of 0.23 for both substituents),²⁶ an equilibrium between products **3f** and **3h-p** should be reached. Indeed, after 6 days of reaction time, a ratio of 1:1 **3f**:**3h-p** was found in both reaction mixtures. This proves that the phenol sulfonates undergo a dynamic covalent reaction – albeit slowly – at room temperature. In addition, the easy control of the driving force of the SuPhenEx reaction via the *para*-substituents on the nucleophile and/or leaving group allows fine tuning of e.g. the degree and rate of replacement. In order to increase the atom efficiency of the reaction, we have studied the recyclability of the sodium 4-nitrophenoxide used in the production of the starting material. We could recover > 85% of the 4-nitrophenol, which was used to make fresh starting material **1** (see Supporting Info).

In addition, the exchange reaction was tested for its ability to degrade a polysulfonate polymer. Such polymers have become easily available via SuFEx click chemistry, both in a step-growth¹¹ as well as in a chain-growth fashion.¹⁰ When the model polymer **8** ($M_n = 27$ kDa) was treated with 10 equiv of sodium phenolate in THF at 80 °C, the molecular weight of degraded products was reduced to ≤ 0.7 kDa within 24 h (as measured by gel permeation chromatography), indicating the complete degradation of polymer **8** (Figure 2). Furthermore, LC-MS analysis of the

degraded polymer showed fragments **9**, **10** and **11** as the major degradation products (Figure 3). Additionally, trace amounts of product **12** as observed in LC/MS confirmed the formation of also this degradation product. Based on this, we propose a possible degradation pathway of the polymer (Figure 3, see Supporting Info for more details). This result shows the potential of the reversible SuPhenEx reaction in depolymerization.

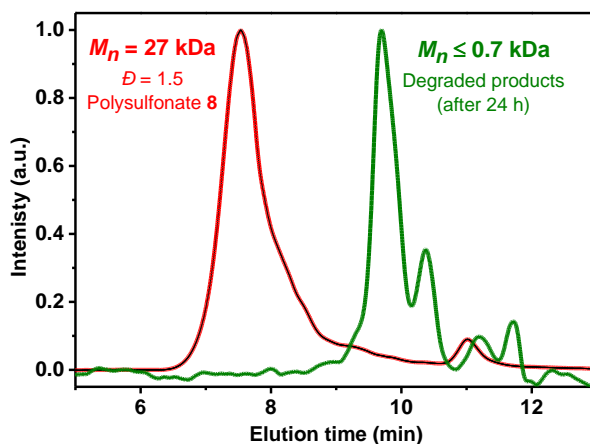


Figure 2. GPC traces of polymer and degraded products.

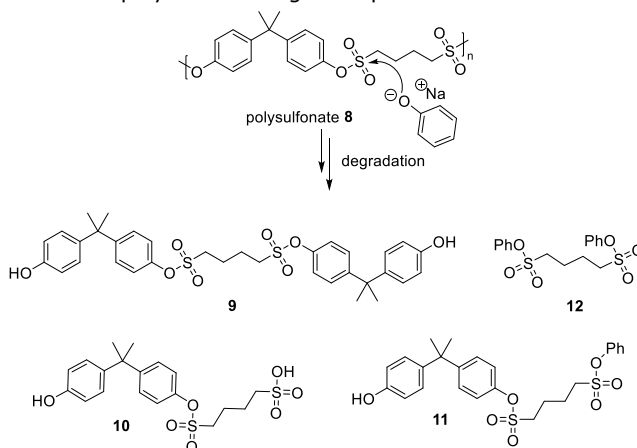


Figure 3. Degradation of polysulfonate **8**.

In conclusion, we provide a simple, fast, and highly efficient click reaction to create a wide range of S(VI) alcohol exchange compounds starting from a single easy-to-produce and stable starting material. The reaction is fluorine-free, fast and typically quantitative, the work-up facile, the driving force tunable, and the reaction shows a very wide functional group tolerance, which we thus expect to have significant use in a wide range of the molecular sciences.

References

- (1) Xi, W.; Scott, T. F.; Kloxin, C. J.; Bowman, C. N. Click Chemistry in Materials Science. *Adv. Funct. Mater.* **2014**, *24*, 2572–2590.
- (2) Hoyle, C. E.; Bowman, C. N. Thiol-Ene Click Chemistry. *Angew. Chem. Int. Ed.* **2010**, *49*, 1540–1573.
- (3) Dong, J.; Krasnova, L.; Finn, M. G.; Barry Sharpless, K. Sulfur(VI) Fluoride Exchange (SuFEx): Another Good Reaction for Click Chemistry. *Angew. Chem. Int. Ed.* **2014**, *53*, 9430–9448.
- (4) Xu, L.; Wu, P.; Dong, J. New Polymers From SuFEx Click Chemistry: Syntheses and Perspectives. *Synth. Polym. Chem. Innov. Outlook* **2019**, No. 32, 1–31.
- (5) Smedley, C. J.; Li, G.; Barrow, A. S.; Gialelis, T. L.; Giel, M.-C.; Ottonello, A.; Cheng, Y.; Kitamura, S.; Wolan, D. W.; Sharpless, K. B.; Moses, J. E. Diversity Oriented Clicking (DOC): Divergent Synthesis of SuFExable Pharmacophores from 2-Substituted-Alkynyl-1-Sulfonyl Fluoride (SASF) Hubs. *Angew. Chem. Int. Ed.* **2020**, *59*, 12460–12469.
- (6) Liang, D. D.; Pujari, S. P.; Subramaniam, M.; Besten, M.; Zuilhof, H. Configurationally Chiral SuFEx-Based Polymers. *Angew. Chem. Int. Ed.* **2022**, *61*, e202116158.
- (7) Li, S.; Li, G.; Gao, B.; Pujari, S. P.; Chen, X.; Kim, H.; Zhou, F.; Klivansky, L. M.; Liu, Y.; Driss, H.; Liang, D. D.; Lu, J.; Wu, P.; Zuilhof, H.; Moses, J.; Sharpless, K. B. SuFExable Polymers with Helical Structures Derived from Thionyl Tetrafluoride. *Nat. Chem.* **2021**, *13*, 858–867.
- (8) Barrow, A. S.; Smedley, C. J.; Zheng, Q.; Li, S.; Dong, J.; Moses, J. E. The Growing Applications of SuFEx Click Chemistry. *Chem. Soc. Rev.* **2019**, *48*, 4731–4758.
- (9) Wang, H.; Zhou, F.; Ren, G.; Zheng, Q.; Chen, H.; Gao, B.; Klivansky, L.; Liu, Y.; Wu, B.; Xu, Q.; Lu, J.; Sharpless, K. B.; Wu, P. SuFEx-Based Polysulfonate Formation from Ethenesulfonyl Fluoride–Amine Adducts. *Angew. Chem. Int. Ed.* **2017**, *56*, 11203–11208.
- (10) (a) Kim, H.; Zhao, J.; Bae, J.; Klivansky, L. M.; Dailing, E. A.; Liu, Y.; Cappiello, J. R.; Sharpless, K. B.; Wu, P. Chain-Growth Sulfur(VI) Fluoride Exchange Polycondensation: Molecular Weight Control and Synthesis of Degradable Polysulfates. *ACS Cent. Sci.* **2021**, *7*, 1919–1928. (b) Subramaniam, M.; Ruggeri, F.S.; Zuilhof, H. Degradable click reaction-based polymers as highly functional materials. *Matter.* **2022**, *3*, 2490–2492.
- (11) Gao, B.; Zhang, L.; Zheng, Q.; Zhou, F.; Klivansky, L. M.; Lu, J.; Liu, Y.; Dong, J.; Wu, P.; Sharpless, K. B. Bifluoride-Catalysed Sulfur(VI) Fluoride Exchange Reaction for the Synthesis of Polysulfates and Polysulfonates. *Nat. Chem.* **2017**, *9*, 1083–1088.
- (12) Randall, J. D.; Eyckens, D. J.; Stojcevski, F.; Francis, P. S.; Doeven, E. H.; Barlow, A. J.; Barrow, A. S.; Arnold, C. L.; Moses, J. E.; Henderson, L. C. Modification of Carbon Fibre Surfaces by Sulfur-Fluoride Exchange Click Chemistry. *ChemPhysChem* **2018**, *19*, 3176–3181.
- (13) Gembus, V.; Marsais, F.; Levacher, V. An Efficient Organocatalyzed

- Interconversion of Silyl Ethers to Tosylates Using DBU and P-Toluenesulfonyl Fluoride. *Synlett* **2008**, No. 10, 1463–1466.
- (14) Gahtory, D.; Sen, R.; Pujari, S.; Li, S.; Zheng, Q.; Moses, J. E.; Sharpless, K. B.; Zuilhof, H. Quantitative and Orthogonal Formation and Reactivity of SuFEx Platforms. *Chem. - A Eur. J.* **2018**, *24*, 10550–10556.
 - (15) Liu, F.; Wang, H.; Li, S.; Bare, G. A. L.; Chen, X.; Wang, C.; Moses, J. E.; Wu, P.; Sharpless, K. B. Biocompatible SuFEx Click Chemistry: Thionyl Tetrafluoride (SOF₄)-Derived Connective Hubs for Bioconjugation to DNA and Proteins. *Angew. Chem. Int. Ed.* **2019**, *58*, 8029–8033.
 - (16) Liang, D. D.; Streefkerk, D. E.; Jordaan, D.; Wagemakers, J.; Baggerman, J.; Zuilhof, H. Silicon-Free SuFEx Reactions of Sulfonimidoyl Fluorides: Scope, Enantioselectivity, and Mechanism. *Angew. Chem. Int. Ed.* **2020**, *59*, 7494–7500.
 - (17) Chao, Y.; Krishna, A.; Subramaniam, M.; Liang, D.-D.; Pujari, S. P.; Sue, A. C.-H.; Li, G.; Miloserdov, F. M.; Zuilhof, H. Sulfur-Phenolate Exchange: SuFEx-Derived Dynamic Covalent Reactions and Degradation of SuFEx Polymers. *Angew. Chem. Int. Ed.* **2022**, *61*, e202207456.
 - (18) Smedley, C. J.; Homer, J. A.; Gialelis, T. L.; Barrow, A. S.; Koelln, R. A.; Moses, J. E. Accelerated SuFEx Click Chemistry For Modular Synthesis. *Angew. Chem. Int. Ed.* **2022**, *61*, e202112375.
 - (19) Zeng, D.; Ma, Y.; Deng, W.-P.; Wang, M.; Jiang, X. Divergent Sulfur(VI) Fluoride Exchange Linkage of Sulfonimidoyl Fluorides and Alkynes. *Nat. Synth.* **2022**, *1*, 455–463.
 - (20) Wei, M.; Liang, D.; Cao, X.; Luo, W.; Ma, G.; Liu, Z.; Li, L. A Broad-Spectrum Catalytic Amidation of Sulfonyl Fluorides and Fluorosulfates. *Angew. Chem. Int. Ed.* **2021**, *60*, 7397–7404.
 - (21) Zasukha, S. V.; Timoshenko, V. M.; Tolmachev, A. A.; Pivnytska, V. O.; Gavrylenko, O.; Zherish, S.; Shermolovich, Y.; Grygorenko, O. O. Sulfonimidamides and Imidosulfuric Diamides: Compounds from an Underexplored Part of Biologically Relevant Chemical Space. *Chem. - A Eur. J.* **2019**, *25*, 6928–6940.
 - (22) Borne, A. L.; Brulet, J. W.; Yuan, K.; Hsu, K. L. Development and Biological Applications of Sulfur-Triazole Exchange (SuTEx) Chemistry. *RSC Chem. Biol.* **2021**, *2*, 322–337.
 - (23) (a) Alonso, F.; Moglie, Y.; Vitale, C.; Radivoy, G.; Yus, M. A New Mild Deprotecting Method for O-Benzylsulfonyl Phenols and Alcohols Based on a DTBB-Catalyzed Lithiation. *Synthesis*. **2005**, No. 12, 1971–1976. (b) Davy, M. B.; Douglas, K. T.; Loran, J. S.; Steltner, A.; Williams, A. Elimination-Addition Mechanisms of Acyl Group Transfer: Hydrolysis and Aminolysis of Aryl Phenylmethanesulfonates. *J. Am. Chem. Soc.* **1977**, *99*, 1196–1206. (c) Dai, Q.; Liu, L.; Zhang, J. Palladium / Xiao-Phos-Catalyzed Kinetic Resolution of Sec -Phosphine Oxides by P -Benzylation. *Angew. Chem. Int. Ed.* **2021**, *60*, 27247–27252. (d) Mahapatra, M. K.; Kumar, R.; Kumar, M. Synthesis, Biological Evaluation and in Silico Studies of 5-(3-Methoxybenzylidene)Thiazolidine-2,4-Dione Analogues as PTP1B Inhibitors. *Bioorg. Chem.* **2017**, *71*, 1–9. (e) Maji, A.; Bhaskararao, B.; Singha, S.; Sunoj, R. B.; Maiti, D. Directing Group Assisted: Meta -Hydroxylation by C-H Activation.

- Chem. Sci.* **2016**, *7*, 3147–3153. (f) Moghaddam, F. M.; Hoor, A. A.; Dekamin, M. G. Microwave-Promoted Pseudo-Thia-Fries Rearrangement of Aryl Benzyldisulfonates; Highly Reactive Benzyl Cation Generation. *J. Sulfur Chem.* **2004**, *25*, 125–130. (g) Truce, W. E.; Christensen, L. W. Base-Induced α -Sulfonylation of Aryl Alkanedisulfonates. *J. Org. Chem.* **1970**, *35*, 3968–3970.
- (24) Gao, J.; Pan, X.; Liu, J.; Lai, J.; Chang, L.; Yuan, G. Iodine-Induced Synthesis of Sulfonate Esters from Sodium Sulfinates and Phenols under Mild Conditions. *RSC Adv.* **2015**, *5*, 27439–27442.
- (25) Bahrami, K.; Khodaei, M. M.; Abbasi, J. Synthesis of Sulfonamides and Sulfonic Esters via Reaction of Amines and Phenols with Thiols Using H_2O_2 - POCl_3 System. *Tetrahedron* **2012**, *68*, 5095–5101.
- (26) Hansch, C.; Leo, A.; Taft, R. W. A Survey of Hammett Substituent Constants and Resonance and Field Parameters. *Chem. Rev.* **1991**, *91*, 165–195.

Supporting Information

General information

Chemicals

Sodium hydride (60% dispersion in mineral oil), 4-nitrophenol, phenylmethylsulfonyl fluoride, phenol, 4-methoxyphenol, 4-cyanophenol, 4-chlorophenol, 4-aminophenol, p-cresol, m-cresol, 4-hydroxybenzamide, 3,4,5-trifluorophenol, 3,5-bis(trifluoromethyl)phenol, 4-bromophenol, 2-bromophenol, 3-bromophenol, 4-fluorophenol, 2-fluorophenol, 4-methyl-2-nitrophenol, acetaminophen, 4-hydroxybenzyl alcohol, resorcinol, vanillic acid, bisphenol A, 2-cyanophenol, sesamol, trans-ferulic acid, salicylaldehyde, vanillin, β -estradiol, dopamine hydrochloride, and (–)-epinephrine were bought from Merck Life Science N.V.; acetonitrile-d₃, 2,6-dichlorophenol, 4-hydroxybenzoic acid, 3-fluorophenol, and 4-hydroxyphenylboronic acid were bought from Fisher Scientific B.V.; o-cresol, 2,4,6-trimethylphenol, 3-hydroxypyridine, 2-tert-butylphenol, 4-hydroxybenzaldehyde, eugenol, 4-(4-hydroxyphenyl)-2-butanone, 2-(4-hydroxyphenyl)ethanol, and thymol were bought from TCI EUROPE N.V.; 4-(trifluoromethoxy)phenol and 4-((4-isopropoxyphenyl)sulfonyl) phenol were bought from Fluorochem Ltd; 4-iodophenol was bought from VWR International B.V. All chemicals were used as received.

Analysis

NMR measurements were conducted on a 400 MHz Bruker Avance III at 298K, and the resulting data were analyzed using MestReNova software, version 14.1.0-24037. Spectra were calibrated relative to signals corresponding to the non-deuterated solvents (CH₃CN solvent peak) – at 1.94 ppm for ¹H spectra, and 1.32 ppm for ¹³C spectra. For spectra measured in CDCl₃ calibration was performed with the CHCl₃ peaks at 7.26 ppm (¹H spectra) and 77.16 ppm (¹³C spectra). ¹⁹F spectra were not calibrated. Abbreviations used in the description of NMR data are as follows: chemical shift (δ = ppm), multiplicity (s = singlet, d = doublet, t = triplet, q = quartet, p = pentet, sextet = sext, h = heptet, dt = doublet of triplets, m = multiplet, br = broadened), coupling constant (*J*, Hz).

High-resolution mass spectra (HRMS) were recorded on a Thermo Scientific Exactive 1.1 with an orbitrap mass analyzer, using a DART gun from Ion Sense. The temperature of the DART gun was set to 400 °C, with a helium gas flow. Data were analyzed using Thermo Xcalibur software, version 2.2 SP1.48.

IR spectra were recorded on a Bruker Tensor 27 spectrometer equipped with a diamond ATR accessory (64 scans; 4 cm⁻¹ resolution; range 4000-350 cm⁻¹). Strong

or indicative peaks in the region 4000-1000 cm^{-1} are mentioned for each novel compound.

TLC analysis was performed on pre-coated, alumina-backed silica gel plates. TLC plates were analyzed by UV fluorescence (254 nm) or KMnO_4 stain followed by heating.

Column chromatography for isolated yields and full characterization was performed using silica (40-63 μm , 230-400 mesh) and 20-50% ethyl acetate in hexane, depending on the polarity of the product. To perform flash chromatography, a connector connected to a compressed-air flow was installed on the column.

Gel Permeation Chromatography (GPC). The polymer molecular weight (M_n^{PS}) and polydispersity (Đ) relative to a set of polystyrenes were measured on an Agilent Technologies 1200 Gel Permeation Chromatography (GPC) system. It was equipped with a diode-array detector (DAD, G1315D, data obtained using a 250 nm, 260 nm, and 290 nm UV-vis detector), a refractive index detector (RID, G1362A), autosampler (ALS, G1329A), bin pump (G1312A), solvent degasser (G1322A). GPC equipped with VARIAN GPC/SEC column from PLgel 5 μm MIXED-D (300 \times 7.5 mm) part number: PL1110-6504. The system was calibrated with EasyVial PS-M and EasyVial PS-L polystyrene standards (Agilent Technologies), GPC polystyrene standards with a combined range from M_p 400 to 2,000,000 Da (Fluka). HPLC-grade *N,N*-dimethylformamide (DMF, Biosolve®, unstabilized, HPLC grade) with 0.01% LiBr (ReagentPlus®, $\geq 99\%$ from Sigma-Aldrich) was used as mobile phase for determining the molecular weight polymers. The elution rate was 1.0 mL/min (all GPC performed at room temperature).

Liquid chromatography–mass spectrometry LC-MS analysis was performed using Agilent 1290 Infinity UHPLC system and Thermo Scientific Q Exactive Focus Mass Spectrometer in electrospray ionization (ESI^+) mode. LC-MS grade acetonitrile (HiPerSolv CHROMANORM®) and millipore water with 0.1 % formic acid were used as mobile phase in gradient flow. Eclipse XDB C-18 HPLC column was used with flow rate 0.4 mL/min, oven temperature 25 $^\circ\text{C}$, detector wavelength 240 nm and 280 nm.

Synthetic procedures

Unless mentioned otherwise, all reactions were performed at room temperature under ambient atmosphere.

4-Nitrophenyl phenylmethanesulfonate **1**

NaH (60% in oil, 293 mg, 7.34 mmol, 1.4 equiv) was added to 4-nitrophenol (948 mg, 6.82 mmol, 1.3 equiv) in 80 ml of dry tetrahydrofuran, and the solution was stirred for 5 min. Next, phenylmethanesulfonyl chloride (1.0 g, 5.25 mmol, 1.0 equiv) was added, and stirring was continued for 24 h. Then, the reaction mixture was diluted with 150 ml of DCM and transferred to a separatory funnel, where it was washed with water (3 × 150 ml). The organic phase was isolated, dried over sodium sulphate, and the solvent was evaporated. Next, the product was further purified by column chromatography (n-hex/EA) (using a Biotage® system and SiliCycle® precast silica columns (200–300 mesh or 300–400 mesh)) to yield compound **1** (1.37 g, 89%) as white crystals.

General procedure for the synthesis of products (for NMR screening)

In a typical exchange reaction, 5 mg of NaH (0.124 mmol, 1.2 equiv) and 0.113 mmol (1.1 equiv) of phenol/alcohol were dissolved in 0.9 mL of CD₃CN, and the reaction was stirred for ~5 min to generate the phenolate. After this time, 30 mg (0.103 mmol, 1.0 equiv) of **1** was added, and stirring was continued. TLC (25% ethyl acetate in hexane) was used to monitor the progress of the reaction by the disappearance of the spot belonging to 4-nitrophenyl phenylmethanesulfonate. When this spot had fully disappeared, the reaction mixture was filtered into an NMR tube through a short silica plug, to remove the sodium nitrophenolate. The filtered reaction mixture was then directly analyzed using ¹H NMR. No internal standard was needed in this case, as the sodium nitrophenolate was filtered off, and no other side products – except in the case of degradation – are formed during the reaction. As a result, the reaction mixture only contains the product and any remaining starting material, both of which provide well-separated signals in ¹H NMR. The yield could therefore be determined by the disappearance of the signals belonging to 4-nitrophenol, with a simultaneous appearance of product signals. A reference spectrum of the reactant phenol was recorded in all cases, and successful binding was further confirmed by a change in chemical shift for the signals belonging to the added phenol upon attachment to the S(VI) hub. When the reaction was filtered prematurely – or when conversion was <100% – signals from an attached nitrophenol group were still visible (though with a lower integral value), and the product signals of the partially attached phenol had lower integrals than expected based on full conversion. When degradation took place, no product signals were observed, and signals from the starting material had shifted or disappeared.

Products for isolated yields and full characterization

Compounds for which the isolated yield was determined, and novel compounds that had to be characterized more extensively, were synthesized in the same way as described above for the NMR products, using non-deuterated acetonitrile as the solvent, on a scale of 150 mg (0.51 mmol) of **1**. After the reaction was completed,

the solvent was evaporated, and the products were purified using flash column chromatography (silica gel) with 25%-40% ethyl acetate in hexane, depending on the polarity of the product. For highly polar products (e.g. **7i**), 5% methanol in DCM was used as the mobile phase.

Reaction with 2-tert-butyl-1,1,3,3-tetramethylguanidine (BTMG) or DBU

25 μ l of BTMG or 17.5 μ l of DBU (0.117 mmol, 1.1 equiv) and 0.113 mmol (1.1 equiv) of phenol were dissolved in 0.9 mL of CD₃CN, and the reaction was stirred for ~10 min to generate the phenolate. After this time, 30 mg (0.103 mmol, 1 equiv) of **1** was added, and stirring was continued. TLC (25% ethyl acetate in hexane) was used to monitor the progress of the reaction by the disappearance of the spot belonging to 4-nitrophenyl phenylmethanesulfonate. When this spot had fully disappeared, the reaction mixture was either transferred into an NMR tube for direct analysis using ¹H NMR, or purified for characterization.

Base screening

For the base screening, the same protocol was used as described above for BTMG, with a few adjustments: 0.117 mmol of the base mentioned in the left column of Table S1 was used instead of BTMG; compound **1** was added after 20 min instead of 10; and the exchange reaction after addition of **1** was run for 15 min, before the reaction mixture was filtered into an NMR tube for analysis.

Reaction with 4-cyanophenyl- or 4-chlorophenyl phenylmethanesulfonate

Reactions using either 4-cyanophenyl phenylmethanesulfonate or 4-chlorophenyl phenylmethanesulfonate as starting material (instead of **1**) were performed in the same way as described in the general procedure, though CH₃CN was used instead of CD₃CN. After synthesis had been completed, the solvent was evaporated on a rotavapor, and the products were purified using flash column chromatography (silica gel, 30% ethyl acetate in hexane).

Reaction with 4-nitrophenyl 4-methylbenzenesulfonate

Reactions performed with 4-nitrophenyl 4-methylbenzenesulfonate instead of **1** as a starting material were performed as described in the general procedure, on a scale of 90 mg (0.307 mmol) 4-nitrophenyl 4-methylbenzenesulfonate, and using CH₃CN as the solvent. When full conversion was reached, the solvent was evaporated on a rotavapor, and the crude product was purified using flash column chromatography (silica gel, 30% ethyl acetate in hexane).

Hydrolytic stability

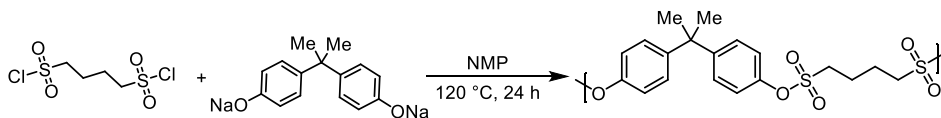
To test the hydrolytic stability of compound **1**, 50 mg of **1** was added to 5 ml of a 20% solution of DMSO in water. As compound **1** does not dissolve in this solution, the resulting suspension was stirred vigorously on a stir plate. Degradation of **1**

was followed by absorption measurements on a spectrophotometer. The increase in absorption arising from the nitrophenol degradation product was taken as a measure for the amount of degradation.

Recycling experiment

The starting material **1** (1.0 g, 3.41 mmol, 1 equiv) was added to a stirred solution of sodium phenolate (0.395 g, 3.41 mmol, 1 equiv) in dry CH₃CN (15 mL) and allowed to stir for an hour. The reaction mixture was quenched with water (100 mL), diluted with CH₂Cl₂ (100 mL) and adjusted to pH = 10 with 1 M NaOH (aq). Then the aqueous layer was separated, diluted with CH₂Cl₂ (100 mL), adjusted to pH = 6 with 1 M NaOH (aq) and two layers were separated. The aqueous layer was extracted with CH₂Cl₂ (2 × 30 mL) and the combined organic layers were dried over Na₂SO₄ and concentrated under vacuum to give 4-nitrophenol (0.408 g, 86%). This 4-nitrophenol was reacted to NaH (60% in oil, 164 mg, 4.10 mmol, 1.4 equiv) followed by phenylmethanesulfonyl chloride (559 mg, 2.93 mmol, 1.0 equiv) in dry THF (10 mL) to prepare the fresh starting material **1** (705 mg, 82%).

Polymer synthesis

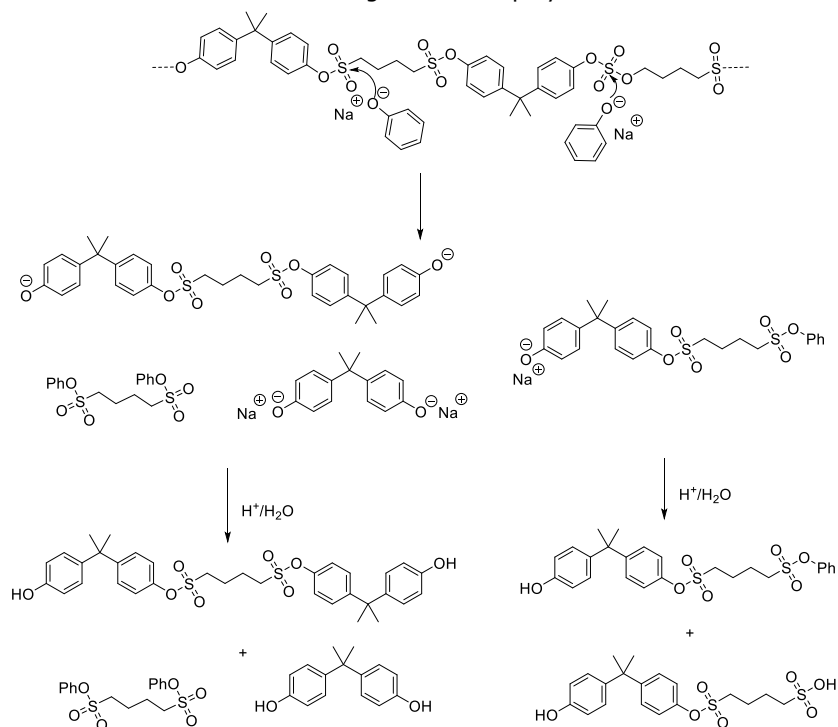


Inside an argon-filled glovebox (MBRAUN's MB 20 G-LMF gas purifier with H₂O and O₂ values of <0.1 ppm), butane-1,4-disulfonyl dichloride (0.5 g, 1.96 mmol, 1 equiv) and disodium bis-phenolate (0.53 g, 1.96 mmol, 1 equiv) were added in a 5 mL screw-capped glass vial equipped with a magnetic stir bar. 1.25 mL of anhydrous *N*-methyl-2-pyrrolidone (Thermo Scientific 99.9+% Extra Dry over Molecular Sieve, AcroSeal®) was added, and the vial was taken out of the glovebox. The reaction mixture was heated to 120 °C using an oil bath, and stirred for 24 h, during which course the reaction mixture turned viscous. Next, the reaction mixture was cooled, and 4 mL DMF was added to dissolve the crude polymer. The resulting solution was poured slowly into 30 mL of MeOH under constant stirring. After a precipitate formed, the stirring was continued for another 10 min. The formed precipitate was then allowed to sediment for 10 min, after which the methanol layer was removed and a minimal amount of DMF was added to re-dissolve the precipitate. This precipitate, sediment, and re-dissolve cycle was repeated, for a total of 4 cycles. Afterwards, the polymer was purified by dialysis (Sigma-Aldrich, Pur-A-Lyzer™ Mega 6000) in DMSO, and subsequently used for degradation experiments. The molecular weight M_n of polymer **8** was found to be 27 kDa ($\mathcal{D} = 1.54$) with GPC measurement.

Degradation of polysulfonate **8**

NaH (9.8 mg, 0.24 mmol, 10 equiv) was added to phenol (23 mg, 0.24 mmol, 10 equiv) in 1 ml of tetrahydrofuran, and the solution was stirred for 5 min. Next, polysulfonate **8** (10 mg, 1.0 equiv) was added, and the stirring was continued for 24 h at 80 °C in an oil bath. Then the mixture was diluted with DCM (3 mL) and water (3 mL), adjusted to pH ~ 5 with 0.05 M HCl. Then, the organic layer was washed with water (2 × 3 mL), dried over Na₂SO₄, and used for GPC and LC-MS analysis.

Plausible mechanism for the degradation of polymer **8**:



Supporting tables & figures

Hydrolytic stability

To measure the degradation of **1**, the optical absorption at 418 nm was followed, as at this wavelength **1** does not have any significant absorption (Figure S1). The degree of degradation (in %) was calculated using a calibration curve of 4-nitrophenol in 20% DMSO in water.

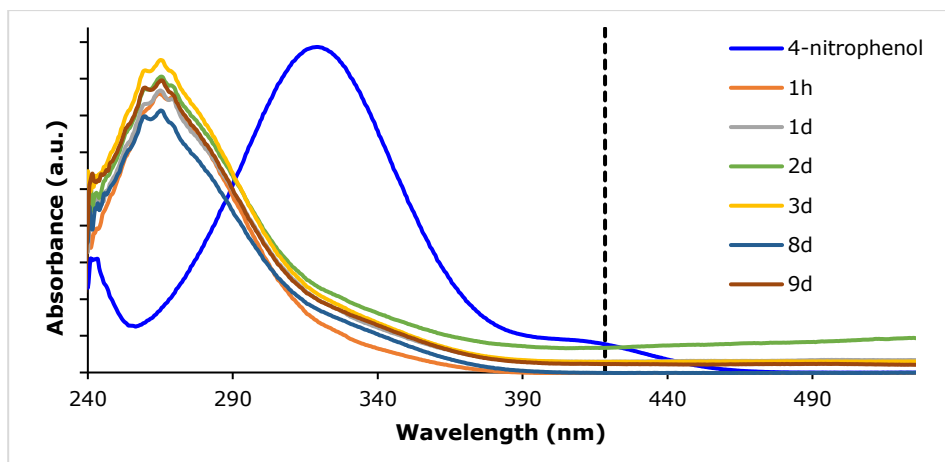


Figure S1: absorption spectra of **1** in 20% DMSO in water after different exposure times. The spectrum of 4-nitrophenol is shown in blue. The vertical dashed line indicates the wavelength at which the amount of degradation was determined (418 nm).

The results after 9 days of exposure to 20% DMSO in water show only minimal degradation (<0.09%, Figure S2). However, the actual degradation is even lower, as the absorption across the whole spectrum was increased for several time points, due to the turbidity of the sample. This can also be clearly seen in Figure S1 above for the spectra of *e.g.* 2d, 3d, and 9d.

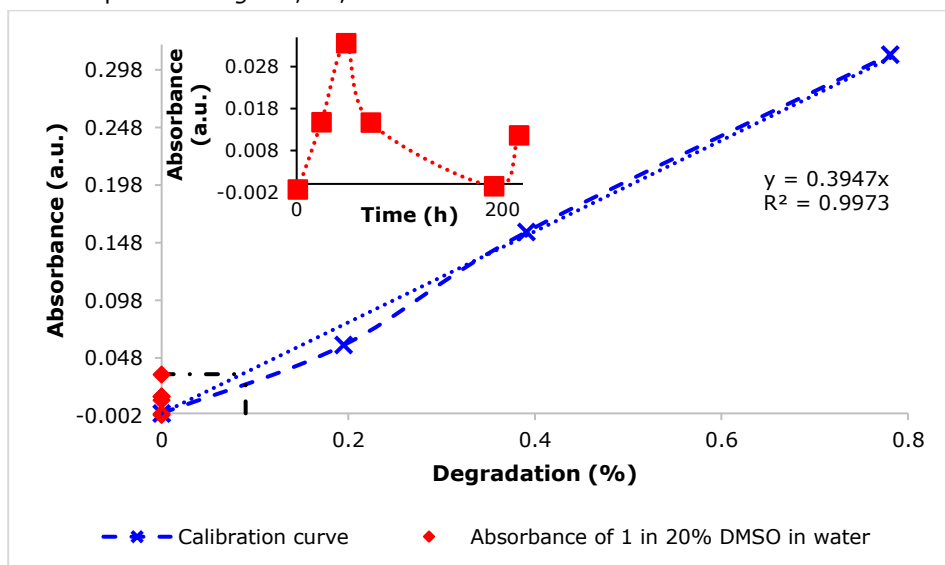


Figure S2: Optical absorption values at 418 nm for **1** in 20% DMSO in water, compared to the absorption of different concentrations of 4-nitrophenol in the same solvent mixture (calibration curve). The insert shows the absorption at 418 nm over time, for the solution of **1** in 20% DMSO in water.

An NMR spectrum taken after 9 days of the exposed sample confirms no degradation has taken place.

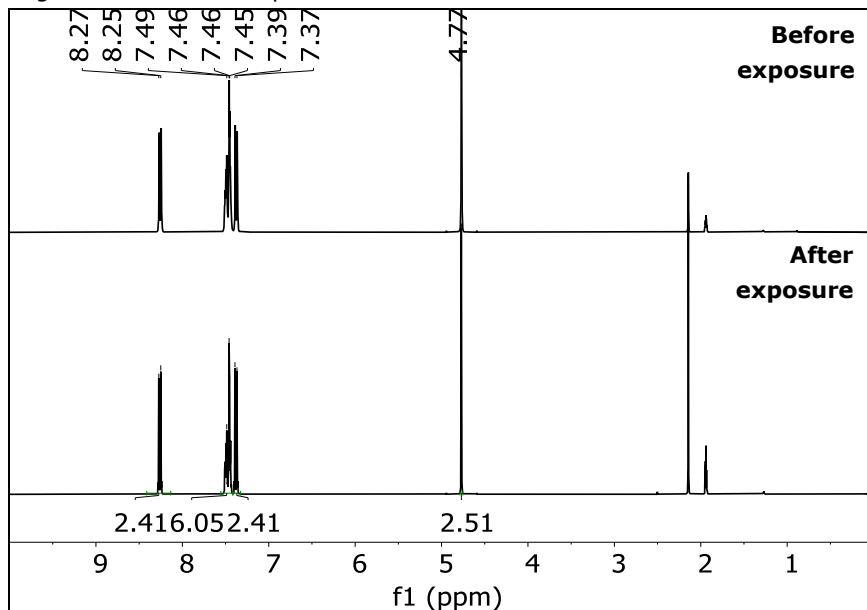


Figure S3: ^1H NMR spectrum (400 MHz, CD_3CN) of **1** before (blue upper spectrum) and after (red bottom spectrum) 9 days exposure to a 20% solution of DMSO in water.

Base screening

In the table below, conversion refers to the percentage of **1** that has reacted, while yield refers to the percentage of the desired product found in the reaction mixture. In cases where the conversion is higher than the yield, side reactions or degradation of **1** occurred.

Table S1: Overview of common bases tested for the exchange reaction of **1** with phenol.

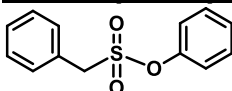
<p>2a, 1.1 equiv 1.2 equiv 1, 1 equiv 3a</p>		
Base	Yield (%)	Conversion (%)
Sodium hydride (NaH)	100	100
Potassium hydride (KH)	Degraded	100
Lithium hydride (LiH)	50	50
Potassium hydroxide (KOH)	55	55
Cesium hydroxide monohydrate ($\text{CsOH} \cdot \text{H}_2\text{O}$)	84	84

Potassium tert-butoxide (KOtBu)	25	100
Lithium diisopropylamide (LDA)	Degraded	100
Triethylamine (Et) ₃ N	53	53
N,N-Diisopropylethylamine (DIPEA)	46	46
2-tert-Butyl-1,1,3,3-tetramethylguanidine (BTMG)	100	100
1,4-Diazabicyclo[2.2.2]octane (DABCO)	72	72
1,8-Diazabicyclo[5.4.0]undec-7-ene (DBU)	100	100
None	0	0

Characterization of compounds

Spectra of all novel compounds can be found online at:
<https://pubs.acs.org/doi/10.1021/acs.orglett.2c03421>

3a. Phenyl benzyldisulfonate

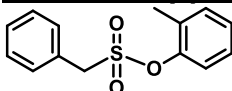


Prepared according to the general procedure described above using phenol as the phenol. White solid. Yield: 121 mg (95%)

¹H NMR (CD₃CN, 400 MHz): δ 7.53 – 7.41 (m, 7H), 7.39 – 7.33 (m, 1H), 7.25 – 7.18 (m, 2H), 4.68 (s, 2H).

This product has been reported in >20 publications, with the first mention in Zaborsky & Kaiser (1966).¹

3b-o. 2-Methylphenyl benzyldisulfonate



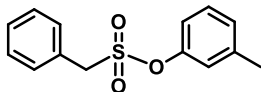
Prepared according to the general procedure described above using *o*-cresol as the phenol. NMR yield: 100%

HRMS: *m/z* C₁₆H₁₇NNaO₃S⁺ ([M+ACN+Na]⁺): calculated 326.0821, found 326.0822

¹H NMR (CD₃CN, 400 MHz): δ 7.55 – 7.48 (m, 2H), 7.48 – 7.43 (m, 3H), 7.33 – 7.27 (m, 1H), 7.26 – 7.20 (m, 2H), 7.16 – 7.10 (m, 1H), 4.73 (s, 2H), 2.22 (s, 3H).

¹³C NMR (CD₃CN, 101 MHz): δ 148.9, 132.8, 132.7, 132.1, 130.1, 129.8, 129.1, 128.3, 128.2, 123.1, 57.7, 16.7.

$\bar{\nu}_{\text{max}}$: 3062, 3032, 2935, 1593, 1489, 1456, 1363, 1180, 1146, 1099 cm⁻¹.

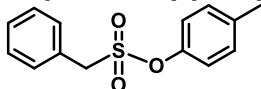
3b-m. 3-Methylphenyl benzylsulfonate

Prepared according to the general procedure described above using *m*-cresol as the phenol. White solid. NMR yield: 100%

HRMS: m/z $C_{16}H_{17}NNaO_3S^+$ ($[M+ACN+Na]^+$): calculated 326.0821, found 326.0824.

1H NMR (CD_3CN , 400 MHz): δ 7.52 – 7.42 (m, 5H), 7.35 – 7.27 (m, 1H), 7.18 (d, J = 7.6 Hz, 1H), 7.04 – 6.97 (m, 2H), 4.67 (s, 2H), 2.35 (s, 3H). **^{13}C NMR (CD_3CN , 101 MHz):** δ 150.39, 141.63, 132.02, 130.70, 130.10, 129.84, 129.03, 128.95, 123.51, 120.01, 57.19, 21.25

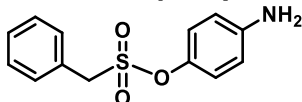
$\bar{\nu}_{max}$: 3066, 3035, 2927, 1610, 1583, 1487, 1456, 1367, 1174, 1122 cm^{-1} .

3b-p. 4-Methylphenyl benzylsulfonate

Prepared according to the general procedure described above using *p*-cresol as the phenol. NMR yield: 100%

1H NMR (CD_3CN , 400 MHz): δ 7.53 – 7.38 (m, 5H), 7.24 (d, J = 8.3 Hz, 2H), 7.09 (d, J = 8.5 Hz, 2H), 4.65 (s, 2H), 2.34 (s, 3H).

Product was previously reported in Alonso *et al.* (2005) & Moghaddam *et al.* (2004).^{2,3}

3c. 4-Aminophenyl benzylsulfonate

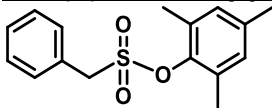
Prepared according to the general procedure described above using 4-aminophenol as the phenol. brown solid. The secondary product that was formed during this reaction – where phenol **2c** had attached to **1** via the $-NH_2$ moiety – was separated from the desired product using column chromatography (silica gel, gradient of 53–65% ethyl acetate in hexane), and the product distribution that was found using NMR (75% **3c**, 25% secondary product) was confirmed by isolating and weighing both products.

HRMS: m/z $C_{13}H_{14}NO_3S^+$ ($[M+H]^+$): calculated 264.0689, found 264.0690.

1H NMR (CD_3CN with 20% MeOD, 400 MHz): δ 7.50 – 7.40 (m, 5H), 6.93 (d, J = 8.9 Hz, 2H), 6.64 (d, J = 8.9 Hz, 2H), 4.58 (s, 2H), 4.27 (s, 2H). **^{13}C NMR (CD_3CN with 20% MeOD, 101 MHz):** δ 148.3, 141.3, 132.0, 130.0, 129.8, 129.2, 123.8, 115.8, 56.5.

$\bar{\nu}_{max}$: 3475, 3385, 3063, 3034, 2924, 2854, 1622, 1502, 1362, 1169, 1144 cm^{-1} .

3d. 2,4,6-Trimethylphenyl benzylsulfonate

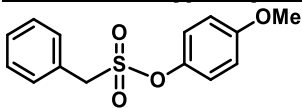


Prepared according to the general procedure described above using 2,4,6-trimethylphenol as the phenol. White solid. Yield: 143 mg (96%)

¹H NMR (CD₃CN, 400 MHz): δ 7.54 (dd, *J* = 6.6, 3.2 Hz, 2H), 7.48 – 7.41 (m, 3H), 6.92 (s, 2H), 4.77 (s, 2H), 2.25 (s, 3H), 2.22 (s, 6H).

Product was previously reported in Alonso *et al.* (2005) & Truce *et al.* (1970).^{2,4}

3e. 4-Methoxyphenyl benzylsulfonate

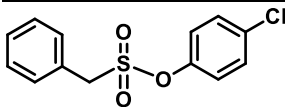


Prepared according to the general procedure described above using 4-methoxyphenol as the phenol. White solid. Yield: 142 mg (100%)

¹H NMR (CD₃CN, 400 MHz): δ 7.51 – 7.40 (m, 5H), 7.13 (d, *J* = 9.2 Hz, 2H), 6.95 (d, *J* = 9.2 Hz, 2H), 4.64 (s, 2H), 3.79 (s, 3H).

Product was previously reported in Moghaddam *et al.* (2004) & Betts *et al.* (2006).^{3,5}

3f. 4-Chlorophenyl benzylsulfonate

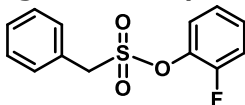


Prepared according to the general procedure described above using 4-chlorophenol as the phenol. White solid. Yield: 143 mg (99%)

¹H NMR (CD₃CN, 400 MHz): δ 7.51 – 7.40 (m, 7H), 7.20 (dt, *J* = 8.9, 3.2 Hz, 2H), 4.69 (s, 2H).

Product was previously reported in Alonso *et al.* (2005), Moghaddam *et al.* (2004), Gao *et al.* (2015) and Davy *et al.* (1977).^{2,3,6,7}

3g-o. 2-Fluorophenyl benzylsulfonate



Prepared according to the general procedure described above using 2-fluorophenol as the phenol. White solid. Yield: 129 mg (95%)

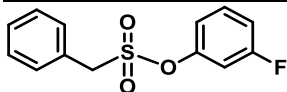
HRMS: *m/z* C₁₃H₁₁FN₃O₃S⁺ ([M+Na]⁺): calculated 289.0305, found 289.0306.

¹H NMR (CD₃CN, 400 MHz): δ 7.56 – 7.41 (m, 5H), 7.40 – 7.28 (m, 2H), 7.29 – 7.17 (m, 2H), 4.76 (s, 2H). **¹³C NMR (CD₃CN, 101 MHz):** δ 155.5 (d, *J* = 242.4

Hz), 137.7 (d, $J = 10.1$ Hz), 132.1, 130.3, 129.9, 129.8 (d, $J = 8.1$ Hz), 128.6, 126.2 (d, $J = 3.8$ Hz), 126.16, 125.63, 57.8 (d, $J = 1.4$ Hz). **^{19}F NMR (CD_3CN , 376 MHz, decoupled):** δ -129.28.

$\bar{\nu}_{\text{max}}$: 3068, 3036, 2931, 1599, 1497, 1458, 1373, 1252, 1159, 1099, 1028 cm^{-1} .

3q-m. 3-Fluorophenyl benzylsulfonate

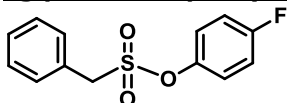


Prepared according to the general procedure described above using 3-fluorophenol as the phenol. NMR yield: 100%

^1H NMR (CD_3CN , 400 MHz): δ 7.51 – 7.42 (m, 7H), 7.06 (dd, $J = 8.3$, 2.3 Hz, 1H), 6.99 (dt, $J = 9.6$, 2.4 Hz, 1H), 4.71 (s, 2H).

Product was previously reported in Davy *et al.* (1977).⁷

3q-p. 4-Fluorophenyl benzylsulfonate

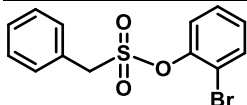


Prepared according to the general procedure described above using 4-fluorophenol as the phenol. NMR yield: 100%

^1H NMR (CD_3CN , 400 MHz): δ 7.51 – 7.41 (m, 5H), 7.25 – 7.13 (m, 4H), 4.67 (s, 2H).

Product was previously reported in Alonso *et al.* (2005).²

3h-o. 2-Bromophenyl benzylsulfonate



Prepared according to the general procedure described above using 2-bromophenol as the phenol. White solid. NMR yield: 100%

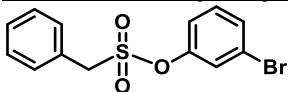
HRMS: m/z $\text{C}_{13}\text{H}_{11}\text{BrNaO}_3\text{S}^+$ ($[\text{M}+\text{Na}]^+$): calculated 348.9504, found 348.9506.

^1H NMR (CD_3CN , 400 MHz): δ 7.71 (dd, $J = 8.0$, 1.6 Hz, 1H), 7.55 – 7.50 (m, 2H), 7.48 – 7.42 (m, 3H), 7.43 – 7.36 (m, 1H), 7.33 – 7.17 (m, 2H), 4.80 (s, 2H).

^{13}C NMR (CD_3CN , 101 MHz): δ 147.7, 135.0, 132.1, 130.3, 130.2, 129.9, 129.7, 128.6, 124.9, 117.0, 58.5.

$\bar{\nu}_{\text{max}}$: 3088, 3063, 3034, 2982, 2933, 1464, 1371, 1207, 1167, 1155, 1142, 1041 cm^{-1} .

3h-m. 3-Bromophenyl benzylsulfonate



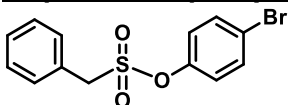
Prepared according to the general procedure described above using 3-bromophenol as the phenol. White solid. NMR yield: 100%

HRMS: m/z $C_{13}H_{11}BrNaO_3S^+$ ($[M+Na]^+$): calculated 348.9504, found 348.9507.

1H NMR (CD_3CN , 400 MHz): δ 7.57 – 7.40 (m, 6H), 7.41 – 7.29 (m, 2H), 7.21 (dd, J = 6.7, 2.3 Hz, 1H), 4.71 (s, 2H). **^{13}C NMR (CD_3CN , 101 MHz):** δ 150.8, 132.4, 132.0, 131.4, 130.2, 129.9, 128.7, 126.3, 123.1, 122.3, 57.4.

$\bar{\nu}_{max}$: 3093, 3064, 3034, 2983, 2929, 1579, 1466, 1358, 1205, 1186, 1149 cm^{-1} .

3h-p. 4-Bromophenyl benzylsulfonate

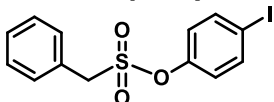


Prepared according to the general procedure described above using 4-bromophenol as the phenol. NMR yield: 100%

1H NMR (CD_3CN , 400 MHz): δ 7.58 (dt, J = 9.1, 3.4 Hz, 2H), 7.51 – 7.42 (m, 5H), 7.12 (dt, J = 8.9, 3.4 Hz, 2H), 4.68 (s, 2H).

Product was previously reported in Alonso *et al.* (2005), Truce *et al.* (1970), and Smedley *et al.* (2022).^{2,4,8}

3i. 4-Iodophenyl benzylsulfonate



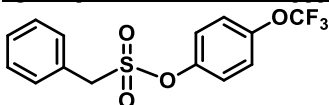
Prepared according to the general procedure described above using 4-iodophenol as the phenol. White solid. NMR yield: 100%

HRMS: m/z $C_{13}H_{11}INaO_3S^+$ ($[M+Na]^+$): calculated 396.9366, found 396.9367.

1H NMR (CD_3CN , 400 MHz): δ 7.78 (d, J = 8.7 Hz, 2H), 7.53 – 7.41 (m, 5H), 6.99 (d, J = 8.7 Hz, 2H), 4.68 (s, 2H). **^{13}C NMR (CD_3CN , 101 MHz):** δ 150.4, 140.1, 132.0, 130.2, 129.9, 128.7, 125.3, 92.1, 57.2.

$\bar{\nu}_{max}$: 3084, 3060, 3005, 2955, 1572, 1477, 1354, 1209, 1194, 1173, 1151, 1007 cm^{-1} .

3j. 4-(Trifluoromethoxy)phenyl benzylsulfonate



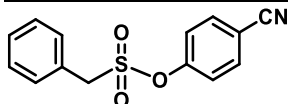
Prepared according to the general procedure described above using 4-(trifluoromethoxy)phenol as the phenol. White solid. Yield: 170 mg (100%)

HRMS: m/z $C_{14}H_{15}F_3NO_4S^+$ ($[M+NH_4]^+$): calculated 350.0668, found 350.0659.

1H NMR (CD_3CN , 400 MHz): δ 7.55 – 7.40 (m, 5H), 7.36 (d, J = 9.3 Hz, 2H), 7.31 – 7.25 (m, 2H), 4.71 (s, 2H). **^{13}C NMR (CD_3CN , 101 MHz):** δ 148.8, 148.3, 132.0, 130.2, 129.9, 128.7, 124.9, 123.8, 121.4 (q, J = 259.3 Hz), 57.28. **^{19}F NMR (CD_3CN , 376 MHz):** δ -58.92.

$\bar{\nu}_{max}$: 3076, 2949, 1498, 1354, 1223, 1215, 1146, 1014 cm^{-1} .

3k-p. 4-Cyanophenyl benzyisulfonate



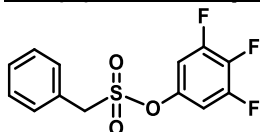
Prepared according to the general procedure described above using 4-cyanophenol as the phenol. White solid. NMR yield: 100%

HRMS: m/z $C_{14}H_{12}NO_3S^+$ ($[M+H]^+$): calculated 274.0532, found 274.0527.

1H NMR (CD_3CN , 400 MHz): δ 7.79 (d, J = 8.8 Hz, 2H), 7.47 (dd, J = 12.4, 3.1 Hz, 5H), 7.33 (d, J = 8.8 Hz, 2H), 4.74 (s, 2H). **^{13}C NMR (CD_3CN , 101 MHz):** δ 153.4, 135.4, 132.0, 130.3, 129.9, 128.5, 124.1, 118.8, 111.9, 57.7.

$\bar{\nu}_{max}$: 3101, 3063, 2237, 1597, 1493, 1458, 1361, 1151, 1144, 1103, 1016 cm^{-1} .

3l. 3,4,5-Trifluorophenyl benzyisulfonate



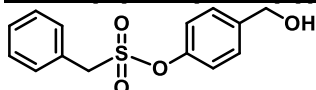
Prepared according to the general procedure described above using 3,4,5-trifluorophenol as the phenol. White solid. NMR yield: 100%

HRMS: m/z $C_{13}H_{13}F_3NO_3S^+$ ($[M+NH_4]^+$): calculated 320.0563, found 320.0555.

1H NMR (CD_3CN , 400 MHz): δ 7.50 – 7.43 (m, 5H), 7.06 – 6.97 (m, 2H), 4.73 (s, 2H). **^{13}C NMR (CD_3CN , 101 MHz):** δ 151.9 (ddd, J = 249.5, 10.7, 5.2 Hz), 145.0 (td, J = 12.8, 4.6 Hz), 140.5 (dd, J = 249.3, 15.1 Hz), 132.1, 130.4, 130.0, 128.4, 109.1 (dd, J = 25.6, 7.1 Hz), 57.4. **^{19}F NMR (CD_3CN , 376 MHz, decoupled):** δ -134.01, -134.06, -163.71 (t, J = 20.0 Hz).

$\bar{\nu}_{max}$: 3093, 3007, 2956, 1633, 1514, 1454, 1338, 1228, 1171, 1105, 1051 cm^{-1} .

3m. 4-(Hydroxymethyl)phenyl benzyisulfonate



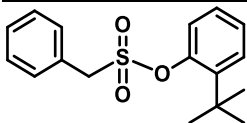
Prepared according to the general procedure described above using 4-hydroxybenzyl alcohol as the phenol. White solid. NMR yield: 100%

HRMS: m/z $C_{14}H_{18}NO_4S^+$ ($[M+NH_4]^+$): calculated 296.0951, found 296.0949.

1H NMR (CD_3CN , 400 MHz): δ 7.50 – 7.44 (m, 5H), 7.40 (dt, J = 8.5, 2.6 Hz, 2H), 7.17 (dt, J = 8.5, 2.8 Hz, 2H), 4.67 (s, 2H), 4.59 (s, 2H). **^{13}C NMR (CD_3CN , 101 MHz):** δ 149.2, 142.5, 132.0, 130.1, 129.9, 129.1, 122.9, 115.6, 63.9, 57.1

$\bar{\nu}_{max}$: 3541, 3066, 3036, 2931, 2875, 1595, 1502, 1354, 1142, 1014 cm^{-1} .

3o-o. 2-Tert-butylphenyl benzylsulfonate



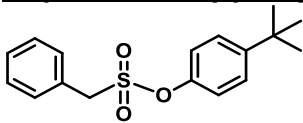
Prepared according to the general procedure described above using 2-tert-butylphenol as the phenol. White solid. NMR yield: 100%

HRMS: m/z $C_{17}H_{20}NaO_3S^+$ ($[M+Na]^+$): calculated 327.1025, found 327.1027.

1H NMR (CD_3CN , 400 MHz): 7.64 – 7.37 (m, 6H), 7.38 – 7.27 (m, 1H), 7.26 – 7.20 (m, 2H), 4.80 (s, 2H), 1.36 (s, 9H). **^{13}C NMR (CD_3CN , 101 MHz):** δ 150.0, 142.1, 132.1, 130.2, 129.9, 129.2, 128.8, 128.4, 127.3, 122.2, 59.1, 35.4, 30.7.

$\bar{\nu}_{max}$: 3066, 2956, 2872, 1485, 1443, 1354, 1203, 1180, 1147, 1076 cm^{-1} .

3o-p. 4-Tert-butylphenyl benzylsulfonate



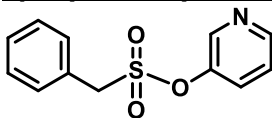
Prepared according to the general procedure described above using 4-tert-butylphenol as the phenol. White solid. NMR yield: 100%

HRMS: m/z $C_{17}H_{20}NaO_3S^+$ ($[M+Na]^+$): calculated 327.1025, found 327.1027.

1H NMR (CD_3CN , 400 MHz): δ 7.52 – 7.41 (m, 7H), 7.12 (d, J = 8.8 Hz, 2H), 4.66 (s, 2H), 1.32 (s, 9H). **^{13}C NMR (CD_3CN , 101 MHz):** δ 151.5, 148.1, 132.0, 130.1, 129.8, 129.0, 127.9, 122.6, 57.2, 35.3, 31.5.

$\bar{\nu}_{max}$: 3061, 2960, 2870, 1502, 1367, 1205, 1176, 1149, 1016 cm^{-1} .

3p. Pyridin-3-yl benzylsulfonate



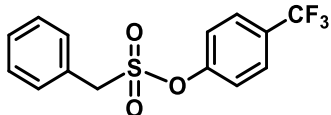
Prepared according to the general procedure described above using 3-hydroxypyridine as the phenol. White solid. NMR yield: 100%

HRMS: m/z $C_{12}H_{12}NO_3S^+$ ($[M+H]^+$): calculated 250.0532, found 250.0533.

^1H NMR (CD_3CN , 400 MHz): δ 8.53 (dd, J = 4.7, 1.4 Hz, 1H), 8.44 (d, J = 2.2 Hz, 1H), 7.58 (ddd, J = 8.4, 2.8, 1.4 Hz, 1H), 7.53 – 7.39 (m, 6H), 4.75 (s, 2H).
 ^{13}C NMR (CD_3CN , 101 MHz): δ 149.3, 147.5, 144.6, 132.1, 130.7, 130.3, 129.9, 128.6, 125.6, 57.4.

$\bar{\nu}_{\text{max}}$: 3095, 3055, 2980, 2926, 1572, 1473, 1421, 1369, 1207, 1188, 1159, 1022 cm^{-1} .

3q. 4-(Trifluoromethyl)phenyl benzylsulfonate



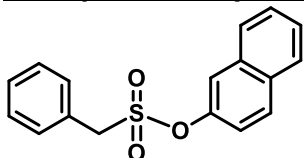
Prepared according to the general procedure described above using 4-(trifluoromethyl)phenol as the phenol. White solid. Yield: 155 mg (96%)

HRMS: m/z $\text{C}_{16}\text{H}_{14}\text{F}_3\text{NNaO}_3\text{S}^+$ ($[\text{M}+\text{ACN}+\text{Na}]^+$): calculated 380.0539, found 380.0541.

^1H NMR (CD_3CN , 400 MHz): δ 7.76 (d, J = 8.5 Hz, 2H), 7.53 – 7.41 (m, 5H), 7.37 (d, J = 8.5 Hz, 2H), 4.74 (s, 2H). **^{13}C NMR (CD_3CN , 101 MHz):** δ 153.0, 132.1, 130.3, 129.9, 129.6 (q, J = 34.3 Hz), 128.6, 128.4 (q, J = 3.8 Hz), 124.9 (q, J = 270.8 Hz) 123.8, 57.5. **^{19}F NMR (CD_3CN , 376 MHz, decoupled):** δ -62.89.

$\bar{\nu}_{\text{max}}$: 3064, 3005, 2953, 1610, 1510, 1327, 1215, 1151, 1119, 1066, 1014 cm^{-1} .

3r. Naphthalen-2-yl benzylsulfonate

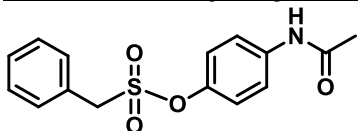


Prepared according to the general procedure described above using 2-naphthol as the phenol. NMR yield: 100%

^1H NMR (CD_3CN , 400 MHz): δ 8.00 – 7.86 (m, 3H), 7.72 (d, J = 2.5 Hz, 1H), 7.61 – 7.54 (m, 2H), 7.54 – 7.48 (m, 2H), 7.48 – 7.42 (m, 3H), 7.34 (dd, J = 8.9, 2.5 Hz, 1H), 4.74 (s, 2H).

Product was previously reported in Bahrami *et al.* (2012).⁹

3s. 4-acetamidophenyl benzylsulfonate



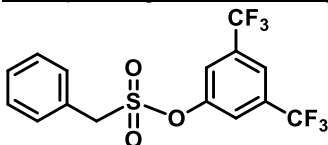
Prepared according to the general procedure described above using acetaminophen as the phenol. White solid. NMR yield: 100%

HRMS: m/z $\text{C}_{15}\text{H}_{15}\text{NNaO}_4\text{S}^+$ ($[\text{M}+\text{Na}]^+$): calculated 328.0614, found 328.0614.

^1H NMR (CD_3CN with 37.5% CD_3OD , 400 MHz): δ 7.57 (dt, J = 8.9, 3.6 Hz, 2H), 7.48 – 7.38 (m, 5H), 7.12 (dt, J = 8.9, 3.4 Hz, 2H), 4.66 (s, 2H), 2.06 (s, 3H).
 ^{13}C NMR (CD_3CN with 37.5% CD_3OD , 101 MHz): δ 171.4, 146.5, 139.4, 132.5, 130.5, 130.3, 129.5, 123.9, 122.3, 57.4, 24.4.

$\bar{\nu}_{\text{max}}$: 3313, 3074, 2995, 2941, 2447, 1651, 1595, 1508, 1362, 1190, 1147, 1018 cm^{-1} .

3u. 3,5-Bis(trifluoromethyl)phenyl benzylsulfonate



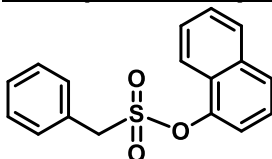
Prepared according to the general procedure described above using 3,5-bis(trifluoromethyl)phenol as the phenol. White solid. Yield: 167 mg (85%)

HRMS: m/z $\text{C}_{15}\text{H}_{14}\text{F}_6\text{NO}_3\text{S}^+$ ($[\text{M}+\text{NH}_4]^+$): calculated 402.0593, found 402.0582.

^1H NMR (CD_3CN , 400 MHz): δ 7.97 (s, 1H), 7.67 (s, 2H), 7.55 – 7.39 (m, 5H), 4.81 (s, 2H). **^{13}C NMR (CD_3CN , 101 MHz):** δ 151.1, 133.8 (q, J = 33.9 Hz), 132.1, 130.5, 130.0, 128.3, 124.4 (q, J = 4.0 Hz), 122.2 (hept, J = 3.6 Hz), 121.1 (q, J = 272.7 Hz), 57.9. **^{19}F NMR (CD_3CN , 376 MHz, decoupled):** δ -63.49.

$\bar{\nu}_{\text{max}}$: 3086, 2989, 2933, 1614, 1458, 1360, 1275, 1128 cm^{-1} .

3v. Naphthalen-1-yl benzylsulfonate

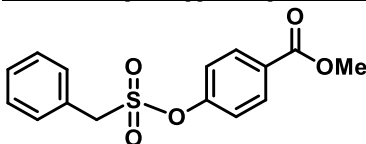


Prepared according to the general procedure described above using 1-naphthol as the phenol. NMR yield: 100%

^1H NMR (CD_3CN , 400 MHz): δ 7.98 – 7.92 (m, 2H), 7.87 (d, J = 8.3, 1.1 Hz, 1H), 7.60 – 7.53 (m, 4H), 7.50 – 7.44 (m, 4H), 7.34 (dd, J = 7.7, 1.2 Hz, 1H), 4.85 (s, 2H).

Product was previously reported in Alonso *et al.* (2005) & Moghaddam *et al.* (2004).^{2,3}

3w. methyl 4-((benzylsulfonyl)oxy)benzoate



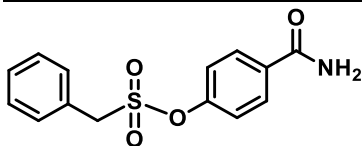
Prepared according to the general procedure described above using methyl 4-hydroxybenzoate as the phenol. White solid. NMR yield: 100%

HRMS: m/z $C_{15}H_{15}O_5S^+$ ($[M+H]^+$): calculated 307.0635, found 307.0632.

1H NMR (CD_3CN , 400 MHz): δ 8.05 (d, J = 8.8 Hz, 2H), 7.52 – 7.41 (m, 5H), 7.29 (d, J = 8.8 Hz, 2H), 4.72 (s, 2H), 3.88 (s, 3H). **^{13}C NMR (CD_3CN , 101 MHz):** δ 166.7, 153.7, 132.3, 132.0, 130.2, 130.1, 129.9, 128.7, 123.1, 57.5, 53.0.

$\bar{\nu}_{max}$: 3007, 2955, 1716, 1602, 1504, 1433, 1356, 1277, 1215, 1157, 1153, 1097, 1018 cm^{-1} .

3y. 4-carbamoylphenyl phenylmethanesulfonate



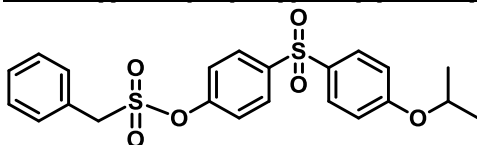
Prepared according to the description of the BTMG/DBU reaction provided above.

3y was isolated by precipitation from the reaction mixture using an acetone/water mixture. The solid was collected using vacuum filtration, washed with an acetone/water mixture, followed by hexane, and then dried under vacuum. White solid.

HRMS: m/z $C_{14}H_{12}NO_4S^-$ ($[M-H]^-$): calculated 290.0493, found 290.0497

1H NMR (MeOD with 50% CD_3CN , 400 MHz): δ 7.93 (dt, J = 8.9, 2.8 Hz, 2H), 7.55 – 7.49 (m, 2H), 7.49 – 7.43 (m, 3H), 7.29 (dt, J = 8.8, 2.8 Hz, 2H), 4.79 (s, 2H). **^{13}C NMR (MeOD with 50% CD_3CN , 101 MHz):** δ 170.9, 153.6, 134.3, 132.7, 131.1, 130.8, 130.4, 129.5, 123.6. (Aliphatic peak is hidden underneath MeOD solvent peak.)

3aa. 4-((4-Isopropoxyphenyl)sulfonyl)phenyl benzyisulfonate



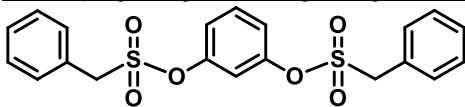
Prepared according to the general procedure described above using 4-((4-isopropoxyphenyl)sulfonyl)phenol as the phenol. White solid. NMR yield: 100%

HRMS: m/z $C_{22}H_{23}O_6S_2^+$ ($[M+H]^+$): calculated 447.0931, found 447.0939.

1H NMR (CD_3CN , 400 MHz): δ 7.95 (d, J = 8.8 Hz, 2H), 7.84 (d, J = 9.0 Hz, 2H), 7.49 – 7.36 (m, 5H), 7.33 (d, J = 8.8 Hz, 2H), 7.02 (d, J = 9.0 Hz, 2H), 4.71 (s, 2H), 4.68 (hept, 1H), 1.29 (d, J = 6.0 Hz, 6H). **^{13}C NMR (CD_3CN , 101 MHz):** δ 163.3, 153.5, 142.2, 132.9, 132.0, 130.9, 130.4, 130.3, 129.9, 128.5, 124.1, 117.1, 71.6, 57.6, 22.0.

$\bar{\nu}_{max}$: 3097, 3066, 2980, 2933, 1589, 1489, 1373, 1319, 1292, 1259, 1144, 1101, 1014 cm^{-1} .

3ab. 1,3-phenylene-bis(benzylsulfonate)



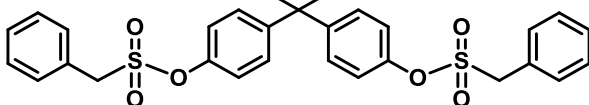
Prepared according to the general procedure described above, with 2 equiv of NaH, using resorcinol as the phenol. White solid. NMR yield: 100%

HRMS: m/z $C_{20}H_{22}NO_6S_2^+$ ($[M+NH_4]^+$): calculated 436.0883, found 436.0875.

1H NMR (CD_3CN , 400 MHz): δ 7.52 – 7.42 (m, 11H), 7.21 (d, J = 2.3 Hz, 1H), 7.19 (d, J = 2.3 Hz, 1H), 7.03 (t, J = 2.3 Hz, 1H), 4.70 (s, 4H). **^{13}C NMR (CD_3CN , 101 MHz):** δ 150.8, 132.0, 130.3, 129.9, 128.7, 122.0, 117.4, 57.4.

$\bar{\nu}_{max}$: 3066, 3037, 2929, 1595, 1477, 1356, 1171, 1101 cm^{-1} .

3ac. Propane-2,2-diylbis(4,1-phenylene) bis(benzylsulfonate)



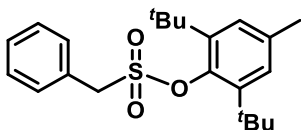
Prepared according to the general procedure described above, with 2 equiv of NaH, using bisphenol A as the phenol. White solid. NMR yield: 100%

HRMS: m/z $C_{29}H_{32}NO_6S_2^+$ ($[M+NH_4]^+$): calculated 554.1666, found 554.1672.

1H NMR (CD_3CN , 400 MHz): δ 7.57 – 7.35 (m, 10H), 7.28 (d, J = 8.8 Hz, 4H), 7.11 (d, J = 8.8 Hz, 4H), 4.66 (s, 4H), 1.67 (s, 6H). **^{13}C NMR (CD_3CN , 101 MHz):** δ 150.4, 148.4, 132.0, 130.1, 129.8, 129.3, 129.0, 122.6, 57.2, 43.4, 30.9.

$\bar{\nu}_{max}$: 3066, 3036, 2970, 1498, 1365, 1207, 1176, 1146, 1016 cm^{-1} .

3ae. 2,6-Di-tert-butyl-4-methylphenyl benzylsulfonate

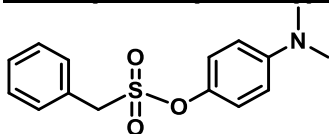


Prepared according to the general procedure described above using 2,6-di-tert-butyl-4-methylphenol as the phenol. White solid. NMR yield: 100%

HRMS: m/z $C_{22}H_{34}NO_3S^+$ ($[M+NH_4]^+$): calculated 392.2254, found 392.2255.

1H NMR (CD_3CN , 400 MHz): δ 7.58 – 7.42 (m, 5H), 7.22 (s, 2H), 4.75 (s, 2H), 2.31 (s, 3H), 1.39 (s, 18H). **^{13}C NMR (CD_3CN , 101 MHz):** δ 145.9, 136.2, 132.4, 130.1, 130.0, 129.7, 128.6, 58.1, 37.6, 33.2, 30.7, 20.9.

$\bar{\nu}_{max}$: 3039, 2958, 1670, 1595, 1346, 1267, 1178, 1157, 1088 cm^{-1} .

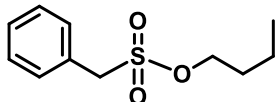
3af. 4-(Dimethylamino)phenyl benzylsulfonate

Prepared according to the general procedure described above using 4-(dimethylamino)phenol as the phenol. Pinkish solid. NMR yield: 100%

HRMS: m/z $C_{15}H_{18}NO_3S^+$ ($[M+H]^+$): calculated 292.1002, found 292.1001.

1H NMR (CD_3CN , 400 MHz): δ 7.52 – 7.40 (m, 5H), 7.05 (d, J = 9.2 Hz, 2H), 6.72 (d, J = 9.2 Hz, 2H), 4.59 (s, 2H), 2.92 (s, 6H). **^{13}C NMR (CD_3CN , 101 MHz):** δ 150.80, 140.71, 131.97, 129.98, 129.79, 129.20, 123.61, 113.72, 56.61, 40.88.

$\bar{\nu}_{max}$: 3070, 3037, 2985, 2937, 2808, 1605, 1514, 1336, 1198, 1174, 1142, 1070 cm^{-1} .

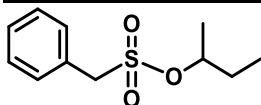
5a. 1-Butoxy benzylsulfonate

Prepared according to the general procedure described above using 1-butanol as the alcohol. White solid. NMR yield: 100%

HRMS: m/z $C_{11}H_{20}NO_3S^+$ ($[M+NH_4]^+$): calculated 246.1158, found 246.1156.

1H NMR (CD_3CN , 400 MHz): δ 7.42 (m, 5H), 4.44 (s, 2H), 4.16 (t, J = 6.5 Hz, 2H), 1.64 (p, 2H), 1.37 (sext, J = 7.5 Hz, 2H), 0.91 (t, J = 7.4 Hz, 3H). **^{13}C NMR (CD_3CN , 101 MHz):** δ 131.77, 129.85, 129.76, 129.69, 72.28, 56.23, 31.86, 19.36, 13.77.

$\bar{\nu}_{max}$: 3066, 3036, 2962, 2875, 1497, 1456, 1352, 1203, 1169, 1140 cm^{-1} .

5b. 2-Butoxy benzylsulfonate

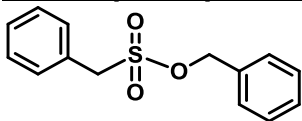
Prepared according to the general procedure described above using 2-butanol as the alcohol. White solid. NMR yield: 100%

HRMS: m/z $C_{11}H_{20}NO_3S^+$ ($[M+NH_4]^+$): calculated 246.1158, found 246.1156.

1H NMR (CD_3CN , 400 MHz): δ 7.47 – 7.37 (m, 5H), 4.68 (sext, J = 6.2 Hz, 1H), 4.42 (s, 2H), 1.71 – 1.59 (m, 2H), 1.31 (d, J = 6.3 Hz, 3H), 0.90 (t, J = 7.4 Hz, 3H). **^{13}C NMR (CD_3CN , 101 MHz):** δ 131.8, 130.0, 129.7, 129.6, 83.2, 57.5, 30.3, 20.8, 9.6.

$\bar{\nu}_{max}$: 3066, 3034, 2978, 2935, 2881, 1497, 1456, 1336, 1171 cm^{-1} .

5d. benzyl benzyldisulfonate

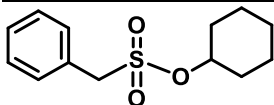


Prepared according to the general procedure described above using benzyl alcohol as the alcohol. NMR yield: 100%

¹H NMR (CD₃CN, 400 MHz): δ 7.46 – 7.33 (m, 10H), 5.21 (s, 2H), 4.57 (s, 2H).

Product was previously reported in Dai *et al.* (2021).¹⁰

5e. cyclohexyl benzyldisulfonate

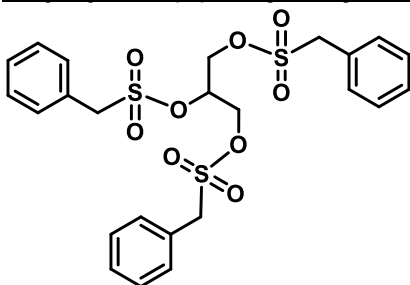


Prepared according to the general procedure described above using cyclohexanol as the alcohol. NMR yield: 100%

¹H NMR (CD₃CN, 400 MHz): δ 7.50 – 7.35 (m, 5H), 4.59 (hept, *J* = 8.7, 3.9 Hz, 1H), 4.42 (s, 2H), 1.93 – 1.86 (m, 2H), 1.76 – 1.65 (m, 2H), 1.61 – 1.46 (m, 3H), 1.43 – 1.20 (m, 3H).

Product was previously reported in Alonso *et al.* (2005).²

5f. propane-1,2,3-triyl tris(benzyldisulfonate)

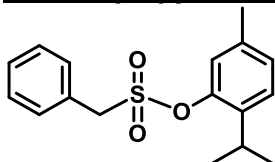


Prepared according to the general procedure described above, using 3 equiv of NaH and 3 equiv of **1**, and using glycerol as the alcohol. White solid. Yield: 95 mg (100%)

HRMS: *m/z* C₂₄H₃₀NO₉S₃⁺ ([M+NH₄]⁺): calculated 572.1077, found 572.1074.

¹H NMR (CD₃CN, 400 MHz): δ 7.49 – 7.37 (m, 15H), 5.01 (tt, *J* = 5.6, 3.7 Hz, 1H), 4.51 (s, 4H), 4.45 (s, 2H), 4.30 (qd, *J* = 11.8, 4.7 Hz, 4H). **¹³C NMR (CD₃CN, 101 MHz):** δ 131.92, 131.87, 130.07, 130.06, 129.89, 129.85, 129.08, 128.90, 77.14, 68.75, 57.76, 56.78.

$\tilde{\nu}_{\text{max}}$: 3066, 3034, 3007, 2955, 1493, 1456, 1358, 1169, 1090, 1014 cm⁻¹.

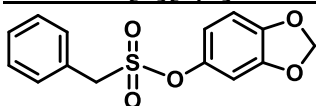
7a. 2-isopropyl-5-methylphenyl benzyldisulfonate

Prepared according to the general procedure described above using thymol as the phenol. White solid. NMR yield: 100%

HRMS: m/z $C_{17}H_{24}NO_3S^+$ ($[M+NH_4]^+$): calculated 322.1471, found 322.1470.

1H NMR (CD_3CN , 400 MHz): δ 7.59 – 7.41 (m, 5H), 7.26 (d, J = 8.0 Hz, 1H), 7.11 (d, J = 8.0 Hz, 1H), 6.88 (s, 1H), 4.75 (s, 2H), 3.06 (hept, J = 6.9 Hz, 1H), 2.27 (s, 3H), 1.11 (d, J = 6.9 Hz, 6H). **^{13}C NMR (CD_3CN , 101 MHz):** δ 147.32, 139.65, 138.28, 132.11, 130.11, 129.84, 129.23, 129.17, 128.03, 123.31, 57.90, 27.31, 23.45, 20.79.

$\bar{\nu}_{max}$: 3064, 3034, 2962, 2929, 2872, 1620, 1502, 1456, 1352, 1234, 1173, 1142, 1076 cm^{-1} .

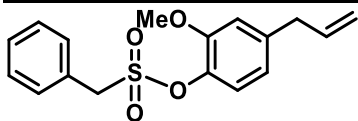
7b. benzo[d][1,3]dioxol-5-yl benzyldisulfonate

Prepared according to the general procedure described above using sesamol as the phenol. White solid. NMR yield: 100%

HRMS: m/z $C_{14}H_{16}NO_5S^+$ ($[M+NH_4]^+$): calculated 310.0744, found 310.0744.

1H NMR (CD_3CN , 400 MHz): δ 7.53 – 7.40 (m, 5H), 6.84 (d, J = 8.4 Hz, 1H), 6.75 – 6.66 (m, 2H), 6.02 (s, 2H), 4.65 (s, 2H). **^{13}C NMR (CD_3CN , 101 MHz):** δ 149.4, 147.7, 144.4, 132.0, 130.1, 129.8, 128.9, 116.0, 109.0, 104.9, 103.6, 56.9.

$\bar{\nu}_{max}$: 3064, 2985, 2897, 1633, 1610, 1479, 1354, 1246, 1157, 1111, 1090, 1034 cm^{-1} .

7c. 4-Allyl-2-methoxyphenyl benzyldisulfonate

Prepared according to the general procedure described above using eugenol as the phenol. White solid. NMR yield: 100%

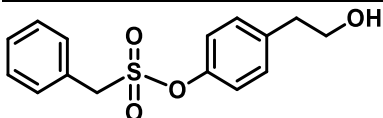
HRMS: m/z $C_{17}H_{19}O_4S^+$ ($[M+H]^+$): calculated 319.0999, found 319.1001.

1H NMR (CD_3CN , 400 MHz): δ 7.57 – 7.35 (m, 5H), 7.07 (d, J = 8.2 Hz, 1H), 6.99 (d, J = 2.0 Hz, 1H), 6.79 (dd, J = 8.2, 2.0 Hz, 1H), 6.00 (ddt, J = 16.9, 10.0, 6.8 Hz, 1H), 5.14 (dd, J = 17.1, 1.8 Hz, 1H), 5.09 (d, J = 10.0 Hz, 1H), 4.68 (s, 2H), 3.88 (s, 3H), 3.40 (d, J = 6.7 Hz, 2H). **^{13}C NMR (CD_3CN , 101 MHz):** δ 152.6,

142.1, 138.2, 137.8, 132.1, 130.0, 129.7, 129.3, 124.8, 121.6, 116.7, 114.5, 58.0, 56.7, 40.5.

$\bar{\nu}_{\text{max}}$: 3066, 3007, 2978, 2939, 2839, 1601, 1504, 1456, 1381, 1367, 1267, 1169, 1109, 1113, 1030 cm^{-1} .

7e. 4-(2-hydroxyethyl)phenyl benzylsulfonate



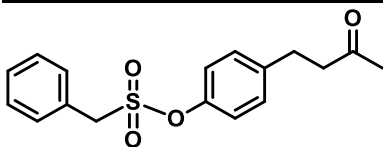
Prepared according to the general procedure described above, using 2 equiv of NaH, and using 2-(4-hydroxyphenyl)ethanol as the phenol. White solid. NMR yield: 100%

HRMS: m/z $\text{C}_{15}\text{H}_{20}\text{NO}_4\text{S}^+$ ($[\text{M}+\text{NH}_4]^+$): calculated 310.1108, found 310.1110.

^1H NMR (CDCl_3 , 400 MHz): δ 7.38 – 7.29 (m, 5H), 7.01 (dt, J = 8.7, 2.6 Hz, 2H), 6.76 (dt, J = 8.5, 2.9 Hz, 2H), 4.26 (s, 2H), 4.16 (t, J = 7.0 Hz, 2H), 2.86 (t, J = 7.0 Hz, 2H). **^{13}C NMR (CDCl_3 , 101 MHz):** δ 154.7, 130.8, 130.4, 129.2, 129.0, 128.5, 127.9, 115.6, 71.6, 57.0, 35.0.

$\bar{\nu}_{\text{max}}$: 3066, 3036, 2926, 2854, 1734, 1502, 1456, 1356, 1238, 1171, 1144 cm^{-1} .

7g. 4-(3-oxobutyl)phenyl benzylsulfonate



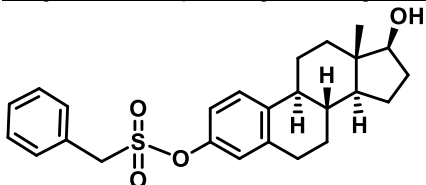
Prepared according to the general procedure described above using 4-(4-hydroxyphenyl)-2-butanone as the phenol. White solid. NMR yield: 100%

HRMS: m/z $\text{C}_{17}\text{H}_{19}\text{O}_4\text{S}^+$ ($[\text{M}+\text{H}]^+$): calculated 319.0999, found 319.1000.

^1H NMR (CD_3CN , 400 MHz): δ 7.52 – 7.41 (m, 5H), 7.26 (dt, J = 8.8, 2.8 Hz, 2H), 7.11 (dt, J = 8.6, 2.8 Hz, 2H), 4.66 (s, 2H), 2.87 – 2.75 (m, 4H), 2.09 (s, 3H). **^{13}C NMR (CD_3CN , 101 MHz):** δ 208.4, 148.5, 142.0, 132.0, 130.8, 130.1, 129.8, 123.0, 116.1, 57.1, 45.1, 30.1, 29.6.

$\bar{\nu}_{\text{max}}$: 3066, 3036, 2926, 1711, 1502, 1365, 1205, 1173, 1144 cm^{-1} .

7i. β -Estradiol, benzylsulfonyl ester



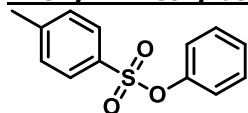
Prepared according to the general procedure described above, using 2 equiv of NaH, and using β -estradiol as the phenol. White solid. NMR yield: 100%

HRMS: m/z $C_{25}H_{34}NO_4S^+$ ($[M+NH_4]^+$): calculated 444.2203, found 444.2211.

1H NMR ($CDCl_3$, 400 MHz): δ 7.43 – 7.31 (m, 5H), 7.19 – 7.17 (m, 1H), 6.81 (dd, J = 8.6, 2.6 Hz, 1H), 6.75 (d, J = 2.6 Hz, 1H), 4.43 (s, 2H), 3.66 (t, J = 8.5 Hz, 1H), 2.80 – 2.71 (m, 2H), 2.27 – 2.20 (m, 1H), 2.17 – 2.03 (m, 2H), 1.89 (dt, J = 12.5, 3.6 Hz, 1H), 1.85 – 1.78 (m, 1H), 1.70 – 1.58 (m, 1H), 1.38 – 1.08 (m, 8H), 0.71 (s, 3H). **^{13}C NMR ($CDCl_3$, 101 MHz):** δ 147.2, 139.7, 139.1, 131.0, 129.4, 129.1, 127.6, 126.9, 122.1, 119.0, 82.0, 56.8, 50.2, 44.3, 43.4, 38.5, 36.8, 30.8, 29.7, 27.1, 26.3, 23.3, 11.2.

$\bar{\nu}_{max}$: 3456, 3066, 3034, 2924, 2868, 1720, 1605, 1491, 1456, 1367, 1169, 1130, 1055 cm^{-1} .

Phenyl 4-methylbenzenesulfonate

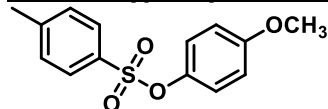


Prepared according to the procedure for reactions with 4-nitrophenyl 4-methylbenzenesulfonate, using phenol as the phenol. White solid. Yield: 127 mg (100%)

1H NMR (CD_3CN , 400 MHz): δ 7.70 (dt, J = 8.4, 2.2 Hz, 2H), 7.40 (d, J = 8.1 Hz, 2H), 7.37 – 7.26 (m, 3H), 7.04 – 6.98 (m, 2H), 2.43 (s, 3H).

Product was previously reported in many publications, the earliest mention being Gilman *et al.* (1925).¹¹

4-Methoxyphenyl 4-methylbenzenesulfonate

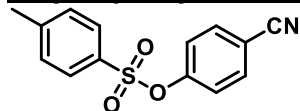


Prepared according to the procedure for reactions with 4-nitrophenyl 4-methylbenzenesulfonate, using 4-methoxyphenol as the phenol. White solid. Yield: 142 mg (100%)

1H NMR (CD_3CN , 400 MHz): δ 7.68 (dt, J = 8.4, 2.0 Hz, 2H), 7.41 – 7.36 (m, 2H), 6.91 (dt, J = 9.3, 3.5 Hz, 2H), 6.82 (dt, J = 9.3, 3.5 Hz, 2H), 3.73 (s, 3H), 2.42 (s, 3H).

Product was previously reported in many publications, the earliest mention being Borrows *et al.* (1949).¹²

4-Cyanophenyl 4-methylbenzenesulfonate

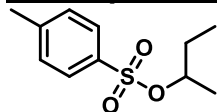


Prepared according to the procedure for reactions with 4-nitrophenyl 4-methylbenzenesulfonate, using 4-cyanophenol as the phenol. White solid. Yield: 119 mg (85%)

^1H NMR (CD_3CN , 400 MHz): δ 7.75 – 7.66 (m, 4H), 7.44 – 7.35 (m, 2H), 7.17 (dt, J = 8.9, 2.6 Hz, 2H), 2.42 (s, 3H).

Product was previously reported in many publications, the earliest mention being Takikawa *et al.* (1972).¹³

2-butoxy 4-methylbenzenesulfonate

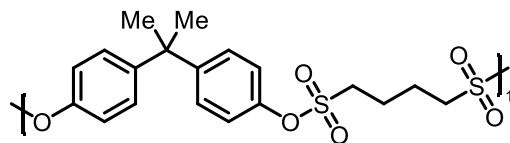


Prepared according to the procedure for reactions with 4-nitrophenyl 4-methylbenzenesulfonate, using 2-butanol as the alcohol. White solid. Yield: 111 mg (95%)

^1H NMR (CD_3CN , 400 MHz): δ 7.76 (dt, J = 8.4, 1.9 Hz, 2H), 7.47 – 7.36 (m, 2H), 4.53 (h, J = 6.2 Hz, 1H), 2.43 (s, 3H), 1.61 – 1.45 (m, 2H), 1.19 (d, J = 6.3 Hz, 3H), 0.75 (t, J = 7.4 Hz, 3H).

Product was previously reported in many publications, the earliest mention being Kenyon *et al.* (1935).¹⁴

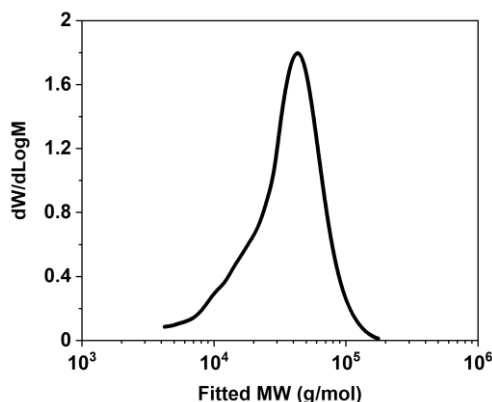
Polymer 8



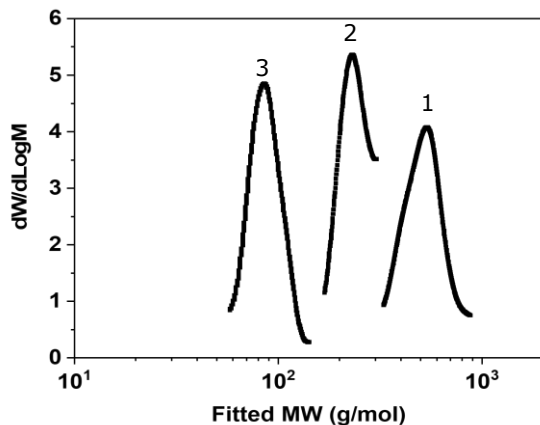
Product was previously reported in Gao *et al.* (2017).¹⁵

^1H NMR (400 MHz, CD_2Cl_2): δ 7.27 (d, J = 8.5 Hz, 4H), 7.17 (d, J = 8.4 Hz, 4H), 3.31 (s, 4H), 2.14 (s, 5H), 1.67 (s, 6H).

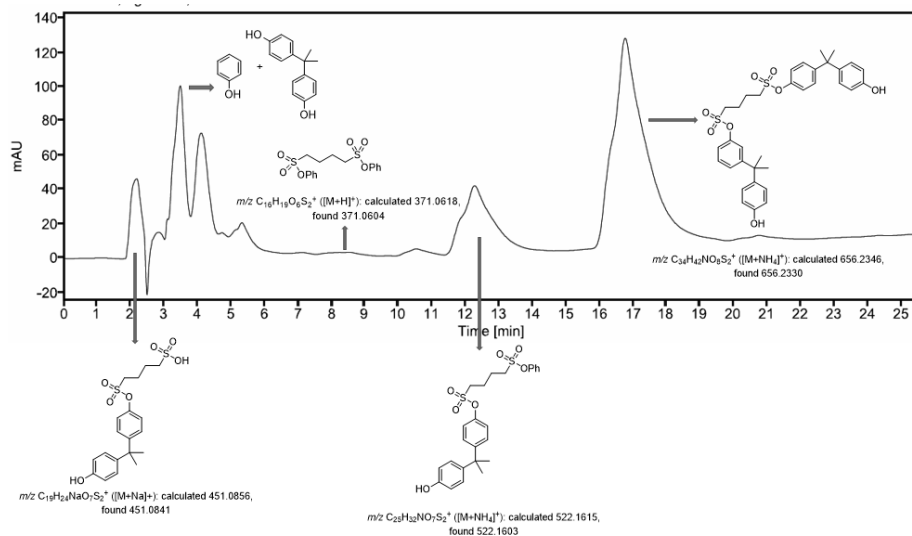
GPC and LC mass data for polysulfonate 8



Molecular Weight Averages							
Peak	Mp (g/mol)	Mn (g/mol)	Mw (g/mol)	Mz (g/mol)	Mz+1 (g/mol)	Mv (g/mol)	PD
Peak 1	43179	28575	40891	54573	88197	52833	1.539

Figure S4: GPC distribution plot and analyzed data for polysulfonate 8.

Molecular Weight Averages							
Peak	Mp (g/mol)	Mn (g/mol)	Mw (g/mol)	Mz (g/mol)	Mz+1 (g/mol)	Mv (g/mol)	PD
Peak 1	555	509	534	559	584	555	1.049
Peak 2	238	228	232	236	240	235	1.018
Peak 3	87	85	87	90	92	89	1.024

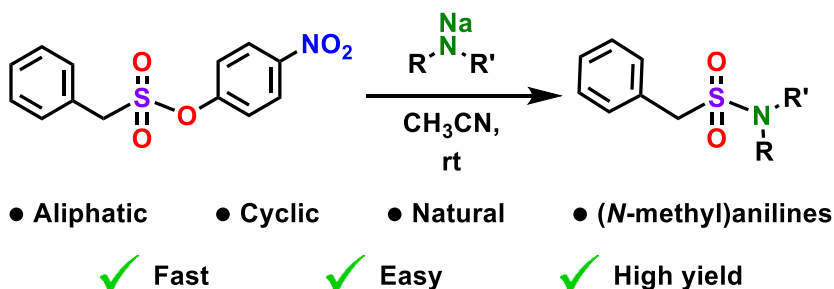
Figure S5: GPC distribution plot for degraded polysulfonate 8.**Figure S6:** LC mass spectrum of the degraded polysulfonate 8.

References

- (1) Zaborsky, O. R.; Kaiser, E. T. A Comparative Study of the Alkaline Hydrolysis of O-Hydroxy- α -Toluenesulfonic Acid Sultone and Phenyl α -Toluenesulfonate. *J. Am. Chem. Soc.* **1966**, *88* (13), 3084–3087.
- (2) Alonso, F.; Moglie, Y.; Vitale, C.; Radivoy, G.; Yus, M. A New Mild Deprotecting Method for O-Benzylsulfonyl Phenols and Alcohols Based on a DTBB-Catalyzed Lithiation. *Synthesis (Stuttg.)*. **2005**, No. 12, 1971–1976.
- (3) Moghaddam, F. M.; Hoor, A. A.; Dekamin, M. G. Microwave-Promoted Pseudo-Thia-Fries Rearrangement of Aryl Benzylsulfonates; Highly Reactive Benzyl Cation Generation. *J. Sulfur Chem.* **2004**, *25* (2–3), 125–130.
- (4) Truce, W. E.; Christensen, L. W. Base-Induced α -Sulfonylation of Aryl Alkanesulfonates. *J. Org. Chem.* **1970**, *35* (11), 3968–3970.
- (5) Betts, L. M.; Tam, N. C.; Kabir, S. M. H.; Langer, R. F.; Crandall, I. Ether Aryl Sulfonic Acid Esters with Improved Antimalarial/Anticancer Activities. *Aust. J. Chem.* **2006**, *59* (4), 277–282.
- (6) Gao, J.; Pan, X.; Liu, J.; Lai, J.; Chang, L.; Yuan, G. Iodine-Induced Synthesis of Sulfonate Esters from Sodium Sulfinates and Phenols under Mild Conditions. *RSC Adv.* **2015**, *5* (35), 27439–27442.
- (7) Davy, M. B.; Douglas, K. T.; Loran, J. S.; Steltner, A.; Williams, A. Elimination-Addition Mechanisms of Acyl Group Transfer: Hydrolysis and Aminolysis of Aryl Phenylmethanesulfonates. *J. Am. Chem. Soc.* **1977**, *99* (4), 1196–1206.
- (8) Smedley, C. J.; Homer, J. A.; Gialelis, T. L.; Barrow, A. S.; Koelln, R. A.; Moses, J. E. Accelerated SuFEx Click Chemistry For Modular Synthesis. *Angew. Chem. Int. Ed.* **2022**, *61* (4).
- (9) Bahrami, K.; Khodaei, M. M.; Abbasi, J. Synthesis of Sulfonamides and Sulfonic Esters via Reaction of Amines and Phenols with Thiols Using H₂O₂-POCl₃ System. *Tetrahedron* **2012**, *68* (25), 5095–5101.
- (10) Dai, Q.; Liu, L.; Zhang, J. Palladium / Xiao-Phos-Catalyzed Kinetic Resolution of Sec -Phosphine Oxides by P -Benzylation. *Angew. Chem. Int. Ed.* **2021**, *60*, 27247–27252.
- (11) Gilman, H.; Beaber, N. J.; Myers, C. H. THE REACTION BETWEEN ARYL SULFONATES AND ORGANOMAGNESIUM HALIDES. *J. Am. Chem. Soc.* **1925**, *47* (7), 2047–2052.
- (12) Borrows, E. T.; Clayton, J. C.; Hems, B. A.; Long, A. G. S 43. The Synthesis of Thyroxine and Related Substances. Part II. The Preparation of Dinitrodiphenyl Ethers. *J. Chem. Soc.* **1949**, No. 0, S190–S199.
- (13) Takikawa, Y.; Saburo, T. Reactions of Organic Compounds with Sodium Hydrosulfide in Liquid Ammonia. IV. Reactions of Aromatic Nitriles with Sodium Hydrosulfide in Liquid Ammonia. *Nippon Kagaku Kaishi* **1972**, 1972 (4), 766–770.
- (14) Kenyon, J.; Phillips, H.; Pittman, V. P. 250. Walden Inversion Reactions of d- β -Butyl, d- β -Octyl, and d-Benzylmethylcarbinyl p-Toluenesulphonates. *J. Chem. Soc.* **1935**, No. 0, 1072–1084.
- (15) Gao, B.; Zhang, L.; Zheng, Q.; Zhou, F.; Klivansky, L. M.; Lu, J.; Liu, Y.; Dong, J.; Wu, P.; Sharpless, K. B. Bifluoride-Catalysed Sulfur(VI) Fluoride Exchange Reaction for the Synthesis of Polysulfates and Polysulfonates. *Nat. Chem.* **2017**, *9* (11), 1083–1088.

Chapter 5

Sulphur-Phenolate Exchange as a mild, fast, and high-yielding method towards the synthesis of sulfonamides



This Chapter was published as:

Alyssa F.J. van den Boom and Han Zuilhof (2023); Sulphur-Phenolate Exchange as a mild, fast, and high-yielding method towards the synthesis of sulfonamides; *Organic Letters*, **25**, 788–793.

<https://doi.org/10.1021/acs.orglett.2c04292>

Abstract: Sulfonamides have many important biological applications, yet their synthesis often involves long reaction times under dry and non-ambient conditions. Here, we report the synthesis of a large range of sulfonamides at room temperature, using 4-nitrophenyl benzyisulfonate as a starting material. Sulfonamides were prepared from a wide range of aliphatic, linear, and cyclic amines, anilines, and *N*-methylanilines. The yields and reaction times observed here were comparable to or better than those reported previously, establishing SuPhenEx as a viable alternative.

The recent (re-)discovery and development of the sulfur fluoride exchange (SuFEx) reaction, in which an S-F bond is replaced by an S-O or S-N bond,¹ has greatly expanded the range of sulfonyl-containing compounds that are available to molecular scientists.² As a result, products of the SuFEx reaction can be found in fields ranging from polymer chemistry via organic synthesis to medicinal chemistry.^{3–9} For this last field, sulfonamides in particular are an important class of compounds, with many applications as e.g. anti-cancer¹⁰ or antiviral¹¹ drugs, protein^{12–14} or enzyme^{15–19} inhibitors. It is therefore not surprising that there has been much research into the synthesis of sulfonamides. Currently, the most common synthesis pathway is the reaction of the desired sulfonyl chloride with the desired amine under dry and basic conditions. While the yields obtained using this method are generally good, long reaction times,²⁰ (microwave) heating and/or non-ambient conditions^{16,17,21} are often needed, unless the amine is first activated by the addition of a lithium agent.^{22,23} Apart from this, the sulfonyl chlorides used as starting material generally display poor hydrolytic stability, leading to lower yields when the reaction medium is not thoroughly dried. While there are examples of the use of other leaving groups, such as thiazoles²⁴ or phosphates,²⁵ these routes suffered from poor yields. Sulfonyl fluorides can also be used as starting material, and indeed show good yields and a higher stability against hydrolysis than the corresponding sulfonyl chlorides.²⁶ Yet, for such use of sulfonyl fluorides, elevated temperatures or catalysts are often needed.^{27–30} Furthermore, there is an environment-driven trend to limit the use of fluorine-containing chemicals in industry. As a result, there is clearly a need for a fluorine-free alternative that is easy to make and a more stable starting material than sulfonyl chlorides, and that can still produce sulfonamides in a good yield, without catalysts, in <12 h of reaction time.

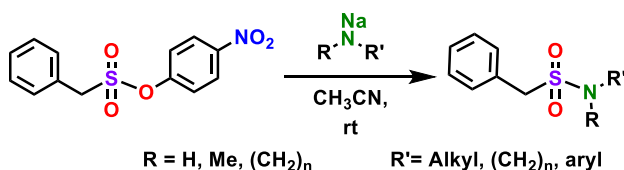


Figure 1: Overview of the SuPhenEx reaction with amines.

Previously, we have shown that the *p*-nitrophenolate moiety can function as an excellent leaving group in S(VI) exchange chemistry, making the corresponding sulfur-phenolate exchange (SuPhenEx) an efficient, fluorine-free alternative for the SuFEx reaction.^{31,32} Specifically, 4-nitrophenyl benzylsulfonate was shown to be a good alternative to benzylsulfonyl chloride or fluoride as a starting material, by creating in a near-quantitative fashion a large library of sulfonates using a simple and fast SuPhenEx reaction at room temperature.³² Now, we demonstrate that the same class of starting materials can also be used to create a large array of sulfonamides in good yields via the reaction with a wide range of alkyl amines and

N-alkylated anilines (Figure 1). To this end, we first allowed 4-nitrophenyl benzyldisulfonate (**1**) to exchange with aliphatic amines, using different primary butylamines as model compounds, and – as in the entire current study – NaH to create the corresponding N-centered anion (Table 1; briefly: NaH was added to the amine, stirred for 5 min, after which **1** was added; see Supporting Information for more details). All primary alkylamines reacted quantitatively within 5 min to form the corresponding sulfonamides. So, while even the *tert*-isomer (product **3c**) reacted readily, a significant increase to 2 h reaction time for quantitative product formation (all still at rt) was observed upon reaction of **1** with *N*-methylbutylamine (**2d**). For the corresponding *N*-ethyl derivative, yielding product **3e**, the reaction time increased to 6 h, though without compromising the yield. These results are in line with literature, where similarly high yields were obtained for aliphatic amines reacting with benzyldisulfonyl chloride, though typically after longer reaction times (2 – 19 h).^{10,18}

Table 1: SuPhenEx reaction of **1** with linear and cyclic aliphatic amines.

1	2
 3a , 5 min, 100%	 3b , 5 min, 100% (92%)
 3c , 5 min, 100%	 3d , 2 h, 100% (95%)
 3e , 6 h, 100% (91%)	
 3f , 10 min, 100%	 3g , 40 min, 100%
 3h , 4 h, 100% ^a (100%)	 3i , 3 h, 100% (100%)
 3j , 2 h, 100% (100%)	 3k , 3 h, 100% ^a (100%)
 3l , 3 h, 100% ^a (97%)	 3m , 4 h, 83% ^a (77%)
 3n , 24 h, 88% (88%)	 3o , 10 min, 90% (85%) ^b

Yields were determined by ¹H NMR measurements. Isolated yields are reported between brackets. Reaction times refer to the time needed for full conversion of **1**. Reaction conditions: 0.20 mmol **1** and 1.1 equiv **2** in 0.6 ml CH₃CN.

^a NMR yield confirmed using an internal standard. ^b 2 equiv of NaH were used.

For benzylic amines, the effect of an extra substituent on the amine was less pronounced, as demonstrated by the reaction times of **3f** and **3g**. In literature, no comparable reactions in solution are known, but 4-iodobenzylamine required 2 h to be coupled to surfaces functionalized with sulfonyl fluoride,³³ while amines with two

benzylic groups were coupled to benzylsulfonyl chloride with <86% yield after an overnight reaction.³⁴ The reaction times found here (10 – 40 min at rt) thus show a considerable improvement on these previous results.

After determining the effect of additional substitutions on the reactivity of amines, we turned our attention to the effect of ring size and ring strain, by performing the exchange reaction with simple cyclic amines ranging from 4- (azetidine) to 8-membered (azocane) rings as model compounds (yielding products **3h-3l**). The highest reactivity was found for piperidine (**2j**), with a reaction time of 2 h. This is in line with literature, where the basicity and charge on the N atom of piperidine is calculated – and basicity also experimentally determined – to be the highest from all cyclic amines studied here.³⁵ This is a direct effect of the low ring strain in piperidine; as the ring strain increases, the orbitals forming the N-C bonds are forced to increase in *p*-character, which leads the orbitals involved in the N-H bond and nitrogen lone pair to increase in *s* character. As the *s*-orbital is closer to the nucleus, this stabilizes the N-H bond and nitrogen lone pair, thereby lowering the basicity of the amine. In piperidine, the N-C bonds are closest to the natural angles of the *p*-orbitals, which explains the higher reactivity compared to both smaller and larger rings. In previous studies using 6-membered cyclic amines and benzylsulfonyl chloride, yields were either lower (60-90%) when the reaction was performed at 0-25 °C,^{13,14,36} or equal to the yield obtained here when the reaction was performed under reflux conditions.³⁷ The combination of reduced reaction times, quantitative yields and removal of the need for ultra-dry conditions shows the SuPhenEx reaction to be at least a viable alternative to these previous methods.

The previously demonstrated stability of **1** in aqueous solutions³² is, of course, especially effective in the SuPhenEx reactivity for use in many biological applications, specifically those involving polar natural amines (Table 1). To demonstrate its scope, we thus used several amino acids to attach to **1**. Since previous studies in our lab showed an incompatibility of carboxylic acid groups with the SuPhenEx reaction,³² a benzyl protecting group was used on the C-terminus of the amino acids. With this precaution, it was possible to obtain all three products **3m-o** in good yield, *i.e.* comparable to but minimally slightly faster than previously reported coupling reactions of benzylsulfonyl chloride to (benzyl-protected) amino acids.^{20,38} The longer reaction times for glycine (**3m**) and *L*-proline (**3n**), for which reaction times of minutes (glycine) or a couple of hours (*L*-proline) were expected, can be explained by the low solubility of these more polar amines in acetonitrile. Indeed, when 1 equiv of 15-crown-5 was added during the reaction, both products **3m** and **3n** were obtained in <30 minutes.

After these first studies, we tested a series of anilines and *N*-methylanilines (Table 2). Here, as opposed to the trend observed in Table 1, the reactivity was increased for secondary amines with respect to primary amines, and a wide variety of *N*-methylanilines reacted in good yields (83 – 100%) within 2 h. Only two *N*-methyl anilines did not react well: *N*-methyl-4-nitroaniline (**4f**), with the same

strongly electron-withdrawing substituent as the phenolate leaving group in **1**, gave no more than trace amounts of product. Additionally, the product from *p*-NH₂-substituted *N*-methyl aniline **5g** was obtained in low yield as well, due to side reactions with the additional amine moiety on this molecule. Interestingly, the only SuPhenEx product that was observed was the one with attachment *via* the *N*-methylamine group, demonstrating the difference in reactivity between anilines and *N*-methylanilines.

Table 2: SuPhenEx reaction of **1** with *N*-methylanilines and anilines.

1, 0.1 mmol	4, 1.1 equiv	dry CH ₃ CN (0.6 mL), rt	5	
5a , incomplete, 87%	5b , 1 h, 100 % (98%)	5c , 2 h, 100% (92%)	5d , 1.5 h, 100% (94%)	5e , 2 h, 100%
5f , trace amounts	5g , 3.5 h, 42% (36%) ^b	5h , 30 min, 77%	5i , incomplete, 90%	5j , incomplete, 90% (85%)
5k , incomplete, 88%	5l , trace amounts	5m , trace amounts	5n , no reaction	5o , incomplete, 83% (79%)
5p , degradation of 1	5q , incomplete, 40% (25%) ^b	5r , no product ^b	5s , 5 min, 25% (15%)	

Yield determined by ¹H NMR measurements, after filtering through a short silica plug. Isolated yields are reported between brackets.

^a Yield confirmed with an internal standard. ^b 2 equiv of NaH were used. Note: Incomplete reactions were stopped after 5 days.

For the primary anilines, only aniline itself gave full conversion, although good yields were still obtained for anilines with electronically moderate substituents (**5h-k**, **5o**) after longer reaction times than observed for *N*-methylanilines. When a stronger electron-withdrawing substituent was attached to the aniline, *e.g.* a nitro- (**5m,n**) or cyano- (**5p**) group, only trace amounts of product were found, or the starting material **1** degraded before product was formed. This is in line with previous room-temperature methods using benzyisulfonyl chloride as a starting material,^{39–42} although Cheng *et al.* reported the formation of a dinitro product in 89% yield using a 50% excess of aniline and base.⁴¹ Higher yields have also been reported for anilines using a microwave reaction at 130 °C.^{16,17,21} For **5r**, which is stabilized by resonance after deprotonation, no product was found, while the sterically hindered

and strained indole (**5s**) gave a low yield of 25% product, yet had a surprisingly short reaction time, comparable to those of aliphatic primary amines. As a result of the reduced reaction rate, the SuPhenEx reactions with anilines were also more susceptible to water. When the reaction vial was opened to air during a test reaction, the observed yield was lower, and more degradation of **1** could be observed. At the same time, if the reaction was performed under completely dry – but not oxygen-free – conditions, product formation took significantly longer, showing that trace amounts of water do actually seem to favor the reaction. Analysis of a crystalline side product found after degradation indicated hydrolysis of **1**. ^1H NMR of the crude reaction mixture after degradation also indicated side reactions on the amine itself, though the exact products were not analyzed in detail. As the corresponding reaction with phenols showed no such dependency on the presence of water,³² we postulate that a reaction occurs between the deprotonated amine and water. As a result of this, the amount of amine available for reaction with **1** is decreased, causing a lower yield and eventual base-catalyzed hydrolysis of **1**.

Next, **1** was reacted with other nitrogen-based nucleophiles, such as hydroxylamines, a hydrazine, a hydrazide, and an amide (Table 3), and some interesting results were found; where *O,N*-dimethyl-hydroxylamine **6a** gave 100% yield, the NH_2 -bearing hydroxylamine **6b** gave only trace amounts of product. Similarly, substituted hydrazine **6c** gave full conversion into the desired product, while hydrazide **6d** only gave 30% yield after 5 days. For amide **6e**, the negative charge on the nitrogen atom is stabilized by the carbonyl group, preventing product formation and leading to the eventual degradation of **1**.

Table 3: SuPhenEx reaction of **1** with other nitrogen-containing nucleophiles.

7a , 3 d, 100%	7b , trace amounts	7c , 2 h, 100% (78%)	7d , incomplete, 30% ^a (28%)	7e , degradation of 1

Yields were determined by ^1H NMR measurements. Isolated yields are reported between brackets. Reaction conditions: 0.20 mmol **1** and 1.1 equiv **2** in 0.6 ml CH_3CN . ^a NMR yield confirmed using an internal standard. Note: incomplete reactions were stopped after 5 days.

Finally, to further investigate the scope of the sulfonamide-forming SuPhenEx reaction, we varied the leaving group to a series of other phenolic moieties with less electron-withdrawing substituents on the *para*-position, and to a non-phenolic leaving group, namely the 2-butoxy moiety. To this aim, we repeated the SuPhenEx reaction with butylamine **2a** with several alternative starting materials (Table 4).

Changing the substituent on the phenolate leaving group from 4-nitro to 4-cyano leads to a small increase in reaction time, from 5 min to 15 min. When a trifluoromethyl group is used instead, the yield of **3a** decreases to 85%, while for the unsubstituted phenolate, the yield decreases even further, to just 40%. Finally, when an aliphatic 2-butoxy leaving group was used, no conversion was observed at all. This demonstrates that the reactivity of the SuPhenEx reaction can gradually be tuned by the substituent on the leaving group.

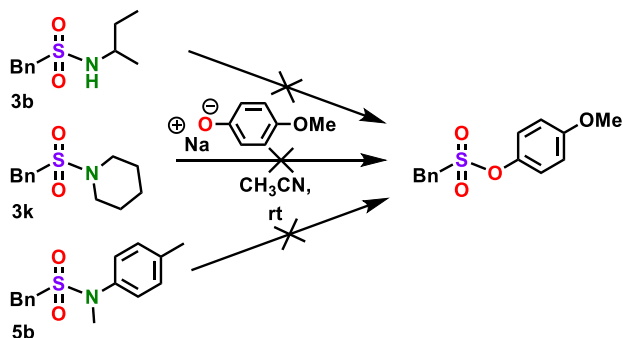
Table 4: The effect of the leaving group on the reactivity of the SuPhenEx reaction with butylamine.

<p>0.15 mmol, 1 equiv 1.1 equiv 3a</p>		
Leaving group	Yield	Time
4-Nitrophenolate	100%	5 min
4-Cyanophenolate	100%	15 min
4-Trifluoromethylphenolate	85%	Incomplete reaction
Phenolate	40%	Incomplete reaction
2-Butoxy	0%	No reaction

After determining the scope of the SuPhenEx reaction for the synthesis of sulfonamides, we investigated the degree of exchange with a good O-centered nucleophile. This is a.o. relevant, as for O-centered nucleophiles, we recently discovered the SuPhenEx reaction to be a dynamic covalent reaction, with e.g. potential for controlled polymer degradation.³¹ To this end, we selected three sulfonamide products **3b**, **3k**, and **5b**, and reacted these with sodium 4-methoxyphenolate, a strong oxygen-based nucleophile (Scheme 1). For all three reactions, no conversion or degradation of the sulfonamides was observed after 6 days of reaction time, and the starting products **3b**, **3k**, **5b** could be recovered quantitatively. This high stability of the sulfonamide products under these reaction conditions thus adds to the features of the SuPhenEx reaction in multistep synthesis.

Sulphur-Phenolate Exchange as a mild, fast and high-yielding method towards the synthesis of sulfonamides

Scheme 1: Sulfonamides remain stable under SuPhenEx conditions with a strong nucleophile.



In conclusion, we have demonstrated that the SuPhenEx reaction is a powerful S(VI) exchange chemistry alternative to conventional synthesis methods for the production of sulfonamides, using a stable and easy-to-use starting material. The reaction works well for a wide range of linear and cyclic aliphatic amines, (C-protected) amino acids, and *N*-alkylanilines. Yields obtained with the SuPhenEx reaction are comparable to or higher than those reported previously, while reaction times are often shorter and no rigorous drying is needed. Finally we demonstrated the stability of the created sulfonamides towards nucleophilic attack, allowing the SuPhenEx reaction to be used in orthogonal syntheses. With all this, we hope to expand the synthetic toolbox available to (bio-)molecular scientists.

References

- (1) Dong, J.; Krasnova, L.; Finn, M. G.; Barry Sharpless, K. Sulfur(VI) Fluoride Exchange (SuFEx): Another Good Reaction for Click Chemistry. *Angew. Chem. Int. Ed.* **2014**, *53* (36), 9430–9448.
- (2) Smedley, C. J.; Homer, J. A.; Gialelis, T. L.; Barrow, A. S.; Koelln, R. A.; Moses, J. E. Accelerated SuFEx Click Chemistry For Modular Synthesis. *Angew. Chem. Int. Ed.* **2022**, *61* (4).
- (3) Xu, L.; Wu, P.; Dong, J. New Polymers From SuFEx Click Chemistry : Syntheses and Perspectives. *Synthetic Polymer Chemistry: Innovations and Outlook* **2019**, No. 32, 1–31.
- (4) Smedley, C. J.; Li, G.; Barrow, A. S.; Gialelis, T. L.; Giel, M.-C.; Ottonello, A.; Cheng, Y.; Kitamura, S.; Wolan, D. W.; Sharpless, K. B.; Moses, J. E. Diversity Oriented Clicking (DOC): Divergent Synthesis of SuFExable Pharmacophores from 2-Substituted-Alkynyl-1-Sulfonyl Fluoride (SASF) Hubs. *Angew. Chem. Int. Ed.* **2020**, *59*, 12460–12469.
- (5) Liang, D. D.; Pujari, S. P.; Subramaniam, M.; Besten, M.; Zuilhof, H. Configurationally Chiral SuFEx-Based Polymers. *Angew. Chem. Int. Ed.* **2022**, *61* (8), e202116158.
- (6) Li, S.; Li, G.; Gao, B.; Pujari, S. P.; Chen, X.; Kim, H.; Zhou, F.; Klivansky, L. M.; Liu, Y.; Driss, H.; Liang, D. D.; Lu, J.; Wu, P.; Zuilhof, H.; Moses, J.; Sharpless, K. B. SuFExable Polymers with Helical Structures Derived from Thionyl Tetrafluoride. *Nat Chem* **2021**, *13* (9), 858–867.
- (7) Barrow, A. S.; Smedley, C. J.; Zheng, Q.; Li, S.; Dong, J.; Moses, J. E. The Growing Applications of SuFEx Click Chemistry. *Chem Soc Rev* **2019**, *48* (17), 4731–4758.
- (8) Abdul Fattah, T.; Saeed, A.; Albericio, F. Recent Advances towards Sulfur (VI) Fluoride Exchange (SuFEx) Click Chemistry. *J Fluor Chem* **2018**, *213*, 87–112.
- (9) Liang, D. D.; Streefkerk, D. E.; Jordaan, D.; Wagemakers, J.; Baggerman, J.; Zuilhof, H. Silicon-Free SuFEx Reactions of Sulfonylimidoyl Fluorides: Scope, Enantioselectivity, and Mechanism. *Angew. Chem. Int. Ed.* **2020**, *59* (19), 7494–7500.
- (10) Ling, T.; Tran, M.; González, M. A.; Gautam, L. N.; Connelly, M.; Wood, R. K.; Fatima, I.; Miranda-Carboni, G.; Rivas, F. (+)-Dehydroabietylamine Derivatives Target Triple-Negative Breast Cancer. *Eur J Med Chem* **2015**, *102*, 9–13.
- (11) Tomassi, C.; Nguyen Van Nhlen, A.; Marco-Contelles, J.; Balzarini, J.; Pannecouque, C.; de Clercq, E.; Postel, D. Synthesis and Anti-HIV1 Biological Activity of Novel 5"-ATSAO Compounds. *Bioorg Med Chem* **2008**, *16* (8), 4733–4741.
- (12) Whitman, D. B.; Askew, B. C.; Duong, L. T.; Fernandez-Metzler, C.; Halczenko, W.; Hartman, G. D.; Hutchinson, J. H.; Leu, C. T.; Prueksaritanont, T.; Rodan, G. A.; Rodan, S. B.; Duggan, M. E. Nonpeptide Av β 3 Antagonists. Part 9: Improved Pharmacokinetic Profile through the Use of an Aliphatic, Des-Amide Backbone. *Bioorg Med Chem Lett* **2004**, *14* (17), 4411–4415.

- (13) Zhu, J.; Chen, H.; Guo, X. E.; Qiu, X. L.; Hu, C. M.; Chamberlin, A. R.; Lee, W. H. Synthesis, Molecular Modeling, and Biological Evaluation of Novel RAD51 Inhibitors. *Eur J Med Chem* **2015**, *96*, 196–208.
- (14) Coburn, C. A.; Luo, Y.; Cui, M.; Wang, J.; Soll, R.; Dong, J.; Hu, B.; Lyon, M. A.; Santarelli, V. P.; Kraus, R. L.; Gregan, Y.; Wang, Y.; Fox, S. v.; Binns, J.; Doran, S. M.; Reiss, D. R.; Tannenbaum, P. L.; Gotter, A. L.; Meinke, P. T.; Renger, J. J. Discovery of a Pharmacologically Active Antagonist of the Two-Pore-Domain Potassium Channel K2P9.1 (TASK-3). *ChemMedChem* **2012**, *7* (1), 123–133.
- (15) Smallheer, J. M.; Wang, S.; Laws, M. L.; Nakajima, S.; Hu, Z.; Han, W.; Jacobson, I.; Luettggen, J. M.; Rossi, K. A.; Rendina, A. R.; Knabb, R. M.; Wexler, R. R.; Lam, P. Y. S.; Quan, M. L. Sulfonamidolactam Inhibitors of Coagulation Factor Xa. *Bioorg Med Chem Lett* **2008**, *18* (7), 2428–2433.
- (16) Perez, C.; Barkley-Levenson, A. M.; Dick, B. L.; Glatt, P. F.; Martinez, Y.; Siegel, D.; Momper, J. D.; Palmer, A. A.; Cohen, S. M. Metal-Binding Pharmacophore Library Yields the Discovery of a Glyoxalase 1 Inhibitor. *J Med Chem* **2019**, *62* (3), 1609–1625.
- (17) Rouffet, M.; de Oliveira, C. A. F.; Udi, Y.; Agrawal, A.; Sagi, I.; McCammon, J. A.; Cohen, S. M. From Sensors to Silencers: Quinoline- and Benzimidazole-Sulfonamides as Inhibitors for Zinc Proteases. *J Am Chem Soc* **2010**, *132* (24), 8232–8233.
- (18) Saupe, S. M.; Steinmetzer, T. A New Strategy for the Development of Highly Potent and Selective Plasmin Inhibitors. *J Med Chem* **2012**, *55* (3), 1171–1180.
- (19) Saupe, S. M.; Leubner, S.; Betz, M.; Klebe, G.; Steinmetzer, T. Development of New Cyclic Plasmin Inhibitors with Excellent Potency and Selectivity. *J Med Chem* **2013**, *56* (3), 820–831.
- (20) Ajani, O. O.; FAMILONI, O. B.; Echeme, J. O.; Wu, F. Ecofriendly Synthesis in Aqueous Medium: An Expeditious Approach to New N,N-Diethyl Amide Bearing Benzenemethanesulfonamides. *The Open Organic Chemistry Journal* **2013**, *7*, 1–10.
- (21) Adamek, R. N.; Credille, C. v.; Dick, B. L.; Cohen, S. M. Isosteres of Hydroxypyridinethione as Drug-like Pharmacophores for Metalloenzyme Inhibition. *Journal of Biological Inorganic Chemistry* **2018**, *23* (7), 1129–1138.
- (22) Chazallette, C.; Rivière-Baudet, M.; Supuran, C. T.; Scozzafava, A. Carbonic Anhydrase Inhibitors: Allylsulfonamide, Styrene Sulfonamide, N-Allyl Sulfonamides and Some of Their Si, Ge, and B Derivatives. *J Enzyme Inhib* **2001**, *16* (6), 475–489.
- (23) Lee, T.; Park, J. H.; Jeon, M. K.; Gong, Y. D. Solid-Phase Synthesis of 1,3,6-Trisubstituted-LH-Thiazolo[4,5-c][1,2] Thiazin-4(3H)One-2,2-Dioxide Derivatives Using Traceless Linker. *J Comb Chem* **2009**, *11* (2), 288–293.
- (24) Day, J. J.; Neill, D. L.; Xu, S.; Xian, M. Benzothiazole Sulfinic Acid Transfer Reagent under Oxidation-Free Conditions. *Org Lett* **2017**, *19* (14), 3819–3822.
- (25) Harger, M. J. P. Competing Sulfonylation and Phosphonylation Following Rearrangement of an O-Sulfonyl-N-Phosphinoylhydroxylamine with Tert-Butylamine: Demonstration of a Phosphonamidic-Sulfonic Anhydride

- Intermediate and 18O-Labeling Evidence on How It May Be Formed. *Org Biomol Chem* **2003**, 1 (19), 3390–3395.
- (26) Lou, T. S.-B.; Willis, M. C. Sulfonyl Fluorides as Targets and Substrates in the Development of New Synthetic Methods. *Nat Rev Chem* **2022**, 6 (2), 146–162.
- (27) Mahapatra, S.; Woroch, C. P.; Butler, T. W.; Carneiro, S. N.; Kwan, S. C.; Khasnavis, S. R.; Gu, J.; Dutra, J. K.; Vetelino, B. C.; Bellenger, J.; Am Ende, C. W.; Ball, N. D. SuFEx Activation with Ca(NTf₂)₂: A Unified Strategy to Access Sulfamides, Sulfamates, and Sulfonamides from S(VI) Fluorides. *Org Lett* **2020**, 22 (11), 4389–4394.
- (28) Dondoni, A.; Marra, A. SuFEx: A Metal-Free Click Ligation for Multivalent Biomolecules. *Org Biomol Chem* **2017**, 15 (7), 1549–1553.
- (29) Zelli, R.; Tommasone, S.; Dumy, P.; Marra, A.; Dondoni, A. A Click Ligation Based on SuFEx for the Metal-Free Synthesis of Sugar and Iminosugar Clusters. *European J Org Chem* **2016**, 2016 (30), 5102–5116.
- (30) Wei, M.; Liang, D.; Cao, X.; Luo, W.; Ma, G.; Liu, Z.; Li, L. A Broad-Spectrum Catalytic Amidation of Sulfonyl Fluorides and Fluorosulfates**. *Angewandte Chemie International Edition* **2021**, 60 (13), 7397–7404.
- (31) Chao, Y.; Krishna, A.; Subramaniam, M.; Liang, D.-D.; Pujari, S. P.; Sue, A. C.-H.; Li, G.; Miloserdov, F. M.; Zuilhof, H. Sulfur-Phenolate Exchange: SuFEx-Derived Dynamic Covalent Reactions and Degradation of SuFEx Polymers. *Angew. Chem. Int. Ed.* **2022**, No. e202207456.
- (32) van den Boom, A. F. J.; Subramaniam, M.; Zuilhof, H. Sulfur-Phenolate Exchange As a Fluorine-Free Approach to S(VI) Exchange Chemistry on Sulfonyl Moieties. *Org Lett* **2022**, 24 (47), 8621–8626.
- (33) Gahtory, D.; Sen, R.; Pujari, S.; Li, S.; Zheng, Q.; Moses, J. E.; Sharpless, K. B.; Zuilhof, H. Quantitative and Orthogonal Formation and Reactivity of SuFEx Platforms. *Chemistry - A European Journal* **2018**, 24 (41), 10550–10556.
- (34) Hill, B.; Liu, Y.; Taylor, S. D. Synthesis of α -Fluorosulfonamides by Electrophilic Fluorination. *Org Lett* **2004**, 6 (23), 4285–4288.
- (35) Radić, N.; Despotović, I.; Vianello, R. Ring Strain and Other Factors Governing the Basicity of Nitrogen Heterocycles - An Interpretation by Triadic Analysis. *Croatica Chemica Acta* **2012**, 85 (4), 495–504.
- (36) Ivachtchenko, A. v.; Tkachenko, S. E.; Sandulenko, Y. B.; Vvedensky, V. Y.; Khvat, A. v. A Parallel Solution-Phase Synthesis of Substituted 3,7-Diazabicyclo[3.3.1] Nonanes. *J Comb Chem* **2004**, 6 (5), 828–834.
- (37) Naredla, R. R.; Klumpp, D. A. Preparation of Sulfonamides from N-Silylamines. *Tetrahedron Lett* **2013**, 54 (45), 5945–5947.
- (38) Tang, J.; Chen, H.; He, Y.; Sheng, W.; Bai, Q.; Wang, H. Peptide-Guided Functionalization and Macrocyclization of Bioactive Peptidosulfonamides by Pd(II)-Catalyzed Late-Stage C–H Activation. *Nat Commun* **2018**, 9 (1).
- (39) Park, H. G.; Choi, J. Y.; Choi, S. H.; Park, M. K.; Lee, J.; Suh, Y. G.; Cho, H.; Oh, U.; Lee, J.; Kang, S. U.; Lee, J.; Kim, H. D.; Park, Y. H.; Jeong, Y. S.; Choi, J. K.; Jew, S. S. N-4-Substituted-Benzyl-N'-Tert-Butylbenzyl Thioureas as Vanilloid Receptor Ligands: Investigation on the Role of Methanesulfonamido Group in Antagonistic Activity. *Bioorg Med Chem Lett* **2004**, 14 (3), 787–791.

Sulphur-Phenolate Exchange as a mild, fast and high-yielding method towards
the synthesis of sulfonamides

- (40) Chen, H.; Wang, L.; Han, J. Deacetylative Aryl Migration of Diaryliodonium Salts with C(Sp²)-N Bond Formation toward Ortho-Iodo N-Aryl Sulfonamides. *Org Lett* **2020**, 22 (9), 3581–3585.
- (41) Cheng, G.; Wang, P.; Yu, J.-Q. Meta -C–H Arylation and Alkylation of Benzylsulfonamide Enabled by a Palladium(II)/Isoquinoline Catalyst . *Angewandte Chemie* **2017**, 129 (28), 8295–8298.
- (42) Dai, H. X.; Stepan, A. F.; Plummer, M. S.; Zhang, Y. H.; Yu, J. Q. Divergent C-H Functionalizations Directed by Sulfonamide Pharmacophores: Late-Stage Diversification as a Tool for Drug Discovery. *J Am Chem Soc* **2011**, 133 (18), 7222–7228.

Supporting Information

General information

Chemicals

Sodium hydride (60% dispersion in mineral oil), 4-nitrophenol, phenylmethylsulfonyl fluoride, aniline, benzylamine, *n*-butylamine, *sec*-butylamine, *tert*-butylamine, *N*-ethylbutylamine, glycine benzyl ester hydrochloride, *L*-proline benzyl ester, *L*-tryptophan benzyl ester, piperidine, 3-nitro-*N*-methylaniline, *N*-methyl-4-nitroaniline, *p*-toluidine, 4-fluoroaniline, 4-chloroaniline, 3'-aminoacetophenone, 3-nitroaniline, adenine, 3-aminobenzonitrile, methyl 4-aminobenzoate, 4-nitroaniline, phenol, 2-butanol, 4-cyanophenol, 4-(trifluoromethyl)phenol were bought from Merck Life Science N.V.; acetonitrile- d_3 was bought from Fisher Scientific B.V.; 4-(methylamino)benzoate was bought from Alfa Aesar; *N*-1-methylbenzene-1,4-diamine dihydrochloride was bought from Fluorochem Ltd; *N*-methyl-1-butylamine, 1-aminopiperidine, 1-cyclohexylhydrazine hydrochloride, hexanehydrazine, *O*-benzylhydroxylamine, *O,N*-dimethyl-hydroxylamine hydrochloride, benzamide, *N*-methyl-*p*-toluidine, 4-chloro-*N*-methylaniline, 4-fluoro-*N*-methylaniline, heptamethyleneimine were bought from ABRC GmbH; azetidine, pyrrolidine, indole, *N*-methylbenzylamine, *N*-methylaniline, hexamethyleneimine, 4,4'-diaminodiphenyl ether were bought from TCI Europe N.V. All chemicals were used as received. Phenyl benzyisulfonate, 2-butoxy benzyisulfonate, 4-cyanophenyl benzyisulfonate, and 4-(trifluoromethyl)phenyl benzyisulfonate were prepared as described in ¹.

Analysis

NMR measurements were conducted on a 400 MHz Bruker Avance III at 298K, and the resulting data were analyzed using MestReNova software, version 14.1.0-24037. Spectra were calibrated relative to signals corresponding to the non-deuterated solvents (CH₃CN solvent peak) – at 1.94 ppm for ¹H spectra, and 1.32 ppm for ¹³C spectra. Spectra recorded in CDCl₃ were calibrated on the non-deuterated solvent peak at 7.26 ppm (¹H spectra) and 77.16 ppm (¹³C spectra). ¹⁹F spectra were not calibrated. Abbreviations used in the description of NMR data are as follows: chemical shift (δ = ppm), multiplicity (s = singlet, d = doublet, t = triplet, q = quartet, p = pentet, sextet = sext, h = heptet, dt = doublet of triplets, m = multiplet, br = broadened), coupling constant (*J*, Hz).

High-resolution mass spectra (HRMS) were recorded on a Thermo Scientific Exactive 1.1 with an orbitrap mass analyzer, using a DART gun from Ion Sense. The temperature of the DART gun was set to 300-550 °C, with a nitrogen gas flow. Data were analyzed using Thermo Xcalibur software, version 2.2 SP1.48.

IR spectra were recorded on a Bruker Tensor 27 spectrometer equipped with a diamond ATR accessory (64 scans; 4 cm⁻¹ resolution; range 4000-350 cm⁻¹). Strong or indicative peaks in the region 4000-1000 cm⁻¹ are mentioned for each novel compound.

TLC analysis was performed on pre-coated, alumina-backed silica gel plates. TLC plates were analyzed by UV fluorescence (254 nm) or KMnO₄ stain followed by heating.

Column chromatography for isolated yields and full characterization was performed using silica (40-63 µm, 230-400 mesh) and 35-60% ethyl acetate in hexane, depending on the polarity of the product. To perform flash chromatography, a connector connected to a compressed-air flow was installed on the column.

Synthetic procedures

All reactions were performed at room temperature, under ambient atmosphere.

4-Nitrophenyl phenylmethanesulfonate **1**

NaH (60% in oil, 293 mg, 7.34 mmol, 1.4 equiv) was added to 4-nitrophenol (948 mg, 6.82 mmol, 1.3 equiv) in 80 ml of dry tetrahydrofuran, and the solution was stirred for 5 min. Next, phenylmethanesulfonyl chloride (1.0 g, 5.25 mmol, 1.0 equiv) was added, and stirring was continued for 24 h. Then, the reaction mixture was diluted with 150 ml of DCM and transferred to a separatory funnel, where it was washed with water (3 × 150 ml). The organic phase was isolated, dried over sodium sulphate, and the solvent was evaporated. Next, the product was further purified by column chromatography (n-hex/EA) (using a Biotage® system and SiliCycle® precast silica columns (200–300 mesh or 300–400 mesh)) to yield compound **1** (1.37 g, 89%) as white crystals.

General procedure for the synthesis of products (for NMR screening)

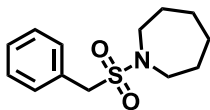
In a typical exchange reaction, 5 mg of NaH (0.124 mmol, 1.2 equiv) and 0.113 mmol (1.1 equiv) of aniline/amine were dissolved in 0.9 mL of CH₃CN (stored over NaSO₄), and the reaction was stirred for ~5 min to generate the deprotonated amine. After this time, 30 mg (0.103 mmol, 1.0 equiv) of **1** was added, and stirring was continued. TLC (35% ethyl acetate in hexane) was used to monitor the progress of the reaction by the disappearance of the spot belonging to 4-nitrophenyl phenylmethanesulfonate. When necessary, staining with a standard permanganate stain was performed to better visualize spots. When the spot for **1** had fully disappeared, the reaction mixture was filtered through a short silica plug to remove the sodium nitrophenolate. The solvents were evaporated, and the mixture was

directly analyzed using ^1H NMR. No internal standard was needed in this case, as the sodium nitrophenolate was filtered off, and no other side products – except in the case of degradation – are formed during the reaction. As a result, the reaction mixture only contains the product and any remaining starting material, both of which provide well-separated signals in ^1H NMR. The yield could therefore be determined by the disappearance of the signals belonging to 4-nitrophenol, with a simultaneous appearance of product signals. A reference spectrum of the reactant amine was recorded in all cases, and successful binding was further confirmed by a change in chemical shift for the signals belonging to the added amine upon attachment to the S(VI) hub. When the reaction was filtered prematurely – or when conversion was $<100\%$ – signals from an attached nitrophenol group were still visible (though with a lower integral value), and the product signals of the partially attached amine had lower integrals than expected based on full conversion. When degradation took place, no product signals were observed, and signals from the starting material had shifted or disappeared. To confirm the accuracy of this method, an internal standard (vinyltrimethylsilane) was added to several reaction mixtures after evaporation of the solvent, and the yield was determined both with and without internal standard. The difference in yield determined in this way was $<1\%$, confirming the accuracy of the NMR yields determined without internal standard.

Products for isolated yields and full characterization

Compounds for which the isolated yield was determined, and novel compounds that had to be characterized more extensively, were synthesized in the same way as described above for the NMR products, on a scale of 60 mg (0.21 mmol) of **1**. After the reaction was completed, the reaction mixture was transferred to an extraction funnel, diluted with ~ 15 ml of ethyl acetate, and washed with ~ 4 ml fractions of water, until the water layer was colorless (typically 5 fractions were needed). Then, the organic layer was washed 3x with ~ 4 ml of an 1M aqueous solution of KHSO_4 . The organic layer was isolated, dried with Na_2SO_4 , filtered, and concentrated on a rotavapor. The crude product was further purified using flash column chromatography (silica gel) with 35%-60% ethyl acetate in hexane, depending on the polarity of the product. A representative example of the synthesis of 1-(benzylsulfonyl)azepane (**3k**) on a scale of 0.31 mmol **1** is provided below.

3k: 1-(benzylsulfonyl)azepane

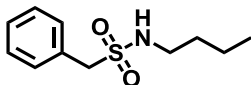


15.0 mg (60% dispersion, 0.38 mmol, 1.2 equiv) NaH was weighed into a 4 mL vial equipped with a stir bar, and 33.6 mg (0.34 mmol, 1.1 equiv) hexamethyleneimine was added. Next, 1.8 ml of acetonitrile – stored over sodium sulfate – was added, and the resulting mixture was stirred for 5 min. 90.0 mg (0.31 mmol, 1 equiv) of 4-nitrophenyl phenylmethanesulfonate **1** was added, and the reaction was allowed to stir at room temperature. Reaction progress was monitored by TLC (35% ethyl acetate in hexane), and full conversion was confirmed by the disappearance of the spot belonging to **1**. After 3 h, this spot had fully disappeared, and the reaction mixture was transferred to an extraction funnel along with 20 ml of ethyl acetate. The organic layer was washed 5× with 5 ml of water, until the water layer was completely colorless. The organic layer was collected, dried over sodium sulfate, and concentrated on a rotavapor. The product was further purified by flash column chromatography (silica gel, 35% ethyl acetate in hexane) to yield 77.7 mg (0.31 mmol, 100%) of **3k** as an off-white solid.

Characterization of compounds

Spectra of all novel compounds can be found online at:
<https://doi.org/10.1021/acs.orglett.2c04292>.

3a: N-butyl-1-phenylmethanesulfonamide

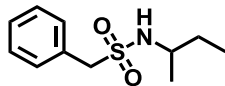


Prepared according to the general procedure described above using butylamine as the amine. NMR yield: 100%

HRMS: m/z $C_{11}H_{18}NO_2S^+$ ($[M+H]^+$): calculated 228.1053, found 228.1053.

1H NMR (CD_3CN , 400 MHz): δ 7.44 – 7.33 (m, 5H), 5.10 (s, 1H), 4.25 (s, 2H), 2.97 (q, J = 7.0 Hz, 2H), 1.45 (p, J = 7.0 Hz, 2H), 1.32 (h, J = 7.0 Hz, 2H), 0.89 (t, J = 7.3 Hz, 3H).

These values match previously reported data.²

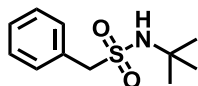
3b: *N*-(*sec*-butyl)-1-phenylmethanesulfonamide

Prepared according to the general procedure described above using *sec*-butylamine as the amine. Purified by column: 35% ethyl acetate in hexane. White crystals. NMR yield: 100%; isolated yield: 42.6 mg, 92%.

HRMS: m/z $C_{11}H_{18}NO_2S^+$ ($[M+H]^+$): calculated 228.1053, found 228.1052.

1H NMR (CD_3CN , 400 MHz): δ 7.49 – 7.33 (m, 5H), 5.01 (d, J = 7.8 Hz, 1H), 4.26 (s, 2H), 3.28 (dh, J = 8.1, 6.6 Hz, 1H), 1.61 – 1.36 (m, 2H), 1.14 (d, J = 6.6 Hz, 3H), 0.89 (t, J = 7.4 Hz, 3H). **^{13}C NMR (CD_3CN , 101 MHz):** δ 131.4, 131.0, 129.0, 128.8, 117.9, 59.5, 52.1, 30.8, 21.3, 10.1.

$\bar{\nu}_{max}$: 3284, 3066, 2995, 2966, 2924, 2875, 1492, 1456, 1429, 1298, 1265, 1157, 1109 cm^{-1}

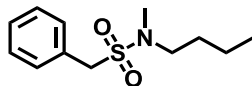
3c: *N*-(*tert*-butyl)-1-phenylmethanesulfonamide

Prepared according to the general procedure described above using *tert*-butylamine as the amine. NMR yield: 100%

HRMS: m/z $C_{11}H_{18}NO_2S^+$ ($[M+H]^+$): calculated 228.1053, found 228.1053.

1H NMR (CD_3CN , 400 MHz): δ 7.47 – 7.32 (m, 5H), 4.93 (s, 1H), 4.26 (s, 2H), 1.33 (s, 9H).

These values match previously reported data.³

3d: *N*-butyl-*N*-methyl-1-phenylmethanesulfonamide

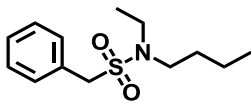
Prepared according to the general procedure described above using *N*-methylbutylamine as the amine. Purified by column: 35% ethyl acetate in hexane. Light yellow crystals. NMR yield: 100%; isolated yield: 46.9 mg, 95%.

HRMS: m/z $C_{12}H_{20}NO_2S^+$ ($[M+H]^+$): calculated 242.1209, found 242.1210.

1H NMR (CD_3CN , 400 MHz): δ 7.48 – 7.30 (m, 5H), 4.24 (s, 2H), 3.01 (t, J = 7.2 Hz, 2H), 2.73 (s, 3H), 1.47 (p, J = 7.3 Hz, 2H), 1.27 (h, J = 7.3 Hz, 2H), 0.89 (t, J = 7.4 Hz, 3H). **^{13}C NMR (CD_3CN , 101 MHz):** δ 131.9, 130.9, 129.5, 129.3, 118.3, 55.9, 50.7, 35.2, 30.8, 20.3, 13.9.

$\bar{\nu}_{max}$: 3063, 3034, 2956, 2929, 2870, 1603, 1495, 1456, 1317, 1205, 1144, 1086, 1018 cm^{-1}

3e: *N*-butyl-*N*-ethyl-1-phenylmethanesulfonamide



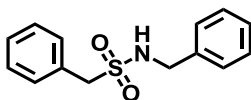
Prepared according to the general procedure described above using *N*-ethylbutylamine as the amine. Purified by column: 35% ethyl acetate in hexane. Thick yellowish oil. NMR yield: 100%; isolated yield: 47.5 mg, 91%.

HRMS: m/z $C_{13}H_{22}NO_2S^+$ ($[M+H]^+$): calculated 256.1366, found 256.1376.

1H NMR (CD_3CN , 400 MHz): δ 7.44 – 7.33 (m, 5H), 4.22 (s, 2H), 3.14 (q, J = 7.1 Hz, 2H), 3.05 (t, J = 7.6 Hz, 2H), 1.48 (p, J = 7.8 Hz, 2H), 1.27 (h, J = 7.4 Hz, 2H), 1.10 (t, J = 7.1 Hz, 3H), 0.90 (t, J = 7.4 Hz, 3H). **^{13}C NMR (CD_3CN , 101 MHz):** δ 131.9, 131.2, 129.4, 129.2, 57.7, 48.5, 43.9, 32.1, 20.5, 15.3, 14.0.

$\bar{\nu}_{max}$: 3064, 3034, 2958, 2931, 2874, 1595, 1497, 1456, 1331, 1192, 1146, 1122, 1024 cm^{-1}

3f: *N*-benzyl-1-phenylmethanesulfonamide



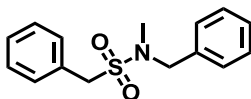
Prepared according to the general procedure described above using benzylamine as the amine. NMR yield: 100%.

HRMS: m/z $C_{14}H_{16}NO_2S^+$ ($[M+H]^+$): calculated 262.0896, found 262.0888.

1H NMR (CD_3CN , 400 MHz): δ 7.43 – 7.26 (m, 10H), 5.62 (s, 1H), 4.26 (s, 2H), 4.17 (d, J = 6.4 Hz, 2H).

This compound was first reported by Johnson *et al.* (1914).⁴

3g: *N*-benzyl-*N*-methyl-1-phenylmethanesulfonamide

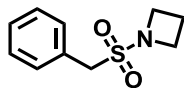


Prepared according to the general procedure described above using *N*-methylbenzylamine as the amine. NMR yield: 100%.

HRMS: m/z $C_{15}H_{18}NO_2S^+$ ($[M+H]^+$): calculated 276.1053, found 276.1052.

1H NMR (CD_3CN , 400 MHz): δ 7.46 – 7.39 (m, 5H), 7.39 – 7.33 (m, 2H), 7.33 – 7.27 (m, 3H), 4.34 (s, 2H), 4.17 (s, 2H), 2.64 (s, 3H).

This product was previously reported in Nikam *et al.* (1998).⁵

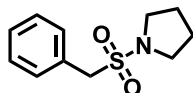
3h: 1-(benzylsulfonyl)azetidine

Prepared according to the general procedure described above using azetidine as the amine. Purified by column: 35% ethyl acetate in hexane. White solid. NMR yield: 100%; NMR yield (IS): 100%; isolated yield: 43.2 mg, 100%.

HRMS: m/z $C_{10}H_{14}NO_2S^+$ ($[M+H]^+$): calculated 212.0740, found 212.0738.

1H NMR ($CDCl_3$, 400 MHz): δ 7.45 – 7.40 (m, 2H), 7.41 – 7.33 (m, 3H), 4.19 (s, 2H), 3.78 (t, J = 7.7 Hz, 4H), 2.15 (p, J = 7.8 Hz, 2H). **^{13}C NMR ($CDCl_3$, 101 MHz):** δ 130.9, 128.9, 128.82, 128.77, 57.7, 51.0, 15.3.

$\bar{\nu}_{max}$: 3059, 3028, 2978, 2906, 1593, 1493, 1454, 1335, 1309, 1288, 1234, 1207, 1149, 1126, 1065, 1030 cm^{-1}

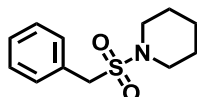
3i: 1-(benzylsulfonyl)pyrrolidine

Prepared according to the general procedure described above using pyrrolidine as the amine. Purified by column: 35% ethyl acetate in hexane. Light yellow solid. NMR yield: 100%; isolated yield: 46.1 mg, 100%.

HRMS: m/z $C_{11}H_{16}NO_2S^+$ ($[M+H]^+$): calculated 226.0896, found 226.0893.

1H NMR (CD_3CN , 400 MHz): δ 7.45 – 7.36 (m, 5H), 4.27 (s, 2H), 3.22 – 3.14 (m, 4H), 1.84 (t, J = 3.5 Hz, 2H), 1.83 (t, J = 3.6 Hz, 2H).

These values match previously reported values for this compound.⁶

3j: 1-(benzylsulfonyl)piperidine

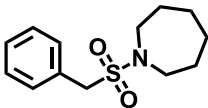
Prepared according to the general procedure described above using piperidine as the amine. Purified by column: 35% ethyl acetate in hexane. Light yellow solid. NMR yield: 100%; isolated yield: 49 mg, 100%.

HRMS: m/z $C_{12}H_{18}NO_2S^+$ ($[M+H]^+$): calculated 240.1053, found 240.1049.

1H NMR (CD_3CN , 400 MHz): δ 7.45 – 7.34 (m, 5H), 4.20 (s, 2H), 3.18 – 3.07 (m, 4H), 1.58 – 1.47 (m, 6H).

These values match previously reported values for this compound.⁶

3k: 1-(benzylsulfonyl)azepane



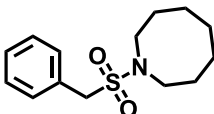
Prepared according to the general procedure described above using hexamethyleneimine as the amine. Purified by column: 35% ethyl acetate in hexane. Off-white solid. NMR yield: 100%; NMR yield (IS): 100%; isolated yield: 51.8 mg, 100%.

HRMS: m/z $C_{13}H_{20}NO_2S^+$ ($[M+H]^+$): calculated 254.1209, found 254.1207.

1H NMR ($CDCl_3$, 400 MHz): δ 7.36 (s, 5H), 4.22 (s, 2H), 3.08 (t, J = 5.5 Hz, 4H), 1.66 – 1.53 (m, 8H). **^{13}C NMR ($CDCl_3$, 101 MHz):** δ 130.7, 129.7, 128.8, 128.6, 57.1, 49.1, 29.9, 26.8.

$\bar{\nu}_{max}$: 3063, 3030, 2920, 2850, 1603, 1493, 1446, 1323, 1286, 1225, 1144, 1043 cm^{-1}

3l: 1-(benzylsulfonyl)azocane



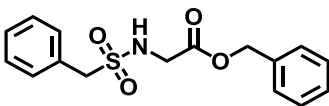
Prepared according to the general procedure described above using heptamethyleneimine as the amine. Purified by column: 35% ethyl acetate in hexane. Light yellow solid. NMR yield: 100%; NMR yield (IS): 100%; isolated yield: 53.1 mg, 97%.

HRMS: m/z $C_{14}H_{22}NO_2S^+$ ($[M+H]^+$): calculated 268.1366, found 268.1364.

1H NMR (CD_3CN , 400 MHz): δ 7.72 – 7.09 (m, 5H), 4.23 (s, 2H), 3.11 (t, J = 5.5 Hz, 4H), 1.69 – 1.50 (m, 10H). **^{13}C NMR (CD_3CN , 101 MHz):** δ 131.8, 131.0, 129.5, 129.2, 55.6, 50.2, 28.8, 27.6, 25.5.

$\bar{\nu}_{max}$: 3063, 3034, 2926, 2854, 1495, 1454, 1327, 1149, 1122, 1082, 1028 cm^{-1}

3m: benzyl (benzylsulfonyl)glycinate



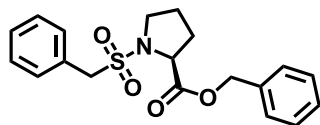
Prepared according to the general procedure described above using glycine benzyl ester as the amine. Purified by extraction with ethyl acetate and water, as described in the general procedure for isolated compounds. White needles. NMR yield: 84%; NMR yield (IS): 83%; isolated yield: 50.3 mg, 77%.

HRMS: m/z $C_{16}H_{21}N_2O_4S^+$ ($[M+NH_4]^+$): calculated 337.1217, found 337.1218.

^1H NMR (CD_3CN , 400 MHz): δ 7.46 – 7.20 (m, 10H), 5.61 (s, 1H), 5.17 (s, 2H), 4.33 (s, 2H), 3.79 (d, J = 6.0 Hz, 2H). **^{13}C NMR (CD_3CN , 101 MHz):** δ 170.7, 136.9, 131.9, 130.9, 129.6, 129.5, 129.4, 129.33, 129.25, 67.8, 59.8, 45.3.

$\bar{\nu}_{\text{max}}$: 3263, 3063, 3036, 2937, 1743, 1593, 1497, 1454, 1419, 1379, 1329, 1309, 1238, 1213, 1198, 1147, 1111, 1026 cm^{-1}

3n: benzyl (benzylsulfonyl)-L-prolinate

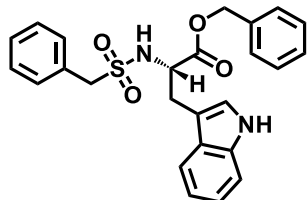


Prepared according to the general procedure described above using *L*-proline benzyl ester as the amine. Purified by recrystallization from 25% ethyl acetate in hexane. Light yellow solid. NMR yield: 88%; isolated yield: 64.7 mg, 88%.

HRMS: m/z $\text{C}_{19}\text{H}_{22}\text{NO}_4\text{S}^+$ ($[\text{M}+\text{H}]^+$): calculated 360.1264, found 360.1259.

^1H NMR (CD_3CN , 400 MHz): δ 7.47 – 7.30 (m, 10H), 5.15 (s, 2H), 4.32 (q, J = 13.7 Hz, 2H), 4.17 (dd, J = 8.7, 3.6 Hz, 1H), 3.36 – 3.21 (m, 2H), 2.23 – 2.12 (m, 1H), 1.98 – 1.92 (m, 1H), 1.92 – 1.81 (m, 2H). **^{13}C NMR (CD_3CN , 101 MHz):** δ 173.4, 137.1, 131.9, 130.7, 129.6, 129.5, 129.4, 129.3, 129.1, 67.6, 61.8, 57.4, 49.6, 31.7, 25.6.

3o: benzyl (benzylsulfonyl)-L-tryptophanate



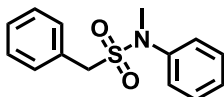
Prepared according to the general procedure described above using 2 equiv of NaH, and *L*-tryptophan benzyl ester as the amine. Purified by recrystallization from 25% ethyl acetate in hexane. Yellow-brown solid. NMR yield: 90%; isolated yield: 78.0 mg, 85%.

HRMS: m/z $\text{C}_{25}\text{H}_{28}\text{N}_3\text{O}_4\text{S}^+$ ($[\text{M}+\text{NH}_4]^+$): calculated 466.1795, found 466.1801.

^1H NMR (CD_3CN , 400 MHz): δ 9.17 (s, 1H), 7.49 (d, J = 8.1 Hz, 1H), 7.41 (d, J = 8.2 Hz, 1H), 7.35 – 7.27 (m, 6H), 7.26 – 7.18 (m, 4H), 7.15 (t, J = 7.0 Hz, 1H), 7.10 – 7.01 (m, 2H), 5.62 (d, J = 8.7 Hz, 1H), 5.04 (q, J = 12.3 Hz, 2H), 4.19 (dt, J = 8.7, 6.7 Hz, 1H), 4.14 – 4.05 (m, 2H), 3.23 – 3.10 (m, 2H). **^{13}C NMR (CD_3CN , 101 MHz):** δ 172.8, 137.4, 136.7, 131.8, 130.8, 129.5, 129.4, 129.33, 129.26, 129.2, 125.2, 122.7, 120.1, 119.4, 112.5, 110.0, 67.9, 60.0, 58.2, 29.9.

$\bar{\nu}_{\text{max}}$: 3379, 3284, 3060, 3036, 2935, 2253, 1738, 1497, 1456, 1425, 1333, 1201, 1151, 1126, 1101 cm^{-1}

5a: *N*-methyl-*N*,1-diphenylmethanesulfonamide



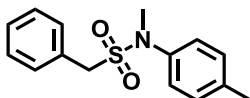
Prepared according to the general procedure described above using *N*-methylaniline as the amine. NMR yield: 87%.

HRMS: m/z $C_{14}H_{19}N_2O_2S^+$ ($[M+NH_4]^+$): calculated 279.1162, found 279.1161.

1H NMR (CD_3CN , 400 MHz): δ 7.40 – 7.35 (m, 7H), 7.31 – 7.26 (m, 3H), 4.35 (s, 2H), 3.23 (s, 3H).

These values match previously reported data.⁶

5b: *N*-methyl-1-phenyl-*N*-(*p*-tolyl)methanesulfonamide



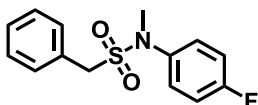
Prepared according to the general procedure described above using *N*-methyl-*p*-toluidine as the amine. Purified by column: 35% ethyl acetate in hexane. White crystals. NMR yield: 100%; isolated yield: 55.2 mg, 98%.

HRMS: m/z $C_{15}H_{18}NO_2S^+$ ($[M+H]^+$): calculated 276.1053, found 276.1056.

1H NMR (CD_3CN , 400 MHz): δ 7.39 (s, 5H), 7.28 – 7.06 (m, 4H), 4.33 (s, 2H), 3.20 (s, 3H), 2.34 (s, 3H). **^{13}C NMR (CD_3CN , 101 MHz):** δ 140.2, 138.1, 132.0, 130.6, 130.4, 129.6, 129.4, 127.6, 56.0, 39.3, 21.0.

$\bar{\nu}_{max}$: 3064, 3034, 2926, 1510, 1456, 1342, 1265, 1171, 1144, 1065, 1020 cm^{-1}

5c: *N*-(4-fluorophenyl)-*N*-methyl-1-phenylmethanesulfonamide

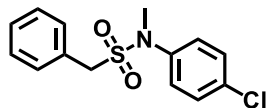


Prepared according to the general procedure described above using 4-fluoro-*N*-methylaniline as the amine. Purified by column: 35% ethyl acetate in hexane. Off-white solid. NMR yield: 100%; isolated yield: 52.6 mg, 92%.

HRMS: m/z $C_{14}H_{15}FNO_2S^+$ ($[M+H]^+$): calculated 280.0802, found 280.0798.

1H NMR (CD_3CN , 400 MHz): δ 7.39 (s, 5H), 7.31 – 7.25 (m, 2H), 7.15 – 7.06 (m, 2H), 4.35 (s, 2H), 3.21 (s, 3H). **^{13}C NMR (CD_3CN , 101 MHz):** δ 162.2 (d, J = 244.6 Hz), 132.0, 130.2, 129.8, 129.7, 129.6, 129.5, 116.6 (d, J = 22.9 Hz). **^{19}F NMR (CD_3CN , 376 MHz):** δ 116.62.

$\bar{\nu}_{max}$: 3074, 2989, 2928, 1504, 1456, 1344, 1217, 1171, 1144, 1057 cm^{-1}

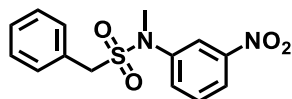
5d: *N*-(4-chlorophenyl)-*N*-methyl-1-phenylmethanesulfonamide

Prepared according to the general procedure described above using 4-chloro-*N*-methylaniline as the amine. Purified by column: 35% ethyl acetate in hexane. White crystals. NMR yield: 100%; isolated yield: 56.9 mg, 94%

HRMS: m/z $C_{14}H_{15}ClNO_2S^+$ ($[M+H]^+$): calculated 296.0507, found 296.0508.

1H NMR (CD_3CN , 400 MHz): δ 7.66 – 7.30 (m, 7H), 7.24 (dt, J = 9.0, 3.0 Hz, 2H), 4.36 (s, 2H), 3.21 (s, 3H). **^{13}C NMR (CD_3CN , 101 MHz):** δ 141.60, 132.75, 131.99, 130.08, 129.93, 129.61, 129.57, 128.72, 56.20, 38.95.

$\bar{\nu}_{max}$: 3091, 3059, 3055, 2941, 1491, 1456, 1406, 1331, 1267, 1163, 1136, 1090, 1065, 1014 cm^{-1}

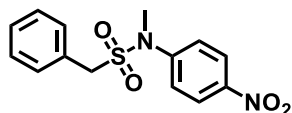
5e: *N*-methyl-*N*-(3-nitrophenyl)-1-phenylmethanesulfonamide

Prepared according to the general procedure described above using 3-nitro-*N*-methylaniline as the amine. NMR yield: 100%.

HRMS: m/z $C_{14}H_{18}N_3O_4S^+$ ($[M+NH_4]^+$): calculated 324.1013, found 324.1014.

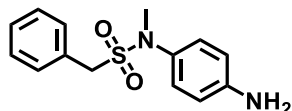
1H NMR (CD_3CN , 400 MHz): δ 8.04 (ddd, J = 8.1, 2.2, 1.1 Hz, 1H), 7.98 (t, J = 2.2 Hz, 1H), 7.61 (ddd, J = 8.2, 2.3, 1.1 Hz, 1H), 7.54 (t, J = 8.0 Hz, 1H), 7.38 – 7.35 (m, 5H), 4.44 (s, 2H), 3.30 (s, 3H).

This product was previously reported in Wojciechowski, K. (1997).⁷

5f: *N*-methyl-*N*-(4-nitrophenyl)-1-phenylmethanesulfonamide

Prepared according to the general procedure described above using *N*-methyl-4-nitroaniline as the amine. Trace amounts.

HRMS: m/z $C_{14}H_{18}N_3O_4S^+$ ($[M+NH_4]^+$): calculated 324.1013, found 324.1011.

5g: *N*-(4-aminophenyl)-*N*-methyl-1-phenylmethanesulfonamide

Prepared according to the general procedure described above using 2 equiv of NaH, and *N*1-methylbenzene-1,4-diamine as the amine. Purified by gradient column: 35-

Sulphur-Phenolate Exchange as a mild, fast and high-yielding method towards
the synthesis of sulfonamides

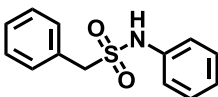
60% ethyl acetate in hexane. Green-brownish crystals. NMR yield: 42%; isolated yield: 20.4 mg, 36%.

HRMS: m/z $C_{14}H_{17}N_2O_2S^+$ ($[M+H]^+$): calculated 277.1005, found 277.1008.

1H NMR (CD_3CN , 400 MHz): δ 7.43 – 7.35 (m, 5H), 7.02 (dt, J = 8.8, 3.2 Hz, 2H), 6.61 (dt, J = 8.9, 3.1 Hz, 2H), 4.29 (s, 4H), 3.15 (s, 3H). **^{13}C NMR (CD_3CN , 101 MHz):** δ 148.6, 132.00, 131.98, 130.7, 129.5, 129.4, 129.3, 115.4, 55.5, 39.7.

$\bar{\nu}_{max}$: 3435, 3344, 3051, 2924, 2852, 1622, 1512, 1456, 1336, 1257, 1142, 1061 cm^{-1}

5h: *N*,1-diphenylmethanesulfonamide



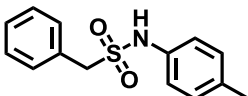
Prepared according to the general procedure described above using aniline as the amine. NMR yield: 77%.

HRMS: m/z $C_{13}H_{17}N_2O_2S^+$ ($[M+NH_4]^+$): calculated 265.1005, found 265.0996.

1H NMR (CD_3CN , 400 MHz): δ 7.39 – 7.32 (m, 5H), 7.32 – 7.27 (m, 2H), 7.25 – 7.19 (m, 2H), 7.20 – 7.14 (m, 1H), 4.36 (s, 2H).

These values match previously reported data.⁸

5i: 1-phenyl-*N*-(*p*-tolyl)methanesulfonamide



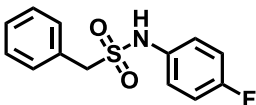
Prepared according to the general procedure described above using *p*-toluidine as the amine. NMR yield: 90%.

HRMS: m/z $C_{14}H_{19}N_2O_2S^+$ ($[M+NH_4]^+$): calculated 279.1162, found 279.1164.

1H NMR (CD_3CN , 400 MHz): δ 7.40 – 7.34 (m, 3H), 7.33 – 7.26 (m, 2H), 7.17 (d, J = 8.0 Hz, 2H), 7.11 (dt, J = 8.5, 2.2 Hz, 2H), 4.32 (s, 2H), 2.31 (s, 3H).

This product was previously reported in King *et al.* (1975).⁹

5j: *N*-(4-fluorophenyl)-1-phenylmethanesulfonamide



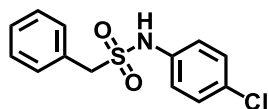
Prepared according to the general procedure described above using 4-fluoroaniline as the amine. Purified by column: 35% ethyl acetate in hexane. White crystals. NMR yield: 90%; isolated yield: 46.1 mg, 85%.

HRMS: m/z $C_{13}H_{16}FN_2O_2S^+$ ($[M+NH_4]^+$): calculated 283.0911, found 283.0914.

1H NMR (CD_3CN , 400 MHz): δ 7.53 (s, 1H), 7.40 – 7.35 (m, 3H), 7.33 – 7.27 (m, 2H), 7.25 – 7.16 (m, 2H), 7.12 – 7.05 (m, 2H), 4.34 (s, 2H). **^{13}C NMR (CD_3CN , 101 MHz):** δ 162.1, 147.3 (d, J = 2485.1 Hz), 132.0, 130.2, 129.6, 129.5, 123.8 (d, J = 8.3 Hz), 116.9 (d, J = 22.9 Hz), 58.1. **^{19}F NMR (CD_3CN , 376 MHz):** 119.99

$\bar{\nu}_{max}$: 3261, 3068, 3037, 2929, 1506, 1396, 1327, 1292, 1211, 1147 cm^{-1}

5k: N-(4-chlorophenyl)-1-phenylmethanesulfonamide



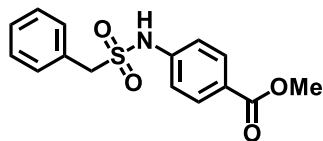
Prepared according to the general procedure described above using 4-chloroaniline as the amine. NMR yield: 88%.

HRMS: m/z $C_{13}H_{16}ClN_2O_2S^+$ ($[M+NH_4]^+$): calculated 299.0616, found 299.0617.

1H NMR (CD_3CN , 400 MHz): δ 7.38 – 7.35 (m, 3H), 7.33 (dt, J = 9.0, 3.1 Hz, 2H), 7.30 – 7.26 (m, 2H), 7.17 (dt, J = 9.0, 3.1 Hz, 2H), 4.37 (s, 2H).

This product was previously reported in Marvel *et al.* (1926).¹⁰

5l: methyl 4-((phenylmethyl)sulfonamido)benzoate

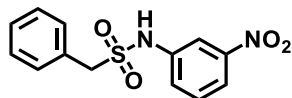


Prepared according to the general procedure described above using methyl 4-aminobenzoate as the amine. Trace amounts.

HRMS: m/z $C_{15}H_{16}NO_4S^+$ ($[M+H]^+$): calculated 306.0795, found 306.0793.

These values match previously reported data.¹¹

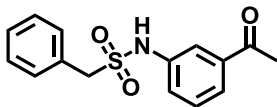
5m: N-(3-nitrophenyl)-1-phenylmethanesulfonamide



Prepared according to the general procedure described above using 3-nitroaniline as the amine. Trace amounts.

HRMS: m/z $C_{13}H_{16}N_3O_4S^+$ ($[M+NH_4]^+$): calculated 310.0856, found 310.0858.

5o: N-(3-acetylphenyl)-1-phenylmethanesulfonamide



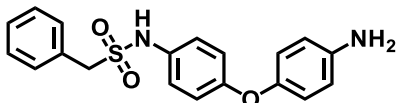
Prepared according to the general procedure described above using 3'-aminoacetophenone as the amine. Purified by column: 40% ethyl acetate in hexane. Light yellow crystals. NMR yield: 83%; isolated yield: 46.8 mg, 79%.

HRMS: m/z $C_{15}H_{16}NO_3S^+$ ($[M+H]^+$): calculated 290.0845, found 290.0845.

1H NMR (CD_3CN , 400 MHz): δ 7.74 – 7.71 (m, 1H), 7.71 (d, J = 1.7 Hz, 1H), 7.46 (t, J = 8.2 Hz, 1H), 7.43 – 7.30 (m, 4H), 7.33 – 7.24 (m, 2H), 4.40 (s, 2H), 2.55 (s, 3H). **^{13}C NMR (CD_3CN , 101 MHz):** δ 198.4, 139.5, 139.3, 132.0, 130.7, 130.1, 129.60, 129.58, 125.1, 125.0, 119.9, 58.5, 27.1.

$\bar{\nu}_{max}$: 3286, 3063, 3036, 2924, 1676, 1589, 1497, 1456, 1406, 1333, 1284, 1257, 1246, 1151, 1130 cm^{-1}

5g: N-(4-(4-aminophenoxy)phenyl)-1-phenylmethanesulfonamide



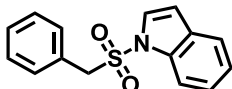
Prepared according to the general procedure described above using 2 equiv of NaH, and 4,4'-diaminodiphenyl ether as the amine. Purified by gradient column: 35-75% ethyl acetate in hexane. White solid. NMR yield: 40%; isolated yield: 18.1 mg, 25%.

HRMS: m/z $C_{19}H_{20}N_2O_3S^{2+}$ ($[M+2H]^{2+}$): calculated (m/z) 178.0592, found 178.0589.

1H NMR (CD_3CN , 400 MHz): δ 7.43 (s, 1H), 7.39 – 7.34 (m, 3H), 7.34 – 7.28 (m, 2H), 7.14 (dt, J = 8.9, 3.6 Hz, 2H), 6.87 (dt, J = 9.1, 3.4 Hz, 2H), 6.81 (dt, J = 8.9, 3.4 Hz, 2H), 6.66 (dt, J = 8.8, 3.4 Hz, 2H), 4.31 (s, 2H), 4.07 (s, 2H). **^{13}C NMR (CD_3CN , 101 MHz):** δ 157.5, 148.5, 145.7, 132.7, 132.0, 130.4, 129.54, 129.45, 124.1, 121.8, 118.7, 116.5, 57.9.

$\bar{\nu}_{max}$: 3622, 3394, 3329, 3107, 3047, 2931, 2850, 2679, 1606, 1495, 1317, 1213, 1136, 1011 cm^{-1}

5s: 1-(benzylsulfonyl)-1H-indole



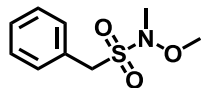
Prepared according to the general procedure described above using indole as the amine. Very light orange/brown solid. This product is difficult to separate from the left-over indole after the reaction. Purified by column: 30% ethyl acetate in hexane. NMR yield: 25%; isolated yield: 8.3 mg, 15%.

HRMS: m/z $C_{15}H_{14}NO_2S^+$ ($[M+H]^+$): calculated 272.0740, found 272.0743.

^1H NMR (CDCl_3 , 400 MHz): δ 7.81 (d, J = 7.3 Hz, 1H), 7.59 (d, J = 7.7 Hz, 1H), 7.31 – 7.26 (m, 3H), 7.18 (t, J = 7.2 Hz, 2H), 7.03 (d, J = 3.3 Hz, 1H), 6.88 (d, J = 8.0 Hz, 2H), 6.51 (d, J = 3.7 Hz, 1H), 4.49 (s, 2H) **^{13}C NMR (CDCl_3 , 101 MHz):** δ 130.6, 129.4, 128.8, 127.1, 127.0, 124.7, 123.4, 121.6, 113.2, 107.8, 59.9.

$\bar{\nu}_{\text{max}}$: 3144, 3113, 3064, 3034, 2924, 1444, 1362, 1259, 1205, 1163, 1122, 1074 cm^{-1}

7a: *N*-methoxy-*N*-methyl-1-phenylmethanesulfonamide



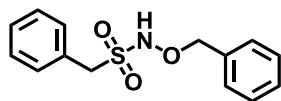
Prepared according to the general procedure described above using *O,N*-Dimethylhydroxylamine as the amine. NMR yield: 100%.

HRMS: m/z $\text{C}_9\text{H}_{17}\text{N}_2\text{O}_3\text{S}^+$ ($[\text{M}+\text{NH}_4]^+$): calculated 233.0954, found 233.0956.

^1H NMR (CD_3CN , 400 MHz): δ 7.47 – 7.36 (m, 5H), 4.40 (s, 2H), 3.78 (s, 3H), 3.03 (s, 3H).

This product was previously reported in Abdulla *et al.* (2017).¹²

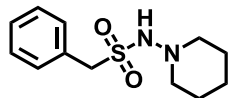
7b: *N*-(benzyloxy)-1-phenylmethanesulfonamide



Prepared according to the general procedure described above using *o*-benzylhydroxylamine as the amine. Trace amounts.

HRMS: m/z $\text{C}_{14}\text{H}_{19}\text{N}_2\text{O}_3\text{S}^+$ ($[\text{M}+\text{NH}_4]^+$): calculated 295.1111, found 295.1111.

7c: 1-phenyl-*N*-(piperidin-1-yl)methanesulfonamide



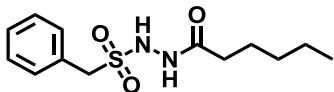
Prepared according to the general procedure described above using 1-aminopiperidine as the amine. Purified by column: 45% ethyl acetate in hexane. White crystals. NMR yield: 100%; isolated yield: 40.6 mg, 78%.

HRMS: m/z $\text{C}_{12}\text{H}_{19}\text{N}_2\text{O}_2\text{S}^+$ ($[\text{M}+\text{H}]^+$): calculated 255.1162, found 255.1161.

^1H NMR (CD_3CN , 400 MHz): δ 7.44 – 7.35 (m, 5H), 6.18 (s, 1H), 4.36 (s, 2H), 2.82 (t, J = 5.3 Hz, 4H), 1.65 (p, J = 5.9 Hz, 4H), 1.39 (p, J = 5.9 Hz, 2H). **^{13}C NMR (CD_3CN , 101 MHz):** δ 131.9, 130.6, 129.5, 129.3, 58.8, 56.3, 26.6, 23.9.

$\bar{\nu}_{\text{max}}$: 3178, 3064, 2937, 2920, 2856, 1497, 1454, 1315, 1255, 1149, 1122, 1018 cm^{-1}

7d: N'-hexanoyl-1-phenylmethanesulfonohydrazide



Prepared according to the general procedure described above using hexanehydrazide as the amine. Purified by column: 50% ethyl acetate in hexane. White solid. NMR yield: 31%; NMR yield (IS): 30%; isolated yield: 16.3 mg, 28%.

HRMS: m/z $C_{13}H_{21}N_2O_3S^+$ ($[M+H]^+$): calculated 285.1267, found 285.1268.

1H NMR (CD_3CN , 400 MHz): δ 8.38 (s, 1H), 7.50 – 7.34 (m, 6H), 4.33 (s, 2H), 2.21 (t, J = 6.6 Hz, 2H), 1.63 (p, J = 7.5 Hz, 2H), 1.37 – 1.30 (m, 4H), 0.91 (t, J = 6.0 Hz, 3H). **^{13}C NMR (CD_3CN , 101 MHz):** δ 173.7, 132.1, 130.1, 129.5, 58.6, 34.3, 32.0, 25.7, 23.0, 14.2.

$\tilde{\nu}_{max}$: 3311, 3132, 3066, 3036, 2953, 2928, 2870, 1687, 1591, 1518, 1497, 1456, 1335, 1153 cm^{-1}

References

- (1) van den Boom, A. F. J.; Subramaniam, M.; Zuilhof, H. Sulfur-Phenolate Exchange As a Fluorine-Free Approach to S(VI) Exchange Chemistry on Sulfonyl Moieties. (2022), *Org Lett*, **24** (47), 8621–8626.
- (2) Day, J. J.; Neill, D. L.; Xu, S.; Xian, M. Benzothiazole Sulfinic Acid Transfer Reagent under Oxidation-Free Conditions. (2017), *Org Lett*, **19** (14), 3819–3822.
- (3) Harger, M. J. P. Competing Sulfonylation and Phosphonylation Following Rearrangement of an O-Sulfonyl-N-Phosphinoylhydroxylamine with Tert-Butylamine: Demonstration of a Phosphonamidic-Sulfonic Anhydride Intermediate and 18O-Labeling Evidence on How It May Be Formed. (2003), *Org Biomol Chem*, **1** (19), 3390–3395.
- (4) Johnson, T. B.; Ambler, J. A. Researches on Amines. IV. The Alkylation and Hydrolysis of Aliphatic Sulfonamides. A New Synthesis of Sarcosine. (1914), *J Am Chem Soc*, **36** (2), 372–385.
- (5) Nikam, S. S.; Kornberg, B. E.; Ault-Justus, S. E.; Rafferty, M. F. Novel Quenchers for Solution Phase Parallel Synthesis. (1998), *Tetrahedron Lett*, **39** (10), 1121–1124.
- (6) Zhou, G.; Ting, P.; Aslanian, R.; Piwinski, J. J. A Useful Pd-Catalyzed Negishi Coupling Approach to Benzylic Sulfonamide Derivatives. (2008), *Org Lett*, **10** (12), 2517–2520.
- (7) Wojciechowski, K. Synthesis of Nitrobenzophenones from Nitro- α -Sulfonyldiphenylmethane Derivatives. (1997), *Synth Commun*, **27** (1), 135–144.
- (8) Hill, B.; Liu, Y.; Taylor, S. D. Synthesis of α -Fluorosulfonamides by Electrophilic Fluorination. (2004), *Org Lett*, **6** (23), 4285–4288.
- (9) King, J. F.; Kang, Y. I. Basic Catalysis in the Trapping of Sulphenes. (1975), *J Chem Soc Chem Commun*, No. 2, 52–53.
- (10) Marvel, C. S.; Gillespie, H. B. Identification of Amines. III. Benzylsulfonamides. (1926), *J Am Chem Soc*, **48** (11), 2943–2944.
- (11) Wydysh, E. A.; Medghalchi, S. M.; Vadlamudi, A.; Townsend, C. A. Design and Synthesis of Small Molecule Glycerol 3-Phosphate Acyltransferase Inhibitors. (2009), *J Med Chem*, **52** (10), 3317–3327.
- (12) Abdulla, O.; Clayton, A. D.; Faulkner, R. A.; Gill, D. M.; Rice, C. R.; Walton, S. M.; Sweeney, J. B. Catalytic Sp³–Sp³ Functionalisation of Sulfonamides: Late-Stage Modification of Drug-Like Molecules. (2017), *Chemistry – A European Journal*, **23** (7), 1494–1497.

Chapter 6

General Discussion & Outlook

The aim of the research described in this book was to find new and more environmentally friendly alternatives to existing processes and reactions, and to sensitize silicon solar cells with singlet fission material for more efficient energy conversion. In this chapter, we will briefly reflect on the results obtained from this research, and provide some future perspectives. A more detailed discussion of the results can be found in the corresponding chapter.

Chapter 2. Silicon nanoparticles

Silicon nanoparticles (Si NPs) are a less-toxic and biodegradable alternative to lead- or cadmium-based nanoparticles,¹⁻⁶ with an emission range from the visible to the infrared (~ 1000 nm) region, depending on the size and crystallinity of the NPs.^{7,8} The low toxicity, wide absorption/emission range, and excellent electronic and electric properties of crystalline silicon mean that Si NPs can be used in bio-imaging, electronics, solar cells, and medicine.⁹⁻¹⁴ For all these purposes, however, it is important that the surface of the often hydrogen-terminated H-Si NPs is well-passivated, to prevent oxidation and (premature) degradation of the particles. For lead- and cadmium-based NPs, passivation is often done during synthesis, yet this is (often) not possible for H-Si NPs. Luckily, several passivation methods exist for H-Si NPs, such as thermal hydrosilylation or thiolation,^{8,15} etching using phosphorous pentachloride followed by modification with an amine,^{16,17} halogenation followed by a Grignard reaction,¹⁸ platinum-catalyzed reactions,^{19,20} or reactions in the presence of radical initiators.^{21,22} We added one more method to this list in **Chapter 2**, where we describe the passivation of Si NPs with silanols. Unlike these previously mentioned methods, our reaction proceeds in one step, at room temperature, without harsh/corrosive chemicals, and without catalysts. And while a room-temperature hydrosilylation reaction with ω -ester- and ω -acid-terminated alkenes was reported by the group of Korgel, this reaction took 20 h under constant nitrogen flow, instead of the 1 h required for our silanol passivation.²³ As such, the silanol method provides great improvements in terms of waste reduction, safety, and energy consumption. However, compared to some high-temperature and halogenation methods, passivation with silanols yields a lower packing density, which results in increased oxidation of the Si NPs over time. This is especially the case for silanols with shorter alkyl chains, as these have a smaller footprint on the NP surface; for longer alkyl chains, the oxidation over time is limited, and good passivation is achieved. Nevertheless, in both cases, the oxygen present in the silanol ligand itself poses a problem. As described in **Chapter 2**, the oxygen atoms from the ligands can bury themselves into the Si NP, where the presence of oxygen causes trap states and (surface) defects. This distorts the near-ideal electronic and electrical properties of the Si NPs, and shifts the excitation and emission maxima towards shorter wavelengths – as observed while measuring the optical properties of our Si NPs before and after passivation. As such, the silanol

passivation method is likely not suitable for electronics or solar cell applications, where trap states greatly reduce charge transfer and efficiencies.

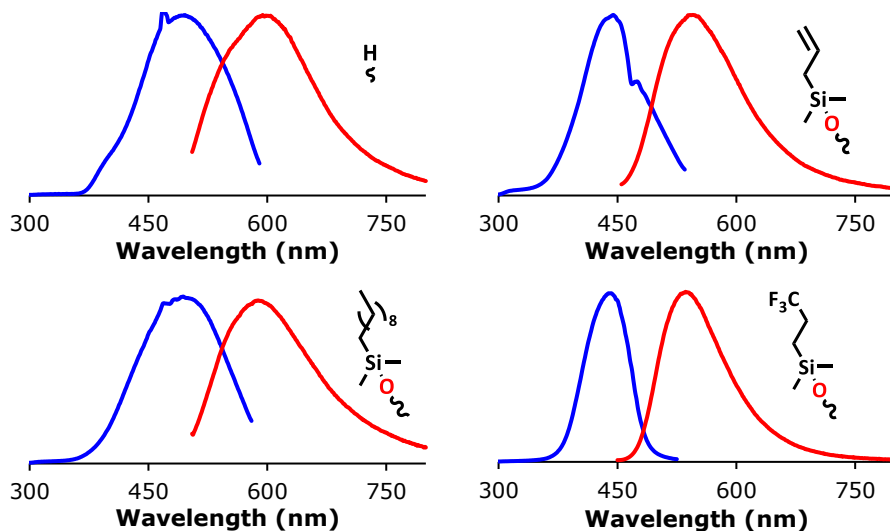


Figure 1: Excitation (blue) and emission (red) spectra of the Si NPs produced in this thesis. The structure in each graph indicates the coating on the particle.

Still, the room temperature method does provide great benefits in the possibility for further functionalization of the coating. This was demonstrated in **Chapter 2** by coupling a thiol sugar to Si NPs passivated with a silanol containing a terminal vinyl group. Previous methods often did not allow such further functionalization of the coating (though examples of *e.g.* acid- or amine-terminated coatings exist),^{23–25} as the presence of an additional functional group on the ligand caused problems during the passivation of the Si NPs. The silanol method developed here therefore shows greater flexibility in terms of end groups on the passivated Si NP surface, which opens the way to fully tunable surface coatings. With the increased interest in and development of NPs for *e.g.* targeted cancer treatments (where NPs – which have been shown to accumulate in tumors – are functionalized with anti-cancer drugs),^{1,9,11} medicine,² bio-imaging,^{10,12} and biosensing,²⁶ such fully tunable coatings have become indispensable.

Chapter 3. Sensitized solar cells

In **Chapter 3**, we attempted to improve the efficiency of silicon solar cells by sensitizing them with tetracene, a compound capable of undergoing singlet fission (SF). As introduced in **Chapter 1**, sensitization with singlet fission materials has several environmental and practical advantages over sensitization with dyes or quantum dots, or the use of perovskites or tandem solar cell designs: 1) with dye sensitization, liquid electrolytes (and dyes) are needed, that can corrode the electrodes and leach into the environment upon improper encapsulation;²⁷ 2) for

quantum dot sensitization, lead- or cadmium-based quantum dots are generally used, which are toxic to both humans and the environment;²⁸ 3) perovskites – while promising – often contain toxic lead cations, are unstable, and cannot be properly deposited onto full-scale solar cells;^{29–33} and 4) tandem solar cells require expensive materials and complicated production techniques.^{34–37} With singlet-fission sensitization, no (liquid) electrolytes are needed, and the SF material itself (tetracene) is a non-toxic solid, that can be deposited onto a silicon solar cell after thermal evaporation in a vacuum chamber, with no other major changes required to the production process of the silicon solar cells. And while the photostability of tetracene is low as well, it has the benefit that even after degradation, it helps reduce the temperature in the underlying silicon solar cell, thereby increasing its lifetime.³⁸ Thus, sensitization with tetracene is a safe and sustainable solution to boost solar cell efficiency and lifespan. However, as mentioned in **Chapter 1**, successful transfer of triplet energy from tetracene to silicon has only been observed after aging and with a suitable HfO_xN_y interlayer, when the overlap in wavefunctions between tetracene and silicon was large enough to allow Dexter energy transfer.^{39,40} As the aging method is highly dependent on the deposition parameters used, and the HfO_xN_y interlayer requires strictly controlled production methods, an easier method to transfer the triplet energy from tetracene to silicon is still needed to produce an efficient tetracene-sensitized solar cell. In **Chapter 3**, we used a covalently attached seed layer of tetracene derivatives to facilitate the triplet energy transfer (Figure 2), an approach that has not been attempted before. To this end, two derivatives were synthesized and tested: 5-ethynyltetracene and 2-ethynyltetracene. Both derivatives were synthesized on gram-scale, and were successfully attached to the silicon surface.

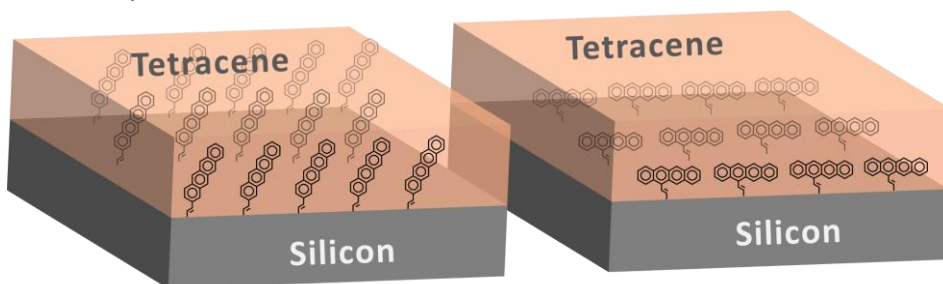


Figure 2: Schematic representation of the solar cell models made in this thesis.

Unfortunately, when the crystallinity of the subsequently deposited tetracene layer was measured, the surface functionalized with 5-ethynyltetracene showed low crystallinity, possibly due to the backfilling process with 1-pentyne. Further measurements also concluded no triplet energy transfer occurred for these surfaces. For surfaces functionalized with 2-ethynyltetracene, high crystallinity and ordering of the tetracene layer was observed, and a change in crystal structure was visible within the deposited tetracene layer. Instead of only polymorph Tc I, XRD

spectra also showed peaks belonging to the polymorph Tc II. Previously, triplet energy transfer to (unfunctionalized) silicon was observed when the ratio of Tc II in the deposited tetracene layer was increased from a small minority (48%) to a small majority (52%).³⁹ Unfortunately, in our model system, the ratio of Tc II is only 7%. While it is postulated that the Tc II polymorph is present near the seed layer – as no other functionalization showed peaks belonging to Tc II – the thickness of the Tc II layer is likely too small in our sensitized cell. As a result, no triplet energy transfer was observed. Still, the ability of 2-ethynyltetracene to influence the orientation and ordering of a deposited tetracene layer is promising and worthy of further exploration. In addition, the effect of the temperature in the deposition chamber on the crystal structure of the deposited tetracene layer is another interesting factor. It has been shown that at higher temperatures, a higher ratio of polymorph Tc II is found in the tetracene layer. As such, it would be interesting to combine an optimized seed layer – perhaps with a longer linker – with an optimized deposition temperature, to allow more control over the crystal structure of tetracene, and increase the ratio of Tc II.

Chapter 4 & 5. Fluorine-free S(VI) exchange reactions

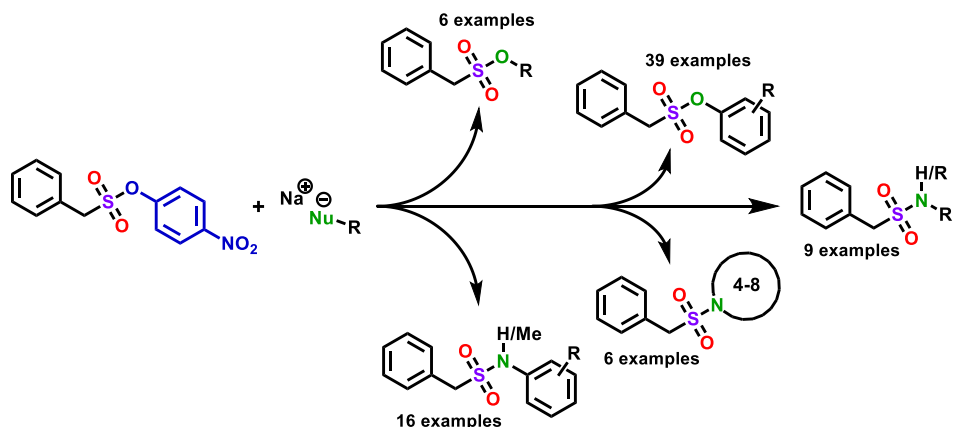


Figure 3: Overview of products created using the SuPhenEx method.

SuFEx chemistry – as outlined in **Chapter 1** – has become an invaluable tool for the discovery and development of enzyme inhibitors,^{41,42} and has also shown promise in polymer synthesis and functionalization.^{43,44} However, with recent discoveries into the toxicity of fluorine-containing chemicals, and legislation to ban or limit their use, SuFEx may lose its applicability. To prevent this, we developed a fluorine-free alternative to SuFEx towards the synthesis of sulfonyl esters and sulfonamides. **Chapter 4** describes the scope of the reaction between 4-nitrophenyl benzenesulfonate and various aromatic alcohols, where the 4-nitrophenolate is used to replace fluorine as the leaving group. The yields and reaction times found using

this SuPhenEx reaction were higher and shorter, respectively, than those reported previously for the same reaction with a chlorine or fluorine leaving group.^{45,46} Only when the substrate contains a second base-sensitive group does the SuPhenEx reaction cause degradation, though this could in some cases be solved by changing the base used during the reaction. For saturated aliphatic alcohols, quantitative yields were found as well, using only a minor (1.1 equiv) excess of the alcohol. Under traditional SuFEx conditions, such alcohols could only be induced to react upon the addition of a catalyst. Yet with SuPhenEx, even quantitative triple addition to glycerol occurred overnight at room temperature, using just 3.1 equiv of the SuPhenEx starting material. This reaction time could be decreased by the addition of 15-crown-5, as demonstrated for several slow-reacting substrates in **Chapter 4**. The scope of SuPhenEx was then expanded even further with natural alcohols, where – in the absence of other base-sensitive groups – quantitative yields were again observed. Finally, as one of the strengths of SuFEx is its applicability in aqueous media,⁴⁷ we tested the stability of our starting material in an 80% solution of water in DMSO. Even after several weeks, no signs of degradation could be seen, further confirming SuPhenEx as an excellent alternative to SuFEx and S(VI) exchange reactions starting from sulfonyl chlorides.

We then used the same SuPhenEx reaction for the synthesis of sulfonamides in **Chapter 5**. Sulfonamides can be found in medicinal chemistry as e.g. anti-cancer⁴⁸ or antiviral drugs,⁴⁹ protein inhibitors,^{50–52} or enzyme inhibitors,^{53–57} and are usually made from sulfonyl chlorides. However, sulfonyl chlorides suffer from poor hydrolytic stability, and require extensive drying of solvents and reagents before use. Synthesis from sulfonyl fluorides is also possible, but often requires heating or the use of catalysts to reach high yields.^{58–61} And – especially for biological studies – the release of toxic fluorine atoms during this reaction provides a major drawback. Since the hydrolytic stability of our nitrophenolate-based starting material was already proven, we hypothesized that the SuPhenEx reaction could also be of use here. And indeed, for a range of aliphatic, cyclic, and natural amino acids, the SuPhenEx reaction gave near quantitative yields after just a few hours of reaction time. For most of these substrates – when known from literature – the reaction times found here were shorter,^{48,56} and yields were either comparable or higher than those found for sulfonyl chloride-based syntheses,^{51,52,62} establishing SuPhenEx as an improvement on the use of sulfonyl chlorides for these compounds. For *N*-methylanilines, similarly high yields were obtained within two hours of reaction time, except for the substrates bearing a NH₂- or NO₂- substituent on the *para*-position, for which lower yields or trace amounts of product were found. When primary anilines were used as substrate, longer reaction times and lower yields were found, as compared to the corresponding *N*-methylanilines. The decreased reactivity of primary anilines was expected based on literature on room-temperature reactions using sulfonyl chlorides,^{63–66} and was previously overcome

by the group of Cohen by heating the reaction mixture to 130 °C in a microwave reactor.^{54,55,67} Here, high yields could still be obtained for primary anilines with halide- or methyl substituents on the *para*-position, while larger substituents or more electron-withdrawing substituents gave low or negligible yields. Thus, for primary anilines, heating or the addition of a catalyst may be inescapable to reach high yields. Finally, although the SuPhenEx reaction with (primary) anilines was more susceptible to water compared to the reaction with aliphatic amines or alcohol-based substrates, no extensive drying of solvents was needed, and reactions could still be performed under atmospheric conditions. The SuPhenEx reaction therefore poses an excellent and more environmentally friendly alternative to the use of sulfonyl chlorides and fluorides for the synthesis of sulfonamides, as no heating, cooling, distillation of solvent, or argon atmosphere is needed.

For some final general environmental considerations, **Chapter 4** describes the possibility to recycle the excess sodium 4-nitrophenolate that precipitates during the production of the starting material into the next production cycle of starting material. This greatly enhances the atom efficiency of the reaction, and reduces chemical waste. In addition, the hydrogen gas formed during the formation of the starting material and deprotonation of the nucleophiles can be captured and used to generate electricity or heat. This energy can then be used to power equipment or heat buildings, further increasing the economically friendly character of the SuPhenEx reaction.

Outlook & future research

Silicon nanoparticles

With an increase in methods available to chemists to both create and functionalize silicon nanoparticles,⁶⁸ the applications for such particles have increased as well. Porous silicon nanoparticles have started to appear as drug carriers,^{1,9,11,69} while highly crystalline particles have found applications in solar cells, bio-imaging, and electronics.⁷⁰⁻⁷⁴ With the development of synthesis methods for near-infrared emitting nanoparticles with a diameter close to twice the Bohr radius of silicon (~5 nm), and the growing amount of control chemists have over the nanoparticle size, coating, and optical properties, it is now possible to almost completely tune silicon nanoparticles to your specific needs.⁶⁸ This, combined with the highly-abundant starting material, low toxicity, and biodegradable properties, make silicon nanoparticles increasingly better competitors to lead- and cadmium-based nanoparticles. And since research into silicon nanoparticles is far from exhausted, more interesting applications of silicon nanoparticles will likely be discovered in the (near) future.

Singlet-fission-sensitized solar cells

One possible application for near-infrared emitting silicon nanoparticles would be as an interlayer between tetracene and silicon in a singlet-fission-sensitized solar cell, to facilitate the energy transfer from tetracene to the silicon bulk. From literature we know that triplet transfer from tetracene to nanoparticles is possible for PbS nanoparticles, with a transfer efficiency of over 90%.^{75,76} The benefit of transferring the triplet energy to nanoparticles lies in the degenerate energy levels of the latter: where relaxation *via* emission of the triplet energy is spin-forbidden in tetracene, this process is allowed in nanoparticles. As such, the nanoparticles can indirectly transfer the triplet energy from tetracene to silicon *via* FRET or emission/absorption.

With this information, we propose a new solar cell design, in which (modified) tetracene is deposited onto or co-deposited with a layer of silicon nanoparticles with a bandgap of ~ 1.1 eV. This hybrid layer would be deposited onto a conventional silicon cell, to create the design shown in Figure 4. In this design, the triplets from tetracene are transferred into the silicon nanoparticles *via* Dexter energy transfer. Then, the silicon nanoparticles transfer the energy to the silicon bulk *via* FRET, effectively increasing the current generated by high-energy photons within the solar cell. For the singlet fission material, unmodified tetracene could be used, or 5,12-bis((triisopropylsilyl)ethynyl)tetracene (TIPS-tetracene), a compound with increased photostability compared to unmodified tetracene, to increase the lifespan of the sensitized cell. Furthermore, the various orientations of the tetracene molecules on the Si NPs will likely imply a significant fraction of them are parallel to the surface, which may improve transfer efficiencies even further by direct transfer of triplets to silicon, without the intermediary transfer to the Si NPs.

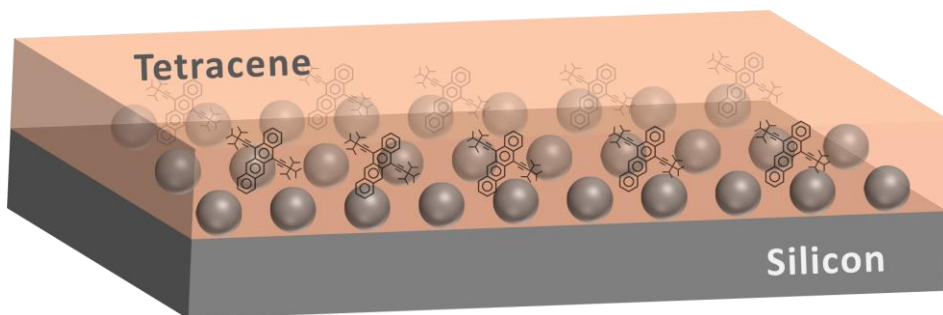


Figure 4: Proposed solar cell design, featuring near-infrared emitting Si NPs and TIPS-tetracene for an optimized energy transfer and a longer lifespan.

SuPhenEx

In **Chapters 4 & 5**, we introduced the SuPhenEx reaction for sulfonyl compounds as an alternative to SuFEx and sulfonyl chloride exchange reactions. While a large range of alcoholic and amine-based substrates was tested, further investigations into the scope of the SuPhenEx reaction are desired. As described in

Chapter 1, one of the main applications of SuFEx is the development of enzyme inhibitors. As such, it would be interesting to see how SuPhenEx reactions perform here. The hydrolytic stability of 4-nitrophenyl benzyisulfonate is certainly high enough to allow its use in biological media, yet the formation of the nitrophenolate ion could have adverse effects. In addition, the degradation of our SuPhenEx starting material in the presence of acid groups – which are certainly present in proteins and biological samples – requires further research, to more fully understand the degradation process, and to find possible solutions. On the other hand, the bright orange color produced by the nitrophenolate leaving group in aqueous media may provide an easy way to ascertain the reaction progress, and allow for a quick method of confirming successful binding events in a screening setting. Finally, as one of the main benefits of click chemistry lies in its orthogonal nature, a study into the cross-reactivity of SuPhenEx with e.g. CuAAC or thiol-ene reactions would elevate the importance of the SuPhenEx reaction.

Conclusion

To conclude, we have developed a room-temperature method to passivate silicon nanoparticles (Si NPs) that requires little solvent, no catalysts, and relatively short reaction times. As such, we were able to reduce the energy requirement, waste production, and use of toxic chemicals compared to previously used methods. With longer ligands, the passivated nanoparticles showed good stability towards oxidation, and only minor shifts in optical properties compared to unpassivated hydrogen-terminated Si NPs. While the presence of oxygen in the ligand limits the use of this method for electronic applications, the tunability of the ligand end-group provides an excellent handle for further functionalization, for example *via* the SuPhenEx reaction developed in this thesis. As a result, this passivation method shows good promise for use in biological and medicinal applications, where such flexibility is indispensable.

We then created model systems for singlet-fission-sensitized solar cells with a higher theoretical efficiency and lifetime, using two tetracene derivatives to act as seed layers to orient subsequently deposited tetracene layers. While a promising tilt in the orientation of the deposited tetracene layer was seen with a 2-ethynyltetracene seed layer, no effect on triplet energy transfer was observed. In addition, the more favorable orientation seemed limited to the tetracene layers closest to the seed layer, with the tetracene layers further away assuming a less favorable orientation. More research is therefore needed into novel tetracene derivatives, likely with slightly longer linker parts, as well as on the effect of the seed layer on the structure of deposited tetracene layers of different thicknesses.

Finally, we developed a fluorine-free approach to S(VI) exchange chemistry for sulfonyl moieties with the introduction of the SuPhenEx reaction, to reduce the amount of fluorine-containing chemicals needed for S(VI) exchange reactions. For

the synthesis of aromatic and aliphatic sulfonyl esters, SuPhenEx reactions showed a quantitative yield for most substrates, with shorter reaction times compared to previously reported reactions. SuPhenEx reactions can furthermore be performed in a single pot at room temperature under atmospheric conditions, and show good tolerance towards water and oxygen. For the synthesis of sulfonamides – where SuPhenEx replaces the hydrolysis-prone sulfonyl chloride exchange reaction – quantitative yields were reached for aliphatic and cyclic amines, whereas aromatic amines showed lower yields. Still, these yields were comparable or higher than those reported previously, and were reached after shorter reaction times. In addition, with SuPhenEx, no extensive drying of solvents is required, and the reaction can be performed at room temperature. This decreases the energy consumption compared to previous methods requiring extensive drying or microwave reactors.

All in all, the results in this thesis provide scientists with more economically friendly and energy-saving alternatives to available methods, and we hope this trend is continued in future research.

References

- (1) Bertucci, A.; Kim, K. H.; Kang, J.; Zuidema, J. M.; Lee, S. H.; Kwon, E. J.; Kim, D.; Howell, S. B.; Ricci, F.; Ruoslahti, E.; Jang, H. J.; Sailor, M. J. Tumor-Targeting, MicroRNA-Silencing Porous Silicon Nanoparticles for Ovarian Cancer Therapy. (2019), *ACS Appl Mater Interfaces*, **11** (27), 23926–23937.
- (2) Ferreira, M. P. A.; Ranjan, S.; Correia, A. M. R.; Mäkilä, E. M.; Kinnunen, S. M.; Zhang, H.; Shahbazi, M. A.; Almeida, P. v.; Salonen, J. J.; Ruskoaho, H. J.; Airaksinen, A. J.; Hirvonen, J. T.; Santos, H. A. In Vitro and in Vivo Assessment of Heart-Homing Porous Silicon Nanoparticles. (2016), *Biomaterials*, **94**, 93–104.
- (3) Kustov, L. M.; Mashkin, P. v.; Zakharov, V. N.; Abramenko, N. B.; Krysanov, E. Y.; Aslanov, L. A.; Peijnenburg, W. Silicon Nanoparticles: Characterization and Toxicity Studies. (2018), *Environ Sci Nano*, **5** (12), 2945–2951.
- (4) Bimbo, L. M.; Sarparanta, M.; Santos, H. A.; Airaksinen, A. J.; Mäkilä, E.; Laaksonen, T.; Peltonen, L.; Lehto, V. P.; Hirvonen, J.; Salonen, J. Biocompatibility of Thermally Hydrocarbonized Porous Silicon Nanoparticles and Their Biodistribution in Rats. (2010), *ACS Nano*, **4** (6), 3023–3032.
- (5) Choi, J.; Zhang, Q.; Reipa, V.; Wang, N. S.; Stratmeyer, M. E.; Hitchins, V. M.; Goering, P. L. Comparison of Cytotoxic and Inflammatory Responses of Photoluminescent Silicon Nanoparticles with Silicon Micron-Sized Particles in RAW 264.7 Macrophages. (2009), *Journal of Applied Toxicology*, **29** (1), 52–60.
- (6) Ivanov, S.; Zhuravsky, S.; Yukina, G.; Tomson, V.; Korolev, D.; Galagudza, M. In Vivo Toxicity of Intravenously Administered Silica and Silicon Nanoparticles. (2012), *Materials*, **5** (10), 1873–1889.
- (7) Yu, Y.; Fan, G.; Fermi, A.; Mazzaro, R.; Morandi, V.; Ceroni, P.; Smilgies, D. M.; Korgel, B. A. Size-Dependent Photoluminescence Efficiency of Silicon Nanocrystal Quantum Dots. (2017), *Journal of Physical Chemistry C*, **121** (41), 23240–23248.
- (8) Hessel, C. M.; Reid, D.; Panthani, M. G.; Rasch, M. R.; Goodfellow, B. W.; Wei, J.; Fujii, H.; Akhavan, V.; Korgel, B. A. Synthesis of Ligand-Stabilized Silicon Nanocrystals with Size-Dependent Photoluminescence Spanning Visible to near-Infrared Wavelengths. (2012), *Chemistry of Materials*, **24** (2), 393–401.
- (9) Secret, E.; Maynadier, M.; Audrey, G.; Gary-Bobo, M.; Chaix, A.; Belamie, E.; Maillard, P.; Sailor, M. J.; Garcia, M.; Durand, J. O.; Cunin, F. Anionic Porphyrin-Grafted Porous Silicon Nanoparticles for Photodynamic Therapy. (2013), *Chemical Communications*, **49** (39), 4202–4204.
- (10) Singh, M. P.; Atkins, T. M.; Muthuswamy, E.; Kamali, S.; Tu, C.; Louie, A. Y.; Kauzlarich, S. M. Development of Iron-Doped Silicon Nanoparticles as Bimodal Imaging Agents. (2012), *ACS Nano*, **6** (6), 5596–5604.
- (11) Luo, M.; Lewik, G.; Ratcliffe, J. C.; Choi, C. H. J.; Mäkilä, E.; Tong, W. Y.; Voelcker, N. H. Systematic Evaluation of Transferrin-Modified Porous Silicon Nanoparticles for Targeted Delivery of Doxorubicin to Glioblastoma. (2019), *ACS Appl Mater Interfaces*, **11** (37), 33637–33649.
- (12) Park, J. H.; Gu, L.; von Maltzahn, G.; Ruoslahti, E.; Bhatia, S. N.; Sailor, M. J. Biodegradable Luminescent Porous Silicon Nanoparticles for in Vivo Applications. (2009), *Nat Mater*, **8** (4), 331–336.

- (13) Seo, H.; Wang, Y.; Sato, M.; Uchida, G.; Koga, K.; Itagaki, N.; Kamataki, K.; Shiratani, M. The Improvement on the Performance of Quantum Dot-Sensitized Solar Cells with Functionalized Si. (2013), *Thin Solid Films*, **546**, 284–288.
- (14) Seo, H.; Wang, Y.; Uchida, G.; Kamataki, K.; Itagaki, N.; Koga, K.; Shiratani, M. The Reduction of Charge Recombination and Performance Enhancement by the Surface Modification of Si Quantum Dot-Sensitized Solar Cell. (2013), *Electrochim Acta*, **87**, 213–217.
- (15) Yu, Y.; Rowland, C. E.; Schaller, R. D.; Korgel, B. A. Synthesis and Ligand Exchange of Thiol-Capped Silicon Nanocrystals. (2015), *Langmuir*, **31** (24), 6886–6893.
- (16) Dasog, M.; Veinot, J. G. C. Size Independent Blue Luminescence in Nitrogen Passivated Silicon Nanocrystals. (2012), *physica status solidi (a)*, **209** (10), 1844–1846.
- (17) Dasog, M.; de los Reyes, G. B.; Titova, L. v; Hegmann, F. A.; Veinot, J. G. C. Size vs Surface: Tuning the Photoluminescence of Freestanding Silicon Nanocrystals Across the Visible Spectrum via Surface Groups. (2014), *ACS Nano*, **8** (9), 9636–9648.
- (18) Dasog, M.; Bader, K.; Veinot, J. G. C. Influence of Halides on the Optical Properties of Silicon Quantum Dots. (2015), *Chemistry of Materials*, **27** (4), 1153–1156.
- (19) Biesta, W.; van Lagen, B.; Gevaert, V. S.; Marcelis, A. T. M.; Paulusse, J. M. J.; Nielen, M. W. F.; Zuilhof, H. Preparation, Characterization, and Surface Modification of Trifluoroethyl Ester-Terminated Silicon Nanoparticles. (2012), *Chemistry of Materials*, **24** (22), 4311–4318.
- (20) Rosso-Vasic, M.; Spruijt, E.; Popović, Z.; Overgaag, K.; van Lagen, B.; Grandidier, B.; Vanmaekelbergh, D.; Domínguez-Gutiérrez, D.; de Cola, L.; Zuilhof, H. Amine-Terminated Silicon Nanoparticles: Synthesis, Optical Properties and Their Use in Bioimaging. (2009), *J Mater Chem*, **19** (33), 5926–5933.
- (21) Höhlein, I. M. D.; Kehrle, J.; Purkait, T. K.; Veinot, J. G. C.; Rieger, B. Photoluminescent Silicon Nanocrystals with Chlorosilane Surfaces – Synthesis and Reactivity. (2015), *Nanoscale*, **7** (3), 914–918.
- (22) Buriak, J. M. Illuminating Silicon Surface Hydrosilylation: An Unexpected Plurality of Mechanisms. (2014), *Chemistry of Materials*, **26** (1), 763–772.
- (23) Yu, Y.; Hessel, C. M.; Bogart, T. D.; Panthani, M. G.; Rasch, M. R.; Korgel, B. A. Room Temperature Hydrosilylation of Silicon Nanocrystals with Bifunctional Terminal Alkenes. (2013), *Langmuir*, **29** (5), 1533–1540.
- (24) Warner, J. H.; Hoshino, A.; Yamamoto, K.; Tilley, Richard. D. Water-Soluble Photoluminescent Silicon Quantum Dots. (2005), *Angewandte Chemie International Edition*, **44** (29), 4550–4554.
- (25) Sato, S.; Swihart, M. T. Propionic-Acid-Terminated Silicon Nanoparticles: Synthesis and Optical Characterization. (2006), *Chemistry of Materials*, **18** (17), 4083–4088.
- (26) Chu, B.; Wang, H.; Song, B.; Peng, F.; Su, Y.; He, Y. Fluorescent and Photostable Silicon Nanoparticles Sensors for Real-Time and Long-Term Intracellular PH Measurement in Live Cells. (2016), *Anal Chem*, **88** (18), 9235–9242.

- (27) Grätzel, M. Dye-Sensitized Solar Cells. (2003), *Journal of Photochemistry and Photobiology C: Photochemistry Reviews*, **4** (2), 145–153.
- (28) Kramer, I. J.; Sargent, E. H. The Architecture of Colloidal Quantum Dot Solar Cells: Materials to Devices. (2014), *Chem Rev*, **114** (1), 863–882.
- (29) Correa-Baena, J. P.; Abate, A.; Saliba, M.; Tress, W.; Jesper Jacobsson, T.; Grätzel, M.; Hagfeldt, A. The Rapid Evolution of Highly Efficient Perovskite Solar Cells. (2017), *Energy Environ Sci*, **10** (3), 710–727.
- (30) Correa-Baena, J.-P.; Saliba, M.; Buonassisi, T.; Grätzel, M.; Abate, A.; Tress, W.; Hagfeldt, A. Promises and Challenges of Perovskite Solar Cells. (2017), *Science* (1979), **358**, 739–744.
- (31) Asghar, M. I.; Zhang, J.; Wang, H.; Lund, P. D. Device Stability of Perovskite Solar Cells – A Review. (2017), *Renewable and Sustainable Energy Reviews*, **77**, 131–146.
- (32) Rong, Y.; Hu, Y.; Mei, A.; Tan, H.; Saidaminov, M. I.; Seok, S. il; McGehee, M. D.; Sargent, E. H.; Han, H. Challenges for Commercializing Perovskite Solar Cells. (2018), *Science* (1979), **361** (6408).
- (33) Chen, J.; Park, N. G. Causes and Solutions of Recombination in Perovskite Solar Cells. (2019), *Advanced Materials*, **31** (47).
- (34) Li, H.; Zhang, W. Perovskite Tandem Solar Cells: From Fundamentals to Commercial Deployment. (2020), *Chem Rev*, **120** (18), 9835–9950.
- (35) Dupré, O.; Niesen, B.; de Wolf, S.; Ballif, C. Field Performance versus Standard Test Condition Efficiency of Tandem Solar Cells and the Singular Case of Perovskites/Silicon Devices. (2018), *Journal of Physical Chemistry Letters*, **9** (2), 446–458.
- (36) Todorov, T. K.; Bishop, D. M.; Lee, Y. S. Materials Perspectives for Next-Generation Low-Cost Tandem Solar Cells. (2018), *Solar Energy Materials and Solar Cells*, **180**, 350–357.
- (37) Zhang, Z.; Li, Z.; Meng, L.; Lien, S. Y.; Gao, P. Perovskite-Based Tandem Solar Cells: Get the Most Out of the Sun. (2020), *Adv Funct Mater*, **30** (38).
- (38) Jiang, Y.; Nielsen, M. P.; Baldacchino, A. J.; Green, M. A.; McCamey, D. R.; Tayebjee, M. J. Y.; Schmidt, T. W.; Ekins-Daukes, N. J. Singlet Fission and Tandem Solar Cells Reduce Thermal Degradation and Enhance Lifespan. (2021), *Progress in Photovoltaics: Research and Applications*, **29** (8), 899–906.
- (39) Daiber, B.; Maiti, S.; Ferro, S. M.; Bodin, J.; van den Boom, A. F. J.; Luxembourg, S. L.; Kinge, S.; Pujari, S. P.; Zuilhof, H.; Siebbeles, L. D. A.; Ehrler, B. Change in Tetracene Polymorphism Facilitates Triplet Transfer in Singlet Fission-Sensitized Silicon Solar Cells. (2020), *Journal of Physical Chemistry Letters*, **11** (20), 8703–8709.
- (40) Einzinger, M.; Wu, T.; Kompalla, J. F.; Smith, H. L.; Perkinson, C. F.; Nienhaus, L.; Wiegbold, S.; Congreve, D. N.; Kahn, A.; Bawendi, M. G.; Baldo, M. A. Sensitization of Silicon by Singlet Exciton Fission in Tetracene. (2019), *Nature*, **571** (7763), 90–94.
- (41) Wilson Lucas, S.; Zijian Qin, R.; Rakesh, K. P.; Sharath Kumar, K. S.; Qin, H.-L. Chemical and Biology of Sulfur Fluoride Exchange (SuFEx) Click Chemistry for Drug Discovery. (2023), *Bioorg Chem*, **130**, 106227.
- (42) Jones, L. H.; Kelly, J. W. Structure-Based Design and Analysis of SuFEx Chemical Probes. (2020), *RSC Med Chem*, **11** (1), 10–17.

- (43) Wang, H.; Zhou, F.; Ren, G.; Zheng, Q.; Chen, H.; Gao, B.; Klivansky, L.; Liu, Y.; Wu, B.; Xu, Q.; Lu, J.; Sharpless, K. B.; Wu, P. SuFEx-Based Polysulfonate Formation from Ethenesulfonyl Fluoride–Amine Adducts. (2017), *Angewandte Chemie International Edition*, **56** (37), 11203–11208.
- (44) Xiao, X.; Zhou, F.; Jiang, J.; Chen, H.; Wang, L.; Chen, D.; Xu, Q.; Lu, J. Highly Efficient Polymerization via Sulfur(vi)-Fluoride Exchange (SuFEx): Novel Polysulfates Bearing a Pyrazoline–Naphthylamide Conjugated Moiety and Their Electrical Memory Performance. (2018), *Polym Chem*, **9** (8), 1040–1044.
- (45) van den Boom, A. F. J.; Subramaniam, M.; Zuilhof, H. Sulfur-Phenolate Exchange As a Fluorine-Free Approach to S(VI) Exchange Chemistry on Sulfonyl Moieties. (2022), *Org Lett*, **24** (47), 8621–8626.
- (46) Smedley, C. J.; Homer, J. A.; Gialelis, T. L.; Barrow, A. S.; Koelln, R. A.; Moses, J. E. Accelerated SuFEx Click Chemistry For Modular Synthesis. (2022), *Angew. Chem. Int. Ed.*, **61** (4).
- (47) Dong, J.; Krasnova, L.; Finn, M. G.; Barry Sharpless, K. Sulfur(VI) Fluoride Exchange (SuFEx): Another Good Reaction for Click Chemistry. (2014), *Angewandte Chemie - International Edition*, **53** (36), 9430–9448.
- (48) Ling, T.; Tran, M.; González, M. A.; Gautam, L. N.; Connolly, M.; Wood, R. K.; Fatima, I.; Miranda-Carboni, G.; Rivas, F. (+)-Dehydroabietylamine Derivatives Target Triple-Negative Breast Cancer. (2015), *Eur J Med Chem*, **102**, 9–13.
- (49) Tomassi, C.; Nguyen Van Nhien, A.; Marco-Contelles, J.; Balzarini, J.; Pannecouque, C.; de Clercq, E.; Postel, D. Synthesis and Anti-HIV1 Biological Activity of Novel 5''-ATSAO Compounds. (2008), *Bioorg Med Chem*, **16** (8), 4733–4741.
- (50) Whitman, D. B.; Askew, B. C.; Duong, L. T.; Fernandez-Metzler, C.; Halczenko, W.; Hartman, G. D.; Hutchinson, J. H.; Leu, C. T.; Prueksaritanont, T.; Rodan, G. A.; Rodan, S. B.; Duggan, M. E. Nonpeptide Avβ3 Antagonists. Part 9: Improved Pharmacokinetic Profile through the Use of an Aliphatic, Des-Amide Backbone. (2004), *Bioorg Med Chem Lett*, **14** (17), 4411–4415.
- (51) Zhu, J.; Chen, H.; Guo, X. E.; Qiu, X. L.; Hu, C. M.; Chamberlin, A. R.; Lee, W. H. Synthesis, Molecular Modeling, and Biological Evaluation of Novel RAD51 Inhibitors. (2015), *Eur J Med Chem*, **96**, 196–208.
- (52) Coburn, C. A.; Luo, Y.; Cui, M.; Wang, J.; Soll, R.; Dong, J.; Hu, B.; Lyon, M. A.; Santarelli, V. P.; Kraus, R. L.; Gregan, Y.; Wang, Y.; Fox, S. v.; Binns, J.; Doran, S. M.; Reiss, D. R.; Tannenbaum, P. L.; Gotter, A. L.; Meinke, P. T.; Renger, J. J. Discovery of a Pharmacologically Active Antagonist of the Two-Pore-Domain Potassium Channel K2P9.1 (TASK-3). (2012), *ChemMedChem*, **7** (1), 123–133.
- (53) Smallheer, J. M.; Wang, S.; Laws, M. L.; Nakajima, S.; Hu, Z.; Han, W.; Jacobson, I.; Luetttgen, J. M.; Rossi, K. A.; Rendina, A. R.; Knabb, R. M.; Wexler, R. R.; Lam, P. Y. S.; Quan, M. L. Sulfonamidolactam Inhibitors of Coagulation Factor Xa. (2008), *Bioorg Med Chem Lett*, **18** (7), 2428–2433.
- (54) Perez, C.; Barkley-Levenson, A. M.; Dick, B. L.; Glatt, P. F.; Martinez, Y.; Siegel, D.; Momper, J. D.; Palmer, A. A.; Cohen, S. M. Metal-Binding Pharmacophore Library Yields the Discovery of a Glyoxalase 1 Inhibitor. (2019), *J Med Chem*, **62** (3), 1609–1625.
- (55) Rouffet, M.; de Oliveira, C. A. F.; Udi, Y.; Agrawal, A.; Sagi, I.; McCammon, J. A.; Cohen, S. M. From Sensors to Silencers: Quinoline- and Benzimidazole-

- Sulfonamides as Inhibitors for Zinc Proteases. (2010), *J Am Chem Soc*, **132** (24), 8232–8233.
- (56) Saupe, S. M.; Steinmetzer, T. A New Strategy for the Development of Highly Potent and Selective Plasmin Inhibitors. (2012), *J Med Chem*, **55** (3), 1171–1180.
- (57) Saupe, S. M.; Leubner, S.; Betz, M.; Klebe, G.; Steinmetzer, T. Development of New Cyclic Plasmin Inhibitors with Excellent Potency and Selectivity. (2013), *J Med Chem*, **56** (3), 820–831.
- (58) Mahapatra, S.; Woroch, C. P.; Butler, T. W.; Carneiro, S. N.; Kwan, S. C.; Khasnavis, S. R.; Gu, J.; Dutra, J. K.; Vetelino, B. C.; Bellenger, J.; Am Ende, C. W.; Ball, N. D. SuFEx Activation with Ca(NTf₂)₂: A Unified Strategy to Access Sulfamides, Sulfamates, and Sulfonamides from S(VI) Fluorides. (2020), *Org Lett*, **22** (11), 4389–4394.
- (59) Dondoni, A.; Marra, A. SuFEx: A Metal-Free Click Ligation for Multivalent Biomolecules. (2017), *Org Biomol Chem*, **15** (7), 1549–1553.
- (60) Zelli, R.; Tommasone, S.; Dumy, P.; Marra, A.; Dondoni, A. A Click Ligation Based on SuFEx for the Metal-Free Synthesis of Sugar and Iminosugar Clusters. (2016), *European J Org Chem*, **2016** (30), 5102–5116.
- (61) Wei, M.; Liang, D.; Cao, X.; Luo, W.; Ma, G.; Liu, Z.; Li, L. A Broad-Spectrum Catalytic Amidation of Sulfonyl Fluorides and Fluorosulfates**. (2021), *Angewandte Chemie International Edition*, **60** (13), 7397–7404.
- (62) Ivachtchenko, A. v.; Tkachenko, S. E.; Sandulenko, Y. B.; Vvedensky, V. Y.; Khvat, A. v. A Parallel Solution-Phase Synthesis of Substituted 3,7-Diazabicyclo[3.3.1] Nonanes. (2004), *J Comb Chem*, **6** (5), 828–834.
- (63) Park, H. G.; Choi, J. Y.; Choi, S. H.; Park, M. K.; Lee, J.; Suh, Y. G.; Cho, H.; Oh, U.; Lee, J.; Kang, S. U.; Lee, J.; Kim, H. D.; Park, Y. H.; Jeong, Y. S.; Choi, J. K.; Jew, S. S. N-4-Substituted-Benzyl-N'-Tert-Butylbenzyl Thioureas as Vanilloid Receptor Ligands: Investigation on the Role of Methanesulfonamido Group in Antagonistic Activity. (2004), *Bioorg Med Chem Lett*, **14** (3), 787–791.
- (64) Chen, H.; Wang, L.; Han, J. Deacetylative Aryl Migration of Diaryliodonium Salts with C(Sp²)-N Bond Formation toward Ortho-Iodo N-Aryl Sulfonamides. (2020), *Org Lett*, **22** (9), 3581–3585.
- (65) Cheng, G.; Wang, P.; Yu, J.-Q. Meta -C–H Arylation and Alkylation of Benzylsulfonamide Enabled by a Palladium(II)/Isoquinoline Catalyst . (2017), *Angewandte Chemie*, **129** (28), 8295–8298.
- (66) Dai, H. X.; Stepan, A. F.; Plummer, M. S.; Zhang, Y. H.; Yu, J. Q. Divergent C–H Functionalizations Directed by Sulfonamide Pharmacophores: Late-Stage Diversification as a Tool for Drug Discovery. (2011), *J Am Chem Soc*, **133** (18), 7222–7228.
- (67) Adamek, R. N.; Credille, C. v.; Dick, B. L.; Cohen, S. M. Isosteres of Hydroxypyridinethione as Drug-like Pharmacophores for Metalloenzyme Inhibition. (2018), *Journal of Biological Inorganic Chemistry*, **23** (7), 1129–1138.
- (68) Milliken, S.; Thiessen, A. N.; Cheong, I. T.; O'Connor, K. M.; Li, Z.; Hooper, R. W.; Robidillo, C. J. T.; Veinot, J. G. C. "Turning the Dials": Controlling Synthesis, Structure, Composition, and Surface Chemistry to Tailor Silicon Nanoparticle Properties. (2021), *Nanoscale*, **13** (39), 16379–16404.

- (69) Jung, Y.; Kim, D. Recent Advances in Hybrid System of Porous Silicon Nanoparticles and Biocompatible Polymers for Biomedical Applications. (2021), *Biomed Eng Lett*, **11** (3), 171–181.
- (70) Fermi, A.; Locritani, M.; di Carlo, G.; Pizzotti, M.; Caramori, S.; Yu, Y.; Korgel, B. A.; Bergamini, G.; Ceroni, P. Light-Harvesting Antennae Based on Photoactive Silicon Nanocrystals Functionalized with Porphyrin Chromophores. (2015), *Faraday Discuss*, **185**, 481–495.
- (71) Kwak, G. Y.; Kim, T. G.; Hong, S.; Kim, A.; Ha, M. H.; Kim, K. J. Efficiency Improvement of Si Quantum Dot Solar Cells by Activation with Boron Implantation. (2018), *Solar Energy*, **164**, 89–93.
- (72) Dutta, S.; Chatterjee, S.; Mallem, K.; Cho, Y. H.; Yi, J. Control of Size and Distribution of Silicon Quantum Dots in Silicon Dielectrics for Solar Cell Application: A Review. (2019), *Renew Energy*, **144**, 2–14.
- (73) Pudakalakatti, S.; Enriquez, J. S.; McCowan, C.; Ramezani, S.; Davis, J. S.; Zacharias, N. M.; Bourgeois, D.; Constantinou, P. E.; Harrington, D. A.; Carson, D.; Farach-Carson, M. C.; Bhattacharya, P. K. Hyperpolarized MRI with Silicon Micro and Nanoparticles: Principles and Applications. (2021), *WIREs Nanomedicine and Nanobiotechnology*, **13** (6), e1722.
- (74) Yang, Y.; Yuan, W.; Kang, W.; Ye, Y.; Yuan, Y.; Qiu, Z.; Wang, C.; Zhang, X.; Ke, Y.; Tang, Y. Silicon-Nanoparticle-Based Composites for Advanced Lithium-Ion Battery Anodes. (2020), *Nanoscale*, **12** (14), 7461–7484.
- (75) Thompson, N. J.; Wilson, M. W. B.; Congreve, D. N.; Brown, P. R.; Scherer, J. M.; Bischof, T. S.; Wu, M.; Geva, N.; Welborn, M.; van Voorhis, T.; Bulovi, V.; Bawendi, M. G.; Baldo, M. A. Energy Harvesting of Non-Emissive Triplet Excitons in Tetracene by Emissive PbS Nanocrystals. (2014), *Nat Mater*, **13** (1), 1039–1043.
- (76) Davis, N. J. L. K.; Allardice, J. R.; Xiao, J.; Petty, A. J.; Greenham, N. C.; Anthony, J. E.; Rao, A. Singlet Fission and Triplet Transfer to PbS Quantum Dots in TIPS-Tetracene Carboxylic Acid Ligands. (2018), *Journal of Physical Chemistry Letters*, **9** (6), 1454–1460.

Summary

To protect human, animal, and plant life alike, it is imperative to stop global warming, the depletion of natural resources, and environmental pollution. To do this, humankind needs to take further steps to reduce its CO₂ footprint, minimize its energy consumption, and reduce the amount of harmful materials used and waste generated during production processes. This requires extensive collaboration between consumers, industry, government, and the scientific community. In this thesis, the aim was to – in some small part – contribute to this end goal by improving upon existing methods to generate solar energy, and by developing more environmentally friendly alternatives to existing processes and reactions.

Chapter 1 introduces the basis for the research outlined in the later chapters. First, current photovoltaic methods to generate solar energy are explained, and their advantages and disadvantages are discussed. Then, the basic principles of click chemistry are laid out, and a more elaborate description is provided for three of the more relevant click reactions – CuAAC, thiol-ene, and SuFEx. **Chapter 1** ends by defining the aim of this thesis in more detail.

Chapter 2 describes a one-pot, room-temperature method to passivate hydrogen-terminated silicon nanoparticles (H-Si NPs) using alkyl silanols. H-Si NPs are highly desired due to their non-toxic and biodegradable nature, and their excellent electronic properties. However, H-Si NPs are highly susceptible to oxidation, and require passivation to prevent degradation of their properties. Previously reported passivation methods generally required high temperatures, radical catalysts, or corrosive chemicals, and featured reaction times of up to 16 h, with extensive purification afterwards. In contrast, our alkyl silanol method achieved good passivation after 1 h of reaction time at room temperature, without the use of additional reagents, while the whole process of passivation and purification could be completed within 4 h. Furthermore, the silanol method is specific enough that it allows attachment of ligands with secondary functionalities. This was demonstrated by further functionalizing a vinyl-terminated nanoparticle with a sugar thiol *via* a thiol-ene click reaction, resulting in water-soluble silicon nanoparticles. The silanol reaction therefore provides an easy, room-temperature method to quickly passivate H-Si NPs without the need for corrosive or expensive chemicals, while also allowing further functionalization and tuning of the surface coating.

Chapter 3 describes the fabrication and performance of a model singlet-fission sensitized solar cell. Tetracene is a singlet-fission material that is, in principle, capable of doubling the current generated by high-energy photons in a silicon solar cell, greatly increasing its energy conversion efficiency. However, simply depositing tetracene on top of a silicon solar cell leads to inefficient transfer of triplet energy, and does not improve the performance of the solar cell. Though energy transfer

can be improved with special interlayers, this requires highly precise fabrication techniques. We aimed to improve the energy transfer by covalently functionalizing the silicon surface with tetracene derivatives, bound *via* either the 2- or 5-position, to generate a seed layer capable of more favorably orienting the subsequently deposited tetracene for energy transfer. While functionalization *via* the 5-position seemed to decrease the crystallinity of the deposited tetracene layer, functionalization *via* the 2-position showed signs of increasing the crystallinity and improving the orientation, at least for the tetracene layers closest to the seed layer. Unfortunately, no increase in triplet energy transfer was observed for either surface, indicating a need for further research into the parameters that influence tetracene orientation.

Chapter 4 describes the synthesis of sulfonyl esters using a fluorine-free approach to S(VI) exchange chemistry on sulfonyl moieties. While sulfonyl esters are readily made from sulfonyl chlorides or fluorides, these reactions often require the use of catalysts, an inert atmosphere, or additional reagents. In addition, sulfonyl chlorides suffer from poor hydrolytic stability, while sulfonyl fluorides release fluorine-containing byproducts during the reaction. Considering the environment-driven trend to diminish the use of fluorine-containing chemicals, a fluorine-free alternative that does not require additional reagents is highly desired. In **Chapter 4**, we employ 4-nitrophenyl benzyldisulfonate as a starting material in a sulfur-phenolate exchange (SuPhenEx) reaction, where the 4-nitrophenyl moiety is exchanged for a large range of deprotonated aromatic, aliphatic, and natural alcohols. This reaction proceeds at room temperature under atmospheric conditions, and only produces solid sodium 4-nitrophenolate and H₂ gas as byproducts. The yield obtained using the SuPhenEx reaction was in most cases quantitative, and the reaction time comparable or shorter than for previously reported methods. In addition, purification was straightforward, and only consisted of filtering through silica followed by a short flash chromatography column. Therefore, SuPhenEx is considered a good and more environmentally friendly alternative to SuFEx and sulfonyl chloride exchange reactions.

Chapter 5 continues the research started in **Chapter 4**, yet here the focus lies on the synthesis of sulfonamides, a class of compounds found in many biological studies for their use as medicine or enzyme inhibitors. Generally made from sulfonyl chlorides, the synthesis of sulfonamides often involves extensive drying of solvents, the use of an inert atmosphere, or heating to 130 °C in a microwave reactor. Since the introduction of SuFEx, sulfonamides have also been prepared from sulfonyl fluorides using catalysts or elevated temperatures, yet there is still a lack of easy, uncatalyzed, room-temperature procedures. However, using SuPhenEx, we were able to prepare a large range of sulfonamides *via* a room-temperature reaction under atmospheric conditions. We started by testing several aliphatic and cyclic

amines, all of which were obtained with quantitative yields, after similar or shorter reaction times than previously reported. Then, considering the biological applications of sulfonamides, we tested the SuPhenEx reaction with three amino acids, and found good yields (>80%) for each. After this preliminary study, a collection of *N*-methylanilines and primary anilines was tested. While most of the *N*-methylanilines gave (near-) quantitative yields, the primary anilines were decidedly less reactive, though an improvement upon literature procedures was still seen. Finally, several other nitrogen-based nucleophiles and starting materials were tested, to expand the scope of the SuPhenEx reaction even further, and firmly establish SuPhenEx as a more stable and less energy-consuming alternative to the use of sulfonyl chlorides and fluorides.

Finally, **Chapter 6** provides a general discussion and reflection on the results found for each of the previous chapters, and relates these results to existing knowledge. An outlook is provided, as well as some recommendations for future research. **Chapter 6** ends by stating the main conclusions from this thesis.

Acknowledgements

A thesis represents ~4 years of hard work, excitement, frustration, and perseverance. During this time, you meet a lot of people that help and support you, and without whom you would not be writing this thesis today. So in this chapter, I would like to take the opportunity to thank some of those people.

First of all, I would like to thank my promotor, **Han Zuilhof**. Thank you for giving me the opportunity to work on this project, and for all the meetings, advice, and scientific discussions. The original goal of the project may not have worked out the way we wanted it to, but I think we reached some nice results in the end. Many thanks also go to my project partners from the Mat4Sus project: **Bruno Ehrler**, **Silvia Ferro**, **Laurens Siebbeles**, **Arthur Weeber**, **Sourav Maiti**, **Luc Scheres**, **Sachin Kinge**, and **Stefan Luxembourg**. It was a pleasure collaborating with you, and I am proud of the paper we published together, as well as all the unpublished work we did, and the knowledge we shared.

Then, of course, I would like to thank everyone at ORC for welcoming me into the group, the friendly conversations, the nice atmosphere, and the occasional board games. You are all part of the reason these past 4½ years have seemed to fly past. **Elly Geurtsen**, thank you for arranging countless – sometimes last-minute – meetings, and thank you and **Aleida Ruisch** for arranging the shared lunches, Christmas drinks, cakes, and other social activities within ORC. You are truly the “mothers” of ORC, and we would be lost without you. Thank you **Barend van Lagen** for the many talks in the lab, all your help with the NMR, and always making sure the store room is fully stocked. Thank you **Frank Claassen** for all your explanations and help with the MS, and of course thanks to all technicians for keeping all the equipment and labs running smoothly, so us PhDs can do our research. I will miss you all dearly.

I will also miss all fellow PhD's and PD's – past and present – who I had the pleasure of meeting during my time at ORC. Nobody understands a PhD like people with / working on a PhD, so thanks for all the talks, support, laughs, and occasional complaining sessions. I will not list everyone's name here, but there are a few people who I would like to thank in person. **Dieuwertje Streefkerk**, I know you are not a PhD student, but as a lab mate, thank you for all the advice on reactions and purifications, and the many talks about baking, knitting, and other “old-women” hobbies and habits 😊. **Sevil Şahin**, you are one of the sweetest and kindest people I know, who always sees the best in others. Thank you for your endless positivity, and all the laughs (and food). Also thank you, **Ariadni Geballa-Koukoulou**, and **Fatma Akin** for all the fun during bellydance lessons and every time we meet up. Of course, I would also like to thank the karaoke and boardgame crew: **Pepijn**

Beekman, Jorick Bruins, Alice Guarneri, Sevil & Adem Şahin, Fred van Geenen, Ellen Dautzenberg, and Satesh Gangarapu. I sincerely hope all incriminating videos have been deleted.

Finally, and perhaps most importantly, I would like to thank my family. **Mam**, zonder jou zou ik nooit zijn opgegroeid tot de persoon die ik nu ben. Bedankt voor al je liefde en steun, en je luisterend oor tijdens de stressvolle tijden. **Sem**, bedankt voor alle gezelligheid, spelletjes, en nodige ontspanning. Hopelijk hebben we nu allebei meer tijd om samen leuke dingen te doen. **Corrie, Sjef, Michel, en Bo**, jullie zijn de beste en liefste schoonfamilie die iemand zich kan wensen. Bedankt voor al jullie liefde en steun, en ik ben super gelukkig dat ik een deel mag worden van jullie familie. En ten slotte, **Fred**, bedankt voor al je steun en liefde, het luisteren naar mijn frustraties, het vieren van mijn successen, en dat je altijd voor me klaar staat. Ik zou iedereen zo'n lieve partner als jou toewensen!

Curriculum Vitae

Alyssa Frauke Janique van den Boom was born on May 11th, 1995 in Dedemsvaart, the Netherlands. She attended high school in Zwolle, where she graduated with honors as part of the 10% best-performing students in higher education. She then completed her Bachelor and Master studies in *Molecular Life Sciences* at Wageningen University & Research, with a specialization towards Physical Chemistry. During her Master internship, Alyssa worked on the development of new coatings at Trespa International B.V.; during her Master thesis, she worked in the lab of Organic Chemistry on the coating of silicon nanoparticles. This last project also became the second chapter in this thesis, when she continued this project during her PhD research at the same group. Under the supervision of prof. dr. Han Zuilhof, Alyssa then worked on the development of more efficient solar cells, and research into the scope of novel click chemistry. Nowadays, Alyssa works as a trainee patent attorney at EDP Patent Attorneys B.V.

List of publications:

Van den Boom, Alyssa F.J.; Pujari, Sidharam P.; Bannani, Fatma; Driss, Hafedh; Zuilhof, Han (2020); Fast room-temperature functionalization of silicon nanoparticles using alkyl silanols. *Faraday Discuss.*, **222**, 82-94. DOI: 10.1039/c9fd00102f

Daiber, Benjamin; Maiti, Sourav; Ferro, Silvia M.; Bodin, Joris; van den Boom, Alyssa F.J.; Luxembourg, Stefan L.; Kinge, Sachin; Pujari, Sidharam P.; Zuilhof, Han; Siebbeles, Laurens D.A.; Ehrler, Bruno (2020); Change in Tetracene Polymorphism Facilitates Triplet Transfer in Singlet Fission-Sensitized Silicon Solar Cells. *J. Phys. Chem. Lett.*, **11**, 8703-8709. DOI: 10.1021/acs.jpcclett.0c02163

Van den Boom, Alyssa F.J.; Subramaniam, Muthusamy; Zuilhof, Han (2022); Sulfur-Phenolate Exchange As a Fluorine-Free Approach to S(VI) Exchange Chemistry on Sulfonyl Moieties. *Org. Lett.*, **24**, 8621-8626. DOI: 10.1021/acs.orglett.2c03421

Van den Boom, Alyssa F.J.; Zuilhof, Han (2023); Sulfur-Phenolate Exchange as a Mild, Fast, and High-Yielding Method toward the Synthesis of Sulfonamides. *Org. Lett.*, **25**, 788-793. DOI: <https://doi.org/10.1021/acs.orglett.2c04292>

Overview of completed training activities

Discipline-specific activities	Organizing institute	Year
Advanced Organic Chemistry course	ORC - WUR	2018 – '22
Molecular Life Sciences series	WUR	2018 - '19
* Mat4Sus kick-off meeting	NWO / AMOLF	2019
# CHAINS symposium 2019	NWO	2019
CHAINS symposium 2020	NWO	2020
ACS spring conference	ACS	2021
Wageningen International Symposium on Organic Chemistry	KNCV SOC	2021
CHAINS symposium 2021	NWO	2021
* CHAINS symposium 2022	NWO	2022

* Represents an oral presentation

Represents a poster presentation

General courses	Organizing institute	Year
VLAG PhD week	VLAG	2019
Effective behaviour in your professional surroundings	WGS	2019
Scientific Artwork	WGS	2019
Presenting with impact	WGS	2020
Scientific Publishing	WGS	2020
Critical thinking and argumentation	WGS	2021
De Effectieve Teamleider	IMK opleidingen	2022
Career perspectives	WGS	2022

Additional activities	Organizing institute	Year
Preparation of research proposal	ORC - WUR	2018
Weekly group meetings	ORC - WUR	2018 - '22
Colloquia	ORC - WUR	2018 – '22
Project partner meetings	AMOLF, TUD, WUR	2019 – '20
PhD study tour to Israel	PhDs of ORC - WUR	2019

Teaching activities	Year
SOC-33806 Environmental Analytical Techniques	2019 – '20
BIP-24306 Spectroscopy and Imaging	2019 & '22
ORC-11806 Analytical Methods in Organic Chemistry	2019 – '21
ORC-12803 Organic Chemistry 1	2021
ORC-13803 Bio-Organic Chemistry for Life Sciences	2021

The research presented in this thesis was financially supported by the Dutch Research Council (NWO) in the framework of the Materials for Sustainability program.

Financial support from Wageningen University for printing this thesis is gratefully acknowledged.